ISSN 1068-9761/e-2541-9935

LIGHT & ENGINEERING

Volume 28, Number 4, 2020

Editorial of Journal
"Light & Engineering" (Svetotekhnika), Moscow

The purpose and content of «Light & Engineering» is to develop the science of light within the framework of ray, photometric concepts and the application of results for a comfortable light environment, as well as for visual and non-visual light technologies, including medicine. The light engineering science is a field of science and technology and its subject is the development of methods for generation and spatial redistribution of optical radiation, as well as its conversion to other forms of energy and use for various purposes.

The scope of journal includes articles in the following areas:

- Sources of light;
- Light field theory;
- Photometry, colorimetry and radiometry of optical radiation;
- Visual and non-visual effects of radiation on humans;
- Control and regulation devices for light sources;
- Light devices, their design and production technology;
- Light devices for the efficient distribution and transportation of the light energy: hollow light guides, optical fibers;
- Lighting and irradiation installations;
- Light signaling and light communication;
- Light remote sensing;
- Mathematical modelling of light devices and installations;
- Energy savings in light installation;
- Innovative light design solutions;
- Photobiology, including problems of using light in medicine;
- Disinfection of premises, drinking water and smell elimination by UV radiation technology;
- Light transfer in the ocean, space and other mediums;
- Light and engineering marketing;
- Legal providing and regulation of energy effective lighting;
- Light conversion to other forms of energy;
- Standardization in field of lighting;
- Light in art and architecture design;
- Education in field of light and engineering.

Journal “Light & Engineering” had been founded by Prof. Julian B. Aizenberg in 1993

LIGHT & ENGINEERING

СВЕТОТЕХНИКА

Editorial of Journal “Light & Engineering/Svetotekhnika”

Moscow, 2020

Publishing House: Editorial of Journal "Light & Engineering" (Svetotekhnika), Moscow

Editorial Office:

Russia, VNISI, Rooms 327 and 334
106 Prospekt Mira, Moscow 129626

Tel: +7.495.682.26.54
Tel./Fax: +7.495.682.58.46
E-mail: lights-nr@inbox.ru
http://www.l-e-journal.com

Light & Engineering" is an international scientific Journal subscribed to by readers in many different countries. It is the English edition of the journal "Svetotekhnika" the oldest scientific publication in Russia, established in 1932.

Establishing the English edition "Light and Engineering" in 1993 allowed Russian illumination science to be presented the colleagues abroad. It attracted the attention of experts and a new generation of scientists from different countries to Russian domestic achievements in light and engineering science. It also introduced the results of international research and their industrial application on the Russian lighting market.

The scope of our publication is to present the most current results of fundamental research in the field of illumination science. This includes theoretical bases of light source development, physiological optics, lighting technology, photometry, colorimetry, radiometry and metrology, visual perception, health and hazard, energy efficiency, semiconductor sources of light and many others related directions. The journal also aims to cover the application illumination science in technology of light sources, lighting devices, lighting installations, control systems, standards, lighting art and design, and so on.

"Light & Engineering" is well known by its brand and design in the field of light and illumination. Each annual volume has six issues, with about 80–120 pages per issue. Each paper is reviewed by recognized world experts.

CONTENTS

VOLUME 28 **NUMBER 4** **2020**

LIGHT & ENGINEERING

International Commission on Illumination
Commission Internationale de l'Eclairage
Internationale Beleuchtungskommission

CIE Position Statement on Ultraviolet (UV) Radiation to Manage the Risk of COVID-19 Transmission

May 12, 2020

Introduction

The coronavirus disease (COVID-19) pandemic has accelerated the search for environmental controls to contain or mitigate the spread of the severe acute respiratory syndrome coronavirus 2 (SARS-CoV-2) responsible for the disease. SARS-CoV-2 is usually transmitted from person to person by contact with large respiratory droplets, either directly or by touching virus-contaminated surfaces (also denoted as fomites) and subsequently touching the eyes, nose or mouth. Importantly, there is growing evidence of virus transmission via the airborne route as the large respiratory droplets dry out and form droplet nuclei which can remain airborne for several hours. Depending on the nature of the surface and environmental factors, fomites can remain infectious for several days (van Doremalen, 2020).

The use of germicidal UV radiation (GUV) is an important environmental intervention which can reduce both contact spread and airborne transmission of infectious agents (like bacteria and viruses). GUV within the UV–C range (200 nm-280 nm), primarily 254 nm, has been used successfully and safely for over 70 years. However, GUV must be knowledgably applied with appropriate attention to dose and safety. Inappropriate GUV application can present human health and safety issues and produce insufficient deactivation of infectious agents. Application in the home is not advisable and GUV should never be used to disinfect the skin, except when clinically justified.

What is GUV?

Ultraviolet radiation is that part of the optical radiation spectrum that has more energy (shorter wavelengths) than visible radiation, which we experience as light. GUV is ultraviolet radiation that is used for germicidal purposes.

Based on the biological impact of ultraviolet radiation on biological materials, the ultraviolet spectrum is divided into regions: UV-A is defined by CIE as radiation in the wavelength range between 315 nm and 400 nm; UV-B is radiation in the wavelength range between 280 nm and 315 nm; and the UV–C wavelength range is between 100 nm and 280 nm. The UV–C part of the UV spectrum has the highest energy. Whilst it is possible to damage some microorganisms and viruses with most of the ultraviolet radiation spectrum, UV–C is the most effective and hence UV–C is most commonly used as GUV.

The radiant exposure required for the deactivation of an infectious agent by 90 % (in air or on a surface) depends on the environmental conditions (such as relative humidity) and the kind of infectious agent. It typically ranges between 20 J/m2 and 200 J/m2 for mercury lamps predominantly emitting radiation at 254 nm (CIE, 2003). Previously, GUV of 254 nm has been shown to be effective in disinfecting surfaces contaminated with the Ebola virus (Sagripanti and Lytle, 2011; Jinadatha et al., 2015; Tomas et al., 2015). Other studies have demonstrated

the effectiveness of GUV during an influenza outbreak in the Livermore Veterans Hospital (Jordan, 1961). However, despite ongoing research, at present there is no published data on the effectivity of GUV against SARS-CoV-2.

Applying GUV for disinfection

UV–C has been used successfully for water disinfection for many years. Moreover, UV–C disinfection is routinely incorporated into air handling units to manage the build-up of biofilms and to disinfect air (CIE, 2003).

Until the introduction of polymer materials in healthcare settings and the availability of antibi-

otics and vaccines, UV–C sources were commonly used in several countries to sterilize operating theatres and other rooms overnight. Recently, there has been a resurgence of interest in the use of whole room UV–C exposure devices for healthcare environments intended to disinfect the air and accessible surfaces in the room. Such devices can either be placed in a specific room location for a period of time, or they can be robotic units that move around the environment to minimize shadow effects. For surface disinfection, in addition to the option to place a UV–C source in the room, it is possible to place a UV–C source close to a surface.

Limited use of UV–C for disinfection of personal protective equipment during pandemics has been explored in some countries (Jinadatha et al., 2015; Nemeth et al., 2020).

There is growing evidence that the use of UV–C as an adjunct to standard manual cleaning in hospitals can be effective in practice, although more specific application guidelines still need to be developed as well as standard testing procedures.

Upper air disinfection UV–C sources are usually mounted above head-height in rooms and operate continuously to disinfect circulating air. Such sources have been successfully deployed to limit the transmission of tuberculosis (Mphaphlele, 2015; Escombe et al., 2009; DHHS, 2009). Based on a systematic review of the literature, the World Health Organization (WHO) recommended the use of upper room GUV as a means for tuberculosis infection prevention and control (WHO, 2019).

Some laboratory studies have found that the effectivity of upper-air UV–C disinfection depends on the relative humidity, temperature conditions and air circulation (Ko et al., 2000; Peccia et al., 2001). Escombe et al. (2009) studied upper room GUV in a non-air-conditioned hospital ward in Lima, Peru, and found a marked reduction in the risk of transmission of airborne tuberculosis, despite the high relative humidity of 77 %.

Risks when using UV–C

Most people do not get exposed to UV–C naturally: UV–C from the sun is primarily filtered by the atmosphere, even at high altitudes (Piazena and Häder, 2009). Human exposure to UV–C typically arises from artificial sources. UV–C only penetrates the outermost layers of the skin and hardly reaches the basal layer of the epidermis, neither does it penetrate deeper than the surface layer of the cornea of the eye. Exposure of the eye to UV–C can result in photokeratitis, a very painful condition that feels as if sand has been rubbed onto the eye. Photokeratitis symptoms take up to 24 hours after the exposure to develop and require about another 24 hours for them to subside.

When the skin gets exposed to high levels of UV–C, erythema (a skin reddening similar to sunburn) can develop (ISO/CIE, 2019). Usually erythema is less painful than the effect of UV–C on the eyes. However, the UV–C-induced erythema can be misdiagnosed as dermatitis, especially when it is not known that there was a recent UV–C exposure history. There is some evidence that repeated exposure of the skin to UV–C levels that cause erythema may compromise the body's immune system (Gläser et al., 2009).

Ultraviolet radiation is generally considered to be carcinogenic (ISO/CIE, 2016), however, there is no evidence that UV–C alone causes cancer in humans. The Technical Report CIE187:2010 (CIE, 2010) discusses the question and concludes: "while the UV radiation from low- pressure mercury UVGI[1] lamps has been identified as a potential carcinogen, the relative risk of skin cancer is significantly less than the risk from other sources (such as the sun) to which a worker will be routinely exposed. UV germicidal irradiation can be safely and effectively used for upper-air disinfection without a significant risk of long-term delayed effects such as skin cancer."

Guidance for occupational exposure to UV radiation including UV–C radiation has been provided by the International Commission on Non-Ionizing Radiation Protection (ICNIRP, 2004): UV radiant exposure upon unprotected eyes/skin should not exceed 30 J/m^2 for radiation of 270 nm, the peak wavelength of the spectral weighting function for actinic UV hazard for skin and eye. As the hazard effect of UV radiation depends on wavelength, the maximum exposure limit for radiation of wavelength 254 nm is 60 J/m^2. For radiation of 222 nm the maximum (actinic UV hazard) exposure limit is even higher, around 240 J/m^2. This wavelength has been studied for germicidal purposes in (Buonanno et al., 2017; Welch et al., 2018; Narita et al., 2018; Taylor et al., 2020; Yamano et al., 2020). The preceding (daily) UV exposure limits are given in the

[1] UVGI is the acronym of "ultraviolet germicidal irradiation".

IEC/CIE standard for the photobiological safety of products (IEC/CIE, 2006).

Typical UV–C sources often also emit radiation that includes various wavelengths outside the UV–C range. Some UV–C products may additionally emit UV-B or UV-A, and some UV disinfection sources declared as UV–C sources may not even emit UV–C. As the exposure to UV from such products may increase the risk of skin cancer, protective measures have to be taken to minimize this risk. In normal use, UV sources secured inside ductwork for recirculated air or used for water sterilization should not present a risk of exposure to people. When working in a UV-irradiated zone, workers shall wear personal protective equipment such as industrial clothing (e.g. heavy fabric), and industrial face protection (e.g. face shields) (ICNIRP, 2010). Full-face respirators (CIE, 2006) and hand protection by disposable gloves (CIE, 2007) are also protective against UV.

Measurement of UV–C

In-situ measurement of UV–C is usually performed using handheld UV–C radiometers. Ideally, any radiometer should be calibrated by a laboratory that is accredited to ISO/IEC17025 (ISO/IEC, 2015), so that the calibration is traceable to the International System of Units (SI) (BIPM, 2019a; BIPM, 2019b). Moreover, it is important to check the calibration report and apply any correction factors which are contained within the report when using the instrument. The calibration report is usually only valid for the UV–C source used in the calibration; significant errors may result when measuring other source types with the instrument. Most instrument calibrations are typically done using the 254 nm emission line of a low-pressure mercury source. If the calibrated instrument is then used to measure a UV source with a wavelength (range) that is significantly different from 254 nm, this may result in spectral mismatch errors of tens of per cent. Some UV–C radiometers can be calibrated to account for wavelengths other than 254 nm, for example for use with UV LED sources or excimer lamps.

When a UV radiometer is calibrated, it is best practice for the calibration laboratory to ask the user what type of source will be evaluated with the instrument, so that ideally the instrument will be calibrated using a source with a similar spectral composition as the sources to be measured by the user, in order to reduce these spectral mismatch errors. CIE220:2016 (CIE, 2016) provides guidance for characterization and calibration of UV radiometers. Further information about the measurement of optical radiation hazards is provided in (ICNIRP/CIE, 1998). At present, CIE and ICNIRP are organizing an online tutorial on the measurement of optical radiation and its effects on photobiological systems (CIE/ICNIRP, 2020).

Consumer products

As the present COVID-19 pandemic spreads, many UV–C products promising efficient disinfection of surfaces and air are being put on the market. Specific guidance on the safety of consumer products is the responsibility of international organizations such as the International Electrotechnical Commission (IEC), and is not provided by CIE. As such, this Position Statement only covers the wider issue of the safe use and application of UV radiation for germicidal disinfection. Products available to consumers tend to be marketed as handheld devices. CIE is concerned that users of such devices may be exposed to harmful amounts of UV–C. Moreover, consumers may use/handle UV products inappropriately (and therefore not achieve effective disinfection) or they might be buying products that do not actually emit UV–C.

Summary recommendations

Products that emit UV–C are extremely useful in disinfection of air and surfaces or sterilization of water. CIE and WHO warn against the use of UV disinfection lamps to disinfect hands or any other area of skin (WHO, 2020), unless clinically justified. UV–C can be very hazardous to humans and animals and therefore can only be used in properly constructed products that meet safety regulations, or in very controlled circumstances where safety is taken into account as the first priority, ensuring that the limits of exposure as specified in ICNIRP (2004) and IEC/CIE (2006) are not exceeded. For proper UV assessment and risk management, appropriate UV measurements are essential.

References

BIPM (2019a) *The International System of Units (SI), 9th Edition.*
Downloadable at https://www.bipm.org/utils/common/pdf/si-brochure/SI-Brochure-9-EN.pdf

BIPM (2019b) *The International System of Units (SI), 9th Edition – Appendix 3: Units for photochemical and photobiological quantities.*
Downloadable at https://www.bipm.org/utils/common/pdf/si-brochure/SI-Brochure-9-App3- EN.pdf, accessed 2020–04–24.

Buonanno, M., Ponnaiya, B., Welch, D., Stanislauskas, M., Randers-Pehrson, G., Smilenov, L., Lowy, F.D., Owens, D.M. and Brenner, D.J. (2017) Germicidal Efficacy and Mammalian Skin Safety of 222-nm UV Light. *Radiat Res* 187(4): 483–491. DOI:10.1667/RR0010CC.1

CIE (2003) CIE155:2003 *Ultraviolet Air Disinfection*. Freely available at http://cie.co.at/news/cie-releases-two-key-publications-uv-disinfection[2]

CIE (2006) CIE172:2006 *UV protection and clothing.*

CIE (2007) CIE181:2007 *Hand protection by disposable gloves against occupational UV exposure.*

CIE (2010) CIE187:2010 *UV–C photocarcinogenesis risks from germicidal lamps*.

Freely available at http://cie.co.at/news/cie-releases-two-key-publications-uv-disinfection[2]

CIE (2016) CIE220:2016 *Characterization and Calibration Methods of UV Radiometers.*

CIE/ICNIRP (2020) CIE/ICNIRP *Online Tutorial on the Measurement of Optical Radiation and its Effects on Photobiological Systems, August 25, 2020 to August 27, 2020*. http://cie.co.at/news/cieicnirp-online-tutorial-measurement-optical-radiation-and-its-effects-photobiological-systems, accessed 2020–04–24.

DHHS (2009) *Environmental Control for Tuberculosis: Basic Upper-Room Ultraviolet Germicidal Irradiation Guidelines for Healthcare Settings*, DHHS (NIOSH) Publication Number 2009–105, https://www.cdc.gov/niosh/docs/2009–105/default.html, accessed 2020-04–25.

Escombe, A.R., Moore, D.A., Gilman, R.H., Navincopa, M., Ticona, E., Mitchell, B., Noakes, C., Martínez, C., Sheen, P., Ramirez, R., Quino, W., Gonzalez, A., Friedland, J.S., Evans,

C.A. (2009) *Upper-room ultraviolet light and negative air ionization to prevent tuberculosis transmission*. *PLoS Med*. 6(3): e43. DOI: 10.1371/journal.pmed.1000043.

Gläser, R., Navid, F., Schuller, W., Jantschitsch, C., Harder, J., Schröder, J.M., Schwarz, A., Schwarz, T. (2009) UV-B radiation induces the expression of antimicrobial peptides in human keratinocytes in vitro and in vivo. *Journal of Allergy and Clinical Immunology* 123(5): 1117–1123. DOI: 10.1016/j.jaci.2009.01.043

ICNIRP (2004) ICNIRP Guidelines – On limits of exposure to ultraviolet radiation of wavelengths between 180 nm and 400 nm (incoherent optical radiation), *Health Physics* 87(2):171–186; 2004.

Available at http://www.icnirp.org

ICNIRP (2010) ICNIRP Statement – Protection of workers against ultraviolet radiation, *Health Physics* 99(1):66-87; DOI: 10.1097/HP.0b013e3181d85908

Available at http://www.icnirp.org

ICNIRP/CIE (1998) ICNIRP 6/98 / CIE x016–1998. *Measurement of Optical Radiation Hazards.*

IEC/CIE (2006) IEC62471:2006/CIE S009:2002 *Photobiological safety of lamps and lamp systems / Sécurité photobiologique des lampes et des appareils utilisant des lampes.* (bilingual edition)

ISO/IEC (2015) ISO/IEC17025:2015 *General requirements for the competence of testing and calibration laboratories.*

ISO/CIE (2016) ISO/CIE28077:2016(E) *Photocarcinogenesis action spectrum (non- melanoma skin cancers).*

ISO/CIE (2019) ISO/CIE17166:2019(E) *Erythema reference action spectrum and standard erythema dose.*

Jinadatha, C., Simmons, S., Dale, C., Ganachari-Mallappa, N., Villamaria, F.C., Goulding, N., Tanner, B., Stachowiak, J., Stibich, M. (2015) Disinfecting personal protective equipment with pulsed xenon ultraviolet as a risk mitigation strategy for health care workers. *Am J Infect Control* 43(4): 412–414. DOI: 10.1016/j.ajic.2015.01.013

Jordan, W.S. (1961) The Mechanism of Spread of Asian Influenza, *Am Rev Resp Dis.*

Volume 83, Issue 2P2, Pages 29–40. DOI: 10.1164/arrd.1961.83.2P2.29

Ko, G., First, M.W., Burge, H.A. (2000) Influence of relative humidity on particle size and UV sensitivity of Serratia marcescens and Mycobacterium bovis BCG aerosols. *Tubercle and Lung Disease*. Volume 80, Issues 4–5, Pages 217–228.
DOI: 10.1054/tuld.2000.0249

Mphaphlele, M. (2015) Institutional Tuberculosis Transmission. Controlled Trial of Upper Room Ultraviolet Air Disinfection: A Basis for New Dosing Guidelines*. Am J Respir Crit Care Med*. 192(4):477–84. DOI: 10.1164/rccm.201501–0060OC

Narita, K., Asano, K., Morimoto, Y., Igarashi, T., Hamblin, M.R., Dai, T. and Nakane, A. (2018) Disinfection and healing effects of 222-nm UVC light on methicillin-resistant Staphylococcus aureus infection in mouse wounds. *Journal of Photochemistry and Photobiology B: Biology* 178: 10–18. DOI: 10.1016/j.jphotobiol.2017.10.030

Nemeth, C., D. Laufersweiler, E. Polander, C. Orvis, D. Harnish, S.E. Morgan, M. O'Connor,

S. Hymes, S. Nachman and B. Heimbuch (2020). "Preparing for an Influenza Pandemic: Hospital Acceptance Study of Filtering Facepiece Respirator Decontamination Using Ultraviolet

[2] Limited free access until 2020–06–25.

Germicidal Irradiation." J Patient Saf. DOI 10.1097/PTS.0000000000000600.

Peccia, J., Werth, H.M., Miller, S., Hernandez, M. (2001) Effects of Relative Humidity on the Ultraviolet Induced Inactivation of Airborne Bacteria, *Aerosol Science and Technology*, Volume 35, Issue 3, DOI: 10.1080/02786820152546770

Piazena, H. and Häder, D.-P. (2009) Solar UV-B and UV-A irradiance in arid high-mountain regions: Measurements on the island of Tenerife as compared to previous tropical Andes data. *Journal of Geophysical Research: Biogeosciences.* 114(G4).? DOI: 10.1029/2008JG000820

Sagripanti, J.-L. and Lytle, C.D. (2011) Sensitivity to ultraviolet radiation of Lassa, vaccinia, and Ebola viruses dried on surfaces. *Archives of Virology* 156(3): 489–494.

DOI: 10.1007/s00705–010–0847–1

Taylor, W., Camilleri, E., Craft, D.L., Korza, G., Granados, M.R., Peterson, J., Szczpaniak, R., Weller, S.K., Moeller, R., Douki, T., Mok, W.W.K. and Setlow, P. (2020) DNA Damage Kills Bacterial Spores and Cells Exposed to 222-Nanometer UV Radiation. *Applied and Environmental Microbiology* 86(8): e03039–03019. DOI:10.1128/aem.03039–19

Tomas, M.E., Cadnum, J.L., Jencson, A., Donskey, C.J. (2015) The Ebola disinfection booth: evaluation of an enclosed ultraviolet light booth for disinfection of contaminated personal protective equipment prior to removal. *Infect Control Hosp Epidemiol.* 36(10): 1226–1228. DOI: 10.1017/ice.2015.166

van Doremalen, N., Bushmaker, T., Morris, D.H., Holbrook, M.G., Gamble, A., Williamson, B.N., Tamin, A., Harcourt, J.L., Thornburg, N.J., Gerber, S.I., Lloyd-Smith, J.O., de Wit, E.,

Munster, V.J. (2020) Aerosol and Surface Stability of SARS-CoV-2 as Compared with SARS- CoV-1. *N Engl J Med.* 382: 1564–1567. DOI: 10.1056/NEJMc2004973

Welch, D., Buonanno, M., Grilj, V., Shuryak, I., Crickmore, C., Bigelow, A.W., Randers- Pehrson, G., Johnson, G.W. and Brenner, D.J. (2018) Far-UVC light: A new tool to control the spread of airborne-mediated microbial diseases. *Scientific Reports* 8(1): 2752. DOI: 10.1038/s41598–018–21058-w

WHO (2019) *WHO guidelines on tuberculosis infection prevention and control*. 2019 update. Geneva: World Health Organization.

WHO (2020) https://www.who.int/emergencies/diseases/novel-coronavirus-2019/advice-for-public/myth-busters, accessed 2020–04–22.

Yamano, N., Kunisada, M., Kaidzu, S., Sugihara, K., Nishiaki-Sawada, A., Ohashi, H., Yoshioka, A., Igarashi, T., Ohira, A., Tanito, M. and Nishigori, C. (2020) Long-term effects of 222 nm ultraviolet radiation C sterilizing lamps on mice susceptible to ultraviolet radiation.

Photochemistry and Photobiology. DOI: 10.1111/php.13269

About the CIE and its Position Statements

The International Commission on Illumination – also known as the CIE from its French title, the Commission Internationale de l´Eclairage – is devoted to worldwide cooperation and the exchange of information on all matters relating to the science and art of light and lighting, colour and vision, photobiology and image technology.

With strong technical, scientific and cultural foundations, the CIE is an independent, non-profit organization that serves member countries on a voluntary basis. Since its inception in 1913, CIE has been accepted as representing the best authority on the subject and as such is recognized by ISO as an international standardization body publishing global standards on the fundamentals of light and lighting.

CIE position statements are approved by the CIE Board of Administration, which includes the Directors of all the CIE Divisions (the bodies that carry out the scientific work of the CIE), after first ensuring agreement with the relevant CIE Technical Committees.

For any further information please contact

CIE Central Bureau
Kathryn Nield, General Secretary Babenbergerstraße 9/9A, A-1010 Vienna, Austria Phone: +43 1 714 31 87
Email: kathryn.nield@cie.co.at Website: http:/www.cie.co.at

Light & Engineering
Vol. 28, No. 4, pp. 9–21, 2020
https://doi.org/10.33383/2020-36
Svetotekhnika # 2, 2020, pp. 6–15

AIR DISINFECTION BY UV GERMICIDAL RADIATION

Alexander L. Wasserman

E-mail: alexzo@list.ru; alexlvovzo@outlook.com

ABSTRACT

Since 2005, in our country, the use of UV germicidal radiation for disinfection of the indoor air environment is regulated by the guidance of R3.5.1904–64 (as the recommendations). This radiation is dangerous for humans: skin and especially the eyes are affected. It is necessary to use closed irradiators (recirculators) with germicidal lamps, and not open ones, the radiation of which covers the entire volume of the room in order to avoid exposure of people during disinfection of indoor air. This requires taking people from the premises and observing all relevant safety measures.

Unfortunately, in practice, there may occur, accidentally or out of ignorance of the rules for open irradiators operating by personnel, violations of safety rules leading to grave consequences. To eliminate such violations, it is necessary to increase the level of knowledge of staff, but there is no special educational and technical literature. This article attempts to fill this gap.

Keywords: UV germicidal radiation, spectrum of activity, germicidal effectiveness, productivity of a germicidal irradiator, surface or volume emitter, volumetric dose

FOREWORD

The first studies on the use of UV radiation (UVR) for the destruction of pathogens are the hundred years old. The study of this phenomenon belongs to science – Photobiology.

In solving the problems of applying this technology these days, three important stages can be noted:

- Development, mastering of production and manufacture of UV tube low pressure mercury lamps (LPML) with a power of 15 W and 30 W, with a bulb made of uviole glass blocking ozone-forming radiation; this work was directed by the chief engineer of the Moscow Electric Lamp Plant R.A. Nilender, an outstanding organizer of the lamp industry of the USSR. The first irradiators with these lamps were open and they could be used only in the absence of people in the room;
- Proposed by a doctor Y.E. Neystadtom irradiator with closed design, which could be used in the presence of people – the so-called recirculator [1];
- Development, mastering of production and manufacture of a new type of UV tubular ozoneless LPMLs with a capacity of up to 1000 W and above, with a quartz glass bulb and using not liquid mercury, but a solid solution of mercury in another metal – amalgam; this work was led by the Director General of NPO “LIT” S.V. Kostyuchenko [2, 3].

At present, a scientific and technical line has been formed in Russia on UV technology for air disinfection. At the same time, industrial production was organized and a wide range of germicidal lamps and irradiators has appeared. In 2012, a fundamental work of a high scientific level was published [4], edited by F.V. Karmazinova, S.V. Kostyuchenko, N.N. Kudryavtseva, S.V. Khramenkova. It should be noted the great contribution of domestic scientists to the theory and practice of using UVR for air disinfection: first of all, G.M. Franka, N.F. Galanina, N.M. Danzig, J.E. Neystadt, V.I. Vashkova, A.L. Koshkina, D.N. Lazareva, V.F. Sokolova, M.V. Sokolova, M.G. Shandalu, T.I. Noskov, G.S. Sarycheva, D.A. Shklover, R.A. Nilendera and others. The lack of appropriate technical literature

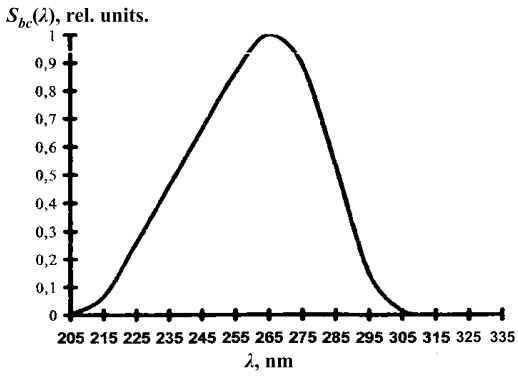

Fig. 1. Relative spectral germicidal efficacy curve $S_{bc}(\lambda)$

hinders the practical application of UV disinfection of indoor air.

When writing the article, the author used previously published materials, some of which were written in collaboration with M.G. Chandaloy and V.G. Yuzbashev [5,6].

The author hopes that this article, prepared for specialists, will improve mutual understanding in solving the practical problems of workers and manufacturers of germicidal lamps and irradiators, designers of germicidal plants, sanitary doctors who carry out epidemiological surveillance and medical students.

1. INTRODUCTION

The epidemiological well-being of the air environment, as the most important component to protecting the health of the country's population, is the socio-economic task of our state. The condition and environmental conditions of a person's living environment are essential for his normal life, especially in enclosed spaces of limited volume, the air environment of which contains pathogens. One of the ways of spreading infectious diseases is aero-genic (or airborne), which refers to the main way of transmitting the spread of diseases such as flu, tuberculosis, diphtheria, etc. This is due to the fact that the airborne droplet bacterial aerosol is constantly suspended in air volume due to air movement, which increases the likelihood of infection of people and unpacked food.

1.1. UV Radiation and its Germicidal Effect

For the prevention of diseases and the improvement of the living environment, various methods and means are used, and in particular, the use of UVR, which has a germicidal effect. The high efficiency of this method is ensured by its following features:

– A wide range of coverage of pathogenic micro-flora in air and water, as well as on surfaces;

– The absence of the need to use additional chemicals;

– Lack of smell and the formation of toxic secondary products;

– A relatively short treatment time for premises to achieve the required level of disinfection, within 1 h;

– Low costs for installation of equipment in the premises and ease of operation.

It should be emphasized that the use of UVR as a physical factor affecting microorganisms can give a disinfection of the environment to a very high degree – up to 99.9 %. In addition, the processing of indoor air using UVR is the final link in the list of sanitary and hygienic measures provided for by regulatory documents of the Federal Service for Supervision of Consumer Protection and Human Well-being.

The germicidal effect of UVR on microorganisms in the spectral range of (205–315) nm

The degree of exposure to microorganisms is determined by the function of the relative spectral germicidal efficacy $S_{bc}(\lambda)$. Its maximum occurs at a wavelength of 265 nm, corresponding to the maximum sensitivity of microorganisms (their nucleic acids), as shown in Fig. 1 and Table 1[1]. This function is also called the relative germicidal spectrum of UVR, i.e. microorganisms are *selective receivers of radiation,* and applying energy quantities to them is impractical. From the Table 1 it can be seen that $S_{bc}(\lambda)$ in the mercury line of 254 nm is 85 % of $S_{bc}(\lambda)$ in the line of 265 nm. Taking into account the indicated selectivity of microorganisms, germicidal radiometers are used to measure the germicidal flux, whose spectral sensitivity is corrected for $S_{bc}(\lambda)$. Such germicidal radiometers exist, for example, the TKA-PKM UV radiometer (models 12 and 13), the TKA-VD UV spectroradiometer, etc. These radiometers measure germicidal irradiation (W/m^2) from solid or linear UV radiation spectrum sources. The main germicidal value is the

[1] It is important to note that germicidal UVR is dangerous for humans. It is fraught with burns on the body and eye damage. Therefore, in rooms in the presence of people, it is permissible to use only closed irradiators with germicidal lamps.

Table 1. Relative Spectral Germicidal Efficacy Function S_{bc} (λ)
[S_{bc} (λ) max = 1 at λ = 265 nm]

λ, nm	S_{bc} (λ)	λ, nm	S_{bc} (λ)
205	0,000	265	1
210	0.009	270	0.98
215	0,066	275	0,900
220	0.160	280	0.760
225	0.260	285	0.540
230	0.360	290	0.330
235	0.460	295	0.150
240	0.560	300	0,030
245	0.660	305	0.006
250	0, 765	310	0.001
254	0.850	315	0,000

Table 2. Germicidal Quantities and Units of Measurement of UV Radiation in the Spectral Range (205–315) nm

Value	Designation and formula	Definition	Unit of measurement
Radiation energy	W_{bc}	Energy carried by radiation	J
Radiation flux (radiation power)	$\Phi_{bc} = W_{bc}/t$	The ratio of radiation energy to the time t	W
Spectral density of the radiation flux	$\Phi_{bc}(\lambda)$	The ratio of the radiation flux in an infinitely narrow range of wavelengths to this interval	W/nm
Intensity of rdiation	I_{bc}	Spatial flux density	W/sr
Irradiation	$E_{bc} = \Phi_{bc}/S$	The ratio of the radiation flux to the irradiated surface area	W/m^2
Surface dose	$H_s = W_{bc}/S$	he ratio of radiation energy to the area of the irradiated surface	J/m^2
Volumetric dose	$H_v = W_{bc}/V$	The ratio of radiation energy to the volume of the irradiated part of space	J/m^3

germicidal flux F_{bc}. With this in mind, a system of germicidal quantities and units of measure has been created, which is used in the UV technology for air disinfection (Table 2). Considering the process of killing bacteria on the surface with germicidal irradiation E_s (W/m^3) and, accordingly, the necessary radiation dose H_s (J/m^2), we can conclude that the estimations of the effective dose of volumetric exposure to air space H_v (J/m^3) cannot be produced by the formulas according to which H_s are calculated.

It was established that the type of S_{bc} (λ) curves for different types of pathogenic microorganisms is almost the same.

Bacteria (in the vegetative form) and viruses are more sensitive to UV radiation. Spores of bacteria and protozoa are less sensitive. The most resistant are mushrooms and moulds.

The absorption of radiation by a microorganism is an intra-molecular discrete physical process of interaction between radiation quanta, molecules and atoms according to the Einstein-Stark quantum equivalence law. As follows from this law, each absorbed quantum is capable of activating only one molecule or atom, i.e. a single shock absorption process occurs. Upon absorption of a quantum of radiation, in the case of a coincidence of the frequency of oscillations of a quantum with the frequency of oscillations of electrons in a macromolecule, resonant absorption occurs with the maximum transfer of quantum energy. This leads to damage to important

Table 3. The Dependence of Germicidal Efficacy and Volumetric Dose on the Cleanliness Class

Room cleanliness class	J_{bc}, %	H_v, J/m^3
Extra Clean (A)	99.9	385
Clean (B)	99	257
Conditionally clean (B)	95	167
Dirty (g)	90	129

structures of the microorganism. Ultimately, microorganisms in the air volume become inactivated and lose their ability to reproduce. The maximum radiation effect occurs at λ = 265 nm, which corresponds to the maximum spectral sensitivity of the nucleic acids of microorganisms. Moreover, the quanta of the germicidal UVR are not sufficiently energetic for ionization of oxygen molecules, i.e. when a neutral molecule absorbs oxygen of one quantum, the molecule does not decay into a negative electron and a positive ion, and, therefore, ozone is not formed in the air. In this regard, germicidal UVR is classified as non-ionizing radiation.

Further, in the case of germicidal irradiation of the air, while maintaining a constant dose level of H_v and a short exposure time, an increase in the volume density of the germicidal radiation flux (W/m^3) is required due to the need to increase the number of quanta, which increases the likelihood of a successful collision of a quantum of germicidal radiation with atoms of macromolecules. A decrease in bulk radiation density reduces the likelihood of a successful collision; to compensate for this, it is necessary to increase the exposure time, while maintaining H_v, i.e. quantum equivalence is respected. It was experimentally established that the process of death of microorganisms in the air during their germicidal irradiation is characterized by an exponential relationship between the number of surviving microorganisms N_{sur} at their initial number N_o and H_v:

$$N_{sur} = N_0 \cdot \exp(-\sigma_v H_v), \qquad (1)$$

where σ_v is the constant characterizing the photosensitivity value of a given type of microorganism under volume exposure. To control the germicidal efficacy J_{bc}, the *Staphyloccous Aureus* microorganism was adopted in our country, the σ_v value of which is equal to 0.0179 m^3 /J (Appendix 1).

J_{bc} is the indicator of the level of reduction of microbial contamination of the air environment as a result of UV radiation, expressed as the ratio of the number of dead microorganisms N_d to N_o (in relative units or in percentage). From the equality $N_d = N_o - N_{sur}$ and expression (1) it follows that:

$$J_{bc} = (N_d / N_0) \cdot 100 = [(1 - \exp(-\sigma_v H_v)] \cdot 100, \%$$

$$H_v = -\ln(1 - J_{bc} \cdot 10^{-2}) / \sigma_v, \text{ J/m}^3. \qquad (2)$$

The recommended modes of exposure to air in dependence on the room class cleanliness are shown in the Table. 3

An increase in relative humidity and dustiness in the room reduces J_{bc}. With an increase in relative humidity from (45–65) % to (80–90) %, J_{bc} decreases by (30–40) %, because drops of water settle on dust particles, which have a screening effect on radiation. It was established that the sensitivity of microorganisms to UVR in moist air is (20–50) times lower than in dry air.

It should be noted that if the UVR contains spectral lines at λ shorter than 200 nm, then ozone[2] is formed in the air of the room, extremely poisonous gas (more toxic than carbon monoxide). According to toxic properties, it belongs to the first hazard class. In the Table 4, the effects caused by the presence of ozone in the indoor air are shown.

2. SOURCES OF GERMICIDAL UV RADIATION

The main sources of germicidal UVR are mercury tube lamps, of which LP mercury lamps are most effective. This is due to the fact that more than 60 %

[2] Ozone is an allotropic modification of oxygen and consists of three of its atoms. At low temperatures, the decomposition of ozone occurs slowly, with increasing temperature it accelerates; at room temperature, the decomposition takes several minutes, and at 100° C it is less than a second. The decay rate of ozone also depends on the relative humidity of the air, at 50 % ozone decays twice as slow as at 80 %.

of the radiation energy of these lamps falls on the resonance line 254 nm, lying in the range of maximum germicidal action, which explains their high germicidal efficacy $\eta_{bc,}$ defined as $\eta_{bc} = (\Phi_{bq} / P_l) \times$ ×100, %, where P_l is the lamp power, and equal about (30–40) %.

According to the main structural features, LP mercury lamps are divided into two groups – lamps with an uviol lamp bulb and bulb made of quartz glass doped with titanium oxide. These bulbs exclude the output of the 185 nm ozone-forming line in the emission spectrum. On this basis, they received the name of the ozone-less. In uviol bulb lamps, mercury is in a liquid state, and in quartz lamps it is replaced by an amalgam. When the lamp is operating, the amalgam heats up and mercury vapours are released into the discharge. On this basis, such lamps are called amalgam. The vapour pressure of mercury over a solid amalgam is orders of magnitude lower than over liquid mercury, therefore, when the bulbs of such lamps are destroyed, mercury vapour in quantities significantly lower than the MPC can enter the air, and there is no need for room demercurization. Amalgam lamps are mechanically stronger than uviol lamps. The latter have a small unit power in the range of (8–75) W, and amalgam ones have a large one, about (100–1000) W. In most uviol lamps, the electrical characteristics at the same power are identical to those of ordinary FLs, so they are operated with similar switching circuits (currently, in most cases, electronic ballasts with a power factor (cos φ) equal to one are used). The useful lifetime decline when Φ_{bc} to 20 % of the initial amounts of amalgam lamps for 12000 h, and for uviol lamp bulb about 8000 h. There are several key parameters describing the technical and operational characteristics of different radiation sources. These include: relative or absolute emission spectra; integral values of germicidal flux or radiation power in a certain spectral range; radiation intensity distribution curves in the longitudinal and transverse planes; power, current and voltage on the lamp; mains voltage; useful life; environmental safety – availability in the radiation spectrum of ozone-forming lines and the possibility of release of toxic substances into the environment during the destruction of a lamp bulb.

In view of the indicatrix of radiation, tubular discharge lamps are divided into two types – with and without coating the bulb. On this basis, the former belong to surface emitters, and the latter to volume

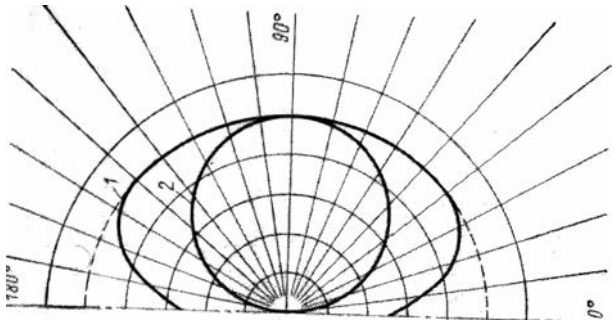

Fig. 2. Indicatrixes of radiation of discharge tube lamps in the longitudinal plane (surface emitter – fluorescent lamp, volume emitter – LP mercury tube lamp)

emitters. For surface emitters, the indicatrix of radiation in the longitudinal plane has a circle, and for bulk emitters – an ellipse (Fig. 2). (Indicators of some other discharge lamps are given in Appendix 2.)

The reason for the difference in the shapes of the radiation indicatrix between the two indicated types of lamps is that in the first type the discharge is not transparent to its own radiation, and in the second it is transparent (due to weak absorption of radiation in the discharge). Plasma is almost completely transparent to visible and UV radiation and the level of its radiation outwardly proportional to the volume occupied by the plasma. This does not depend on the type of discharge in the LP and HP mercury vapour, or in other gases [7, 8].

In this regard, I proposed and published [9] a method for measuring the radiation flux of germicidal mercury tube lamps LP that is an alternative, in particular, to the goniophotometric method [10], which is really unsuitable for routine laboratory measurements. The method is based on three working hypotheses, confirmed experimentally:

– The shape of the radiation indicatrix of tubular mercury lamps without coating the bulb in the longitudinal plane is fairly accurately described by an ellipse;

– The photometric body of such lamps is an ellipsoidal torus;

– The plasma of the electric discharge of LP germicidal lamps is transparent to visible and UV radiation.

3. UV GERMICIDAL IRRADIATORS

The UV germicidal irradiator is an autonomous electrical device containing germicidal lamps (uviol or amalgam), a reflector, ballasts, capacitors (for

Table 4. Effects Due to Ozone

The concentration of ozone, mg /m^3	Exposure time, h	Effect
0,03	8	Plant damage
0.2	1	Irritability, headache
0.3	8	Airway cramps, chest cough
2	2	Nausea, nosebleed, poisoning

Table 5. Some Materials Reflection Coefficients at Wavelength 254 nm

Material type	Reflection coefficient, p
Untreated aluminium	0.4–0.6
Aluminium (surface finish)	0.6–0.9
Duralumin	0.16
Stainless steel	0.25
Chrome plating	0.39
Black enamel	0.05

suppressing radio interference), an electronic meter that records the operating hours of the lamps, as well as auxiliary lamp mounts and fixtures for installing the device. The main objective of the germicidal irradiator is the disinfection of the indoor air from pathogenic microorganisms.

According to their design, the irradiators are divided into the following types: closed (recirculators) and open for to set at floor, wall and ceiling; for placement in rooms or in modules of supply and exhaust ventilation systems. In open irradiators, a direct germicidal flow of lamps, with or without a reflector, covers a wide area in space. In closed irradiators, the germicidal flow of lamps located in a small chamber does not have an outlet to the outside, and air is disinfected during its continuous pumping by means of a fan through the chamber and exit into the room volume. Modules with germicidal lamps located in the supply and exhaust ventilation systems can also be classified as closed irradiators.

On application is the disinfection of air in the absence of people.

According to the efficiency of using the germicidal flux of lamps, taken into account by the total coefficient $\boldsymbol{Z = K_\phi K_o}$, where $\boldsymbol{K_\phi}$ is the coefficient of use of the germicidal flux of lamps, taking into account their mutual shielding, the values of which for open, ceiling open and closed irradiators are approximately equal to 0.8, 0.6 and 0.4; $\boldsymbol{K_o}$ is the coefficient of multiple reflections of the germicidal flow from the inner surface of the reflector with a reflection coefficient ρ at λ = 254 nm, determined for open, ceiling open and closed irradiators as

$\boldsymbol{K_o}$ = 1, $\boldsymbol{K_o}$ =1 / (1–0.3 ρ) and $\boldsymbol{K_o}$ = 1 / (1–0.6 ρ), respectively.

The values of this ρ for some materials are shown in Table. 5.

The main parameter of the irradiator is its germicidal productivity $\mathrm{Pr_{bc}}$ (m^3/h), which characterizes the reduction of microbial contamination of the air medium to the given levels of J_{bc} or H_v for this type of microorganism.

The equations of the mathematical model Pr_{bc} are as follows:

$$\mathrm{Pr}_{bc} = N_l \Phi_{bc} K_\Phi K_0 \cdot 3600 / [-\ln(1 - J_{bc} \cdot 10^{-2})], \text{ or}$$

$$\mathrm{Pr}_{bc} = N_l \Phi_{bc} K_\Phi K_0 \cdot 3600 / H_v, \text{ m}^3\text{/h},$$

where N_l is the number of lamps in the irradiator; Φ_{bc} is the germicidal lamp flux, W.

It should be noted that these formulas are valid when the irradiator operates for a time t during which a given level of J_{bq} is achieved in a room of volume $V_p = \mathrm{Pr}_{bc} \cdot t$, m^3.

Constructive internal elements of a closed irradiator provide a certain resistance to air flow. The degree of hydraulic resistance is taken into account by the total coefficient of local resistance μ, the estimated value of which is in interval of 1.1–1.3. Moreover, the fan performance $\mathrm{Pr_{fan}} = \mu\ \mathrm{Pr_{bc}}$. Pho-

Table 6.1

Initial data	Values
Type of microorganism (SPM)	S aureus
Germicidal efficacy J_{bc}	99.9 %
Microorganism photosensitivity constant σ **v**	0.0179 m^3/J
Type of germicidal lamp	Amalgams
Germicidal lamp flux Φ_{bc}	50 W
Number of lamps N_l	1
The utilization rate of the germicidal lamp flux K_f	0.4
Reflector material	Polished aluminium
Reflectance ρ	0.7
Multiple reflection coefficient K_0 =1/(1–0.6 ρ)	1.72
Coefficient of local resistance to air flow from the fan μ	1,2

Table 6.2

Initial data	Values
Type of microorganism (SPM)	S aureus
Germicidal efficacy J_{bc}	99.9 %
Microorganism photosensitivity constant σ_v	0.0179 m^3/J
Type of germicidal lamp	Amalgams
Germicidal lamp flux Φ_{bc}	50 W
Number of lamps N_l	1
The utilization rate of the germicidal lamp flux K_f	0.6
Reflector material	Polished aluminium
Reflector reflectance ρ	0.7
Multiple reflection coefficient K_0 =1/(1–0.6 ρ)	1,265
Microorganism photosensitivity constant σ_v	0.0179 m 3 / J
Number of lamps N_l	1
The utilization rate of the germicidal lamp flux K_f	0.6

tographs of different types of irradiators are given in Appendix 3.

4. UV GERMICIDAL INSTALLATIONS

UV germicidal installation is a stationary group of indoor UV germicidal irradiators in the room or modules with germicidal lamps in the duct system of the supply and exhaust ventilation, which provide the specified level of the J_{bc} in the room. There are various methods for using irradiators in germicidal plants:

• ***Continuous disinfection of indoor air in the presence of people***

This mode is achieved using closed stationary irradiators (recirculators) or germicidal modules in the supply and exhaust ventilation systems. Such an irradiation regime is recommended to be used to ensure the effective disinfection of rooms with a large number of people, especially if they cannot be moved, for example, in wards with infectious patients, in schools, preschools, etc.

The number of irradiators in the room is determined by the project, according to the terms of technical task (TT). In TT are indicated: J_{bc}, V_p, air exchange rate K_p (h^{-1}), reliability factor K_r = 1.2. Then, the required germicidal performance of the recirculator in the room is determined: $Pr_{bc} = V_p K_p K_r$, with J_{bc} = 99.9 %, H_v = 385 J/m^3 and irradiation time t = 1 h.

For rooms of non-infectious profile, the operating time of the recirculators should be at least

Table 6.3

Initial data	Values
Type of microorganism (SPM)	S aureus
Germicidal efficacy J_{bc}	99.9 %
Microorganism photosensitivity constant σ_v	0.0179 m^3/J
Session exposure time t	0.25 h
Type of germicidal lamp	amalgams
Germicidal lamp stream Φ_{bc}	50 W
Number of lamps N_l	1
The utilization rate of the germicidal lamp flux K_f	0.8
Coefficient of multiple reflections K_0 =1/(1–0.6 ρ)	1

Table 6.4

Initial data	Values
The volume of the premises V_p	400 m^3
Germicidal efficacy J_{bc}	95 %
Air exchange rate K_p	2 h^{-1}
Reliability coefficient K_r	1,2

Table 6.5

Initial data	Values
The volume of the premises V_p	400 m^3
Germicidal efficacy J_{bc}	99.9 %
Session exposure time t	0.25 h
Reliability coefficient K_r	1,2

12 hours. For rooms with infectious patients, the working time of the recirculators should be around the clock. For offices with an infection profile, it is necessary to turn on the recirculator before starting to receive patients for a period of (15–20) minutes. Moreover, J_{bc} should be at least 99 %. For this, the recirculator operating mode is selected for various values of K_r and t <60 min, the doses are estimated by the formula (2).

• ***Intermittent exposure***

In this mode, the irradiation of the room is carried out during the working day with alternating sessions of irradiation at t = 15 min = 0.25 h and pauses between sessions of 3 h by the help of ceiling stationary open irradiators. During a 15-minute exposure session, people are removed from the room. During this time, it is necessary to provide a given level of J_{bc}.

The number of irradiators in the room is determined according to the data in the statement of work, which indicates: $V_{p,}$ J_{bc}, K_p and K_r = 1.2. Then, the required germicidal performance of the irradiator in the room, Pr_{bc}, is determined by the formula $Pr_{bc} = V_p K_p K_r$. From the existing nomenclature irradiator with the same Pr_{bc} or less, Pr_n, is selected but, however, with the predetermined value J_{bc}. Next, the number of indoor irradiators $N_{ir} = Pr_{bc} / Pr_{n.}$ At the same time, the number of irradiators, productivity and dose are proportional to K_p. It should be noted that with an increase in K_p, the costs of a germicidal installation are increasing.

For a long time open irradiators were used to disinfect the indoor air environment. Their use in most cases complicates this procedure due to the need to periodically remove people from the premises. It should be noted that the presence of people in the room between the irradiation sessions leads to secondary contamination by the aero-genic microorganisms of the air in the room due to people carrying infections. This increases the level of nosocomial infections. In addition, between the irradiation sessions, the so-called photo-reactivation of dead microorganisms occurs under the influence of

Table 6.6

Initial data	Values
The volume of the premises V_p	400 m^3
Germicidal efficacy J_{bc}	99.9 %
Air exchange rate K_p	2 h^{-1}
Reliability coefficient K_r	1,2
Coefficient of local resistance to air flow from the fan μ	1,2

Table 6.7

t, min	K_p, h^{-1}	H_v, J/m^3	J_{bc},%	Pr_{bc}, m^3/h
60	1	385	99.9	54
15	1	96.25	81.73	54
20	1	128.3	89.4	54
30	1	192.5	96.8	54
20	2	256.6	99	108
60	2	385	99.9	108

visible light, i.e. restoration of their life. From this we can conclude that such an irradiation regime is ineffective for disinfecting rooms with a large number of people, especially if they cannot be moved. And this mode is not recommended.

In some cases of repeated-short-term exposure, for small rooms, you can use the single mobile open irradiators. The required germicidal performance of such an irradiator $Pr_{bc} = V_p K_r / t$, m^3 /h.

• ***Combined exposure mode***

This mode provides for the use of both open and closed irradiators in operating rooms, blood transfusion rooms and dressing rooms. The irradiators turn on simultaneously before preparing the room for 15 minutes. Then the open irradiators are turned off.

5. TYPICAL EXAMPLES OF CALCULATIONS

The first example: It is necessary to calculate Pr_{bc} of a closed feed and fan performance

The Table 6.1 contains the initial data for the calculation. According to them, Pr_{bc} and Pr_v are defined as

$Pr_{bc} = N_l \cdot \Phi_{bc} \cdot K_\Phi \cdot K_0 \cdot \sigma_v \cdot 3600 / [-\ln (1 - J_{bc} \cdot 10^{-2})] = 1 \cdot 50 \cdot 0.4 \cdot 1.72 \cdot 0.0179 \cdot 3600 / -\ln (1-99.9 \cdot 10^{-2}) = 321$ m^3 / h; $Pr_v = Pr_{bc} \cdot \mu = 321 \cdot 1.2 = 385$ m^3 /h.

The second example: It is necessary to calculate Pr_{bc} of a ceiling open illuminator.

The Table 6.2 contains the initial data for the calculation. According to them, Pr_{bc} is defined as $Pr_{bc} = N_l \cdot \Phi_{bc} \cdot K_\Phi \cdot K_0 \cdot \sigma_v \cdot 3600 / [-\ln (1 - J_{bc} \cdot 10^{-2})] = 1 \cdot 50 \cdot 0.6 \cdot 1.265 \cdot 0,0179 \cdot 3600 / [-\ln (1-99.9 \cdot 10^{-2})] = 351$ m^3 /h.

The third example: It is required to determine Pr_{bc} of a mobile open irradiator at $t = 0.25$ hours.

In the Table 6.3 are input data for the calculation. According to them, Pr_{bc} is calculated according to the previous formula: $1 \cdot 50 \cdot 0.8 \cdot 0.0179 \cdot 3600 / [-\ln (1-99.9 \cdot 10^{-2})] = 373$ m^3/h. The final value of Pr_{bc} for irradiation duration $t = 0.25$ h is $373 \cdot 0.25 = 93.25$ m^3/h.

The fourth example: It is necessary to ensure the disinfection of the air environment of the room with closed irradiators. According to the initial data given in the Table 6.4, the required germicidal performance of the irradiator Pr_{bc} with $J_{bc} = 95$ % is determined: $Pr_{bc} = V_p \cdot K_p \cdot K_r = 400 \cdot 2 \cdot 1.2 = 960$ m^3/h. There is no such irradiator on sale, but there is the DEZAR brand irradiator with a $Pr_v = 100$ m^3/h and $J_{bc} = 99.9$ %. A new operating mode of the selected irradiator is determined at $J_{bc} = 95$ % according to the formula $Pr_r = Pr_v \cdot [-\ln (1-0.999)] / [(-\ln (1-0.95))] = 100 \cdot 6.9/3 = 230$ m^3/h. Consequently, the number of indoor irradiators $N_{ir} = Pr_{bc} / Pr_r = 960/230 \approx 4$, and their location in the room determined by the design documentation.

The fifth example: It is required to ensure the disinfection of the air of the room with open ceiling irradiators. According to the initial data given in the Table 6.5, the required Pr_{bc} with $J_{bc} = 99.9$ % is determining for the irradiation time $t = 0.25$ h as $Pr_{bc} = V_p \cdot K_r / t = 400 \cdot 1.2 / 0.25 = 1920$ m^3/h with

J_{bc} = 99.9 %. There is no such irradiator on sale, but there is another one with Pr_v = 1500 m^3/h and J_{bc} = 99.9 %. A new operating mode of the selected irradiator is determined at t = 0.25 h: $Pr_r = Pr_v \cdot t$ =1500 · 0.25 = 375 m^3/h. Consequently, $N_l = Pr_{bc} / Pr_r$ = 1920/375 ≈ 5 and irradiators location in the room determined by the design documentation.

The sixth example: The germicidal performance of the module Pr_m in the supply and exhaust ventilation system in the room should be determined. The initial data are given in the Table 6.6. According to them, the fan performance is determined as $Pr_v = V_p \cdot K_r \cdot K_p$ = 400 · 2 · 1.2 = 960 m^3 /h, and then the required value of Pr_m according to the formula $Pr_m = Pr_v / \mu$= 960 /1.2 = 800 m^3 / h with germicidal efficacy of 99.9 % is determining.

The seventh example: It is required to determine Pr_{bc} of the recirculator in the office of the infectious profile for a working time of (15–20) minutes, before the start of patient reception. J_{bc} must be at least 99 %. Initial data: V_p = 45 m^3, K_p = 1 h^{-1}, K_r = 1.2. A recirculator with $Pr_{bc} = V_p \cdot K_r \cdot K_p \cdot t$ = 45 · 1 · 1.2 · 1 = 54 m^3/h and J_{bc} = 9.99 % during operation t = 1 h. Then a new operating mode of the recirculator is determined; it is calculated, for different values of K_p and t (60 min), according to the formulas $J_{bc} = [1 - \exp(-\sigma_v \cdot H_v)] \cdot 100$,%, where $H_v = 385 \cdot K_p \cdot t / 60$, J/m^3, and the calculation results are entered in the Table. 6.7.

6. OPERATION AND SAFETY

1. The implementation of germicidal plants should be carried out according to the agreed technical task and the project approved by the services of the Federal Service for Supervision of Consumer Rights Protection and Human Welfare

2. To carry out air disinfection in the presence of people, the required number of irradiators for each room is determined by calculation in accordance with applicable standards (SanPin 2.1.3.2630–10 requirement, clause 11.12).

3. UVR in the germicidal wavelength range is a danger to humans, especially to vision.

4. If it is necessary to find personnel in a room where operating open UV germicidal irradiators are installed or a germicidal flux of UV lamps is measured, face masks, glasses and gloves should be used.

5. Do not use ozonating UV lamps to disinfect the air in the room where people are located. Residual ozone decomposes at room temperature after (30–60) minutes. The appearance of the smell of ozone can serve as an indicator of danger to humans. If it is detected that the concentration of ozone in the room exceeds the permissible norm, the irradiator should be stopped and ozonizing lamps should be detected.

6. When the bulb of mercury lamps is destroyed, mercury vapours can enter the air in quantities significantly higher than the permissible norms, which in the case of uviol lamps requires demercurization of the room, and in the case of amalgam lamps, it needs to be ventilated.

7. The supply and disconnection of the power of open irradiators from the mains must be carried out using switches located outdoors at the front door, which are interlocked with a light panel above the door: “Do not enter! Dangerously! Ultraviolet disinfection is in progress. “

8. Germicidal lamps that have reached their useful life must be stored in a separate room until they are disposed of in accordance with current regulations.

9. It is necessary to periodically clean the reflecting surfaces of the irradiators and the lamp bulb from dust, since even a small layer of dust significantly reduces the value of the germicidal flow. Dust wiping and lamp replacement should be carried out monthly, strictly when the germicidal installation is disconnected from the network.

APPENDICES

Appendix 1: Tab. A.1.
Appendix 2: Fig. A.1 and Tab. A.2.
Appendix 3: Figs. A.2 – A.4.

REFERENCES

1. Neustadt YA.E. Germicidal UV radiation. M .: Medgiz, 1956, 120 p.

2. Kostyuchenko S.V., Krasnochub A.B., Kudryavtsev N.N. A new generation of germicidal irradiators for disinfecting air and water based on highly efficient amalgam lamps // Svetotekhnika, 2004, # 4, pp. 15–19.

3. Vasiliev A.I., Krasnochub A.B., Kuzmenko M.E., Petrenko Yu, Pecherkin A.Y. Analysis of modern industrial sources of germicidal UV radiation // Svetotekhnika, 2004, # 6, pp. 42–45.

Table A.1.Photosensitivity constants for some species microorganisms during surface irradiation (σ_s, m^2 /J) and air volume(σ_v, m^3/J)

Bacteria	σ_s	σ_v	Fungal yeast	σ	σ_v
Bacillus anthracis	0.051	0.0195	*Baker's yeast*	0,060	–
Bacillus megatherium (veg)	0,084	0,034	*Brewer's yeast*	0,070	–
Bacillus megatherium (spores)	0.178	0,0743	Yeast-like mushrooms	0,038	–
Bacillus paratyphosus	0,072	0,0274	*Saccharomyces cerevisiae*	0,038	–
Bacillus subtilis (veg)	0,032	0.0123	*Saccharomyces ellipsoideus*	0,038	–
Bacillus subtilis (spores)	0.019	0.0073	*Saccharomyces sp.*	0,029	–
Campylobacter jejuni	0.209	0,0768	**Mold spores**		
Clostndium tetani	0.019	0.0073			
Corynebacterium diphtheriae	0,069	0,026			
Bacilli dysentery	0.105	0,040	*Aspergillus flavus*	0.003	–
Eberthella typhosa	0.108	0,041	*Aspergillus glaucus*	0.004	–
Escherichia coli	0,077	0,029	*Aspergillus niger*	0.0014	–
Klebsiella terrifani	0,089	0,034	*Mucor racemosus*	0.013	–
Micrococcus candidus	0,038	0.015	*Oospora lactis*	0,046	–
Phytomonas tumefaciens	0,023	0.0088	*Penicillium expansum*	0.018	–
Mycobacterium tuberculosis	0,038	0.015	*Penicillium roqueforti*	0.018	–
Micrococcus sphaeroides	0,053	0,020	**Viruses**		
Pseudomonas aeruginosa	0,042	0.014			
Pseudomonas fluorescens	0,065	0,025			
Proteus vulgaris	0,086	0,035	Hepatitis A	0,032	0.011
Salmonella enteritidis	0.058	0,022	Flu virus	0,064	0.024
Salmonella paratyphi	0,072	0,068	*MS-2 Coliphage*	0.012	0.0045
Salmonella typhimurium	0,029	0.011	Poliovirus	0,040	0.015
Sarcina lutea	0.012	0.0045	Rotavirus	0,028	0.0107
Seratia marcescens	0,095	0,037	**Protozoa**		
Shigella paradysenteriae	0.141	0.051			
Shigella sonnei	0,077	0,029			
Staphylococcus aureus	0.10	0.0179	Cryptosporidium parvum	0,092	0,035
Staphylococcus faecalis	0,053	0,020	Giardia lamblia	0.209	0,0768
Staphylococcus haemolyticus	0.106	0,042	**Seaweed**		
Streptococcus lactus	0,037	0.014			
Streptococcus viridans	0,043	0.115			
Vibrio Cholera (*V.comma)*	0,066	0,025	Chlorella vulgaris	0.019	–

Table A.2. High Intensity Amalgam Lamps

Lamp type	Lamp power, W	Germicidal flux, W	Arc length, mm	Full length mm
ALC100/32	100	23	320	470
ALC120/45	120	thirty	445	595
ALC170/70	170	fifty	695	845
ALC215/95	215	65	945	1095
ALC240/107	240	75	1070	1220

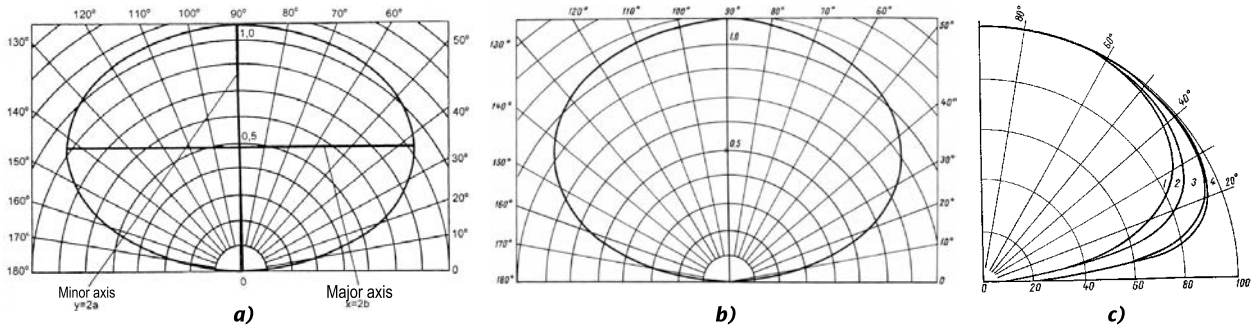

Fig. A.1. Radiation indicatrixes in the longitudinal plane of the discharge tube lamps – volume emitters:
a – mercury lamp HP type DRRT-400; *b* – xenon pulsed tube lamp ISPT 6000;
c – tubular xenon lamps: water-cooled – DKsTV 15000 (*1)* and DKsTV 6000 (*2)*;
air-cooled – DKst 5000 (*3)* and DKst 1000 (*4)*

4. Ultraviolet technology in the modern world: a collective monograph, ed. F.V. Karmazinova et al. Dolgoprudny: Intellect Publishing House, 2012, 392 p.

5. Wasserman A.L. Shandala M.G., Yuzbashev V.G. UV radiation in the prevention of infectious diseases. Moscow: Medicine, 2003, 204 p.

6. Wasserman A.L. Yuzbashev V.G. A mathematical model for calculating the productivity of UV germicidal recirculator // Svetotekhnika, 2015, # 6, pp. 38–39.

7. Artsimovich LA. Elementary plasma physics/ Moscow: Gosatomizdat, 1963, 98 p.

8. Rokhlin G.N. Gas discharge light sources/ Moscow-Leningrad: Energy, 1966, 560 p.

9. Wasserman A.L. Measurement of the germicidal flux of UV mercury lamps of low pressure // Svetotekhnika, 2019, # 1, pp. 69–72.

10. Reference book on lighting. 4th ed., Rev. and add. / Under the total. ed. Yu.B. Eisenberg and G.V. Boos. Mjscow: 2019, 892 p.

THE LIST OF REGULATORY DOCUMENTS

I. GOST R15013 “System for the development and putting products into production. Medical Products. “

Fig. A. 2. Appearance of industrial samples of germicidal closed irradiators (recirculators):
a) “ Stery box “ (*TissiMedica*, USA), productivity (20–50) m^3/h, 5 mercury lamps LP 25 W power each, 500×150×600 mm, 25 kg; *b)* “Dezar-5” (KRONT, RF), productivity 100 m^3/h, 5 mercury lamps LP 15 W power each, 890×150×145 mm, 7.2 kg; *c)* “AEROLIT-200” (NPO “LIT”, RF), productivity 200 m^3/h, 1 amalgam lamp 170 W power, 1100×285×150 mm, 15 kg

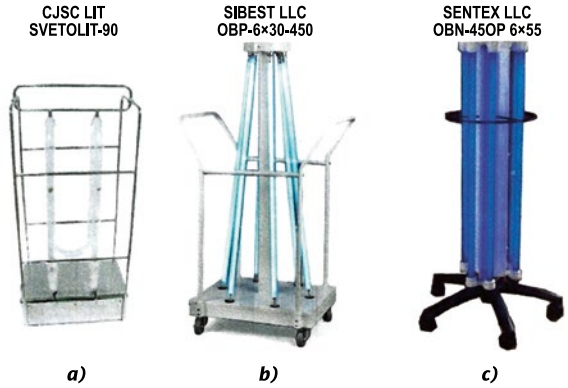

Fig. A.3. Appearance of industrial samples of germicidal open irradiators:
a) SVETOLIT-90 (NPO LIT, RF); *b)* OBP-6×30–450 (SibEST LLC, RF); *c)* OBN-450P 6×55 (LLC TsS SENTEH LLC, RF)

Fig. A.4. Module with germicidal lamps “MEGALIT-6” (NPO “LIT”, RF), which is built into the supply and exhaust ventilation system

II. SanPiN2.1.3.2630–10 “Sanitary and epidemic rules and regulations.”

III. P3.5.1904–04 “ Management. Using UV germicidal radiation to disinfect indoor air. “

IV. SN No. 4557–88 “Sanitary norms of UV – radiation in industrial premises”.

V. Methodological recommendations for monitoring the organization of the current and final demercurization and evaluating its effectiveness No. 4545–87.

VI. Guidelines for the design and operation of ultraviolet germicidal plants for the disinfection of the air in the premises of meat and dairy industry enterprises. Developed by Gipromyasomolprom Institute CJSC

VII. Guide MU2.3.975–10 “The use of UV germicidal radiation for disinfection of the air environment in the premises of organizations of the food industry, public catering and food trade”.

Manufacturers of Germicidal Lamps, Irradiators and UV Radiometers in Russia:

– LLC “NIIIS them. LN Lodygina “, Saransk – Germicidal lamps;

– NPO LIT Moscow – Germicidal lamps and irradiators;

– CJSC KRONT, Moscow – Germicidal irradiators;

– NTP TKA LLC, St. Petersburg, VNIIOFI, Moscow – Radiometers.

Alexander L. Wasserman, Ph.D.
He graduated in 1957 from the electro-physical faculty of VZEI (MPEI TU at present). Alexander Wasserman is the honoured machine builder of the Russian Federation, an invalid of the Great Patriotic War, an oldest scientist of the Russian lighting community

Light & Engineering
Vol. 28, No. 4, pp. 22–26, 2020

https://doi.org/10.33383/2020-010
Svetotekhnika # 3, 2020, pp. 60–63

ON METHODOLOGY FOR DESIGNING ARCHITECTURAL LIGHTING OF PRODUCTION SITE INTERIOR PART III. RESULTS AND CONCLUSIONS

Vladimir V. Voronov and Nikolay I. Shchepetkov

Moscow Institute of Architecture (MARHI, State Academy), Moscow
E-mail: n_shchepetkov@inbox.ru

ABSTRACT

This is the final, third part, on the presentation of Chapter 4 and the results of the Vladimir Voronov thesis [1], successfully defended at the Moscow Architectural Institute in 1985 and devoted to the author's method of designing architectural lighting for industrial interiors with three main upper lantern types of natural daylight and artificial lighting.

The method was developed on the basis of long-term analytical calculations and numerous experiments conducted according to all the laws of statistics in natural conditions and in the camera "Mirror-type artificial sky" created by the author using planar and volumetric (on mock-ups) light modelling with careful measurement of lighting parameters characterizing various states, qualities and options for luminance composition, light saturation of the interior space, contrast of lighting, etc.

The conclusions of the dissertation give a general picture of the research work performed, the main meaning of which is the belief that the design of lighting in industrial (and in any other) interiors is not limited to providing elementary normalized lighting parameters, but is a complex, sophisticated, and creative task of architectural design where the light – natural and artificial – is the main "actor", providing functional and aesthetic qualities to the interior.

Keywords: design method, architectural lighting, industrial interior, luminous image, luminance and luminosity similarity

The dissertation established that the solution to the urgent problem of designing architectural lighting for the interior, achieving a certain visual correspondence of the luminous image in a project that was carried out graphically manually in the recent past and in kind, can be achieved on the basis of the pattern of luminance similarity obtained in the course of experimental studies based on luminosity similarity. Although even today, with the availability and improvement of the digital computer calculation methodology and the visualization of its results, there is no full correspondence for the reasons indicated in [1] as the "ineradicable drawback" of any planar light modelling.

So, to implement the design plan of the architect (and now the lighting designer) without gross distortions in kind based on the research, a method for designing architectural lighting was developed that provides the functional and aesthetic quality of the lighting environment inherent in the project. It is worth noting that with the modern possibilities of controlling LED lighting, the medium can be not only traditionally light-stabilized, but also light-kinetic in a certain scenario.

The lighting design process according to the developed method consists of two stages. The first is the search for a solution and the expression of a conceived (predicted) luminous image using architectural graphics on paper (now possible on a computer screen). The second is the definition of methods for its implementation in kind [3].

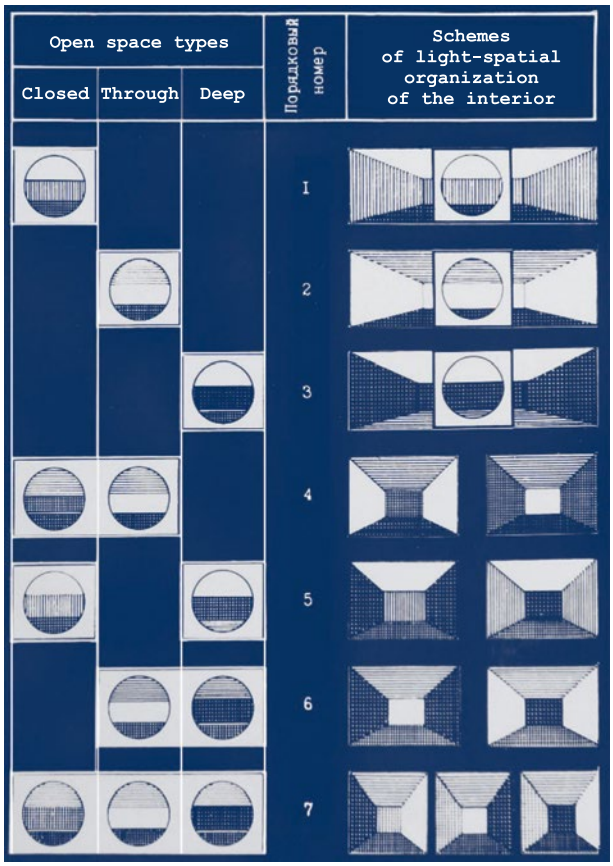

Fig. 1. Schematic diagrams of the light-spatial organization of interiors (see also Fig. 2 [1])

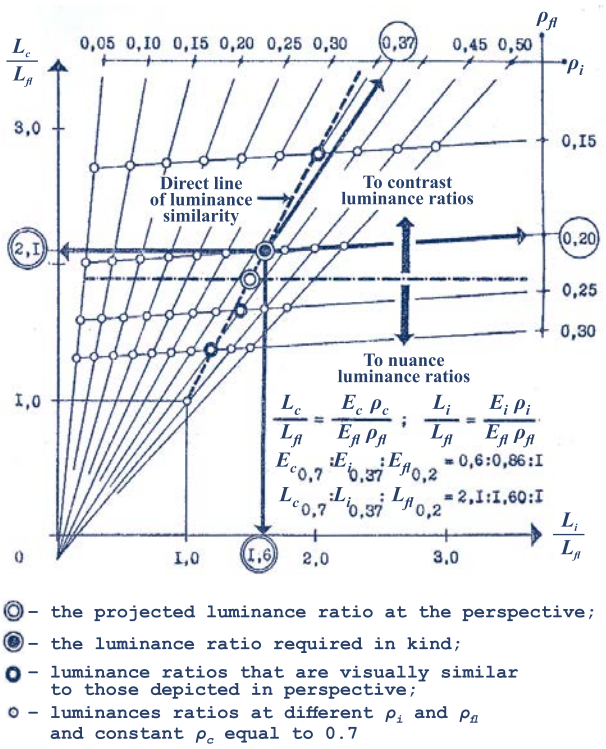

Fig. 2. Determination of the required ratios of luminance: L_c: L_i: L_{fl} and their ρ calculation and graphic method

The first stage includes:

– Selection of the scheme of light-spatial organization of the interior (Fig. 1);

– Achromatic image in the perspective of the predicted distribution of luminance in the interior;

– The luminance of the ceiling (L_c), interior elements (L_i), and floor (L_{fl}) and their ratios with respect to L_c determination.

The second stage includes:

– A graphical definition in daylight of the required ratios L_c: L_i: L_{fl} for nature, which is similar in visual sensation to images in perspective (Fig. 2);

– The choice of the relations L_c: L_i: L_{fl} for their implementation in kind and the determination of the absolute values of L_i and ρ of these surfaces;

– Determination of the quality class of interior lighting according to the quality assessment Table in [1] and the nomogram (Fig. 9 in [1]), in accordance with which (if necessary) the correlation is made L_c: L_w: L_{fl} in perspective (L_w - wall luminance);

– Assessment of the quality of interior lighting according to the luminance range, its harmony and frequency (Fig. 4 [1]);

– Determination E_h /E_z and N and determining their compliance with the required values (Tab. in [1]).

In the dissertation, many of the data mentioned and not mentioned here, provisions and factors of articles that did not fit into the volume, are given more convincingly and extensively. In four, fortunately preserved, but unfortunately not in the best photo quality, exposition tablets, the author's (Vladimir Voronov) method of designing architectural lighting for the interior in comments, graphic diagrams, and tables is more systematically presented (Figs. 3–6).

In those years in our country, an obligatory section of candidate dissertations was the evaluation of the economic effectiveness of the results. It is clear that today it is a completely different, but now rejected idea of this section in dissertations is detrimental to science and practice. By the existing in those time methodology, Vladimir Voronov faithfully found out that the reduced total cost of lighting was the smallest in production interiors with zenith lantern. Costs increase on average by 7 % for buildings with rectangular and 14 % for buildings with shaded lantern. But this does not mean that the shed lights are rejected. They are almost always in the interior according to the impression of the light

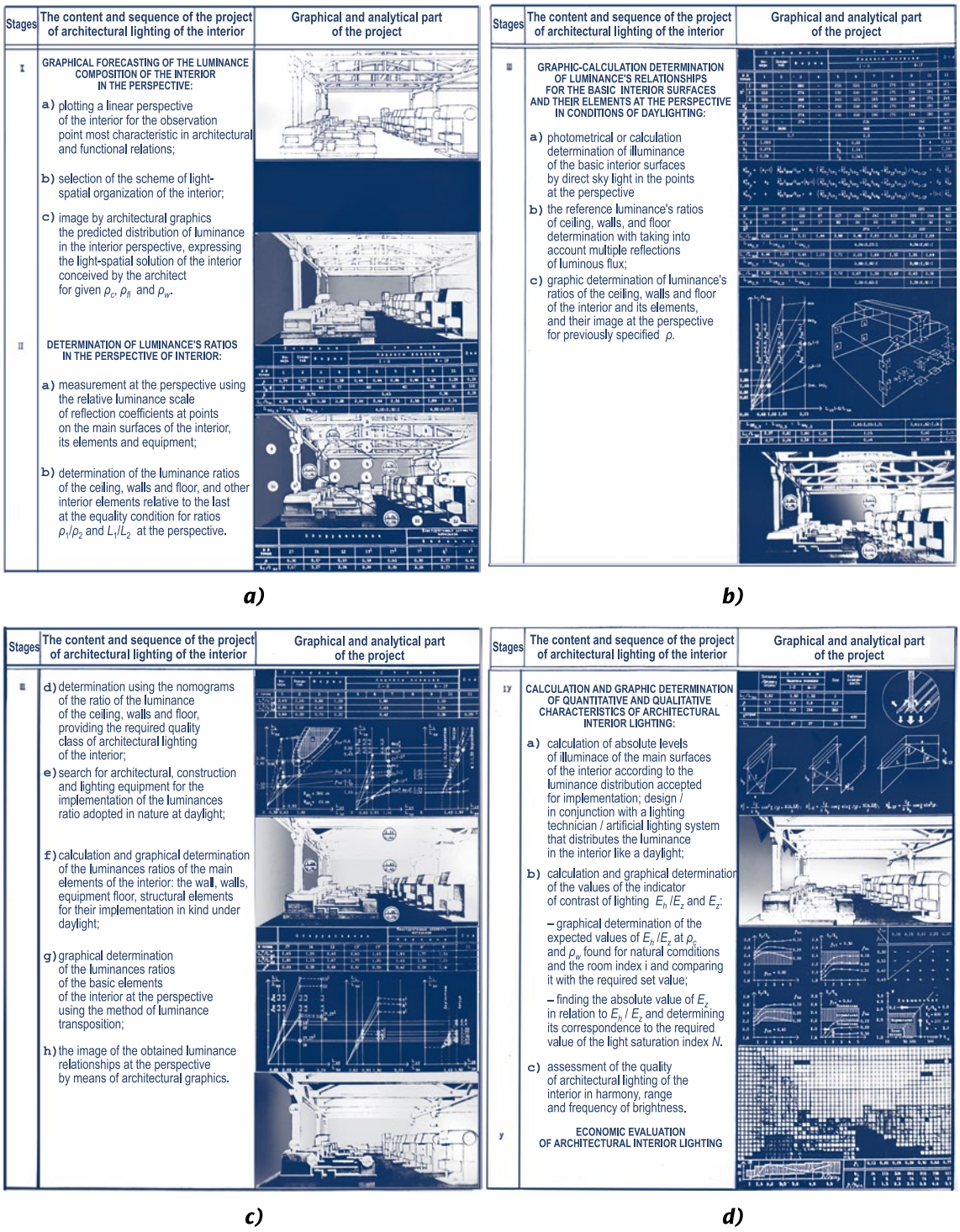

Fig. 3–6. A brief graphic presentation of the method of designing architectural lighting for the interior (stages I–V)

composition aesthetically preferable to others, and for a number of productions in appropriate climatic conditions they can be rational and economical. At the same time, the lump sum costs for daylighting (DL) were determined by the cost of covering the building and for artificial lighting (AL) – by the cost of the originally installed illumination systems (IS) with light sources and their assembly.

The reported costs for the IS were calculated by the VNISI method for the general lighting system (GLS), which in the evening provides a distribution of luminance in the interior that is close to that adopted in daylight. The value of the costs for the light sources ranged from 26 % to 38 % of the total cost of lighting (at the norms and tariffs that were in effect in those years) and depended on the cho-

sen system of light-spatial organization of the interior. Under equal conditions of weighted average luminance ratios of the main surfaces of the interior at DL and light saturation in workshops with shed, rectangular and zenith lamps, the reduced costs for the IS were different. This is due to the fact that the main surfaces of the interior, due to the peculiarities of the light distribution of the lanterns of the upper natural light, are not lit equally during the day. The equality of their weighted average luminance ratios at DL (to achieve a comparable aesthetic effect) is achieved through the use of different internal surfaces $\boldsymbol{\rho}$, which, when calculating the IS, lead to a different amount of illumination devices in the IS. This important circumstance should be taken into account not only as a factor determining the quality of architectural lighting of a production (as well as any other) interior, but also as an important condition for the economic evaluation of a particular illumination installation option.

The results of the dissertation research can be considered, at a minimum, that [1, 2]:

– The theoretical foundations of the light-spatial organization of the production interior with the upper natural and artificial light have been developed, including a relatively universal classification and system of types of interior space, as well as schematic diagrams of its light-space organization;

– Author's methods of objective and subjective assessment of the quality of architectural illumination (AI) of interiors with upper light in natural and laboratory conditions are presented, which showed that it is mainly determined by the light saturation and the distribution of luminance in the interior space;

– A nomogram ("butterfly") was created to assess the quality of AI interior by the distribution of luminance in its space, which is proposed as a tool for controlling light-composition decisions at the design stage and in kind;

– The indicators of quantitative and qualitative assessment of the light saturation of industrial interiors with upper light were determined, characterized objectively by the values of hemispherical ($\boldsymbol{E_{2\pi}}$) and cylindrical ($\boldsymbol{E_{cy}}$) illumination, as well as the contrast of lighting through the ratios $\boldsymbol{E_h / E_{2\pi}}$ and $\boldsymbol{E_h / E_{cy}}$ and subjectively – the author's indicator of light saturation $\boldsymbol{N}$;

– The pattern of luminance similarity was established, on the basis of which an architectural method was developed for the transposition of luminance relations from a planar graphic image of the interior perspective to natural;

– A schedule has been developed for assessing the quality of AI interior according to the range of luminance, harmony and frequency of its series, which allows us to evaluate the luminance composition of the interior at the micrometric level and to differentiate it by categories of monotony, nuance and contrast of lighting;

– It was proved that the permissible (preferred) ranges of luminance ratios in interiors with DL and AL practically coincide, which indicates the subjective desirability of a person to ensure a relative constancy of the luminance distribution in the interior when switching from DL to AL in order to maintain the quality of AI and the constancy of the visual-psychological atmosphere if it is comfort and aesthetic;

– A design method for designing industrial interiors with overhead lights has been developed that is applicable in other typological groups of buildings and allows one to determine the means for realizing the author's design in kind under natural, artificial and combined lighting, ensuring the required quantitative and qualitative characteristics and evaluating their economic efficiency.

All of this is not so little if we talk about the candidate dissertation.

P.S. From the co-author

By his thesis, Vladimir Voronov thoroughly "penetrated" his evidence base into the technical field of lighting engineering, which is little known and obscure in architectural theory and practice.

As far as possible, we, architects from the Department of Architectural Physics, Moscow Institute of Architecture (S.S. Alekseev, N.M. Gusev, V.G. Makarevich, N.V. Obolensky, V.V. Voronov, N.I. Shchepetkov, V.I. Zherdev, G.I. Chirkin, E.V. Sangina, A.G. Batova (Prikhodko), G.S. Matovnikov, etc.), as well as from the NIISF (O.A. Korzin, V.V. Ivanov, A.I. Panurov, Yu.A. Volkov, and others) for decades have tried and have been trying to the best of our abilities and capabilities with our works to expand the range of worldview problems associated with light in architecture and affecting professional tasks – strategic, practical and, at least, operational. Applied lighting, in our opinion, is designed to solve some of the tactical and operational tasks of creating a comfortable, artistically complete, environmentally friendly, and energy-ef-

ficient natural and artificial light architectural environment in the interior and exterior in terms of more accurate criteria-based assessments and methods for their determination.

It is unlikely that it claims to be a separate "science for science", as there once existed the historically failed trend of "art for art", although extreme examples of it still exist today. It makes no sense to argue that a competent architect should formulate strategic tasks in this area – he designs the material-spatial and figurative basis of the anthropogenic environment. And there is practically no productive contact between them today. Few architects who are scientifically engaged in the problems of light, at best, determine some current trends in the development and artistic qualities of this environment, including in the form of ratios of lighting values, without setting the ultimate goal to obtain mathematically accurate results. This is not their area and path. It is here that a productive, systemic, interdisciplinary scientific continuity could be established: professional and important architectural tasks were set, and "narrow specialists" – lighting technicians, on a broad front, are looking for means and methods for solving them.

These are the dreams of an architect who has long plunged into lighting engineering.

Unfortunately, according to the experience of episodic peer-reviewing in recent years, lighting dissertations of applicants at the NIISF, MGSU, MPEI, as well as publications, including in the journal "Lighting & Engineering", I see how fragmented, unsystematic, and partly small-scale research topics are in applied building lighting, and in essence – in light in architecture. It seems that not a single dissertation refers to the works of architects in this area. I don't know what such "caste" isolation means – ignorance, disrespect or, God forbid, contempt for attempts, perhaps not always convincing from their point of view, to use the "outsiders" knowledge of an adjacent respected science. I'm probably mistaken in something. You can consider these estimates as an invitation to discussion.

The dissertation and abstract of V.V. Voronov will be presented on the journal site after converting them to digital form.

REFERENCES

1. Voronov V.V. and Schepetkov N.I. On Methodology for Designing Architectural Lighting of Production Site Interior: Part I. Theoretical foundations and results of scientific research and Part II. Experimental laboratory research // Lighting & Engineering Journal, 2020, Vol. 28, #3, pp. 10–21.

2. Voronov V.V. The method of designing architectural lighting of a production interior // Abstract of the Ph.D. in architecture dissertation. Moscow, MARCHI, 1985.

Nicolay I. Shchepetkov,
Dr. of Architecture, Professor.
He graduated from the Moscow Institute of Architecture in 1965. At present, he is a Head of the Department of "Architectural physics", Moscow Institute of Architecture (SA), Laureate of the State Prize of the Russian Federation (for architectural lighting in Moscow). Corresponding member of the Academy of Natural Sciences, member of the Editorial Board of the Journals "Svetotekhnika" and "Light & Engineering"

***Vladimir V. Voronov*,**
Associate Professor, Ph.D. in architecture, graduated from MARKHi in 1965. Before 2016, he was a Professor of the Architectural Physics sub-department of MARKHI (GA), Honorary Worker of the Higher Education of the Russian Federation.

Light & Engineering
Vol. 28, No. 3, pp. 27–33, 2020

https://doi.org/10.33383/2019–097
Svetotekhnika # 2, 2020, pp. 67–71

ENERGY, INFORMATION, AND SUPERLUMINAL SPEED IN QUANTUM ELECTRODYNAMICS

Boris A. Veklenko

Joint Institute for High Temperatures (JIVT) of the Russian Academy of Sciences, Moscow, Russia
E-mail: veklenkoba@yandex.ru

ABSTRACT

Without using the perturbation theory, the article demonstrates a possibility of superluminal information-carrying signals in standard quantum electrodynamics using the example of scattering of quantum electromagnetic field by an excited atom.

Keywords*:* excited atom, superluminal signal, quantum electrodynamics, scattering

1. INTRODUCTION

Superluminal speeds in optical systems have been attracting attention for many years. And while the matter of information transfer with faster-than-light speeds is fully settled in classical physics after the works by H. Lorentz, J.H. Poincaré and A. Einstein, this categorical assertion does not apply to quantum optics.

In classical physics, the state of an electromagnetic field is described by vectors of electromagnetic strength $E^{\nu}(\mathbf{r},t)$ and vectors of magnetic induction $B^{\nu}(\mathbf{r},t)$ determined at any point of the space $\mathbf{r}$ at any moment of time t. It turns out to be convenient to use vector potential of electromagnetic field $A^{\nu}(\mathbf{r},t)$ in a rationalised Gaussian system of units with zero scalar potential instead of these vectors, so that

$$E^{\nu}(\mathbf{r},t) = -\frac{1}{c}\frac{\partial}{\partial t}A^{\nu}(\mathbf{r},t),\ B^{\nu}(\mathbf{r},t) = rot\mathbf{A}(\mathbf{r},t).$$

Here, c is speed of light in vacuum. Use of vector potential is convenient because just one magnitude $A^{\nu}(\mathbf{r},t)$ should be used instead of two magnitudes $E^{\nu}(\mathbf{r},t)$ and $B^{\nu}(\mathbf{r},t)$. Hereinafter we will often use $A^{\nu}(\mathbf{r},t)$ instead of $E^{\nu}(\mathbf{r},t)$ keeping in mind that the relation between them is rather simple. In quantum physics, the state of an electromagnetic field and the state of particles of finite mass are described by a wave function $\psi(t)$. In quantum optics, analogues of classical magnitudes are calculated as mean quantum magnitudes of corresponding quantum operators $\left\langle \hat{A}^{\nu}(\mathbf{r},t)\right\rangle = \left\langle \psi(t)\right|\hat{A}^{\nu}(\mathbf{r})\left|\psi(t)\right\rangle$. Using the principle of correspondence between the quantum theory and the classical theory, it is safe to assume that mean magnitudes of the quantum theory of electromagnetic field having classical analogues should not change with speeds exceeding the speed of light in vacuum c. The question remains: is it possible to exceed c by means of dispersions, i.e. by means of quantum fluctuations? Such opportunity is not impossible a priori, rather the opposite [1]. If, being interested in the speed of an electromagnetic signal generated at a point $\mathbf{r} = 0$ at a moment $t = 0$, we set a target to measure the strength of the electromagnetic field $\hat{E}^{\nu}(\mathbf{r},t)$ at a point $\mathbf{r}$ of the leading edge of this signal in time t, the Heisenberg uncertainty relation will interfere. According to the definition $\hat{E}^{\nu} = f^{\nu}/q$, where f^{ν} is the force affecting the test charge q placed at the measurement point $\mathbf{r}$. However, $f^{\nu} = dp^{\nu}/dt$, where p^{ν} is the pulse of the test charge measured at the point $\mathbf{r}$.

The uncertainty relation shows that accurately determined **r** and **p** do not exist at the same moment of time. Therefore accurately determined **r** and $E^{\nu}(\mathbf{r},t)$ do not exist simultaneously. Quantum dispersion of coordinates distorting the leading edge of the signal appears. Part of the experimental points will be located behind the leading edge characterised by amplitude $\left\langle \hat{E}^{\nu}(\mathbf{r},t)\right\rangle = \langle\psi(t)|\hat{E}^{\nu}(\mathbf{r},t)|\psi(t)\rangle$, the other part will be located in front of it defining the superluminal signal. So, in a number of experiments, it is possible to predict registration of superluminal signals. We find it essentially necessary to introduce superluminal signals in quantum optics which may affect measurement devices and therefore carry information. It should be noted that the considered dispersion of coordinates in optical measurements does not affect accuracy of measurement of the speed of light itself. The case is that the selected distance between the source of radiation and the measurement coordinate may be arbitrarily large.

What is the nature of superluminal signals? According to the above said, they are ahead of the leading edge of a classical signal, and therefore there is no mean value of field strength in them $\langle\psi(t)|\hat{E}^{\nu}(\mathbf{r})|\psi(t)\rangle = 0$ but the dispersion $\langle\psi(t)|\hat{E}^{\nu}(\mathbf{r})\hat{E}^{\nu}(\mathbf{r})|\psi(t)\rangle \geq 0$ will be different from zero. Such properties are seen in photons [2] which do not have electric and magnetic components, and their energy turns out to be finite. So, non-relativistic quantum mechanics of finite mass particles predicts existence of non-classical states of an electromagnetic field which may form signals with speed exceeding c. It is important to stress that such signals can affect test electrons, excite atoms, transfer energy and information. It should be noted that the existence of photons was predicted (in 1905), by contrast, before establishment of the quantum theory of non-relativistic particles (1925–1926).

Now two questions arise: How much are space domains of superluminal signals and is there a limit of such speeds?

2. QUALITATIVE CONSIDERATION

To answer these questions, appearance of superluminal signals is studied below in their more clear manifestation within another quantum system.

Let transversely polarised light generated by classic current density $f^{\nu}(\mathbf{r},t)$, be scattered by an atom located at the point **R**. According to the quantum theory, scattering of light by a non-excited atom is represented as virtual process of absorption of the photon being diffused and further process of emission of a scattered quantum by this newly excited atom. Such scattering process requires time and is only capable of slowing down ballistic speed of an electromagnetic wave. But in the course of light scattering by an excited atom, another quantum process exists [3] which consists of spontaneous emission of a photon by this excited atom and transfer of the atom into the non-excited state and only then (when the scattered quantum has already started moving) the quantum being scattered is being absorbed by the atom which is no more excited. Such complex process is described by a uniform wave function. That is why the scattered photon and the photon being scattered are mutually correlated and the process generally has nature of scattering. Classical interpretation of this process suggests that such inverse scattering of the photon by an excited atom allows it to gain larger distance $c\tau$, where τ is correlation time of the photons. In front of the leading edge, at distance of $c\tau$ from it, the superluminal precursor appears. If the atom had been in the ground state initially, such inverse possibility of scattering also exists but turns out to be insignificant due to non-resonance of the process.

It is obvious that these speculations are not proven and require detailed research. Until now, superluminal signals transferring information have not manifested themselves in standard quantum electrodynamics.

Let us express the wave function of the quantum system: electromagnetic field plus the scattering atom after the process of scattering through Ψ. Let us expand this function by the complete system of wave functions ψ_i of the scattering atom

$$\Psi = f_0\psi_0 + \sum_{i\neq 0} f_i\psi_i = f_0\psi_0 + \left(\Psi - f_0\psi_0\right),$$

where the initial state of the atom ψ_0 is taken as a separate component. Due to orthogonality of the wave functions of the atom ψ_0 and $\psi_i (i \neq 0)$, scalar products of the functions

$$\left\langle f_0\psi_0 \middle| \sum_{i\neq 0} f_i\psi_i \right\rangle = \left\langle f_0\psi_0 \middle| \Psi - f_0\psi_0 \right\rangle = 0$$

become zero. If the atom has remained in the initial state ψ_0 as a result of scattering, we will call such scattering process a coherent process [4]. This process is reflected by the wave function of electromagnetic field f_0. If ψ_0 corresponds with the excited state, f_0, according to the above mentioned, in particular, describes superluminal signals. If the atom wave function changes as a result of scattering, such process is considered non-coherent by convention.

The magnitudes observed experimentally are calculated as quantum mean magnitudes of corresponding quantum operators. For instance, electric field strength $E^{\nu}(\mathbf{r},t)$ which has a classical analogue and therefore does not have superluminal speeds may be written as

$$\begin{aligned}\left\langle \hat{E}^{\nu}(\mathbf{r},t)\right\rangle &= \left\langle \Psi(t)\middle|\hat{E}^{\nu}(\mathbf{r})\middle|\Psi(t)\right\rangle = \\ &= \left\langle f_0\psi_0\middle|\hat{E}^{\nu}(\mathbf{r})\middle|f_0\psi_0\right\rangle + \\ &+ \left\langle \Psi - f_0\psi_0\middle|\hat{E}^{\nu}(\mathbf{r})\middle|\Psi - f_0\psi_0\right\rangle = \\ &= \left\langle \hat{E}^{\nu}(\mathbf{r},t)\right\rangle_{coh} + \left\langle \hat{E}^{\nu}(\mathbf{r},t)\right\rangle^{ncoh}. \end{aligned} \quad (1)$$

The cross (interference) component is removed here due to orthogonality of the atom wave functions. The first component of the right part of (1) describes coherent scattering and, in the case of scattering by means of an excited atom, as described above, superluminal signals. The second component describes the components of non-coherent scattering, in particular, forced scattering processes in which the initial state ψ_0 of the scatterer transforms into the one that is orthogonal to it $\psi_i (i \neq 0)$. Only interference of the coherent and non-coherent scattering channels makes superluminal signals impossible in the final result of (1). In its turn it means that, in the case of scattering by an excited atom, the wave functions of the non-coherent channel f_i ($i \neq 0$) also describe superluminal signals of opposite in sign. It is important to note that superluminal signals in virtual states appear in calculations of quantum electrodynamics automatically and disappear from the final result only as a result of interference of scattering channels. If the interference is hindered, it is obvious that superluminal signals will appear in the result. It is not difficult to do.

Let us be interested in bilinear normally ordered products of electromagnetic field operators $\left\langle \hat{N}\left(\hat{E}^{\nu}\right)^2\right\rangle$ which determine its local energy characteristics [1]. This magnitude may be estimated lower bound as follows. It is obvious that $\left\langle \left(\hat{E}^{\nu}\right)^2\right\rangle \geq \left\langle \hat{E}^{\nu}\right\rangle\left\langle \hat{E}^{\nu}\right\rangle$.

It is possible to show similarly [2] that, if an electromagnetic field possesses primary components with wave vector $\mathbf{k}_0$, after averaging of the wavelength order over the coordinate range of, it turns out that

$$\left\langle \hat{N}\left(\hat{E}^{\nu}\right)^2\right\rangle \geq \left\langle \hat{E}^{\nu}\right\rangle^2. \quad (2)$$

Therefore, $\left\langle \hat{E}^{\nu}\right\rangle$ determines the lower-bound estimate for the sought $\left\langle \hat{N}\left(\hat{E}^{\nu}\right)^2\right\rangle$. Correctness of the equation (2) does not depend on the specific state over which quantum averaging is done and is not related to the perturbation theory.

If we now write the magnitude $\left\langle \hat{N}\left(\hat{E}^{\nu}\right)^2\right\rangle$ as a sum of the coherent and non-coherent components similarly to (1)

$$\begin{aligned}\left\langle \hat{N}(\hat{E}^{\nu})^2\right\rangle &= \left\langle f_0\psi_0\middle|\hat{N}(\hat{E}^{\nu})^2\middle|f_0\psi_0\right\rangle + \\ &+ \left\langle \Psi - f_0\psi_0\middle|\hat{N}(\hat{E}^{\nu})^2\middle|\Psi - f_0\psi_0\right\rangle = \\ &= \left\langle \hat{N}(\hat{E}^{\nu})^2\right\rangle_{coh} + \left\langle \hat{N}(\hat{E}^{\nu})^2\right\rangle^{ncoh}, \end{aligned}$$

and apply the formula (2) to each component of the right part of this sum, we will find that

$$\begin{aligned}\left\langle \hat{N}(\hat{E}^{\nu})^2\right\rangle &\geq \left\langle f_0\psi_0\middle|\hat{E}^{\nu}\middle|f_0\psi_0\right\rangle^2 + \\ &+ \left\langle \Psi - f_0\psi_0\middle|\hat{E}^{\nu}\middle|\Psi - f_0\psi_0\right\rangle^2 = \\ &= \left\langle \hat{E}^{\nu}\right\rangle_{coh}^2 + \left\langle \hat{E}^{\nu}\right\rangle^{ncoh2}. \end{aligned} \quad (3)$$

Now, due to positive definiteness of the components of the right part of the latter in equation, superluminal signals of different channels will not mutually compensate each other and it will be impossible to avoid them as a result. Therefore, the theory predicts their appearance in the measurements of $\left\langle \hat{N}(\hat{E}^{\nu})^2\right\rangle$, i.e. measurements of the energy of an electromagnetic field.

[1] The operator $\hat{N}$ is called the normal ordering operator. Its presence in the formulas does not affect understanding of further material [2].

3. QUANTITATIVE THEORY

Let us describe some results of exact calculations following from the fundamental equations of quantum electrodynamics described in the Annex. These results were derived by solving the equation (P1) using the method of $\hat{S}$ scatter matrix and R. Feynman diagrams.

To simplify, let us assume that the scattering atom has two energy levels. We will identify the atomic energy at which scattering takes place as ε_{j_0} and the energy of the other state of the atom as ε_{j_2}. Let us assume that these energy levels may possess energetically degenerate magnetic sublevels, using which summation may be done.

First we will assume that the scattering atom is in the non-excited (ground) state. The main scattering channel here will be the coherent channel. The non-coherent scattering channel makes non-resonant low contribution to the result here. Solution of the equation (P. 1) describing the scattered electromagnetic field in this case looks as follows [2]

$$\left\langle \hat{A}^{\nu}(\mathbf{r},t)\right\rangle_{\text{coh}} = \int T^{\nu}(\mathbf{r},\mathbf{r}_3,t,t_3)\theta\left(\varepsilon_{j_2}-\varepsilon_{j_0}\right)\times$$
$$\times\theta\left[\left(c\left(t-t_3\right)-\left|\mathbf{r}-\mathbf{R}\right|-\left|\mathbf{r}_3-\mathbf{R}\right|\right)\right]d\mathbf{r}_3dt_3+c.c., \quad (4)$$

where

$$T^{\nu}\left(\mathbf{r},\mathbf{r}_3,t,t_3\right)=\frac{i}{16\pi^2c^3\hbar}\left(\frac{e}{m}\right)^2\sum_{j_2}p^{\nu_1}_{j_0j_2}p^{\nu_2*}_{j_0j_2}\left(\delta_{\nu\nu_1}-n^{\nu}n^{\nu_1}\right)\times$$
$$\times\left(\delta_{\nu_2\nu_3}-n_3^{\nu_2}n_3^{\nu_3}\right)j^{\nu_3}(\mathbf{r}_3,t_3)\frac{\theta\left(t-t_3\right)}{\left|\mathbf{r}-\mathbf{R}\right|\left|\mathbf{r}_3-\mathbf{R}\right|}\times$$
$$\times\theta\left[\left(c\left(t-t_3\right)-\left|\mathbf{r}_3-\mathbf{R}\right|\right)\right]j^{\nu}\left(\mathbf{r}_3,t_3\right)$$
$$\exp\left[-i\frac{\varepsilon_{j_0}-\varepsilon_{j_2}}{c\hbar}\left(c\left(t-t_3\right)-\left|\mathbf{r}-\mathbf{R}\right|-\left|\mathbf{r}_3-\mathbf{R}\right|\right)\right],$$

$$n_3^{\nu}=\frac{(\mathbf{r}_3-\mathbf{R})^{\nu}}{\left|\mathbf{r}_3-\mathbf{R}\right|}. \quad (5)$$

Since $\varepsilon_{j_2}-\varepsilon_{j_0}>0$, the expression (4) describes the signal scattering by a non-excited atom. Heaviside step function $\theta\left[\left(c\left(t-t_3\right)-\left|\mathbf{r}-\mathbf{R}\right|-\left|\mathbf{r}_3-\mathbf{R}\right|\right)\right]$, prevents the velocity of the leading edge of the scattered signal from exceeding the velocity of classical electromagnetic wave in vacuum. In other words, the magnitude which has a classical analogue does not propagate faster than light. The expression (4) describes only the scattered signal. The signal propagating without scattering is omitted here

$$\left\langle \hat{A}^{\nu}(\mathbf{r},t)\right\rangle=\frac{1}{4\pi}\left(\delta_{\nu\nu_1}-n^{\nu}n^{\nu_1}\right)\int\frac{j^{\nu_1}\left(\mathbf{r}_1,t-\frac{\left|\mathbf{r}-\mathbf{r}_1\right|}{c}\right)}{\left|\mathbf{r}-\mathbf{r}_1\right|}d\mathbf{r}_1.$$

The case is different if an electromagnetic field is scattered by an excited atom. In this case, scattering occurs through two scattering channels: coherent and non-coherent. The solution of the equation (P. 1) shows [2] that, according to the coherent channel

$$\left\langle \hat{A}^{\nu}(\mathbf{r},t)\right\rangle_{coh} = \int T^{\nu}(\mathbf{r},\mathbf{r}_3,t,t_3)\theta\left(\varepsilon_{j_0}-\varepsilon_{j_2}\right)\times$$
$$\times\theta\left[\left(\left|\mathbf{r}-\mathbf{R}\right|+\left|\mathbf{r}_3-\mathbf{R}\right|-c\left(t-t_3\right)\right)\right]d\mathbf{r}_3dt_3+c.c.. \quad (6)$$

Therefore, the coherent channel, which leaves the scattering atom in its ground state, according to the Heaviside function $\theta\left[\left(\left|\mathbf{r}-\mathbf{R}\right|+\left|\mathbf{r}_3-\mathbf{R}\right|-c\left(t-t_3\right)\right)\right]$, and in line with the conclusions of the section 2, instantly forms a scattered channel at any distance $\left|\mathbf{r}-\mathbf{R}\right|$ from the scattering atom if only $\left|\mathbf{r}-\mathbf{R}\right|-c\left(t-t_3\right)+\left|\mathbf{r}_3-\mathbf{R}\right|>0$. We are dealing with infinitely high speed of formation of this signal. Such scattering process does not exist in classical optics.

For non-coherent scattering channel, changing quantum state of the scattering atom, the scattered signal is described by the following formula [2]

$$\left\langle \hat{A}^{\nu}(\mathbf{r},t)\right\rangle^{ncoh} =$$
$$=-\int T^{\nu}(\mathbf{r},\mathbf{r}_3,t,t_3)\theta\left(\varepsilon_{j_0}-\varepsilon_{j_2}\right)d\mathbf{r}_3dt_3+c.c. \quad (7)$$

This signal includes both the area behind the leading edge $\left|\mathbf{r}-\mathbf{R}\right|+\left|\mathbf{r}_3-\mathbf{R}\right|<c(t-t_3)$ and the superluminal area $\left|\mathbf{r}-\mathbf{R}\right|+\left|\mathbf{r}_3-\mathbf{R}\right|>c(t-t_3)$ located in front of the leading edge. Such scattering channel does not have a classical analogue either. Availability of the function $\vartheta(\varepsilon_{j_0}-\varepsilon_{j_2})$ testifies that the non-coherent scattering channel appears only in the case of light scattering by excited atoms.

Using the fact that the complete signal which has a classical analogue is defined by the sum (1) of scattering channels, we find that

$$\left\langle \hat{A}^{\nu}(\mathbf{r},t)\right\rangle = \left\langle \hat{A}^{\nu}(\mathbf{r},t)\right\rangle_{coh} + \left\langle \hat{A}^{\nu}(\mathbf{r},t)\right\rangle^{ncoh} = $$
$$= -\int T^{\nu}(\mathbf{r},\mathbf{r}_3,t,t_3)\theta\left(\varepsilon_{j_0}-\varepsilon_{j_2}\right)\theta\Big[c\left(t-t_3\right)- \tag{8}$$
$$-\left(\left|\mathbf{r}-\mathbf{R}\right|-\left|\mathbf{r}_3-\mathbf{R}\right|\right)\Big]d\mathbf{r}_3dt_3+c.c.$$

As expected, the complete signal determined by the amplitude $\hat{A}^{\nu}(\mathbf{r},t)$, which appears as a result of scattering of electromagnetic field by an excited atom, is completely located behind the leading edge of the wave and does not possess superluminal properties. According to (6) and (7), superluminal components of the amplitudes $\left\langle \hat{A}^{\nu}(\mathbf{r},t)\right\rangle_{coh}$ and $\left\langle \hat{A}^{\nu}(\mathbf{r},t)\right\rangle^{ncoh}$ mutually destroy each other as a result of interference. The expression (8) may be easily derived from the semi-classical radiation theory, which operates by none quantified electromagnetic field.

The case of energy of an electromagnetic field is different. For a time-variable electromagnetic field, presence of a non-zero function $\left\langle \hat{N}(\hat{A}^{\nu})^2\right\rangle$ guarantees difference from zero of the sought $\left\langle \hat{N}(\hat{E}^{\nu})^2\right\rangle$. Similar to the formula (3),

$$\left\langle \hat{N}(\hat{A}^{\nu})^2\right\rangle \geq \left\langle f_0\psi_0\left|\hat{A}^{\nu}\right|f_0\psi_0\right\rangle^2 +$$
$$+\left\langle \Psi-f_0\psi_0\left|\hat{A}^{\nu}\right|\Psi-f_0\psi_0\right\rangle^2 =$$
$$=\left\langle \hat{A}^{\nu}\right\rangle_{coh}^2+\left\langle \hat{A}^{\nu}\right\rangle^{ncoh2}. \tag{9}$$

The functions $\left\langle \hat{A}^{\nu}\right\rangle_{coh}$ and $\left\langle \hat{A}^{\nu}\right\rangle^{ncoh}$, as noted above, have superluminal components. Since the formula (9) contains the squares of these functions, the superluminal components cannot compensate each other as a result of interference now. Therefore, the energy of a scattered electromagnetic signal $\left\langle \hat{N}(\hat{E}^{\nu})^2\right\rangle$ or, according to our assumptions, the function $\left\langle \hat{N}(\hat{A}^{\nu})^2\right\rangle$ turns out to be equal to

$$\left\langle \hat{N}\left(\hat{A}^{\nu}(\mathbf{r},t)\right)^2\right\rangle =$$
$$\left(\int T^{\nu}(\mathbf{r},\mathbf{r}_3,t,t_3)\theta\left(\varepsilon_{j_0}-\varepsilon_{j_2}\right)\theta\Big[\left(\left|\mathbf{r}-\mathbf{R}\right|+\right.\right.$$
$$\left.\left.+\left|\mathbf{r}_3-\mathbf{R}\right|-c\left(t-t_3\right)\right)\Big]d\mathbf{r}_3dt_3+c.c.\right)^2+$$
$$+\left(\int T^{\nu}(\mathbf{r},\mathbf{r}_3,t,t_3)\theta\left(\varepsilon_{j_0}-\varepsilon_{j_2}\right)d\mathbf{r}_3dt_3+c.c.\right)^2.$$

This expression may be written as

$$\left\langle \hat{N}\left(\hat{A}^{\nu}(\mathbf{r},t)\right)^2\right\rangle =$$
$$\left(\int T^{\nu}(\mathbf{r},\mathbf{r}_3,t,t_3)\theta\left(\varepsilon_{j_0}-\varepsilon_{j_2}\right)\theta\Big[c\left(t-t_3\right)-\right.$$
$$\left.-\left|\mathbf{r}-\mathbf{R}\right|-\left|\mathbf{r}_3-\mathbf{R}\right|\Big]d\mathbf{r}_3dt_3+c.c.\right)^2+$$
$$+2\Big(\int T^{\nu}(\mathbf{r},\mathbf{r}_3,t,t_3)\theta\left(\varepsilon_{j_0}-\varepsilon_{j_2}\right)\theta\Big[\left|\mathbf{r}-\mathbf{R}\right|+$$
$$+\left|\mathbf{r}_3-\mathbf{R}\right|-c\left(t-t_3\right)\Big]+c.c.\Big)^2d\mathbf{r}_3dt_3. \tag{10}$$

The first line of (10) describes an ordinary scattered optical signal, which appears in the theory of none quantified field too. It may be calculated by means of the vectors $E^{\nu}(\mathbf{r},t)$ and $B^{\nu}(\mathbf{r},t)$ and standard Maxwell's non-quantified equations. The second line describes the superluminal quantum precursor appeared before this signal. The precursor occupies that area of the space where $E^{\nu}(\mathbf{r},t)=0$ and $B^{\nu}(\mathbf{r},t)=0$. The energy of the precursor is finite. It means that the nature of the precursor is not classical and it reminds a field of Planck photons possessing similar properties. What is more surprising is that the formulas of the quantum precursor does not contain the Planck constant $\hbar$ and fall into the rare set of quantum theory formulas possessing such property. The latter becomes obvious if we suggest that the role of the scattering atom is played by a quantum oscillator. Here $p_{j_0j_2}^{\nu_1}\propto\sqrt{\hbar}$ and, according to (5), the Planck constant falls out of calculations.

Let us stress once more that the precursor possesses energy and may transfer information with superluminal speed. Moreover, since the second line of the formula (10) does not limit the vector $\mathbf{r}$, it means that the signals may be transferred at infinitely high speed by means of the precursor. Availability of energy widths of the scattering atom has an effect on limitation of the magnitude $\left|\mathbf{r}-\mathbf{R}\right|$, which reduces effective value of light speed in measurements [6].

4. CONCLUSION

This review does not use any new hypotheses. It considers only the known equations of quantum

electrodynamics derived relations of which turn out to predict availability of energy-transferring superluminal speeds in nature. Generally speaking, infinite speeds are well-known in quantum theory. Wave function collapse demonstrates such speed in the case of experimental fixation of an electron at some point in space. Another example derives from the property of symmetry of wave functions of identical particles. If the structure of such function is forcefully damaged at some local point of space, symmetry of the wave function will be immediately (infinitely fast) reestablished. Such effect is also encountered in the EPR paradox [7]. One of the distinctive characteristics of the example considered in this work is that obvious possibility of energy and information transfer at infinitely high speed follows from the quantum electrodynamics equations. Such speed is conditioned not by the speed of light but the speed of transfer of correlation properties of wave functions describing the state of a quantum system [9]. Infinitely high speed is Lorentz-invariant and therefore cannot violate the Lorentz transformation.

Let us pay attention to the following circumstance. Non-relativistic quantum mechanics may be described using different mathematical tools. The most well-known are the Heisenberg matrix method (1925) and the Schrödinger differential-equation method (1926).

It is customary to say that quantum mechanics may be exposed in accordance with Heisenberg's representation or in accordance with the Schrödinger's representation. Both methods lead to similar results. In quantum electrodynamics, this property is lost [8] and these two representations have to be considered as substantially two different theories. Selection between them may be determined by an experiment or self-contradictoriness of one of them. In accordance with the Heisenberg's representation, quantum electrodynamics does not lead to existence of superluminal signals [8], which contradicts the basics of quantum theory described in the introduction. That is why only the Schrödinger's representation is used in this review. The experiment [6] which studies the superluminal signal transferring energy also favours this representation.

ANNEX

The quantum electrodynamics equation, whose derivations are reviewed in this paper, is presented below in accordance with the Schrödinger's representation. Let a quantum electromagnetic field generated by classic current density $j^{\nu}(\mathbf{r},t)$ be scattered by an atom located at the point $\mathbf{R}$. We will assume that the atom possesses one valency electron with coordinate $\mathbf{r}$, the spin effects will be neglected. The wave function of the system obeys the Schrödinger equation [2]

$$i\hbar\frac{\partial\Psi(\varsigma,t)}{\partial t}=$$

$$=\left(\int\hat{\psi}^{+}\hat{H}_{a}\hat{\psi}\,d\mathbf{r}+\hat{H}_{ph}-\frac{e}{mc}\int\hat{\psi}^{+}\hat{p}_{\mathbf{r}}^{\nu}\hat{A}^{\nu}\hat{\psi}\,d\mathbf{r}-\right.$$

$$\left.-\frac{1}{c}\int j^{\nu}\hat{A}^{\nu}d\mathbf{r}\right)\Psi(\boldsymbol{\varsigma},t). \qquad \text{(P. 1)}$$

Let us use only quasi-resonant approximation, omit the component proportional to $\hat{\mathbf{A}}^2$, in the Hamiltonian operator, use calibration with zero scalar potential and a rationalised Gaussian system of units. The following indications are used in the equation (P. 1)

$$\hat{H}_{a}=\frac{\hat{p}_{\mathbf{r}}^{2}}{2m}+U(\mathbf{r}-\mathbf{R}),\ \hat{H}_{ph}=$$

$$=\sum_{\mathbf{k}\lambda}\hbar ck\hat{\alpha}_{\mathbf{k}\lambda}^{+}\hat{\alpha}_{\mathbf{k}\lambda},\ \hat{p}_{\mathbf{r}}^{\nu}=$$

$$=-i\hbar\nabla_{\mathbf{r}}^{\nu},\ \hat{\psi}(\mathbf{r})=\sum_{j}\psi_{j}(\mathbf{r}-\mathbf{R})\hat{b}_{j},$$

$$\hat{\psi}^{+}(\mathbf{r})=\sum_{j}\psi_{j}^{*}(\mathbf{r}-\mathbf{R})\hat{b}_{j}^{+},\quad\hat{A}^{\nu}(\mathbf{r})=$$

$$=\sum_{\mathbf{k}\lambda}\sqrt{\frac{\hbar c}{2kV}}e_{\mathbf{k}\lambda}^{\nu}\left(\hat{\alpha}_{\mathbf{k}\lambda}e^{i\mathbf{kr}}+\hat{\alpha}_{\mathbf{k}\lambda}^{+}e^{-i\mathbf{kr}}\right),\ \varsigma=...,\varsigma_{\mathbf{k}\lambda},...,$$

$$\hat{\alpha}_{\mathbf{k}\lambda}=\frac{1}{\sqrt{2}}\left(\varsigma_{\mathbf{k}\lambda}+\frac{\partial}{\partial\varsigma_{\mathbf{k}\lambda}}\right),\ \hat{\alpha}_{\mathbf{k}\lambda}^{+}=\frac{1}{\sqrt{2}}\left(\varsigma_{\mathbf{k}\lambda}-\frac{\partial}{\partial\varsigma_{\mathbf{k}\lambda}}\right).$$

$\hat{b}_j$ and $\hat{b}_j^{+}$ mean the annihilation and creation operators of the atom described by the wave function $\psi_j(\mathbf{r}-\mathbf{R})$ and possessing internal energy $\sum_j$, V is the quantum volume. In the case of temperature none degenerate gas, these operators obey commutation relations of Bose–Einstein fields. Unit vectors $e_{\mathbf{k}\lambda}^{\nu}$ normal to the wave vector $\mathbf{k}$ describe linear polarisation of the photon field ($\lambda=1,2$). $U(\mathbf{r}-\mathbf{R})$ means potential energy of the electron in the atom,

m means the electron mass. Repeating *v* indexes imply summing here and mentioned above.

REFERENCES

1. Heitler W. Quantum Theory of Radiation [Kvantovaya teoriya izlucheniya]. Moscow: Izd-vo inostr. litry, 1956. P. 100.

2. Veklenko B.A. Nonstationary Scattering of Quantum Electromagnetic Field by an Excited Atom [Nestatsionarnoye rasseyaniye kvantovannogo elektromagnitnogo polya na vozbuzhdyonnom atome] // Prikladnaya fizika, 2010, Vol. 3, pp. 10–17.

3. Levich V. G., Vdovin Yu. A., Myamlin V.A. Theoretical Physics Course. P. II [Kurs teoreticheskoy fiziki. Ch. II]. Moscow: Fizmatgiz, 1962, 663 p.

4. Berestetskiy V. B., Lifshits E.M., Pitaevsky L.P. // Quantum Electrodynamics [Kvantovaya elektrodinamika]. Moscow: Nauka, 1980, 257p.

5. Veklenko B.A. The Nature of the Photon and Quantum Optics// Light & Engineering, 2018, Vol. 26, # 2, pp. 7–14.

6. Veklenko B.A., Malakhov Yu.I., Nguen K. Sh. Superluminal Signals in Quantum Optics [Sverkhsvetovyye signaly v kvantovoy optike] // Inzhenernaya fizika, 2013, Vol. 5, pp. 25–38.

7. Einstein A., Podolsky B., Rosen N. Can Quantum-Mechanical Description of Physical Reality be Considered Complete? // UFN, 1936, Vol. 16, pp. 436–457.

8. Veklenko B.A. Superluminal Speeds and Nonequivalence of the Schrödinger's and Heisenberg's Representations in Quantum Electrodynamics [Sverkhsvetovyye skorosti i neekvivalentnost predstavleniy Shryodingera i Geyzenberga v kvantovoy elektrodinamike] // Inzhenernaya fizika, 2013, Vol. 11, pp. 3–9.

9. Kadomtsev B.B. Dynamics and Information [Dinamika i informatsiya] // UFN, 1994, Vol. 164, pp. 449–530.

Boris A. Veklenko,
Prof., Dr. of Phys.-Math. Sc., graduated from the Moscow Power Institute in 1955, defended doctor theses in 1991. At present, he is a Chief Researcher of the JIHT RAS and solves problems of quantum theory of radiation

Light & Engineering
Vol. 28, No. 4, pp. 34–38, 2020

https://dot.org/10.33383/2019-085
Svetotekhnika # 2, 2020, pp. 37–39

ANALYTIC REPRESENTATION OF RELATION BETWEEN SOLAR ALTITUDE ANGLE AND LOCAL TIME FOR CALCULATING DAYLIGHT IRRADIANCE AND ILLUMINANCE OF THE EARTH SURFACE

Alexander V. Leonidov

Senior citizen, Former Researcher of VNISI named after S.I. Vavilov
E-mail: avleonidoff@mail.ru

ABSTRACT

The analytic expression which sets relation between the solar altitude angle and local time at a random point of the Earth surface on a random day of a year is obtained. The obtained expression and derived relations allow one to conduct calculations of daylight irradiance and illuminance of the Earth surface in analytic form.

Keywords: daylight irradiance and illuminance, Earth surface, geocentric equatorial system, analytic form of representation, solar altitude angle, local time, geographic coordinates, year day

1. INTRODUCTION

Daylight illuminance and irradiance of the Earth surface cause determining influence on characteristics of stationary and none-stationary visual processes and characteristics of visual performance [1, 2]. Irradiance caused by solar radiation reaching the surface of the Earth controls circadian activity of human body.

In the course of research of the listed processes, it is quite often necessary to use relation between daily values of solar altitude angle h and local time t_{local} at a design point of the Earth surface with random values of latitude φ on a random day n of a year.

The only publication that presents such data to the fullest extent in the last century was the unique publication [3], which contained the results of the studies conducted in the astrophysical laboratory of the Leningrad University under supervision of Professor V.V. Sharonov. The tabular data presented in [3] include information on relation between solar altitude angle and time of the day with discretisation interval $\Delta t = 1$ hour for different days of a random year with discretisation interval $\Delta n = 10$ days as well as for the values of latitude within the range of $35° \le \varphi \le 70°$ with discretisation interval $\Delta\varphi = 5°$. Tabular representation of data makes it necessary to interpolate within and extrapolate beyond the discretisation intervals used in [3] respectively in the course of lighting engineering calculations. Moreover, tabular representation of data does not allow us to perform lighting engineering calculations in analytic form, which complicates possibilities to use the obtained results and to interpret them substantially.

Nowadays, the copyright holder of [3], which is a rare book, is the University of California. That arouses doubts on the possibility of the book [3] republication in Russia.

Inaccessibility of [3] and general trend of mathematical formalisation of results of lighting engineering studies have defined the main goal of this article: analytic representation of the data on relation between solar altitude angle and local time at a random point of the Earth surface required for calculating its daylight irradiance and illuminance.

Another goal of the work related to active exploration of the polar regions of the Earth is necessity of widening the range of values of latitudes of the Earth surface between the Equator and the North and the South poles of the Earth.

2. USED DATA AND METHODS

Daily and yearly changes of characteristics of illuminance and irradiance of the Earth surface are conditioned by a large amount of spatial motions of the Earth with the most significant of them being daily rotation of the Earth and its movement around the Sun characterised by low orbit eccentricity of the Earth $e = 0.0167$ (the shape of the Earth orbit is nearly circular) [4]. Exclusion of less important motions (Earth axis precession and nutation, etc.) out of consideration, don't introduce any significant errors in the results of lighting engineering calculations.

To obtain an analytic expression relating solar altitude angle during daytime and geographic coordinates of a design point of the Earth surface and local time of central meridian $\xi_{central}$ of a time zone N corresponding with it, the spherical model of the Earth and geocentric equatorial system of the II type [5–7] presented in Fig. 1 were used.

This coordinate system is a projection of geographic coordinates of the Earth surface on an imaginary celestial sphere. The plane perpendicular to the main axis and crossing the centre of the Earth is the main plane, the celestial equator plane, which divides the celestial sphere into the northern and the southern celestial hemispheres and is a projection of the Earth equator on the celestial sphere. The celestial points P and P' lie in the celestial meridian plane. The axis P, P' is the main axis (celestial axis) coincident with the Earth axis. The celestial meridian is a projection of the earth meridian plane on the celestial sphere at a design point of the Earth surface.

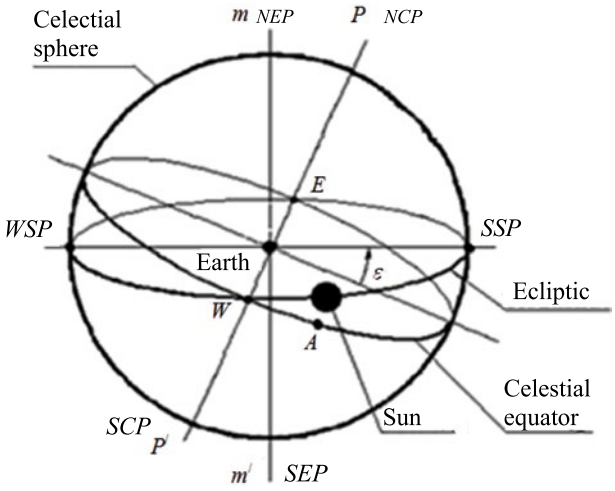

Fig. 1. Geocentric equatorial coordinates system of the II type [5–7]:
NEP – northern ecliptic pole, *NCP* – world northern pole, *SSP* –summer solstice point, *SEP* – southern ecliptic pole, *SCP* – world southern pole, *WSP* - winter solstice point

Visible yearly motion of the Sun centre occurs along the ecliptic. The points m and m' are the northern and the southern ecliptic poles (NEP and SEP respectively). The angle ε between the ecliptic plane and the celestial equator plane equals to $\varepsilon = 23.45°$ [4]. The ecliptic and the celestial equator cross each other at two points: at the western point W which is the vernal equinoctial point and at the eastern point E which is the autumnal equinoctial point. On a random day of the year, the point corresponding to the current position of the Sun centre lies in the celestial meridian plane crossing the celestial axis P, P'.

The great circle of the celestial sphere (declination circle) is the celestial meridian crossing the centre of the Sun, the celestial axis P, P' and crossing the celestial equator at point A. Angular distance between the declination circle and the vernal equinoctial point W measured along the celestial equator is the Sun's right ascension measured in time units, and the angular distance between the centre of the Sun and the point A of the celestial equator in the declination circle is the solar declination (solar declination is positive north of the celestial equator and negative south of the celestial equator).

Since lighting engineering calculations are performed on the surface of the Earth, hereinafter time is used with day duration of 24 hours [4], and the moment of the Sun inferior culmination at the vernal equinoctial point corresponding to 00 hours and 00 minutes of the local time of a selected time zone

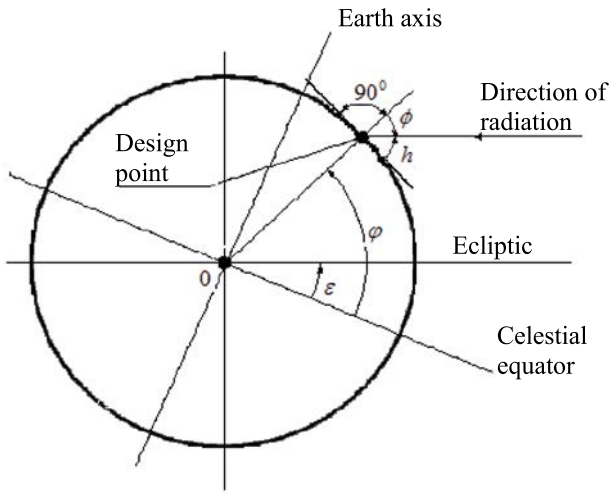

Fig. 2. To the calculation of the angular height of the sun above the horison h

is taken as zero time of the day. The moment of the Sun inferior culmination at the vernal equinoctial point is also taken as a point corresponding to the reference point of year day numbers.

It is convenient to use the projection of the solar declination circle on the Earth surface presented in Fig. 2 to determine the dependence of solar altitude angle on local time.

Solar altitude angle h relative to the horizon (without consideration of solar radiation refraction) is measured within the solar declination circle corresponding to a specific day of the year, current local time and geographic coordinates of the design point of Earth surface.

In the case of the northern hemisphere of the Earth, solar altitude angle above the horizon [5–7] equals to

$$h = 90^0 - \varphi + \varepsilon. \quad (1)$$

For the southern hemisphere, this relation is written as:

$$h = 90^0 + \varphi - \varepsilon. \quad (2)$$

In the relations (1, 2), ε is the angle between the celestial equator plane coincident with the Earth equator plane and the ecliptic plane.

3. RESULTS

Low eccentricity of the Earth orbit making Earth angular velocity relative to the Sun almost constant, the assumptions described above as well as the relations (1, 2) allow us to obtain representation of the sought dependence of solar altitude angle on local time in the geocentric equatorial system. This dependence is represented in the form of the sum of two periodic components corresponding to yearly orbital motion of the Earth around the Sun and daily rotation of the Earth. For the northern and the southern hemispheres, these expressions are written respectively as:

$$h(n,\varphi,t_{local}) = \\ = \varepsilon \sin\Phi(n) - (90^0 - \varphi)\cos\psi(t_{local}), \quad (3)$$

$$h(n,\varphi,t_{local}) = \\ = -\varepsilon \sin\Phi(n) + (90^0 + \varphi)\cos\psi(t_{local}), \quad (4)$$

where Φ is the current phase of yearly orbital motion of the Earth around the Sun, n is the number of full days since zero time, ψ is the current phase of the daily Earth rotation, t_{local} is the local time corresponding to the standard (winter) time for the central meridian ξ_{centre} of the time zone N where the design point of the Earth surface is located, φ is the latitude of the design point.

It is obvious that, in the specified conditions and with consideration of the taken zero time equal to 00 hours and 00 minutes of vernal equinox in the northern hemisphere of the Earth, the expressions for phases $\Phi(n)$ and $\psi(t_{local})$ in the relations (3) and (4) are written as $\Phi(n) = \frac{2\pi n T_{day}}{T_{year}}$, $\psi(t_{local}) = \frac{2\pi t_{local}}{T_{day}}$.

In the relations for phases $\Phi(n)$ and $\psi(t_{local})$, $T_{day} = 24$ *h* is duration of the day, $T_{year} = 8760$ *h* [4] is duration of the year.

Standard (winter) local time t_{local} ($0 \le t_{local} \le 24$ hours) for the central meridian of a random time zone N ($0 \le N \le 23$) is described by means of the following relation:

$$t_{local} = UTC + N, \quad (5)$$

where *UTC* is the Coordinated Universal Time.

The data related to the northern hemisphere of the Earth are of the greatest interest for Russian specialists.

With consideration of the above mentioned expressions for current values of phase $\Phi(n)$ and $\psi(t_{local})$, the relation (3) allows one to calculate dependence of the solar altitude angle on local time for random geographic coordinates of the Earth surface in a specific time zone *N*.

The inverse function for the relation (3) which describes dependence of local time $t_{local}(h)$ and solar altitude angle for values of n and φ within the ranges of $0 \le n \le 365$ and $0° \le \varphi \le 90°$ is written as:

$$t_{local}(h) = \\ = \begin{cases} \frac{T_{day}}{2\pi}\arccos\left[\frac{1}{(90-\varphi)}\left(\varepsilon \sin\frac{2\pi n T_{day}}{T_{year}} - h\right)\right] \text{ first} \\ \text{half of the day,} \\ \frac{T_{day}}{2\pi}\left\{2\pi - \arccos\left[\frac{1}{(90-\varphi)}\left(\varepsilon \sin\frac{2\pi n T_{day}}{T_{year}} - h\right)\right]\right\} \\ \text{second part of the day.} \end{cases} \quad (6)$$

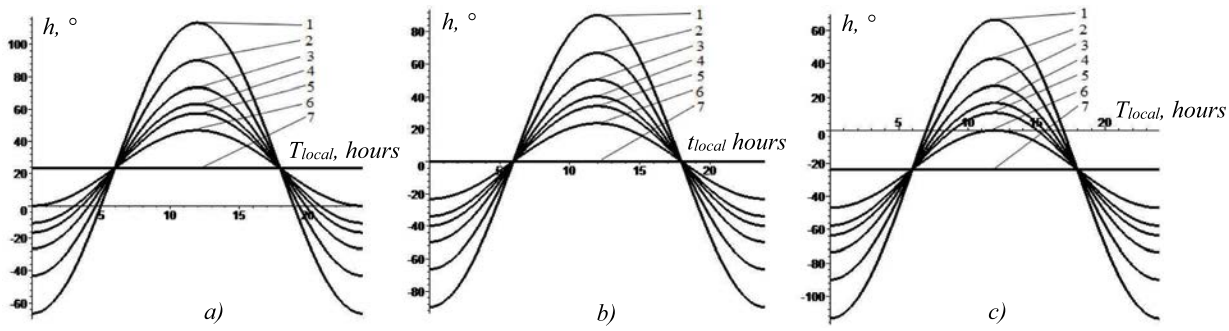

Fig. 3. Dependences of solar altitude angle on local time and geographic latitude of the design point of the Earth surface: ***a)*** n = 91 (June 22), ***b)*** n = 0 (March 21) and n = 182 (September 22), ***c)*** n = 273 (December 22), 1 – φ = 00.00°, 2 – φ = 23.45°, 3 – φ = 40.00°, 4 – φ = 50.00°, 5 – φ = 55.90°, 6 – φ = 66.55°, 7 – φ = 90.00°

The expressions for calculating local sunrise time t_{srise} and sunset time t_{sset} as well as day duration ($t_{sset} - t_{srise}$) directly follow from the relation (6) with h = 0°.

The relation (3) allows us also to calculate the values of solar altitude angle corresponding to the superior culmination (t_{local}=12 hours) and the inferior culmination (t_{local}=00 hours) of the Sun with random combinations of the values of n and φ which lie within the ranges $0 \le n \le 365$ and $0° \le \varphi \le 90°$.

The following relation describes solar altitude angle for the superior culmination:

$$h_{culm.top} = \varepsilon \sin \frac{2\pi n T_{day}}{T_{year}} + \left(90^0 - \varphi\right), \qquad (7)$$

and the following one describes that for the inferior culmination:

$$h_{culm.lower} = \varepsilon \sin \frac{2\pi n T_{day}}{T_{year}} + \left(-90^0 + \varphi\right). \qquad (8)$$

4. DISCUSSION OF RESULTS

As an example, Fig. 3 shows dependences of solar altitude angle and local time as per the expression (3) for different values of geographic latitude φ on the day of summer solstice (n = 91), on the days of vernal and autumnal equinoxes (n = 0, n = 182) and on the day of winter solstice (n = 273).

The projections of the nodes of the curve set presented in Fg. 3 on the local time axis correspond to sunrise and sunset times at a latitude φ = 23.45° on the vernal and autumnal equinox days.

The intercepts of the curves in Fig. 3 with the time axis correspond to local sunrise and sunset times for the central meridian of the considered time zone N and fully correspond to values calculated using the relation (6) with h = 0°.

On the day of the winter solstice in the northern hemisphere, increase in the values of latitude from φ = 00.00° to φ = 90.00° in the expression (7) leads to decrease in maximum daily values of solar altitude angle from h = 66.55° to h = –23.45°. On the days of the vernal equinox n = 0 (March 21) or the autumnal equinox n=182 (September 22), on the days of the summer solstice n = 91 (June 22) and the winter solstice n = 273 (December 22) in the northern hemisphere, the increase in values of latitude of the design point of the Earth surface in the expression (7) from φ = 00.00° to φ = 90.00° lead to decrease in maximum values of solar latitude angle from h = 90.00° to h = 00.00°, from h = 113.45° to h = 23.45° and from h = 66.55° to h = –23.45° respectively.

Comparison of the results of the calculations using the relations (3, 4, 6–8) shows that they are fully coincident with the data provided in [3]. The results of the calculations using the expressions (3, 4, 6–8) also fully comply with the description of instantaneous position and motion of the Sun along the imaginary celestial sphere provided in [5, 7].

Similar results may be obtained using the above mentioned relations for any values of latitude in the northern and southern hemisphere of the Earth on a random day of the year.

5. CONCLUSION

The results obtained in this work allow us to formalise and significantly simplify calculations of daylight irradiance and illuminance of the Earth surface, to make it possible to determine the analytic form of the influence of solar radiation on characteristics of different visual processes, visual performance and circadian activity of human body. Moreover, the results of the work may be used in other

areas of human activity, e.g. in architecture, biophysical studies, research of different aspects of relations between the Sun and the Earth and geophysical processes, in climatology, etc.

REFERENCES

1. Meshkov V.V., Matveev A.B. Basics of Lighting Engineering: Study Guide for Higher Education Institutions. In 2 parts. P. 2. Physiological Optics and Colorimetry [Osnovy svetotekhniki: uchebnoye posobiye dlya vuzov: v 2 ch. Ch. 2. Fiziologicheskaya optika i kolorimetriya]. 2nd edition, revised and supplemented. Moscow: Energoatomizdat, 1989, 432 p.

2. Kravkov S.V. The Eye and its Performance. Psychophysiology of Vision, Lighting Hygiene [Glaz i ego rabota. Psikhofiziologiya zreniya, gigiena osvescheniya]. 4th ed., revised and supplemented. Moscow, Leningrad: Academy of Sciences of the USSR, 1950, 531 p.

3. Tables for Calculating Daylight Illuminance and Visibility. Compiled by the Astrophysical Laboratory of the Leningrad University under Supervision of Professor V.V. Sharonov [Tablitsy dlya raschyota prirodnoy osveschyonnosti i vidimosti. Sostavleny astrofizicheskoy laboratoriyey Leningradskogo universiteta pod rukovodstvom prof. V.V. Sharonova]. Academy of Sciences of the USSR, 1945, 199 p.

4. C.W. Allen Astrophysical Quantities 3rd.ed. University of London, The Athlone Press. 1973.

5. Kononovich, E.V., Moroz, V.I. General Astronomy: Study Guide [Obschiy kurs astronomii: Uschebnoye posobiye] / Eds. V.V. Ivanov. 2nd edition, revised. Moscow: Editorial URSS, 2004, 544 p.

6. Tsesevich V.P. What and How to Observe in the Sky. Guideline on Arranging and Conducting Amateur Astronomical Observations [Chto i kak nablyudat na nebe. Rukovodstvo k organizatsii i provedeniyu lyubitelskikh nablyudeniy nebesnykh tel]. 6th edition, revised. Moscow: Nauka, 1984, 304 p.

7. Klischenko A.P., Shuplyak V.I. Astronomy: Study Guide for Higher Education Institutions [Astronomiya. Uchebnoye posobiye dlya vuzov]. Moscow: Novoye znaniye, 2004, 224 p.

Alexander V. Leonidov,
Ph.D. in Technical Science, graduated from MPEI in 1970 by speciality light and engineering and sources of light. Currently, he is a retired freelance researcher

Light & Engineering
Vol. 28, No. 4, pp. 39–46, 2020

https://doi.org/10.33383/2019-061
Svetotekhnika #2, 2020, pp. 76–81

ON VARIANTS OF THE MAIN ATMOSPHERIC CORRECTION FORMULA

Olga V. Nikolaeva

M.V. Keldysh Applied Mathematics Institute of the Russian Academy of Sciences, Moscow
E-mail: nika@kiam.ru

ABSTRACT

The article studies the accuracy of the main formula of atmospheric correction allowing us to determine albedo of a underlying (earth) surface based on radiance factor of solar light reflected by the system of atmosphere and underlying surface. The problem of atmospheric correction is considered in three-dimensional geometry with spatial non-uniformity of the underlying surface taken into account. It is demonstrated that the accuracy of albedo recovery depends on the used variant of the main formula.

Keywords: atmospheric correction, radiance factor, surface albedo, multidimensional effects

1. INTRODUCTION

During Earth remote sensing, the values of intensity (raiance) of solar radiation (SR) reflected by the system of atmosphere and underlying surface (US) are measured. The measured values of intensity and the known values of extraatmospheric intensity of SR allow one to calculate the radiance factor (RF). Atmospheric correction is required to remove atmospheric distortions from the radiance factor and to determine the reflectance of the Earth surface (albedo). The obtained values of albedo may be further used to determine the surface composition and properties.

In atmospheric correction problems, atmosphere is usually assumed to be horizontally homogeneous and the surface is assumed to be heterogeneous. The surface and the upper border of the atmosphere are divided into pixels. The main atmospheric correction formula relates albedo in Earth pixels and values of RF in atmospheric pixels.

Originally, the main formula was found on the basis of assumption that light gets into an atmospheric pixel only from the Earth pixel located right underneath it. In other words, the problem was solved in Independent Pixel Approximation (IPA). And SR intensity in the problem with random value of the surface albedo was represented by a combination of intensity of light from a black (non-reflecting) US and from a red (isotropic emitting light) US [1]. The formula allows us to determine exactly the US albedo based on the value of RF. This formula is actively used in atmospheric correction problems [2].

With increase of spatial resolution, it became necessary to take into account what contribution is made by light reflected from each Earth pixel to the signal registered in each atmospheric pixel. Two methods are used here.

The first method is based on empirical generalisation of the IPA model, in which RF in an atmospheric pixel depends on albedo in the corresponding Earth pixel and albedo of surroundings of this pixel [3]. It is possible to use an explicit and thus fast algorithm, in which first all surrounding albedos are found and then albedos of all Earth pixels are found [3–5].

In the second method, a system of nonlinear equations is built considering not only reflection of light from an earth's pixel to an atmospheric one but also re-reflection between earth's pixels [4]; unknown variables are albedos of all earth's pixels. The process of solving such system of equation is extremely time-consuming. Required time may be

slightly reduced by simplifying the system of equations by excluding re-reflection between earth's pixels located far from each other. For atmospheric correction in mountainous regions during modelling of re-reflection between earth's pixels, terrain should be taken into account [5].

In [6], the formula of atmospheric correction explicitly relating albedo in each Earth pixel with RF in all atmospheric pixels is proposed. The formula allows one to quickly find albedo in each pixel with consideration of re-reflection from other pixels [7]. The formula is based on representation of SR intensity in the task with random value of albedo as a linear combination of intensities in the problem with black US and in problems with US having one white pixel (reflecting the entire radiation in accordance with the Lambert law) and remainder black pixels.

This work proposes another explicit formula using the conventional linear combination of intensities in the problem with black surface and in problems with one red pixel and remaining black pixels. The matter of identity of these formulas and their accuracies for recovery of albedo of a spatially non-uniform surface is also considered.

2. THE PROBLEM OF LIGHT TRANSFER IN THE ATMOSPHERE

Let us consider the problem of transfer of monochromatic light in a three-dimensional area, Fig. 1.

$$\hat{T}^{3D} I = \mu \frac{\partial I}{\partial z} + \xi \frac{\partial I}{\partial x} + \eta \frac{\partial I}{\partial y} + k(x,y,z) I(x,y,z,\mu,\varphi) - k_s(x,y,z) \int_{\Omega} P(x,y,z,\gamma_s(\mu,\mu',\varphi,\varphi')) I(x,y,z,\mu',\varphi') d\mu' d\varphi' = 0, \quad (1)$$

$$-X < x < X, \quad -Y < y < Y, \quad 0 < z < H, \quad -1 < \mu < 1, \quad 0 < \varphi < 2\pi, \quad (2)$$

$$\xi = \sin\theta\cos\varphi, \ \eta = \sin\theta\sin\varphi, \ \mu = \cos\theta, \quad \gamma_s(\mu,\mu',\varphi,\varphi') = \mu\mu' + \sqrt{1-\mu^2}\sqrt{1-(\mu')^2}\cos(\varphi-\varphi'). \quad (3)$$

The solution $I(x,y,z,\mu,\varphi)$ here is the SR intensity at a spatial point with coordinates (x,y,z) in the $\Omega(\mu=\cos\theta,\varphi)$ direction, Fig. 1. The extinction factor $k(x,y,z)$, the scattering factor $k_s(x,y,z)$, and the scattering indicatrix $P(x,y,z,\gamma_s)$ generally depend both on the height *z* and horizontal coordinates *x*, *y*. The scattering indicatrix depends on $\gamma_s(\mu, \mu', \varphi, \varphi')$, cosine of the angle between the directions (μ,φ) and (μ',φ').

At the upper border, z=0, of the three-dimensional area $-X < x < X$, $-Y < y < Y$, $0 < z < H$, Fig. 1, the condition of incident parallel beam of SR rays in the direction $\Omega_0\,(\mu_0 = \cos\theta_0, \varphi_0)$ is set:

$$I(x,y,0,\mu,\varphi) = I_0\,\delta(\mu-\mu_0)\delta(\varphi-\varphi_0) \quad \text{at } \mu > 0,\ -X < x < X,\ -Y < y < Y. \quad (4)$$

Here I_0 is the extraatmospheric SR and δ is the Dirac delta function.

At the lower border *z* = *H*, let us set reflection from the surface according to the Lambert law

$$I(x,y,H,\mu,\varphi) = A(x,y)\frac{1}{\pi}\int_0^1 d\mu'\,\mu' \int_0^{2\pi} d\varphi'\, I(x,y,H,\mu',\varphi') \quad \text{at } \mu < 0,\ -X < x < X,\ -Y < y < Y, \quad (5)$$

where $A(x,y)$ is the albedo of the US at the point (x,y). We will assume that the US is divided into *N* non-intersecting pixels U_j. Let us set surface albedo within each pixel with its mean value:

$$A_j = \frac{1}{|U_j|}\iint_{U_j} dx\,dy\,A(x,y), \quad (6)$$

where $|U_j|$ is the area of the *j*-th pixel. At irradiated side borders where $\gamma_s(\mu,\mu_0,\varphi,\varphi_0) > 0$, the bound-

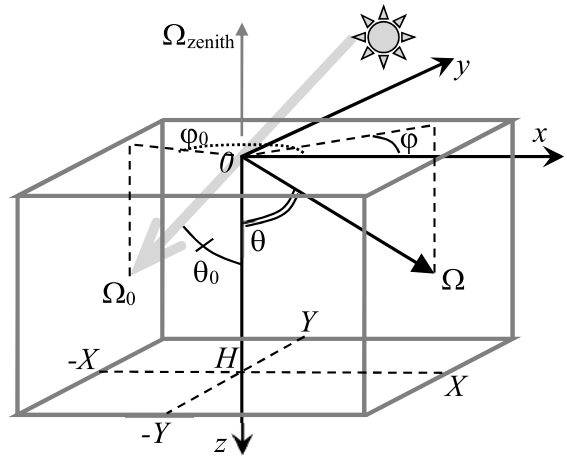

Fig. 1. Area of the solution of the solar light transfer equation

ary condition in the form of (4) is set. At non-irradiated side borders where $\gamma_s(\mu,\mu_0,\varphi,\varphi_0)<0$, zero boundary condition is set. Thus, we have the relations:

$$I(-X,y,z,\mu,\varphi)=J(\mu,\varphi) \quad \text{at } \xi>0,$$

$$-Y<y<Y,\quad 0<z<H, \tag{7}$$

$$I(X,y,z,\mu,\varphi)=J(\mu,\varphi) \quad \text{at } \xi<0,$$

$$-Y<y<Y,\quad 0<z<H, \tag{8}$$

$$I(x,-Y,z,\mu,\varphi)=J(\mu,\varphi) \quad \text{at } \xi>0,$$

$$-X<x<X,\quad 0<z<H, \tag{9}$$

$$I(x,Y,z,\mu,\varphi)=J(\mu,\varphi) \quad \text{at } \xi<0,$$

$$-X<x<X,\quad 0<z<H, \tag{10}$$

where

$$J(\mu,\varphi)=I_0\,\delta(\mu-\mu_0)\delta(\varphi-\varphi_0)$$
$$\text{при } \gamma_s(\mu,\mu_0,\varphi,\varphi_0)>0$$

$$J(\mu,\varphi)=0 \text{ при } \gamma_s(\mu,\mu_0,\varphi,\varphi_0)<0. \tag{11}$$

We will consider the average values of RF of each atmospheric pixel as a solution of the task (1)–(11)

$$R_j=\frac{1}{|U_j|}\frac{\pi}{\mu_0 I_0}\iint\limits_{U_j} dx\,dy\,I(x,y,0,\tilde{\mu},\tilde{\varphi}). \tag{12}$$

The coordinates $(\tilde{\mu},\tilde{\varphi})$ define the direction of reflected SR. Then only the zenith reflection $\Omega_{\text{zenith}}(\tilde{\mu}=-1,\tilde{\varphi}=0)$ is considered, Fig. 1. It should be noted that further speculations are also correct for other directions$(\tilde{\mu},\tilde{\varphi})$.

Let us also determine the transmittance factor of the atmosphere for each Earth pixel

$$T_j=\frac{1}{|U_j|\pi I_0}\iint\limits_{U_j} dx\,dy\int\limits_0^1 d\mu'\mu'\int\limits_o^{2\pi} d\varphi'\,I(x,y,H,\mu',\varphi'). \tag{13}$$

3. UNDERLYING SURFACE ALBEDO DETERMINATION

Let us find an explicit dependence of RF and US albedos. For this purpose, let us introduce basic functions for solving the following problems.

The tasks with black US:

$$\hat{T}^{3D}I^b=0, I^b(x,y,H,\mu,\varphi)=0 \text{ at } \mu<0,$$

$$I^b(x,y,0,\mu,\varphi)=$$
$$=I_0\,\delta(\mu-\mu_0)\delta(\varphi-\varphi_0) \text{ at } \mu>0. \tag{14}$$

The tasks with the US containing one white pixel and remaining black pixels:

$$\hat{T}^{3D}I_i^w=0,$$

$$I_i^w(x,y,0,\mu,\varphi)=$$
$$=I_0\,\delta(\mu-\mu_0)\delta(\varphi-\varphi_0) \text{ at } \mu>0, \tag{15}$$

$$I_i^w(x,y,H,\mu,\varphi)=$$
$$=a_i(x,y)\frac{1}{\pi}\int\limits_0^1 d\mu'\,\mu'\int\limits_0^{2\pi} d\varphi'\,I_i^w(x,y,H,\mu',\varphi') \text{ at } \mu<0,$$

$$a_i(x,y)=0 \text{ at } (x,y)\notin U_i,\ a_i(x,y)=1 \text{ at } (x,y)\in U_i.$$

The tasks with the US containing one red pixel and remaining black pixels

$$\hat{T}^{3D}I_i^r=0,\ I_i^r(x,y,0,\mu,\varphi)=0 \text{ at } \mu>0,$$

$$I_i^r(x,y,H,\mu,\varphi)=a_i(x,y)I_0 \text{ at } \mu<0. \tag{16}$$

In the tasks (14) and (15), boundary conditions (7)–(10) are used at side borders and in the task (16), zero boundary conditions are used.

Let us represent the solution of the problem (1)–(11) as a linear combination of the "black" and the "red" basic functions, the solutions of the problems (14) and (16):

$$I(x,y,z,\mu,\varphi)=$$
$$=I^b(x,y,z,\mu,\varphi)+\sum_{i=1}^{N}\gamma_i\,I_i^r(x,y,z,\mu,\varphi). \tag{17}$$

Really, with any values of γ_i, the function (17) complies with the equation (1) and boundary conditions (4), (7)–(10). The boundary condition (5) in the *j*-th pixel for the function (17) may be written as

$$\gamma_j=\left[\sum_{i=1}^{N}\gamma_i\,T_{j,i}^r+T_j^b\right]A_j,\ j=1,\ldots,N, \tag{18}$$

where $T_{j,i}^r$ and T_j^b are transmittance factors (13) for the basic tasks averaged over the *j*-th Earth pixel

$$T^r_{j,i}=\frac{1}{|U_j|\pi I_0}\iint\limits_{U_j} dxdy\int\limits_0^1 d\mu'\mu'\int\limits_0^{2\pi} I^r_i(x,y,H,\mu',\varphi'), \quad (19)$$

$$T^b_j=\frac{1}{|U_j|\pi I_0}\iint\limits_{U_j} dxdy\int\limits_0^1 d\mu'\mu'\int\limits_o^{2\pi} d\varphi' I^b(x,y,H,\mu',\varphi').$$

Let us introduce two vectors and two matrices:

$$\gamma\{\gamma_j\},\ \hat{\mathbf{A}}\{A_{i,j}=A_j\,\delta_{i,j}\},$$

$$\mathbf{t}^b\{T^b_j\},\ \hat{\mathbf{T}}^r\{T^r_{j,i}\}. \quad (20)$$

Here, $\delta_{i,j}$ is the Kronecker delta. Then the system (18) takes on the following form

$$\gamma=\hat{\mathbf{A}}(\mathbf{t}^b+\hat{\mathbf{T}}^r\gamma).$$

From here, we find the vector γ of unknown values from the factorisation (17)

$$\gamma=\left(\hat{\mathbf{E}}-\hat{\mathbf{A}}\,\hat{\mathbf{T}}^r\right)^{-1}\hat{\mathbf{A}}\mathbf{t}^b. \quad (21)$$

Here, $\hat{\mathbf{E}}$ is the identity matrix. From the expression (17) let us find the RF in the *j*-th pixel

$$R_j=R^b_j+\sum_{i=1}^{N}\gamma_i\,R^r_{j,i}. \quad (22)$$

Here, R^b_j and $R^r_{j,i}$ are the values of RF (12) in the *j*-th pixel for the basic tasks

$$R^b_j=\frac{1}{|U_j|}\frac{\pi}{\mu_0 I_0}\iint\limits_{U_j} dx\,dy\,I^b(x,y,0,-1,0),$$

$$R^r_{j,i}=\frac{1}{|U_j|}\frac{\pi}{\mu_0 I_0}\iint\limits_{U_j} dx\,dy\,I^r_i(x,y,0,-1,0). \quad (23)$$

Let us rewrite the expression (22) in the matrix form

$$\mathbf{r}=\mathbf{r}^b+\hat{\mathbf{R}}^r\gamma, \quad (24)$$

where

$$\mathbf{r}\{R_j\},\ \mathbf{r}^b\{R^b_j\},\ \hat{\mathbf{R}}^r\{R^r_{j,i}\}. \quad (25)$$

By substituting (21) in (24), we obtain the relation

$$\mathbf{r}=\mathbf{r}^b+\hat{\mathbf{R}}^r\left(\hat{\mathbf{E}}-\hat{\mathbf{A}}\,\hat{\mathbf{T}}^r\right)^{-1}\hat{\mathbf{A}}\mathbf{t}^b.$$

This expression is transformed as

$$(\hat{\mathbf{E}}-\hat{\mathbf{A}}\,\hat{\mathbf{T}}^r)(\hat{\mathbf{R}}^r)^{-1}(\mathbf{r}-\mathbf{r}^b)=\hat{\mathbf{A}}\mathbf{t}^b,$$

or

$$(\hat{\mathbf{R}}^r)^{-1}(\mathbf{r}-\mathbf{r}^b)=\hat{\mathbf{A}}\left[\mathbf{t}^b+\hat{\mathbf{T}}^r(\hat{\mathbf{R}}^r)^{-1}(\mathbf{r}-\mathbf{r}^b)\right].$$

Let us introduce the vectors

$$\mathbf{u}=(\hat{\mathbf{R}}^r)^{-1}(\mathbf{r}-\mathbf{r}^b),$$

$$\mathbf{w}=\mathbf{t}^b+\hat{\mathbf{T}}^r(\hat{\mathbf{R}}^r)^{-1}(\mathbf{r}-\mathbf{r}^b). \quad (26)$$

Then the surface albedo in the *j*-th pixel is determined by relation of the elements of these vectors

$$A_j=u_j/w_j. \quad (27)$$

In [6], the values of albedo are obtained by representation of solution of the problem (1)–(11) as a linear combination of the "black" and "white" basic functions: solutions of the problems (14) and (15):

$$A_j=q_j/v_j, \quad (28)$$

where

$$\mathbf{q}=\hat{\mathbf{T}}^{ww}(\hat{\mathbf{R}}^{wb})^{-1}(\mathbf{r}-\mathbf{r}^b),$$

$$\mathbf{v}=\hat{\mathbf{T}}^{wb}(\hat{\mathbf{R}}^{wb})^{-1}(\mathbf{r}-\mathbf{r}^b)+\mathbf{t}^b, \quad (29)$$

$$\hat{\mathbf{R}}^{wb}\{R^{wb}_{j,i}=R^w_{j,i}-R^b_j\},\ \hat{\mathbf{T}}^{wb}\{\mathrm{T}^{wb}_{j,i}=T^w_{j,i}-T^b_j\},$$

$$\hat{\mathbf{T}}^{ww}\{T^w_{i,j}=T^w_{i,i}\,\delta_{i,j}\}. \quad (30)$$

It should be stressed that, in formulae (27), (28), the matrices $\hat{\mathbf{R}}^r$, $\hat{\mathbf{R}}^{wb}$, $\hat{\mathbf{T}}^r$, $\hat{\mathbf{T}}^{wb}$, $\hat{\mathbf{T}}^{ww}$ and the vectors $\mathbf{t}^b$, $\mathbf{r}^b$ describe reflectance and transmittance of the atmosphere for the basic tasks (14)–(16) with consideration of multiple scattering of radiation in the atmosphere and do not depend on the US albedo.

The relations (27), (26) and (28), (29) are the two variants of the main atmospheric correction formula allowing us to find the US albedo based on the values of reflected RF. Each variant of discretisation of the direct problem corresponds to each variant of the main formula. It is not necessary to find the solution of the system of non-linear equations as in the algorithm [6] and to use an iteration process.

It should be noted that, to transfer to the IPA, it is necessary to find mean values of all elements of the matrixs $\hat{\mathbf{R}}^r$, $\hat{\mathbf{T}}^r$ and the vectors $\mathbf{r}^b$ and $\mathbf{t}^b$:

$$\tilde{R}^r=\frac{1}{N}\sum_{j=1}^{N}\sum_{i=1}^{N}R^r_{i,j},\ \tilde{T}^r=\frac{1}{N}\sum_{j=1}^{N}\sum_{i=1}^{N}T^r_{i,j},$$

Table 1. Errors (%) in Determining Albedos by Formulas (27) and (28) According to Pixel Dimension *d* and Aerosol Optical Thickness τ^{aer} Separately for Pixels Located on and outside of the Boundaries of the Media

	τ^{aer}=0.2				τ^{aer}=0.4				τ^{aer}=0.8			
	On the media boundaries		Outside media boundaries		On the media boundaries		Outside media boundaries		On the media boundaries		Outside media boundaries	
d, km	(27)	(28)	(27)	(28)	(27)	(28)	(27)	(28)	(27)	(28)	(27)	(28)
0.25	0.031	0.027	0.091	0.077	0.075	0.069	0.071	0.073	0.071	0.065	0.41	0.26
0.5	0.059	0.053	0.039	0.04	0.12	0.11	0.07	0.07	0.27	0.21	0.1	0.1
1	0.085	0.075	0.13	0.11	0.04	0.05	0.14	0.19	1.01	0.91	1.27	1.07

$$\tilde{r}^b = \frac{1}{N}\sum_{j=1}^{N} R_j^b\,,\ \tilde{t}^b = \frac{1}{N}\sum_{j=1}^{N} T_j^b\,,$$

where $\tilde{R}^r$ and $\tilde{r}^b$ are the mean RF of an image in the tasks with red and black surfaces, $\tilde{T}^r$ and $\tilde{t}^b$ are the mean transmittance factors of an image in these problems. In IPA approximations, the formula (27) of albedo is written as

$$A_j = [R_j - \tilde{r}^b\,]\big/[\tilde{R}^r\,\tilde{t}^b + \tilde{T}^r\,(R_j - \tilde{r}^b)]. \qquad (31)$$

A question whether the formulas (27) and (28) are equivalent arises. Indeed, the radiation emitted by the red pixel does not depend on the light incident on that pixel whereas the light emitted by the white pixel does. The surface of the red pixel is assumed spatially uniform whereas the surface of the white pixel is not. Below the question of equivalency of the formulas (27) and (28) is studied quantitatively,

4. QUANTITATIVE RESULTS

Let us consider the layer of standard atmosphere [8]. We will use the microphysical aerosol model developed for Belarus [9]. We will consider the extinction factor *k*, the scattering factor k_s and the scattering indicatrix $P(\gamma_s)$ as independent of spatial coordinates. Let us find these magnitudes using the Mi-theory [10] for wavelength λ = 0.55μm. It should be noted that the correction formulae (27) and (28) are obtained without any assumptions regarding SR wavelength.

At the first stage, the atmosphere is assumed to be transparent: for aerosol optical thickness τ^{aer} the values of 0.2, 0.4 and 0.8 are used. Rayleigh scattering optical thickness is found using the formula

$$\tau = 0.008569\,\lambda^{-4}\,(1 + 0.0113\,\lambda^{-2} + \\ + 0.00013\,\lambda^{-4})\big|_{\lambda=0.55\ \mathrm{mkm}} \approx 0.097\ [11].$$

Zenith angle of the Sun $\theta_0 = 40^o$ is selected.

The thickness of the atmospheric layer is assumed to be equal to 100 km. Let us consider the region [–5, 5]×[–5, 5] on the earth's surface. Three variants of dimensions of the pixel *d*×*d* are selected: *d* = 1 km, *d* = 0.5 km, and *d* = 0.25 km (the latter dimension complies with parameters of MODIS device). A ploughed field (*A* = 0.06858 [12]) with a rapeseed area located in the centre of it (*A*=0.153 [12]) which has a shape of a circle with radius ρ = 2 km is taken as an US.

Let us consider the case when square pixels uniformly cover the surface area. Let us introduce a mesh with step of 3 km along the height *z* and 0.25 km along *x*, *y*. We find the solutions of the tasks (1)–(11) and (14)–(16) by means of mesh-based discrete-ordinates method [13] in three-dimensional (*x*, *y*, *z*) geometry. Using formulas (19) and (23) we find reflectance and transmittance factors and form matrices (20), (25), and (30) using their values. Inverse matrices $(\hat{\mathbf{R}}^{wb})^{-1}$ and $(\hat{\mathbf{R}}^{r})^{-1}$ are found by means of Krylov subspace method. Finally, using the explicit formulas (27) and (28) we find albedos in each pixel.

Table 1 contains errors of albedo determination using formulas (27) and (28) depending on pixel dimension *d* and aerosol optical thickness $\tau^{aer} < 1$. The errors are listed separately for pixels located at and beyond the interface (border of the circle). The error is determined as the highest pixel variations (%) of the calculated albedos from exact ones. It is seen that accuracy of both formulae (27) and (28) are high.

With that, the errors of both formulas are comparable with the same pixel dimensions. Maximum variation of the calculated albedos from each other for all pixels increases with reduction of pixel dimension *d* and increase in optical thickness τ^{aer} but does not exceed 0.15 % for transparent atmosphere, Table 2.

Table 2. Deviations (%) in Calculating Albedos by Formulas (27) and (28) According to Pixel Dimension *d* and Aerosol Optical Thickness τ^{aer}

d, km	τ^{aer}=0.2	τ^{aer}=0.4	τ^{aer}=0.8
0.25	0.017	0.05	0.15
0.5	0.01	0.022	0.07
1	0.006	0.014	0.025

Then let us consider a denser atmosphere with aerosol optical thickness $1 \le \tau^{aer} \le 10$ for the case of the coarsest spatial resolution (pixel dimension *d* = 1km). With increasing τ^{aer} the influence of the surface albedo on RF becomes less, Fig. 2.

That is why the rows of the matrices $\hat{\mathbf{R}}^{wb}$ and $\hat{\mathbf{R}}^{r}$, see formulas (25) and (30), are becoming less recognisable. As consequence, the norms of the matrices used for calculation of albedo using formulas (27) and (28) are increasing, Fig. 3. That is why even low errors in solving the tasks (1)–(11) and (14)–(16) by means of mesh-based method lead to high errors of the determination of albedo. Therefore, the errors of the determination of albedo by means of both formulas (27) and (28) increase with rise of τ^{aer}, Fig. 4. Similarly higher errors of the determination of albedo will be caused even by low errors of RF measurement when processing actual measurements for higher τ^{aer}.

It should be noted that, with higher τ^{aer} for separate pixels, the error of the determination of albedo is significantly lower than maximum pixel error, compare Fig. 4 with Fig. 5. In its turn, the error of the determination of albedo in IPA approximation is much higher than the errors of formulas (27) and (28); the IPA approximation actually can be used with $\tau^{aer} < 1$.

In IPA approximation, the influence of the values of RF in neighbouring atmospheric pixels on the value of albedo in the current Earth pixel is not taken into account. To estimate this influence, let us write (27) and (26) as:

$$A_j = \left[\sum_{k=1,k\neq j}^{N} f_{j,k}(R_k - R_k^b) + f_{j,j}(R_j - R_j^b) \right] \Big/ \left[T_j^b + \sum_{k=1,k\neq j}^{N} g_{j,k}(R_k - R_k^b) + g_{j,j}(R_j - R_j^b) \right] \quad (32)$$

Here, $f_{j,k}$ and $g_{j,k}$ are (*j*, *k*)-th elements of the matrices $(\hat{\mathbf{R}}^{r})^{-1}$ and $\hat{\mathbf{T}}^{r}(\hat{\mathbf{R}}^{r})^{-1}$. Let us select the number *j* corresponding to central (located in the vicinity of the origin of coordinates) atmospheric and Earth pixels. Let us assign its (*x*, *y*) coordinates to each pixel number *k*. We will obtain the influence functions *f*(*x*, *y*) and *g*(*x*, *y*). Since it turns out that the absolute value of *g*(*x*, *y*) is on average less than the value of *f*(*x*, *y*) by two orders of magnitude, major contribution from the neighbouring pixels depends on the function *f*(*x*, *y*). Let us find the normalised influence function

$$\tilde{f}(x,y) = f(x,y)/\max(f(x,y)).$$

In Fig. 6 it can be seen that with increasing τ^{aer} the influence of the neighbouring pixels grows significantly.

At last, let us mention execution time. Solution of one basic task (14), (15) or (16) using a 3.2 GHz processor speed takes about $t_0 = 28$ seconds. To-

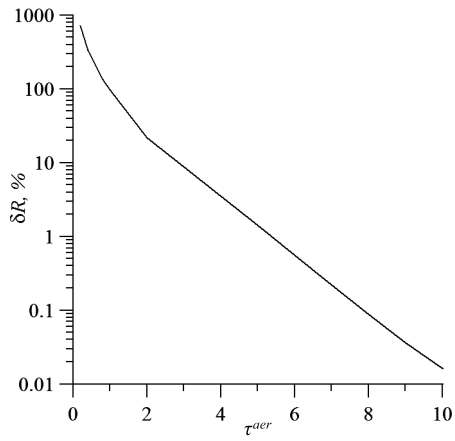

Fig. 2. Maximum pixel variations of luminance factors in problems with reflective (rapeseed area in the ploughed field) and black surfaces, *d* = 1km

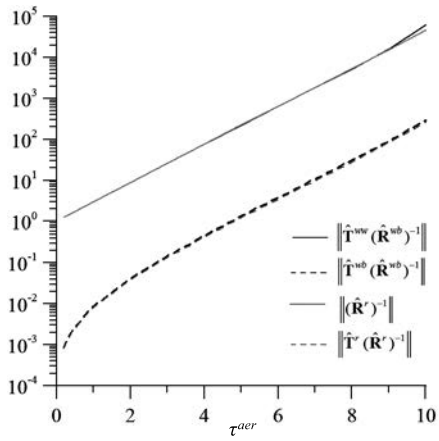

Fig. 3. Norms of the matrices used for determinating albedo, *d* = 1km

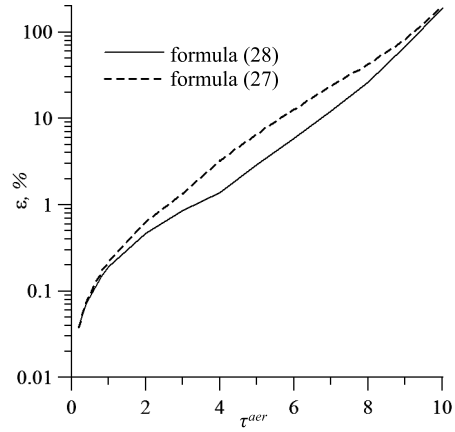

Fig. 4. Maximum pixel errors (%) of the albedo determination, d = 1km

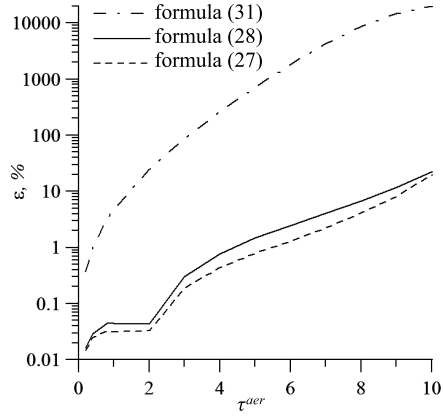

Fig. 5. Errors (%) of the determination of albedo in the central pixel, d = 1km

tal execution time of all basic problems equals to $t_0(2N+1)$ where N is the number of pixels. Time required for inversion of one matrix $\hat{\mathbf{R}}^{wb}$ or $\hat{\mathbf{R}}^{r}$ using the Krylov subspace method is about $(N/100)^4$ seconds.

5. CONCLUSION

The article presents a new variant of the main atmospheric correction formula allowing us to find the values of albedos of spatially non-uniform Lambertian surface using known values of radiance factor of the radiation reflected by the system of atmosphere and underlying surface and known atmosphere parameters. The formula is explicit and allows promptly to recover albedo. Viewing direction is contained in the formula as a free parameter.

In the new variant of the main formula, the solutions of the basic tasks with a black (non-reflective) surface and a surface containing one red pixel (isotropically emitting) and remaining black pixels are used. In the old variant, the basic problems with a underlying surface containing one white pixel (isotropically reflecting) and remaining black pixels are used. The isotropically emitting pixel is assumed spatially uniformed here and the isotropically reflecting one is not.

Two variants of discretisation of the boundary value problem for the solar light atmosphere transfer equation are proposed; each of them leads to the only solution of the problem of recovery of the Earth surface albedo.

Two variants of the formula are compared using the example of the problem of recovery of albedo of a ploughed field which includes an area with vegetation based on nadir measurements. It is demonstrated that both variants of the formula have high accuracy if the surface albedo sufficiently affects the reflected radiance factor, and their accuracy is higher than that of the variant of the formula obtained in the IPA approximation. Therefore, both variants of the formula may be used for atmospheric correction of satellite images.

When applying the presented variants of the atmospheric correction formula to actual satellite images, it is necessary to take into account that the shape of pixels is not set in this formula in any way and different pixels may have different dimensions. Therefore, after selecting a target pixel in an image (where albedo needs to be recovered), it is neces-

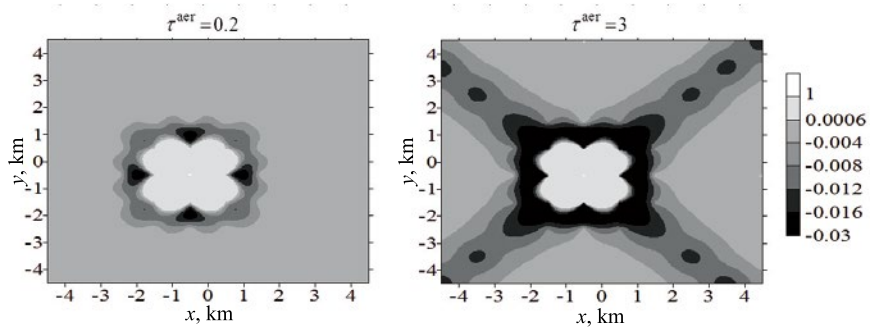

Fig. 6. Normalised influence functions $\tilde{f}(x,y)$, d = 1km

sary to set the surrounding pixels, to calculate radiance factors in them by means of any method of interpolation and then to use the main atmospheric correction formula (such methodology is specified in [7] for the "black-and-white" variant of the formula).

REFERENCES

1. Kaufman Y.J., Tanre D, Gordon H.R., Nakajima T., Lenoble J., Frouin R., Grassl H., Herman B.M., King M.D., Teillet P.M. Passive remote sensing of tropospheric aerosol and atmospheric correction for the aerosol effect // Journal of Geophysical Research, 1997, V. 102, N. D14, pp. 16,815–16,830.

2. Ju J., Roy D.P., Vermote E., Masek J, Kovalskyy V. Continental-scale validation of MODIS-based and LEDAPS Landsat ETM+ atmospheric correction methods // Remote Sensing of Environment, 2012, V. 122, pp. 175–184.

3. ENVI. Atmospheric Correction Module: QUAC and FLAASH User's Guide. 2009. 44 p.

4. Tarasenkov M.V., Belov V.V. A Set of Programmes of Recovery of Reflective Properties of Earth Surface in Visible and UV Ranges [Kompleks programm vosstanovleniya otrazhatelnykh svoistv zemnoy poverkhnosti v vidimom i UF-diapazonakh] // Optika atmosphery i okeana, 2014, Vol. 27, Issue 7, pp. 622–626.

5. Lenot X, Achard V, Poutier L. SIERRA: A new approach to atmospheric and topographic corrections for hyperspectral imagery // Remote Sensing of Environment, 2009, V. 13, pp. 1664–1677

6. Nikolaeva O.V. New Algorithm of Surface Albedo Recovery Based on Sattellite Sensing Data [Novyi algoritm vosstanovleniya albedo poverkhnosti po dannym sputnikovogo zondirovaniya] // Optika atmosphery i okeana, 2016, Vol. 29, Issue 3, pp. 204–209.

7. Nikolaeva O.V. Studying the Accuracy of the Algorithm of Albedo Recovery of a Surface with High Spatial Resolution Using a Fragment of a Satellite Image [Issledovaniye tochnosti algoritma vosstanovleniya albedo poverkhnosti s vysokim prostranstvennym razresheniyem po fragmentu sputnikovogo izobrazheniya] // Optika atmosphery i okeana, 2016, Vol. 29, Issue 7, pp. 541–547.

8. GOST 4401–81: "Standard Atmosphere. Parameters", 2004, 165 p.

9. Katsev I.L., Zaege E.P., Prikhach A.S. Microphisical Model of Aerosol Atmosphere of Belarus and Adjacent Regions [Mikrofizicheskaya model aerozolnoy atmosfery Belarusi i sopredelnykh regionov] // Optika atmosfery i okeana, 2016, Vol. 29, pp. 572–578.

10. Mishchenko M.I., Dlugach J.M., Yanovitskij E.G., Zakharova N.T. Bidirectional reflectance of flat optically thick particulate layers: an efficient radiative transfer solution and applications to snow and soil surfaces // Journal of Quantitative Spectroscopy & Radiative Transfer, 1999, V. 64, pp. 409–432.

11. Hansen J.E., Travis L.D. Light Scattering in Planetary Atmospheres // Space Science Reviews, 1974, V. 16, pp. 527–610.

12. Baula G.G., Brychikhin M.N., Istomina M.N., Krotkov A. Yu., Szhonov E. Yu., Rizvanov A.A., Tretyakov V.N. Formation of the Data Base of Hyperspectral Optical Characteristics of Agricultural Crops in Ultraviolet, Visible and Near-infrared Regions of Spectre [Formirovaniye bazy dannykh giperspektralnykh opticheskikh kharakteristik selskokhozyaystvennykh kultur v ultrfioletovoy, vidimoy i blizhney infrakrasnoy oblastyakh spektra] // Kosmonavtika i raketostroeniye, 2013, Vol. 4, pp. 178–184.

13. Nikolaeva O.V., Bass L.P., Kuznetsov V.S. Raduga-6 – Software for Solution of the Stationary and Non-stationary Radiation Transfer Equations in 1D, 2D and 3D Areas [Raduga-6 – programma resheniya statsionarnogo i nestatsionarnogo uravneniy perenosa izlucheniya v 1D, 2D, 3D oblastyakh]. Abstract Book of the International Symposium "Atmospheric Radiation and Dynamics", Saint Petersburg, June 21–24, 2011, pp. 81–82.

Olga V. Nikolaeva, graduated from the Computational Mathematics Department of the M.V. Lomonosov Moscow State University majoring in Applied Mathematics. At present, she is Senior Researcher of the Applied Mathematics Institute of the Russian Academy of Sciences. Her research interests are the direct and inverse problems for the radiation transfer equation

Light & Engineering
Vol. 28, No. 4, pp. 47–56, 2020

https://doi.org/10.33383/2019-037
Svetotekhnika #2, 2020, pp. 47–55

EFFECTS OF LUMINAIRE ANGLE AND ILLUMINATION TOPOLOGY ON ILLUMINATION PARAMETERS IN ROAD LIGHTING

Mehmet Sait Cengiz

Department of Technical Vocational School, Bitlis Eren University, Turkey
E-mail: msaitcengiz@gmail.com

ABSTRACTS

In this study, refers to two errors in road lighting. It explains the advantages of the staggered layout of luminaires and the problems associated with the use of luminaires located at an angle to the horizontal line of the road. The errors made by the simulation program were proved quantitatively and suggestions for their solution were presented. The loss of luminance of the road surface when illuminated by luminaires located at an angle to the horizontal has been quantitatively proved. In addition, it was found that with the appropriate choice of the layout of luminaires with road lighting, the step between the poles could be reduced by 9.3 %.

Keywords: road lighting, luminaire angle, luminance

1. INTRODUCTION

Primary purpose of road lighting is to ensure safe flow of vehicles or traffic during day and night conditions. Performance of road lighting is evaluated depending on such parameters as illuminance of road surface and walls, overall and longitudinal lighting uniformity, glare control, formation of the contrast required to perceive the objects and flicker frequency [1, 2].

Road lighting improves visibility of pedestrians and other objects. The lighting allows the driver and springs to move safely. Accurately designed road lighting prevents traffic jams and gives people a sense of security.

The driver using any vehicle on highways should have detailed visual information about the way he is driving. Especially at high speeds, the driver should be able to see the route easily, the driver should be able to perceive the position and movements of the vehicle he is driving, be able to monitor the movements of other vehicles, and easily be able to see the obstacles on the road.

CIE reports the results of 30 different studies covering road lighting studies that improve vision conditions. According to this report, fulfillment of road lighting standards: pedestrian accidents decreased from 57 % to 45 %, fatal accidents decreased from 65 % to 48 %, severe injuries decreased from 30 % to 24 %, and the total number of accidents decreased from 53 % to 14 % [3].

Even if there is little traffic at night, the number of accidents that occur on roads or in tunnels without lighting is about three times higher than in daylight hours. The reason for this is the lack of road lighting in accordance with the standards. Ensuring appropriate road lighting to the CIE reduces the rate of crime committed on city roads. According to the studies in the literature, the number of forensic cases on urban roads has decreased by 20 % due to the proper lighting. In terms of the severity of crimes committed, there was a decrease of 40 % [4, 5].

2. ROAD LUMINANCE

The most important objective in design of lighting systems is to obtain sufficient light without supplying excessive lighting and increasing energy cost [6]. Luminance is the most important parameter for

Table 1. Road Lighting Class Selection Parameters

Parameter	Options	Weight factor
Speed	Very high	1
	High	0.5
	Middle	0
Traffic jam	Very high	1
	High	0.5
	Middle	0
	Low	–0.5
	Very low	–1
Traffic layout	Mixed with a high proportion of non-motorized traffic	1
	Mixed	0.5
	Only motor vehicles	0
Middle median strip on the road	Yes	1
	No	0
Intensity of intersection	High	1
	Middle	0
Parked vehicle	Yes	0.5
	No	0
Environmental lighting	High	1
	Middle	0
	Low	–1
Traffic control	Weak	0.5
	Medium or good	0
Total of weight factors		4

road lighting, and L indicates luminance using the cd/m^2 unit. To ensure good visibility of objects and visual comfort of the driver, it is necessary to ensure the uniform distribution of luminance on the road surface. Today, road lighting is based on *ASI* luminance method *Alan*, which is based on road surface luminance. The horizontal illuminance of a point P on an illuminated road is the sum of the horizontal illuminance levels that all the light sources acting at point P have at this point.

2.1. Average Luminance of the Road Surface

In the road lighting, the fund of objects is the road surface that forms the driver's field of view. At the same time, increasing the average luminance of the road surface $L_{average}$ leads to improved visibility, providing more background luminance. Increasing $L_{average}$ increases the sensitivity of the driver's eye by increasing the luminance of the objects located on the road. Therefore, the most important parameter for detection is $L_{average}$. The average luminance is calculated using the glitter values on the selected *mxn* pieces on the road. For $L_{average}$, the luminance values of all the light sources affecting the account area are calculated and collected as vector. In this way, the glare value at each point is calculated. The average luminance of the road surface is calculated separately for each observer [7–9].

2.2. Luminance Uniformity

Although lighting systems provide a good average luminance of the road surface, there may be areas with low luminance where contrast is weak and small obstacles cannot be detected. It is expected that the difference between the minimum and average luminance of the road surface in the field of view will be below a certain value in order to get sufficient lighting at all points of the road. This re-

Table 2. Road Lighting Quality Parameters [18]

Lighting class	$L_{average}$, cd/m^2	U_O	U_I	*TI*, %
M1	>2.0	>0.4	>0.7	<10
M2	>1.5	>0.4	>0.7	<10
M3	>1.0	>0.4	>0.5	<10
M4	>0.75	>0.4	>0.5	<15
M5	>0.50	>0.35	>0.4	<15
M6	>0.30	>0.35	>0.4	<15

quirement leads to the formation of overall and longitudinal uniformity of road surface luminance, which are important secondary characteristics of road lighting.

On the road (on the road surface), there should be an equal distribution of luminance to ensure a clear view for the driver. Two types of uniformity are considered important in road lighting [7–10]. These are overall (resultant) uniformity (U_o) and longitudinal uniformity (U_l).

2.3. Light Sources

High-pressure sodium lamps (HPSL) are preferred in conditions where high levels of brightness are required, including in underwater tunnels, since HPSL have higher luminous flux and are smaller than low-pressure lamps. In previous studies, the photometric properties of luminaires used in road lighting with HPSLs and luminaires with LEDs were compared. In the study, it was shown that lighting of roads of classes *M*3, *M*4, and *M*5 could be ensured by luminaires with LED power of 100 W and 150 W. However, for roads of classes *M*1 and *M*2, these luminaires did not provide the required level of illumination. Since the object of this study is a road of class *M*2 in terms of lighting, the luminaires based on LED are not considered here, but the luminaires with HPSL, which are widely used for road lighting, are considered. As a result, this study simulation was performed with HPSLs accordingly [12–16].

3. ROAD LIGHTING DESIGN

Road types are defined in international technical reports, and the optimal range of solution is technically presented for these road types. Design estimates should be made for luminaires with known photometric characteristics, as a result of which the number and types of luminaires are determined [17–19].

The lighting class of the road that corresponds to a particular road is determined using the table in the *CIE115–2010* [18]. According to Table 1, the *M*2 road lighting class was found, and the corresponding parameter values are also shown in it.

Road lighting class was found with Eq. 1, Eq. 2, and Eq. 3:

$$MX = 6 - total\,of\ weight\ factors, \quad (1)$$

$$MX = 6 - 4 = 2, \quad (2)$$

$$MX = M2. \quad (3)$$

The road lighting quality parameters are shown in Table 2.

3.1. Features of Road Lighting

The road surface is asphalt, class *R*4. Additionally, Q_o = 0.08, and the height of the luminaire is 11 m. The maintenance factor of the luminaire is 0.91, and all calculated luminance values are corrected. The ratio of the minimal luminance value to average luminance value is greater than 0.4 in the calculations for road lighting, ensuring that the rate of the minimal luminance value to the maximum at the latitude coordinate of the observer is greater than 0.7 ($U_I \geq 0.7$).

The levels of luminance and uniformity of road surface luminance conform to the relevant standards. All luminaires were installed in (cross (staggered layout of the luminaires) or mutual (opposite layout of the luminaires)) two lines from the walking ways to the axis of the road and at a height of 11 m. Table 3 illustrates the road and lighting parameters [20–22].

Table 3. Road and Lighting Parameters

Common lighting parameters			
Lighting pole type	Galvanized	Lighting class	*M*2
Number of road lanes	2	Console length (m)	1
Strip Width (m)	3.5	Console Angle	0°/5°/10°/15°
Road Width (m)	7	Luminaire Angle	0°/5°/10°/15°
Road Class	*R*4	Lamp type	HPS
Q_o	0.08	Lamp power (W)	150
Distance to illumination	0	Lamp luminous flux (lm)	17000
Illumination height from ground (m)	11	Maintenance factor (once a year)	0.91

3.2. Simulation Study

The main purpose of the new study is to achieve the most cost-effective results that provide adequate conditions. In the new study on road lighting, classifications are taken into account in various scenarios. The most accurate reference to road lighting are international standards. For this reason, the simulation is adapted to *CIE* standards. According to *CIE140*, the luminance values, average luminance level, overall and longitudinal uniformity of road surface luminance values of all points were calculated for observers.

Luminaires for use in road lighting should be selected taking into account the level of glare, luminance level of the road, uniformity of road surface luminance and efficiency, as well as determined by computer calculations using the luminance method [24–31].

Various options for the road parameters are available in the simulation program. For the road parameters, the lighting system (opposite layout of the luminaires, staggered layout of the luminaires, divided road, road with single luminaire, road with two luminaires, etc.), road class (*R*1, *R*2, *R*3, *R*4, *N*1, *N*2, *N*3, *N*4, etc.), number of lanes, lane width, refuge width, and road lighting class (*M*1, *M*2, *M*3, *M*4, *M*5, *M*6, etc.) can be chosen. For the lighting parameters, select characteristics such as distance between the luminaires, height of the luminaire, distance of the luminaire from the road, console angle, IP protection class, pollution rate, cleaning period, and maintenance factor for post or hanger system lighting. As for the parameters of the luminaire, the name, angle of the luminaire (angle relative to the road), power of the lamp used, lifetime, luminance flux, the power of the ballast and new luminaires can be added into this simulation under the database process at any time [1, 2, 20–23]. A simple and accurate calculation is achieved because of modeling for the lighting system that the data is entered into.

4. APPLICATIONS OF ROAD LIGHTING

In this study, two problems encountered in road lighting were investigated. These problems related to angled lighting and layout of lumanaries under road lighting. For this purpose, it has been proven using a simulation program that the angled lighting, encountered almost everywhere in the road lighting,

Fig. 1. Examples of road lighting console angles

Table 4. Lighting Results for Opposite and Staggered Layout of the Luminaires at 0°, 5°, 10°, and 15° Angles

Angle of illumination	0°		5°		10°		15°	
Observer No	1	2	1	2	1	2	1	2
Location, m	1.75	5.25	1.75	5.25	1.75	5.25	1.75	5.25
Staggered layout of the luminaires								
$L_{average}$, cd/m^2	1.50	1.50	~~1.28~~	~~1.28~~	~~1.11~~	~~1.11~~	~~0.98~~	~~0.98~~
U_o	0.75	0.77	0.80	0.81	0.85	0.81	0.82	0.78
U_1	0.72	0.72	0.80	0,80	0.84	0.84	0.86	0.86
TI,%	5.7	5.8	5.9	5.9	5.7	5.7	5.4	5.4
Opposite layout of the luminaires								
$L_{average}$, cd/m^2	1.64	1.64	~~1.40~~	~~1.40~~	~~1.21~~	~~1.21~~	~~1.07~~	~~1.07~~
U_o	0.67	0.67	0.73	0.73	0.77	0.77	0.77	0.77
U_1	0.70	0.70	0.79	0.79	0.86	0.86	0.86	0.86
TI,%	8.0	8.0	8.0	8.0	7.9	7.9	7.6	7.6

is inaccurate. It is proved instead of angled lighting, it is necessary to perform lighting parallel (by the angle of 0°) to the road surface. The second important problem with road lighting is that it is possible to increase the distance between the lighting poles due to the layout of the luminaires. For this purpose, two-lane road with the opposite layout of the luminaires with HPSLs of 150 W is examined. For the opposite layout of the luminaires, the distance between the poles is 43 m. However, with the help of simulation, when the poles are examined in staggered layout of the luminaires, the distance between the lighting poles is calculated as 47 m. For this road lighting, a 9.3 % longer road with two lanes can be illumitated using staggered layout of the luminaires instead of the opposite one. This example showed that using simulation environment for roads, you could find new solutions for different type of luminaires and lamps of different power.

4.1. Angle Effect in Lighting

Various design tools or physical measurements are used to determine the illumination level of certain points selected in lighting scenes. These are physical measurements carried out by models, numerical equations, and computer programs or illuminance meter under real conditions. In this study, dual luminaires with HPSLs of 150 W installed at a height of 11 m are used on the road. Determination of console angle (0°, 5°, 10° and 15°) for a luminaire with protection class IP65 with HPSL of 150 W is performed simulatively. Fig. 1 illustrates examples of road lighting console and luminaire angles.

As it can be seen in Fig. 1, the luminaires in road lighting are used at an angle due to the console or adjustable fixture mounting. It causes loss efficiency of angled lighting. Efficiency loss was calculat-

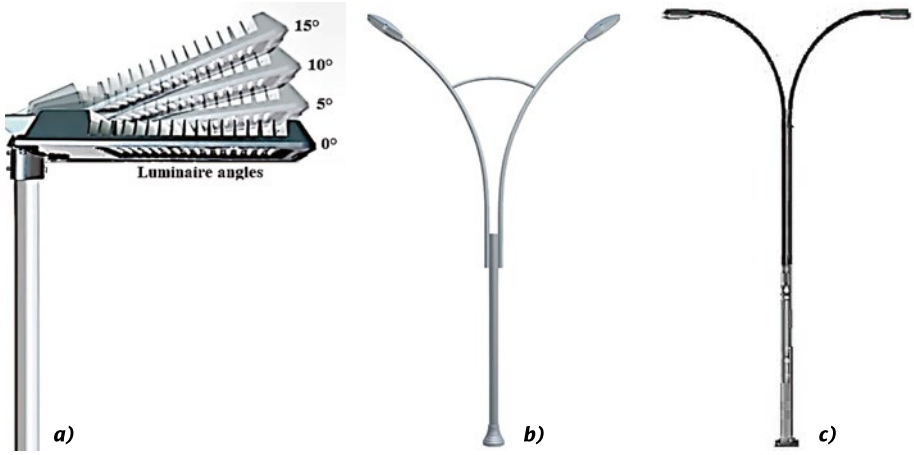

Fig. 2. Luminaire angles (a), inefficient lighting angle (b), and efficient lighting (c)

Table 5. Calculation Results of Road Lighting with Opposite and Staggered Layout of the Luminaires

Parameters of road lighting	Opposite layout of the luminaires		Staggered layout of the luminaires	
Observer location (m)	1.75	5.25	1.75	5.25
$L_{average}$ (cd/m^2)	1.64	1.64	1.5	1.5
U_o	0.67	0.67	0.75	0.77
U_1	0.70	0.70	0.72	0.72
TI (%)	8.00	8.00	5.70	5.80
$E_{average}$ (lx)	25.55		23.4	
E_{min} (lx)	13.31		16.81	
E_{max} (lx)	49.20		34.39	
U_{oa}	0.53		0.73	
U_{la}	0.27		0.49	
Lamp power (W)	150		150	
Luminous flux (lm)	17000		17000	
Distance between illuminations (m)	43		47	

ed based on simulation. As the angle increased, the luminance efficiency in the road decreased. Fig. 2 shows luminaire angles, inefficient (angle) and efficient lighting.

This study investigated a 2-lane road, which is suitable for *CIE140–2000* and *2019* (2nd edition) road lighting calculations in simulated environment. Calculations were made at angles of 0°, 5°, 10°, and 15° for luminaires with HPSL of 150 W. With the exception of 0°, 5°, 10°, and 15° angles, illumination has been found to cause loss of efficiency. For example, if the opposite layout of the luminaires is used, the distance between the poles is 43 m, and luminaire angle 0°, than $L_{average}$ =1.50 cd/m^2. This corresponds to *CIE140–2000* and *2019* (2nd edition) road lighting calculations for *M*2 [10, 11]. By opposite layout of the luminaires, if the luminaire angle is 5°, 10°, and 15°, $L_{average}$ is less than 1.50 cd/m^2 (the distance between the poles is 43 m). If $L_{average}$ =1.50 cd/m^2 less than the lighting is not suitable for *CIE140–2000* and *2019* (2nd edition).

If the staggered layout of the luminaires is used, the distance between the poles is 47 m, and luminaire angle 0°, than $L_{average}$=1.64 cd/m^2. This corresponds to *CIE140–2000* and *2019* (2nd edition) road lighting calculations for *M*2 [10, 11]. By opposite layout of the luminaires, if the luminaire angle is 5°, 10°, and 15°, $L_{average}$ is less than 1.50 cd/m^2 (the distance between the poles is 47 m). If $L_{average}$ =1.50 cd/m^2 less than the lighting is not suitable for *CIE140–2000* and *2019* (2nd edition). Table 4 shows lighting results for opposite and staggered layout of the luminaires at angles of 0°, 5°, 10°, and 15°.

If the he $L_{average}$ for 0° is assumed to be 100 % for each of the opposite and staggered layout of the luminaires in Table 4, than:

– The loss rate for luminaire angle 5° is approximate 15 %;

– The loss rate for the luminaire angle 10° is approximate 26 %;

– The loss rate for the luminaire angle 15° is approximate 35 %.

4.2. Effect of Opposite and Staggered Layout of the Luminaires on Lighting

Another subject examined in this study is the effect of layout of the luminaires in lighting. Despite the fact that all parameters are equal, the layout of lighting poles provides benefits in road lighting. To confirm this, the lighting of a two-lane road was modeled with luminaires with an HPSL of 150 W, arranged in the opposite layout of the luminaires. According to Table 5, all values correspond to *CIE140:2019* road lighting calculations. The distance between the poles is 43 m in the road lighting by the opposite layout of the luminaires. However, the maximum distance between the poles is 47 m. By opposite and staggered layout of the luminaires, all parameters are equal. However, in staggered layout of the luminaires the distance between the poles

Table 6. Luminance Values in Direction of Observer 1 for Opposite Layout of the Luminaires

Observer 1 $L_{average}$=1.64 cd/m², U_o=0.67, U_l=0.70, *TI*=8 % **Opposite layout of the luminaires with HPSL of 150 W**															
	1.43	**4.30**	**7.17**	**10.03**	**12.90**	**15.77**	**18.63**	**21.50**	**24.37**	**27.23**	**30.10**	**32.97**	**35.83**	**38.70**	**41.57**
0.58	1.58	1.51	1.40	1.27	1.35	1.52	1.70	1.79	1.79	1.70	1.56	1.57	1.69	1.67	1.65
1.75	1.74	1.61	1.49	1.42	1.52	1.73	1.91	2.01	1.97	1.84	1.66	1.66	1.82	1.75	1.77
2.92	1.69	1.56	1.42	1.41	1.55	1.82	2.05	2.13	2.00	1.85	1.68	1.66	1.70	1.71	1.72
4.08	1.68	1.55	1.42	1.41	1.55	1.79	1.99	2.06	1.97	1.83	1.66	1.66	1.69	1.70	1.71
5.25	1.65	1.51	1.37	1.28	1.38	1.58	1.79	1.88	1.84	1.76	1.60	1.62	1.77	1.72	1.74
6.42	1.46	1.37	1.23	1.10	1.16	1.32	1.50	1.61	1.61	1.59	1.47	1.50	1.62	1.62	1.58

Table 7. Luminance Values in Direction of Observer 2 for Opposite Layout of the Luminaires

Observer 2 $L_{average}$=1.64 cd/m², U_o=0.67, U_l=0.70, *TI*=8 % **Opposite layout of the luminaires with HPSL of 150 W**															
	1.43	**4.30**	**7.17**	**10.03**	**12.90**	**15.77**	**18.63**	**21.50**	**24.37**	**27.23**	**30.10**	**32.97**	**35.83**	**38.70**	**41.57**
0.58	1.46	1.37	1.23	1.10	1.16	1.32	1.50	1.61	1.61	1.59	1.47	1.50	1.62	1.62	1.58
1.75	1.65	1.51	1.37	1.28	1.38	1.58	1.79	1.88	1.84	1.76	1.60	1.62	1.77	1.72	1.74
2.92	1.68	1.55	1.42	1.41	1.55	1.79	1.99	2.06	1.97	1.83	1.66	1.66	1.69	1.70	1.71
4.08	1.69	1.56	1.42	1.41	1.55	1.82	2.05	2.13	2.00	1.85	1.68	1.66	1.70	1.71	1.72
5.25	1.74	1.61	1.49	1.42	1.52	1.73	1.91	2.01	1.97	1.84	1.66	1.66	1.82	1.75	1.77
6.42	1.58	1.51	1.40	1.27	1.35	1.52	1.70	1.79	1.79	1.70	1.56	1.57	1.69	1.67	1.65

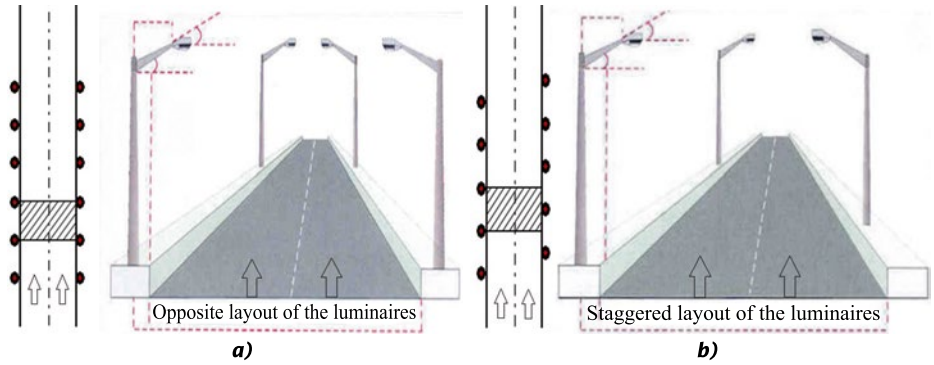

Fig. 3. Opposite and staggered layout of the luminaires

is 4 m higher (suitable for *CIE140:2000* and *2019* (2nd edition)). Therefore, the staggered layout of the luminaires a road that is 9.3 % longer.

For this reason, special solutions, such as in this example should be analyzed in simulated environments with road lighting. This reduces unnecessary costs during initial installation. Energy consumption can be reduced in lighting. Fig. 3 shows the opposite and the staggered layout of the luminaires. Table 5 shows results of calculating road lighting with the opposite and the staggered layout of the luminaires.

Tables 6–9 show the luminance values in the direction of observers 1 and 2, respectively, with opposite and staggered layout of the luminaires. In this case, the requirements *CIE140–2000* and *2019* (2nd edition) are fulfilled at all points [10, 11]. The maximum distance between the poles is 43 m for the opposite layout of the luminaires, and the maximum distance between the poles is 47 m for staggered layout of the luminaires.

Staggered layout of the luminaires increased the maximum distance between the poles by 4 m. Table 6 and Table 7 show luminance values in the di-

Table 8. Luminance Values in Direction of Observer 1 for Staggered Layout of the Luminaires

Observer 1 $L_{average}$=1.50 cd/m², U_o=0.75, U_l=0.72, TI=5.7 % Staggered layout of the luminaires with HPSL of 150 W																
	1.47	4.41	7.34	10.28	13.22	16.16	19.09	22.03	24.97	27.91	30.84	33.78	36.72	39.66	42.59	45.53
0.58	1.58	1.58	1.49	1.35	1.40	1.59	1.59	1.57	1.53	1.48	1.37	1.23	1.21	1.29	1.41	1.55
1.75	1.70	1.68	1.58	1.44	1.51	1.76	1.75	1.82	1.79	1.62	1.47	1.33	1.32	1.40	1.51	1.62
2.92	1.80	1.67	1.51	1.40	1.42	1.58	1.68	1.77	1.78	1.64	1.48	1.38	1.38	1.46	1.60	1.74
4.08	1.87	1.68	1.49	1.35	1.32	1.37	1.47	1.59	1.64	1.59	1.49	1.41	1.49	1.67	1.77	1.85
5.25	1.76	1.58	1.41	1.24	1.21	1.26	1.36	1.49	1.56	1.54	1.49	1.38	1.47	1.72	1.73	1.81
6.42	1.40	1.36	1.26	1.14	1.12	1.20	1.29	1.40	1.46	1.42	1.37	1.24	1.30	1.48	1.50	1.49

Table 9. Luminance Values in Direction of Observer 2 for Staggered Layout of the Luminaires

Observer 2 $L_{average}$=1.50 cd/m², U_o=0.77, U_l=0.72, TI=5.8 % Staggered layout of the luminaires with HPSL of 150 W																
	1.47	**4.41**	**7.34**	**10.28**	**13.22**	**16.16**	**19.09**	**22.03**	**24.97**	**27.91**	**30.84**	**33.78**	**36.72**	**39.66**	**42.59**	**45.53**
0.58	1.58	1.58	1.49	1.35	1.40	1.59	1.59	1.57	1.53	1.48	1.37	1.23	1.21	1.29	1.41	1.55
1.75	1.70	1.68	1.58	1.44	1.51	1.76	1.75	1.82	1.79	1.62	1.47	1.33	1.32	1.40	1.51	1.62
2.92	1.80	1.67	1.51	1.40	1.42	1.58	1.68	1.77	1.78	1.64	1.48	1.38	1.38	1.46	1.60	1.74
4.08	1.87	1.68	1.49	1.35	1.32	1.37	1.47	1.59	1.64	1.59	1.49	1.41	1.49	1.67	1.77	1.85
5.25	1.76	1.58	1.41	1.24	1.21	1.26	1.36	1.49	1.56	1.54	1.49	1.38	1.47	1.72	1.73	1.81
6.42	1.40	1.36	1.26	1.14	1.12	1.20	1.29	1.40	1.46	1.42	1.37	1.24	1.30	1.48	1.50	1.49

rections of observer 1 and observer 2 for the opposite layout of the luminaires. Table 8 and Table 9 show luminance values in the directions of observer 1 and observer 2 for the staggered layout of the luminaires.

5. CONCLUSION

Road lighting installations are important for both driving comfort and safety. The main purpose of the new study is to reach the most cost-effective results that provide adequate conditions. For this reason, when developing new suggestions in the field of road lighting, both the classification of roads by lighting and the corresponding lighting requirements are taken into account.

The most accurate reference to road lighting and the choice of luminaires to be used are international standards. For this reason, simulated road lighting is adapted to *CIE* standards. According to *CIE140–2000*, the luminance values, averaged luminance level, overall and longitudinal uniformity values of road surface luminance in all points were calculated for observers. The data of the used lamp was processed in the simulation database and the results were analyzed.

The HPSL of 150 W conforms the standards specified in *CIE140–2000* and *2019* (2nd edition) road lighting calculations with luminaire angle of 0° in the optimum lighting pole range for the opposite and staggered layout of the luminaires. The angle of the luminaire is 5°, 10°, and 15°, while $L_{average}$ is less than 1.50 cd/m². This is not *CIE* compliant. It was shown that compliance with the regulatory requirements was ensured by inefficient and inaccurate lighting installations.

The layout of lighting poles affects the lighting efficiency. Despite the fact that all parameters are equal, the layout of lighting poles provides benefits in road lighting. The optimum distance between the poles for the opposite layout of the luminaires is 43 m. Moreover, the optimum distance between the poles for staggered layout of the luminaires is 47 m. Staggered layout of the luminaires provides an advantage of 4 m (9.3 %).

Lighting simulations can enhance such special solutions. Therefore, as in this example, special solutions should be analyzed in simulated environments when designing road lighting.

The correct layout of the luminaires and lighting poles reduces unnecessary costs in initial setup of road lighting and increases energy efficiency of road lighting.

REFERENCES:

1. Cengiz M.S. A Simulation and Design Study for Interior Zone Luminance in Tunnel Lighting, Light & Engineering, 2019. V27, #2, pp. 42–51.

2. Cengiz M.S. The Relationship Between Maintenance Factor and Lighting Level in Tunnel Lighting, Light & Engineering, 2019. V27, #3, pp. 75–84.

3. International Commission on Illumination, Road lightings as an Accıdent Countermeasure, CIE93, Vienna-Austria, 1992. p. 92.

4. Painter K.A., Farrington D.P. Evaluating Situational Crime Prevention A Young People's Survey, The British Journal of Criminology, London, 2001. V41, #2, pp. 266–284.

5. Gan F., Grabosky P. Improved street Lighting and Crime Reduction, The Promise of Crime Prevention, 2nd edition ISBN0642241724, Canberra: Australian Institute of Criminology, Canberra, 2000. pp. 1326–6004.

6. Cengiz M.S., Cengiz Ç. Numerical Analysis of Tunnel LED Lighting Maintenance Factor, IIUM Engineering Journal, 2018. V19, #2, pp. 154–163.

7. Ongun, A., The Analysis of Optımum Solution Criteria for The Designing of Road Lighting Installations, M. Sc. Thesis, Gazi University Institute of Science and Technology, Ankara, 2007. p. 174.

8. Bommel W.V. Road Lighting: Fundamentals, Technology and Application, Springer Int. Pub. Switzerland, 2015. p. 333, ISBN: 978–3–319–11465–1.

9. Özkaya M., Aydınlatma Tekniği, Birsen Yayınevi, İstanbul-1994. p. 91.

10. CIE140:2000 – Road Lighting Calculations. CIE140, International Commission on Illumination, Road Lighting Calculations, Vienna-Austria, 2000. p. 33.

11. CIE140:2019 Road Lighting Calculations. CIE140, International Commission on Illumination, 2nd Edition ISBN:978–3–902842–56–5.

12. Onaygil S., Güler Ö., Erkin E. Yol Aydınlatmalarında LED Kullanımı, V. Ulusal Aydınlatma Sempozyumu ve Sergisi, 2009.

13. Cengiz Ç., Kaynaklı M., Gencer G., Eren M. Yapici İ., Yildirim S., Cengiz M.S., Selection Criteria and Economic Analysis of LEDs, Book of Abstracts, Imeset Int. Conf. Mult. Sci. Eng. Tech., Bitlis, Turkey, October 27–29, 2017.

14. UN Economic and Social Council, Economic Commission for Europe, Committee on Sustainable Energy, Steering Committee of the Energy Efficiency 21 Project, Final Report of Energy Efficiency Investment Project Development for Climate Change Mitigation, ECE/ENERGY/WP.4/ 2006/2, (21 March 2006).

15. Gencer G., Eren M., Yildirim S., Kaynaklı M., Palta O., Cengiz M.S., Cengiz Ç. Numerical Approach to City Road Lighting Standards, Book of Abstracts, Imeset Int. Conf. Mult. Sci. Eng. Tech., Bitlis, Turkey, October 27–29, 2017.

16. Yıldırım S., Yapıcı İ., Atiç S., Eren M., Palta O., Cengiz Ç., Cengiz M.S., Yurci Y., Numerical Analysis of Productivity and Redemption Periods in LED Illimunation. Imeset Book of Abstracts, Int. Conf. Mult. Sci. Eng. Tech., Baku, 12–14 July 2017.

17. CIE194–2011 On site measurement of the photometric properties of road and tunnel lighting, 2011.

18. CIE115–2010 (CIE2010) CIE115, International Commission on Illumination, Recommendations far the Lighting of Roads for Motor and Pedestrian Traffic, Vienna-Austria, 1995. p. 25.

19. CIE136–2000, Guide to the lighting of urban areas, 3 August 2000.

20. Onaygil S., TEDAŞ Genel Müdürlüğü Meslek İçi Eğitim Semineri, TEDAŞ Basımevi, Ankara, 2005. pp. 1–70.

21. Onaygil S., 2007. TEDAŞ Genel Müdürlüğü Meslek İçi Eğitim Semineri-Gölbaşı Eğitim Tesisleri, Yol aydnlatma Semineri 23–24 Ocak 2007.

22. Onaygil S., Yol aydınlatma projelerinde yol sınıfının belirlemesinin önemi, Kaynak Elektrik Dergisi, 1998. #12, pp. 125–132.

23. Güler Ö., Onaygil S., The effect of luminance uniformity on visibility level in road lighting, Lighting Research Technology, 2002. V35, pp. 199–215.

24. Tetri, E., Chenani, S.B., Rasanen R.S. Advancement in Road Lighting, Light & Engineering, 2018. V26, #1, pp. 99–109.

25. Tetri E., Bozorg Chenani S., Rasanen R-S., Baumgartner H., Vaaja M., Sierla S., Tahkamo L., Virtanen J-P., Kurkela M., Ikonen E., Halonen L., Hyyppa H., and Kosonen I. Tutorial: Road Lighting for Efficient and Safe Traffic Environments., LEUKOS Journal of the Illuminating Engineering Society of North America, 2017. V13, #4, pp. 223–241.

26. Liping G., Marjukka E., and Halonen L. Luminance monitoring and optimization of luminance meter-

ing in intelligent road lighting control systems, Ingineria Iluminatuluin, 2007. V9, pp 24–40.

27. Barua P., Mazumdar S., Chakraborty S., Bhattacharjee S. Road Classification Based Energy Efficient Design and its Validation for Indian Roads, Light & Engineering, 2018. V26, #2, pp. 110–121.

28. Bozorg Chenani S., Vaaja T M., Kurkela M., Kosonen I., Luttinen T. Target detection distances under different road lighting intensities, European Transport Research Review, 2017. #9, pp. 1–17.

29. Iacomussi Rossi G., Soardo P. Energy Saving and Environmental Compatibility in Road Lighting, Light & Engineering, 2012. V20, #4, pp. 55–63.

30. Tahkamo L. Halonen L. Life cycle assessment of road lighting luminaires -Comparison of light emitting diode and high-pressure sodium technologies, Journal of Cleaner Production, 2015. V93. pp. 234–242.

31. Van Bommel W., Van Den Beld G.,. Van Ooyen M. Industrial Light and Productivity, Lighting & Engineering, 2003. V11, #1, pp. 14–21.

Mehmet Sait Cengiz
Turkey Electricity Distribution Company was made director of research and development in the years 2000-2010. He completed his masters degree in 2011 and his doctorate in 2016 in the field of Electrical and Electronics Engineering. He still works in the field of applied lighting

Light & Engineering
Vol. 28, No. 4, pp. 57–62, 2020
https://doi.org/10.33383/2019-067
Svetotekhnika # 2, 2020, pp. 42–45

ANALYSIS OF CHARACTERISTICS OF HALOGEN AND LED AUTOMOBILE LAMPS

Olga Yu. Kovalenko[1] and Yulia A. Zhuravlyova[2]

[1] N.P. Ogarev Mordovia State University
[2] Russian Technological University MIREA
ulypil@mail.ru

ABSTRACT

This work contains analysis of characteristics of automobile lamps by Philips, KOITO, ETI flip chip LEDs, Osram, General Electric (GE), Gtinthebox, OSLAMPledbulbs with H1, H4, H7, H11 caps: luminous flux, luminous efficacy, correlated colour temperature. Characteristics of the studied samples are analysed before the operation of the lamps. The analysis of the calculation results allows us to make a conclusion that the values of correlated colour temperature of halogen lamps are close to the parameters declared by manufacturers. The analysis of the study results has shown that, based on actual values of correlated colour temperature, it is not advisable to use LED lamps in unfavourable weather conditions (such as rain, fog, snow). The results of the study demonstrate that there is a slight dispersion of actual values of luminous flux of halogen lamps by different manufacturers. Maximum variation between values of luminous flux of different lamps does not exceed 14 %. The analysis of the measurement results has shown that actual values of luminous flux of all halogen lamps comply with the mandatory rules specified in the UN/ECE Regulation No. 37 and luminous flux of LED lamps exceeds maximum allowable value by more than 8 %. Luminous efficacy of LED lamps is higher than that of halogen lamps: more than 82 lm/W and lower power consumption. The results of the measurements have shown that power consumption of a LED automobile lamp is lower than that of similar halogen lamps by 3 times and their luminous efficacy is higher by 5 times.

Keywords: light emitting diode (LED) lamp, halogen lamp, automobile lamp, luminous flux, colour temperature, luminous efficacy, cap, photometric measuring unit, spectral distribution

1. INTRODUCTION

Contemporary automobiles use different types of lamps for illumination of road, signalling and output of information on automobile parameters. Types of these lamps depend on their use and manufacturer. Most of modern automobiles are equipped with headlights with halogen lamps. Light emitting diode (LED) sources of light have become successfully applied in transport industry, namely in traffic lights, road signs, interior indication, brake lights. Drivers and manufacturers have been constantly looking for ways of enhancing headlight because it affects the level of detail of a driver's view during night time and in case of poor visibility and, thus, increasing traffic safety. Nowadays, the Russian market of vehicle lamps is full of a large number of different automobile lamps, from conventional halogen sources of light to relatively new sources of light: LED automobile lamps. A number of studies of characteristics of LED sources of light have revealed problems related to lighting conditions which affect visual performance, efficiency of application of sources of light in agriculture and in other industries [6, 7]. Application of LED sources of light, as automobile headlights, remains a relatively

Table 1. Technical Parameters of the Halogen Lamps

Manufacturer, lamp type	Power consumption, W	Luminous flux, lm	Correlated colour temperature, K
GE, halogen	55	1550	3000
Osram, halogen	55	1550 ±10 %	3000
KOITO, halogen	60	–	4500
Philips, halogen	55	1550 ±10 %	3700

new area hence, it is necessary to study characteristics of LED automobile lamps.

2. THE STUDY OF AUTOMOBILE LAMP CHARACTERISTICS

To evaluate light engineering parameters of lamps for road lighting, in particular luminous flux and correlated colour temperature, halogen and LED lamps produced by different manufacturers were studied: Philips, MTF Titanium, KOITO, ETI flip-chip, Osram, General Electric (GE), Gtinthebox, 1 or 2 samples of each.

The parameters of the studied lamps were measured in the Light Engineering Metrology core facility centre of the Institute for Electronics and Lighting Engineering in accordance with GOST R8.749–2011 [4]. To measure parameters of automobile lamps the Gooch&Housego photo-colorimetric measuring unit was used. It is designed for measuring luminous flux and radiant flux; spectral distribution of radiant flux; correlated colour temperature; general colour rendering index and special colour rendering index; tristimulus values and chromaticity coordinates in *XYZ* (1931), *u v* (1960), *u' v'* (1976) systems [10]. The operation principle of the unit is based on determination of radiant power by measuring spectral distribution of radiation and its integrating. The measuring unit consists of the OL IS7600 photometer sphere with diameter of 2 m, OL 770 VIS/NIR multi-channel spectroradiometer, 770–7G-3.0 fibre-optic cable, OL410–200 PRECISION LAMP SOURCE DC power supply for the AUX LAMP A180 auxiliary lamp, fasteners for fixation of lamps and the computer [9].

Fig. 1. View of the Gtinthebox LED lamps with H1 cap type

Main technical specifications of the unit: spectral range: (380–1100) nm, scan step: 0.75 nm, reflectance of the sphere inner surface: at least 0.986, measurement range of correlated colour temperature: (1500–10,000) K, limits of allowable absolute error of correlated colour temperature: ±25 K, luminous flux indication range: 0.01 to 100,000 lm, measurement range of luminous flux: (5–2500) lm, limits of allowable relative measurement error of luminous flux are about ±9 %.

During measurements, power supply parameters of the lamps were set by means of DPS1060 AC power supply unit. The centre of the image receiving surface of the photometric head lay along the line crossing the photometric centre of the goniophotometer and its plane was perpendicular to this line. The measurements were conducted in a location with its walls, floor and ceiling covered with matt black coating. All calculations were conducted automatically, displayed on the controlling computer of the measuring unit and were presented in a convenient form [2].

To find the value of luminous flux using luminous intensity distribution, the formula 1 is used:

$$\Phi = \int_{\phi=0}^{2\pi} \int_{\theta=0}^{\pi} I(\theta,\phi)\sin\theta d\theta d\phi, \qquad (1)$$

where $I(\theta,\phi)$ is the luminous intensity, θ is the angle characterising the position of the receiver between the poles, ϕ is the angle characterising the position of the receiver in relation to the equator [2].

Figs. 1–6 present view of the sources of light being studied.

The technical specifications of halogen lamps declared by manufacturers are listed in Table 1, their values comply with maximum and nominal

Fig. 2. View of the OSLAMPledbulbs lamp with H4 cap type

Fig. 3. View of the ETI flip-chip LEDs with H11 cap type

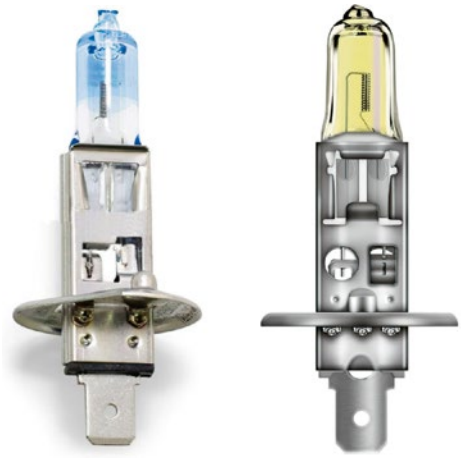

Fig. 4. View of General Electric (GE) and Osram lamps with H1 cap type

Fig. 5. View of KOITO White Beam III Premium halogen lamp with H4 cap type

Fig. 6. View of Philips White Vision H7 cap type halogen lamp

electric and luminous parameters of tungsten halogen lamps specified by [1]. No information on parameters of the LED lamps is specified on their packages. Current of the halogen lamps varied between 4.1 and 5.2 A, current of the LED lamps varied between 0.8 and 1.5 A. The measurement results obtained during the experiment are listed in Table 2.

The results of the study of spectral characteristics of OSLAMPledbulbs LED lamps measured in accordance with GOST are presented in Figs. 7, 8 [3].

The presented spectra demonstrate an intensive emission line in the blue region of the spectrum, which explains much higher values of colour temperature of OSLAMPledbulbs H4 LED lamps (6729 K and 6524 K for low beams and 6456 K and 6530 K for high beams) than the values of colour temperature of KOITO H4 halogen lamps (3548 K and 3562 K for low beams and 3822 K and 3815 K for high beams).

Fig. 9 presents the analysis of luminous efficacy of the lamps being studied.

3. ANALYSIS OF THE STUDY OF AUTOMOBILE LAMP CHARACTERISTICS

The results of the study demonstrate that there is a slight dispersion of actual values of luminous flux

Table 2. Measurement Results of Automobile Lamps

Lamp No.	Manufacturer, lamp type	Supply voltage, V	Power consumption, W	Luminous flux, lm	Correlated colour temperature, K
1	Osram H1, halogen (sample 1)	13.2	67.6	1692	3280
2	Osram H1, halogen (sample 2)		62.0	1491	3150
3	GE H1, halogen		67.3	1671	3212
4	KOITO H4, (low beam, sample 1), halogen		63.8	710	3548
5	KOITO H4, (low beams, sample 2), halogen		63.8	696	3562
6	KOITO H4, (high beams, sample 1), halogen		68.1	1166	3822
7	KOITO H4, (high beams, sample 2), halogen		68.2	1162	3815
8	Philips, halogen, H7 (sample 1)		54.1	1029	3385
9	Philips, halogen, H7 (sample 2)		54.3	1043	3382
10	Gtinthebox H1, LED (sample 1)		23.4	1936	7616
11	Gtinthebox H1, LED (sample 2)		23.6	1940	7515
12	OSLAMPledbulbs H4, LED (low beams, sample 1)		19.5	1340	6524
13	OSLAMPledbulbs H4, LED (low beams, sample 2)		20.6	1705	6729
14	OSLAMPledbulbs H4, LED (high beams, sample 1)		19.1	1815	6530
15	OSLAMPledbulbs H4, LED (high beams, sample 2)		20.2	1929	6456
16	ETI flipchip LEDs H 11 (sample 1)		10.9	878	5306
17	ETI flipchip LEDs H 11 (sample 2)		9.7	789	5142
Requirements of the UN/ECE Regulation No. 37 [8]		13.2 V	no more than 68 W	1550 lm ±15 %	–

of halogen lamps by different manufacturers. Maximum variation between values of luminous flux of different lamps does not exceed 14 %.

The analysis of the results of measurements has shown that:

– Power consumption of halogen lamps exceeds the nominal value more than by 11 % but does not exceed the maximum allowable value, and it should also be noted that the tests were conducted at test voltage 13.2 V and nominal power is specified for supply voltage 12 V;

– Power consumption of LED lamps is less than power consumption of halogen lamps by at least 6;

– LED lamps have much higher luminous efficacy than that of halogen lamps and less energy consumption, wherein luminous efficacy of the sample No. 1 (lamp No. 12) is less than luminous efficacy of the studied sample No. 2 (lamp No. 13) due to less value of luminous flux;

– As seen from the results, colour temperature of tungsten halogen lamps is close to the parameters declared by all manufacturers; correlated colour temperature of LED lamps corresponds to cold light;

– Based on actual values of correlated colour temperature, it is not advisable to use LED lamps in unfavourable weather conditions (such as rain, fog, snow);

– Actual values of luminous flux for halogen lamps are comply with mandatory requirements of the UN/ECE Regulation No. 37, and average luminous flux of LED lamps is higher than the maximum allowable value specified in the UN/ECE Regulation No. 37 by 8 %, with the exception for

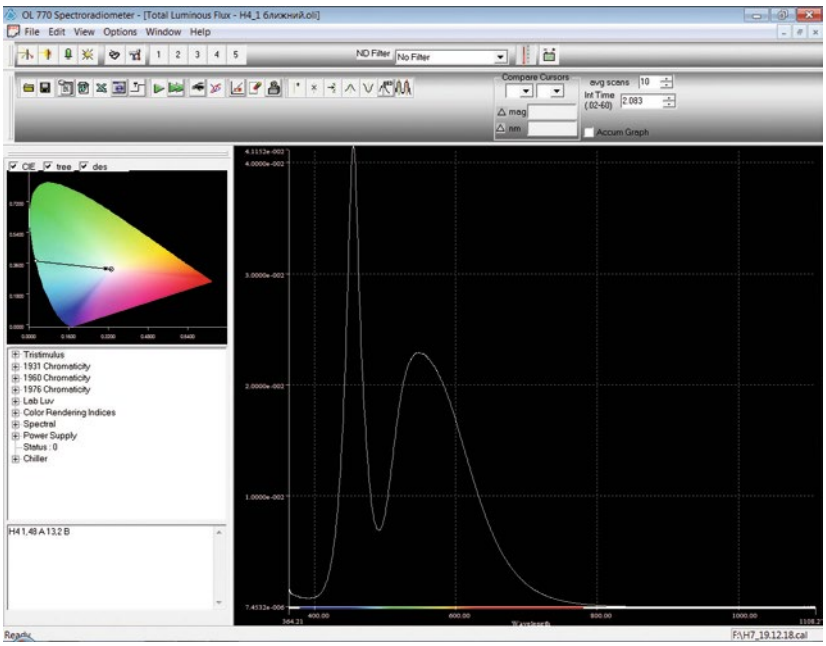

Fig. 7. Results of measurement of OSLAMPledbulbs lamp in low beam mode

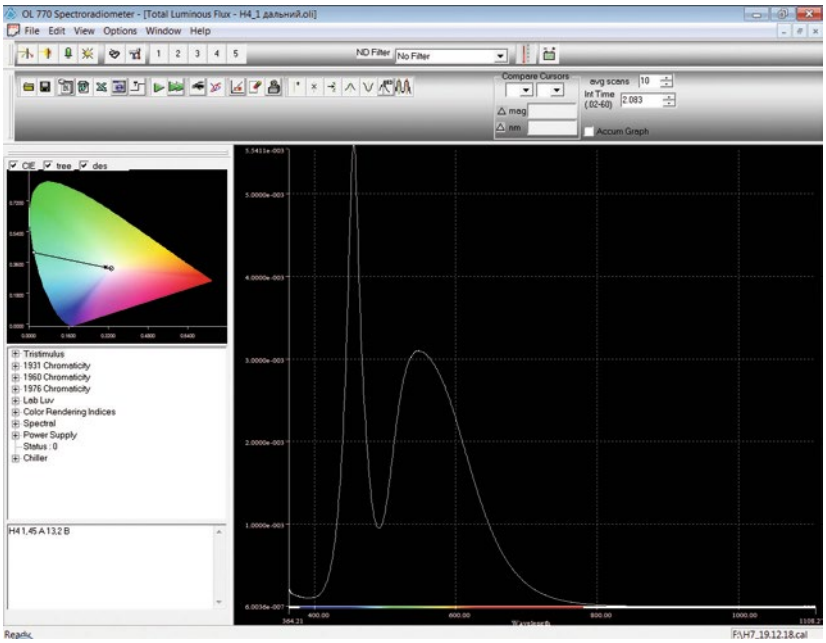

Fig. 8. Results of measurement of OSLAMPledbulbs lamp in high beam mode

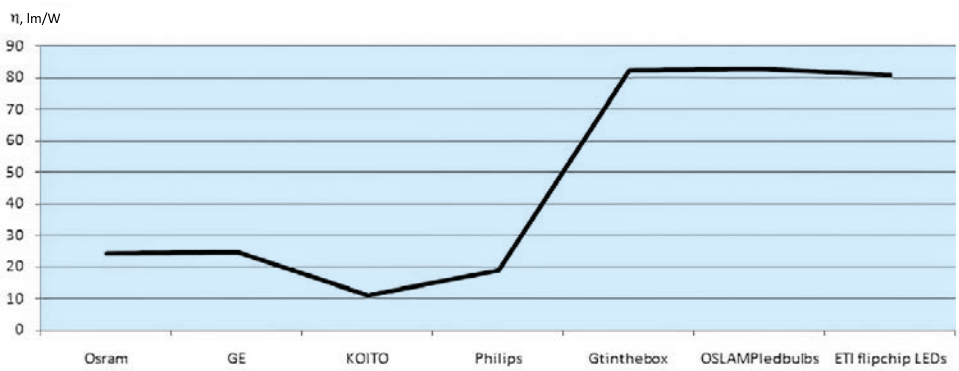

Fig. 9. Luminous efficacy of the studied lamps

the studied OSLAMPledbulbs H4 LED lamp (low beams, sample 1) with its measured value of luminous flux equal to 1340 lm;

– Power consumption of a LED automobile lamp is lower than that of similar halogen lamps by 3 times and their luminous efficacy is higher by 5 times.

REFERENCES

1. GOST R IEC60809–2012: "Lamps for road vehicles: Dimensional, electrical and luminous requirements"// Federal Technical Regulation and Metrology Agency, Moscow, STANDARTINFORM, 2014, 213 p. Date of enactment 01.07.2013.

2. GOST R55702–2013: "Electric light sources. Methods of measuring electrical and luminous characteristics"// Repl. GOST 17616–82, Federal Technical Regulation and Metrology Agency, Moscow, STANDARTINFORM, 2013, 67 p. Date of enactment 01.07.2013.

3. GOST R55702–2013: "Electric light sources. Methods of measuring spectral and colour characteristics"// Federal Technical Regulation and Metrology Agency, Moscow, STANDARTINFORM, 2015, 53 p. Date of enactment 01.07.2014.

4. GOST R8.749–2011: "State system for ensuring the uniformity of measurements. Light emitting diodes Methods of photometric measurements".

5. GO-2000A goniophotometer [Electronic source]. Access mode: http://smart-systems.su/files/modules/items/341/ru/goniofotometr_go-2000a.pdf

6. S.A. Amelkina, O.E. Zheleznikova, and Sinitsyna L.V. LEDs Lighting Effectiveness on Basis of Visual Performance and Visual Fatigue// Light & Engineering, 218, Vol. 26, # 3, pp. 81–87.

7. Kovalenko O. Yu. Increase of Efficiency and Monitoring of Parameters of Light Sources and Irradiating Installations in Agriculture [Povysheniye effektivnosti i kontrol parametrov istochnikov izlucheniya i obluchatelnykh ustanovok v selskom khozyaystve] / O. Yu. Kovalenko, Yu.A. Pilschikova // Photonics [Fotonika], 2017, Vol. 8 (68), pp. 68–73.

8. UN/ECE Regulation No. 37 (Revision 7) Uniform provisions concerning the approval of filament lamps for use in approved lamp units of power-driven vehicles and of their trailers// Federal Technical Regulation and Metrology Agency, Moscow, STANDARTINFORM, 2012,191 p. Date of enactment 11.07.2008.

9. Attachment to Pattern Approval Certificate of Measuring Instruments No. 64752. Description of Measuring Instrument Type. Photocolorimetry Measuring Unit// Moscow, 2017, 7 p.

10. Attachment to Pattern Approval Certificate of Measuring Instruments No. 64753. Description of Measuring Instrument Type. Lighting Engineering Measuring Set// Moscow, 2017, 8 p.

Olga Yu. Kovalenko,
Dr. of Tech. Science, Docent. She graduated from the N.P. Ogarev Mordovia State University majoring in Lighting Engineering and Light Sources in 1983.
At present, she is the Professor of the Metrology, Standardisation and Certification sub-department of the Institute for Electronics and Lighting Engineering of the N.P. Ogarev Mordovia State University, her research interests are measurements and monitoring of parameters of lighting and irradiating systems

Yulia A. Zhuravlyova,
Ph. D., Docent. She graduated from the N.P. Ogarev Mordovia State University majoring in Lighting Engineering and Sources of Light in 2010. At present, she is Associate Professor of the Light Sources sub-department of the Institute for Electronics and Lighting Engineering of the N.P. Ogarev Mordovia State University, Associate Professor of the Electronics sub-department of the Institute for Physics and Technology of RTU MIREA. Her research interests are Energy-efficient lighting installations; parameters of contemporary small-size fluorescent lamps and LED light sources, vacuum equipment

Light & Engineering
Vol. 28, No. 4, pp. 63–67, 2020

https://doi.org/10.33383/2019-038
Svetotekhnika # 2, 2020, pp. 72–75

APPLICABILITY OF A PRISMATIC PANEL TO OPTIMIZE WINDOW SIZE AND DEPTH OF A SOUTH-FACING ROOM FOR A BETTER DAYLIGHT PERFORMANCE

Busra Kose and Tugce Kazanasmaz

Izmir Institute of Technology, Department of Architecture
Email: fatmabusra.kose@gmail.com, tugcekazanasmaz@iyte.edu.tr

ABSTRACT

This study examines the performance of attached prismatic panels, which have shading capability, in a side-lit deep plan room to find out the least possible WWR value in relation to room depth satisfying the required daylight availability. The methodology is based on simulating a base model in Relux and testing it with alternative models composed of incrementally defined WWR and room depth values. In accordance with minimum IES requirements, the most satisfying sDA value was found to be 48.54 % in a room of 12 m depth with 67 % WWR. An sDA of 51.59 % and 59.26 % was achieved in a room of 9m depth with 43 % WWR and 6m depth with 30 % WWR, respectively. The least ASE values were obtained with the least WWR alternative of 30 % in all room depths. This study presents a new approach with the consideration of innovative daylight redirecting systems to propose revisions for the requirements mentioned in standards about daylight in buildings but based on conventional fenestration systems.

Keywords: daylight, prismatic panels, windows, room depth

Abbreviations:

WWR:	Window-to-wall ratio
AR:	Aspect Ratio
sDA:	Spatial Daylight Autonomy
ASE:	Annual Sunlight Exposure
IES:	Illuminating Engineering Society
IEA:	International Energy Agency

1. INTRODUCTION

The effective daylight zone is limited to the window edge in a conventional side lighted space with a vertical window; areas further away from the perimeter zone receive considerably lower daylight [1]. Increasing window size to expand the effective daylight zone can contribute small gains in daylight levels at the rear part of the room but causes excessive solar radiation near the window [2]. This disproportional distribution of daylight in space results in thermal and visual discomfort in front part of the room while additional support from artificial lighting is required at the back, which means undesirable lighting conditions for the occupants [3]. Therefore, determining appropriate room and window ratio according to climatic conditions is significant terms of visual comfort and energy savings [4]. Especially in hot climatic regions, uniform distribution is required to achieve the desired visual and thermal comfort.

Using conventional solar shading devices, such as roller shades or venetian blinds, reduces the amount of daylight entering into room and worsens the daylight distribution across the space [5,6]. Innovative daylight systems have been proposed to overcome shortcomings of conventional daylight techniques. Prismatic daylight-redirecting panels, for instance, improve daylight distribution through sun shadings and redirections [7,8].

The purpose of the study is primarily to test the performance of attached prismatic panels in defining optimum window size and room geometry when

Width	Along the window
Length	750 mm
Thickness	12 mm
Transmission	65 %
Prism angle	45º

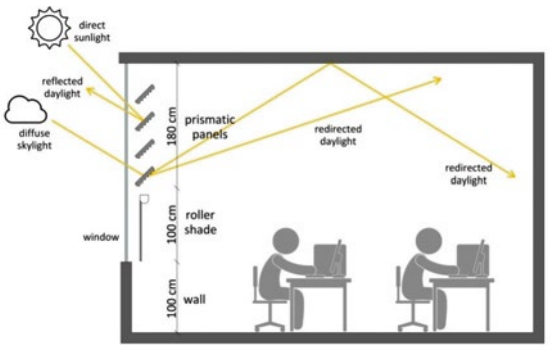

Fig. 1. Schematic illustration of prismatic panel principle and application

prismatic panels are installed in the side windows. The second aim is to provide sufficient daylight as deeply as possible into the space in every WWR-Room depth design alternatives and preventing excessive direct sunlight, which may cause negative impacts on occupants. The climate of Izmir is another significance meaning that, it would be possible to understand the applicability of a prismatic system in such a geographic and climatic location.

2. MODELLING THE BASE CASE ROOM

2.1. Daylight Illuminance and Optical Material Measurements

The base case is a deep-plan room having dimensions of 6 m by 12 m with 3.8 m height. Its window dimension is 5.5 m x 2.8 m. The daylight illuminance measurements were taken on December 21, 2017, at three times a day (9.30, 12.30, and 15.30) under overcast sky condition. A total of 19 measurement points was located with a spacing 0.6 m in the middle line of the room perpendicular to window line. Optical material properties were determined using both a luminance and illuminance meter as in reference [4]. Reflectance values of walls, ceiling and floor are 0.90, 0.85 and 0.60 respectively. The glazing has a transmittance value of 0.80.

Verification process included the comparison to determine how well Relux simulation outputs match up with the actual measurement results. The coefficient of determination (R^2) was calculated to measure the accuracy of the simulation model. They were 0.93, 0.99, 0.97 in simulations ran for times 9.30, 12.30 and 15.30 respectively, indicating the high accuracy and verification of Relux software.

2.2. Prismatic Panel in Relux Model

Prismatic panels (Siteco 45/45) manufactured by company Siteco [9] were chosen to enhance the daylight quality in interior space. They are in louver form, placed inside the window at slat angle of 45°. Prismatic panels were installed at upper part of the window, between 2.00 m and 3.80 m above the floor. This position above the eye level prevents potential glare arising from daylight redirection through prismatic panels. The lower part of the window allows view outside. The distance between each panel was set to be 0.30 m. The identical prismatic panels were applied to all room depth-WWR configurations, Fig. 1.

2.4. Design Alternatives

Alternative room depths and window sizes were determined following standards in literature and modelled in Relux. First, limiting room depth for the reference room was determined using the equa-

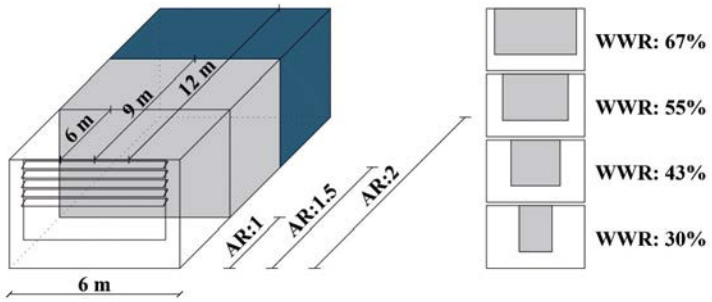

Fig. 2. Schematic view of stages in determining aspect ratios and window-to-wall ratios

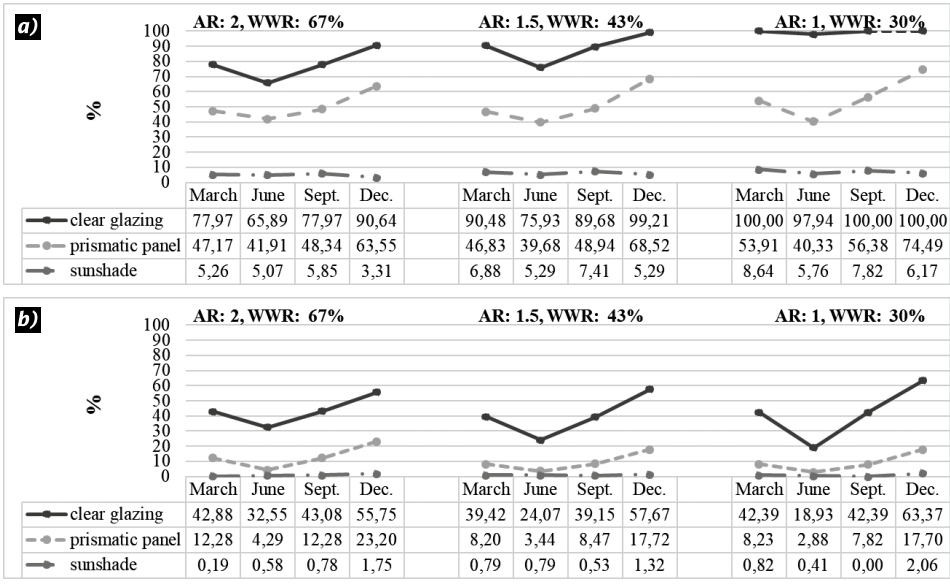

Fig. 3. Daylight performance of the rooms with optimum WWR and with respect to room depths: a) illuminance over 300 lx, b) illuminance over 1000 lx

tion described in The British Code BR8206(Part 2) [10] as:

$$\frac{L}{W}+\frac{L}{H_w}<\frac{2}{1-R_b}, \qquad (1)$$

where L is the room depth, W is the room width, H_w the window head height above floor level and R_b is the average reflectance of surfaces in the rear half of the room.

According to this equation (1), minimum acceptable room depth of the reference room was found as 9 m, indicating that room depth should not exceed this value to avoid gloomy looking and additional electric lighting in the rear half of the room. Taking limiting value into account, three floor aspect ratios of room depth to width were determined as follows:

AR= 1 (when room depth is 6 m, less than limiting value)

AR= 1.5 (when room depth is 9 m, equal to limiting value)

AR = 2 (when room depth is 12 m, greater than limiting value)

Since large windows increases exposure to sun and causes excessive heat gain and visual discomfort, the window area of each determined aspect ratio was incrementally reduced as shown in Fig. 2. Starting from the reference case with WWR of 67 %, the window width was reduced by 50 cm from both sides at each stage until minimum acceptable WWR of 30 % (due to British Code BR8206) [11] was achieved.

The reflectance of walls, ceiling and floor were assigned as 0.50, 0.85, 0.20, according to IEA Task 27 [11]. The measurement points were set to be 75 cm above the floor, 60 cm away from the walls surfaces and 60 cm spacing between each point. Totally 171, 126 and 81 measurement points were determined for the 12 m, 9 m and 6 m deep room, respectively. Simulations were run on solstice and equinox days at 10:00, 13:00 and 16:00. The 10 % transparent sunshade was considered at the lower part of the window to avoid excessive sunlight exposure since all measurements were carried out under CIE clear sky conditions in a room facing to South. In case of overcast sky conditions, additional sunshade would not be necessary, therefore the visual connection with the external environment would be possible.

3. FINDINGS

It is expected that the measurement points with illuminance above 300 lx will be as much as possible, and the measurement points with illuminance above 1000 lx will be as few as possible. Minimum acceptable floor areas are of 55 % for SDA and 7 % for ASE according to IES recommendations.

To simplify the calculation it was found that the illuminance at each measurement point represents the percentage of the annual working hours. For instance, it was assumed that each measurement point simulated in Relux for 21st March at 10:00 represents 180 working hours from 8 am to 11 am in the spring months. It corresponds to 7.5 % of total working hours in a year (considering 2400 working hours per year). Likewise, calculations at 13:00 and 16:00 represents 240 working hours from 11

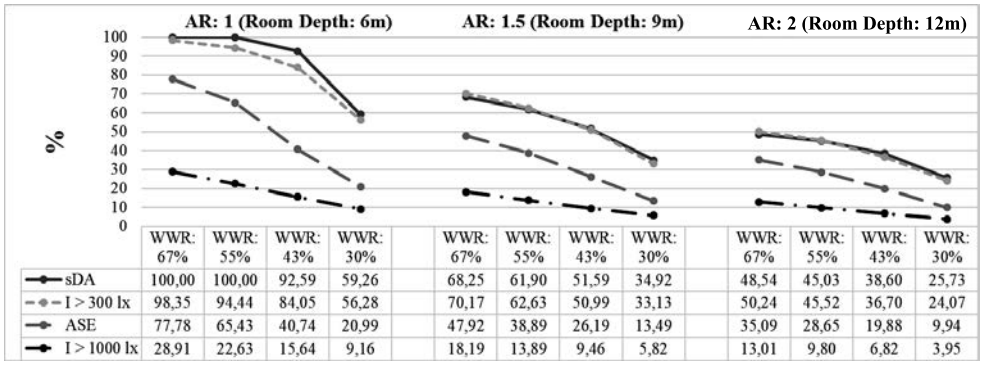

	AR: 1 (Room Depth: 6m)				AR: 1.5 (Room Depth: 9m)				AR: 2 (Room Depth: 12m)			
	WWR: 67%	WWR: 55%	WWR: 43%	WWR: 30%	WWR: 67%	WWR: 55%	WWR: 43%	WWR: 30%	WWR: 67%	WWR: 55%	WWR: 43%	WWR: 30%
sDA	100,00	100,00	92,59	59,26	68,25	61,90	51,59	34,92	48,54	45,03	38,60	25,73
I > 300 lx	98,35	94,44	84,05	56,28	70,17	62,63	50,99	33,13	50,24	45,52	36,70	24,07
ASE	77,78	65,43	40,74	20,99	47,92	38,89	26,19	13,49	35,09	28,65	19,88	9,94
I > 1000 lx	28,91	22,63	15,64	9,16	18,19	13,89	9,46	5,82	13,01	9,80	6,82	3,95

Fig. 4. sDA and ASE values with the percentage of analysis area that meets or exceeds illuminance of 300 lx and 1000 lx

am to 15 pm and 180 working hours from 15 pm to 18 pm respectively. They correspond to 10 % and 7.5 % of total working hours in a year respectively. The same method was applied for 21st June, 23rd September and 21st December. The percentages of annual working hours when illuminance at each measurement point meets or exceeds 300 lx were determined. Finally, the measurement points that meets or exceeds 300 lx at least 50 % of working hours per year were marked on working plane, and ratio of these points to the total measurement points were calculated to achieve sDA value. To calculate ASE, measurement points exposing to illuminance over 1000 lx for more than 250 working hours per year were determined and ratio of these points to the total measurement points were calculated.

Regarding the aspect ratio 2 (12 m depth), the 67 % WWR was found to be the optimum window size achieving the 50.24 % analysis area with sufficient daylight (illuminance over 300 lx) and 13.01 % analysis area exposed to direct sunlight (illuminance over 1000 lx). Daylight levels across the room were decreased due to shading capability of prismatic panels but still remained at an acceptable level.

Regarding the aspect ratio 1.5 (9 m depth), the percentage of area with illuminance above 300 lx was almost halved compared to unshaded room and became 50.99 % when the 43 % WWR was applied.

Regarding the aspect ratio 1 (6 m depth), the configuration with 30 % WWR became the optimum solution, receiving the adequate daylight with the percentage floor area of 56.28 %, Fig. 3.

4. OVERALL ASSESSMENT

• In winter, daylight penetrated deeper into rooms due to the lower position of the sun and illuminance values increased throughout the room. The prismatic panels were incapable of sun shading during these months and the inclined sun rays passed through between panels led to a considerable increase of illuminance values above 1000 lx. This excessive daylight exposure is also the reason for the high ASE values.

• In summer, the amount of daylight entering the room dropped due to the higher position of the sun. The sun-shading effect of the panels was prominent, since sunlight striking from right angles was reflected by the prism structure. This resulted in a decrease in illuminance values above 1000 lx, which ensures ASE to be within the acceptable range in these months.

• In spring and autumn, the amount of daylight entering the room and the daylight distribution is almost identical. The illuminance values throughout the room are higher than those in summer and lower than those in winter.

• The ratio of the area satisfying 300 lx was calculated regardless of a specific time fraction for a space almost corresponds to the estimated sDA value for this space. Contrary to this, the estimated ASE value is considerably greater than the percentage of the area that meets or exceeds illuminance above 1000 lx, Fig. 4.

• Due to IES requirements, the most satisfying sDA value was found to be 48.54 % in a room of 12 m depth with 67 % WWR. An sDA of 51.59 % and 59.26 % was achieved in a room of 9 m depth with 43 % WWR and 6m depth with 30 % WWR respectively.

• The ASE value obtained for each design alternative exceeded the minimum acceptable ASE of 7 % recommended by IES. The closest ASE values were obtained with the least WWR alternative of 30 % in all room depths. This value was 9.94 %, 13.49 % and 20.99 % in room of 12 m, 9 m and 6 m depth respectively.

5. CONCLUSION

This study would make a contribution to establishing availability of the 'useful' daylight, i.e. daylight without over-exposure, in side lighted rooms in terms of improving visual performance, and thus motivation, productivity and well-being of occupants. The current daylighting standards and related previous studies include required window sizes for room geometries, but these are restricted to conventional fenestration systems. However, this study emphasizes that a clear glazing without any daylight system is inadequate to meet the visual performance requirements of the spaces used mostly during the daytime such as educational and office buildings. It has been shown that it is possible to control and use daylight efficiently with the application of advanced daylight systems such as prismatic panels on vertical windows. The consideration of such systems simultaneously with the facade openings in the early design stages is more favourable in terms of avoiding problems related to the amount and distribution of daylight. Therefore, this study suggests new optimal WWR in relation with varying room depths when prismatic panels attached in side windows and recommends rethinking of daylighting requirements mentioned in current daylight standards.

REFERENCES

1. Reinhart, C. F. "A simulation-based review of the ubiquitous window-head-height to daylit zone depth rule-of-thumb," in Proceedings of the Ninth International IBPSA Conference Montréal, Canada, Agust 15–18, 2005.

2. Kim, J., Wineman J. Are windows and views really better? A quantitative analysis of the economic and psychological value of views. New York: Lighting Research Centre, Rensselaer Polytechnic Institute, 2005.

3. Bayram, G., Kazanasmaz, T. Simulation based retrofitting of an educational building in terms of optimum shading device and energy efficient lighting criteria. Light and Engineering, 2016. V24, No.2, pp. 45–55.

4. Littlefair, P.J. Solar shading of buildings. London: Construction Research Communications by permission of Building Research Establishment, 1999.

5. Laura, B., Marino, C., Minichiello, F., Pedace, A. An overview on solar shading systems for buildings. Energy Procedia, 2014. V62, pp. 309–317.

6. Ünver, R. Prediction of interior daylight availability for external obstructions in Istanbul. Light and Engineering, 2009. V17, No.3, pp. 54–64.

7. Ruck, N., Aschehoug, Ø., Aydinli, S., Christoffersen, J., Courret, G., Edmonds, I., Jakobiak, R., Kischkowweit-Lopin, M., Klinger, M., Lee, E., Michel, L., Scartezzini, J-L, & Selkowitz, S. Daylight in Buildings-A source book on daylighting systems and components. Lawrence Berkeley National Laboratory: Washington, DC, USA, 2000.

8. Kazanasmaz, T., Fırat Örs, P. Comparison of advanced daylighting systems to improve illuminance and uniformity through simulation modelling// Light & Engineering, 2014. V 22, No.3, pp. 56–66.

9. Siteco Stationary and Movable Prism Systems. [Online] Available from: https://www.siteco.com/en/home [Accessed August 2017].

10. British Standards Institution. BS8206–2:1992. Code of Practice for daylighting. London: BSI, 1992.

11. van Dijk, D., Platzer, W.J. Reference office for thermal, solar and lighting calculations. IEA-SHC Task 27, 2001.

Busra Kose, MSc, Ph.D. candidate at Department of Architecture from Izmir Institute of Technology. She got her Master's degree in June, 2019. She is interested in lighting design and energy efficiency in buildings

Tugce Kazanasmaz Prof. Dr., held a Doctor of Philosophy in Building Science from Middle East Technical University (METU). She has 19 years academic experience in architectural lighting, building physics and energy efficient design. At present, she is a Professor in the Department of Architecture in İzmir Institute of Technology, Turkey

Light & Engineering
Vol. 28, No. 4, pp. 68–76, 2020

https://doi.org/10.33383/2019-093
Svetotekhnika #2, 2020, pp. 56–62

ENERGY EFFICIENCY IN LIGHTING FOR HISTORICAL BUILDINGS: CASE STUDY OF THE EL AMAN CARAVANSERAI IN PROVINCE OF BITLIS, TURKEY

Behcet Kocaman

Department of Electrical and Electronics Engineering. Bitlis Eren University, Bitlis, Turkey
E-mail: bkocaman@beu.edu.tr

ABSTRACT

Historical buildings are bridges between the past and the present. Moreover, it is a mirror of the life of societies, which lived in other ages. Historic buildings need to be illuminated to provide better visual conditions. The demand for electricity is increasing day by day. Energy must be used efficiently to reduce the amount of energy being dissipated. Therefore, energy efficiency in the lighting for historical buildings is a topic of great importance. Various luminaires are used for interior and exterior lighting of historic buildings. However, new lighting technologies, such as light emitting diode (LED) luminaires, are many times more efficient than traditional technologies, such as incandescent luminaires. The use of new technologies can lead to significant reductions in net energy consumption and associated reductions in greenhouse gas emissions. Historic buildings can serve as powerful and highly visible demonstrations of energy-efficient lighting technologies. In this study, the cost and energy efficiency have been analyzed considering the investment costs and the energy consumption of LED luminaires instead of luminaires with incandescent, halogen and metal halide lamps using almost the same luminous flux in the example of the El Aman Caravanserai in Bitlis, Turkey. As a result, of the calculations, the annual energy consumption (9066.6 kW·h) was reduced by 78.21 % compared to the conventional system (41610 kW·h) installed with incandescent, halogen and metal halide lamps. Thus, the cost of using LED lighting system have been amortised in about 135 days. Later, lighting has been made with less energy consumption, and the energy has been used efficiently.

Keywords: energy efficiency, historic buildings, lighting, LED, interior lighting, exterior lighting

1. INTRODUCTION

Historical buildings are bridges between the past and the present, and sources of cultural identity. They are important investments for the future in order to maintain a balance between energy use and cultural values [1]. They are a mirror of the life of societies and communities that lived in other eras. Therefore, historical buildings need to be exhibited correctly and properly. This is achieved by lighting. Because lighting can change the exterior structure and appearance of a building [2].

The lighting needs to enhance the brand image, highlight the beauty of the building and open the surrounding space for confident exploration and enjoyment.

The visual aspect of historical buildings should be brought to the fore, their details should be revealed. In addition, it should attract attention. However, it should not deteriorate the characteristics of the historical building and should not harm the historical building. For this reason, indoor and outdoor lighting of historical buildings is made [3, 4]. Recently, lighting and energy efficiency have become increasingly important [5]. In addition, studies were conducted on lighting of historical buildings and energy efficiency [6–10].

Fig. 1. View of the satellite of the El Aman Caravanserai

Integrated with advanced control systems, LED is one of the solutions for light quality and energy efficiency in the field of sustainable lighting. When designing illumination, one should take into account the historical value of the building, protection of historical buildings, the most appropriate combination between natural and artificial lighting, human visual welfare, perception and vision quality, visual ergonomics and satisfaction [11].

A number of articles have studied and developed LED lighting systems for either interinal or exterior lighting [12–16].

The increase in energy consumption is due to population growth, increased demand for construction services and comfort levels, as well as increased time spent inside buildings, which ensures that the upward trend in energy demand continues in the future [17]. The development of energy efficiency in buildings is necessary to reduce energy dependency and greenhouse gas emissions [18]. Energy efficiency is a reduction for energy consumed without changing the required brightness level of the illuminated environment.

Lighting is widely used because of the basic need. Therefore, the amount of energy used in lighting increases. According to the report by the International Energy Agency, lighting consumption accounts for 19 % of the world's total energy consumption [19]. At the same time, energy consumption in lighting is 20 % of the total energy consumption in Turkey [20]. For this reason, efficient use of energy in lighting is important. Lighting is one of the potential ways to increase energy savings in buildings [21].

Lighting is not about achieving a certain level of brightness, but about providing good visual conditions. Ensuring good visual conditions depends more on the qualitative and quantitative characteristics of lighting [22]. Lighting should affect those who look at facilities and buildings from an artistic point of view [3].

The main goal of lighting is to provide the correct lighting solution for the installation to achieve the highest quality product, or for the image, while releasing the need for energy efficiency.

When installing lighting, you should choose an installation that will not cause any damage to the stone in the historical building. In addition, the installation made during the initial construction process should not be changed as much as possible.

The purpose of the building to be illuminated and the reason for the need for lighting are the determining criteria for the design of the lighting installation. The characteristics of the illuminated building affect the criteria for selecting the lighting element, in terms of image beauty, as well as in terms of comfort i.e. the gloss and glare, colour and temperature of the lighting used. In this study, the energy efficiency of lighting in historical buildings was analyzed using the example of the El Aman Caravanserai in province of Bitlis in Turkey.

2. A BRIEF HISTORY OF THE EL AMAN CARAVANSERAI

The El Aman Caravanserai is located in Bitlis, the esast point of Turkey (latitude 38°29′28″ N, 42°11′36″ E). It is an example of Ottoman architecture of the second half of the 16th century. The El Aman Caravanserai, which is located about 90 m south of the northeast western axis and the longest distance is about 70 m, is one of the largest caravanserais in Anatolia. This building was built to provide shelter for passengers and caravans traveling along the trade routes connecting Asia with Anatolia and Europe [23]. A satellite image of the El Aman Caravanserai is shown in Fig. 1. This study uses an example of a historical building named the El Aman Caravanserai in Bitlis (Turkey), which is currently used as the cultural centre at Bitlis Eren University. The general image of the El Aman Caravanserai is shown in Fig. 2.

Lighting historical buildings that symbolize the city's history is a special issue [10]. When lighting these buildings, lighting should be done that does

Table 1. Characteristics of Interior and Exterior Lighting Installations

Lighting installation		**Installed power for each Lamp type P (W)**				
Interior lighting		**Power of *I* luminaire (W)**	**Power of *MH* luminaire (W)**	**Power of *H* luminaire (W)**	**Number of luminaire used (pc.)**	**Total power (W)**
Rooms	Staff rooms	100	–	–	15	1500
	Meeting rooms	100	–	–	4	400
	Multi purpose hall	100	–	–	30	3000
	Small cinema	100	–	–	48	4800
	Corridors	100	–	–	10	1000
	Storerooms	100	–	–	4	400
	Toilet	100	–	–	6	600
Total power of interior lighting (W)						11700
Exterior lighting		**Power of *I* luminaire (W)**	**Power of *MH* luminaire (W)**	**Power of *H* luminaire (W)**	**Number of luminaire used**	**Total power (W)**
Facade	Courtyard	–	–	60	9	540
	Northern	–	150	–	2	300
	Western	–	150	–	2	300
	Southern	–	150	–	3	450
	Eastern	–	150	–	3	450
Total power of exterior lighting (W)						2040

***Note to Table 1**: *H* is the halogen lamp, *I* is the incandescent lamp, *MH* is the metal halide lamp.

not physically harm the work and does not describe the person that the work represents. Because while lighting these buildings promotes tourism, lighting architecturally impressive buildings plays an important role in creating the aesthetic identity of the city.

There are no buildings or constructions in the area where the historical structure was built. For this reason, there is no distribution of lighting sources in the interior and on the facade, as well on the front facade territory. Therefore, only luminaires provide night lighting.

At the first stage of construction, the El Aman Caravanserai was illuminated by daylighting. The daylighting of the caravanserai is shown in Fig. 3.

However, after being transformed into a cultural centre, it was illuminated by both daylighting and artificial lighting (Fig. 4).

The light distribution characteristics and physical dimensions of the type of luminaire used in the

Fig. 2. General image of the El Aman Caravanserai

Table 2. Types and Characteristics of Luminaires Used*

Luminaire type	Power (W)	Luminous flux (lm)	Correlated colour temperature (K)	Colour rendering index (CRI)	Lifetime (Hours)
Metal halide	150	12000	4200	85	6000–10000
Halogen	60	630	2800	100	2000–4000
Incandescent	100	1380	2700	100	1000

Note to Table 2 by the scientific editor: here and below, the characteristics of luminaires with traditional lamps such as incandescent, halogen, and metal halide lamps is used for the characteristics of the lamps itselves. When is specified power and lifetime of the luminaire, it is necessary to take into account the power and the lifetime also in relation to electronic components, such as ballast, ignitor and driver, as well as taking into account the optical system of the luminaire for determine luminous flux.

Fig. 3. Daylighting of the El Aman Caravanserai

Fig. 4. Daylighting and artificial lighting of the El Aman Caravanserai

lighting of historical buildings are important. The products should be preferred in dimensions that do not affect the aesthetic integrity of the structure and the general appearance during the daylight, or the application points of the luminaires should be positioned so as not to affect the overall appearance [24].

2.1. Lighting of the El Aman Caravanserai

Daylighting and artificial lighting illuminate the El Aman Caravanserai. For artificial lighting are used 117 luminaires with incandescent lamp 100 W as interior lighting, and 9 luminaires with halogen lamp 60 W and 10 luminaires with metal halide lamp 150 W for exterior lighting. Exterior installation project for outdoor lighting is shown in Fig. 5. The design of the interior installation of indoor lighting is shown in Fig. 6. The names of some parts of the historical building are records in the project. Characteristics of interior and exterior lighting system are given in Table 1. In existing electrical installation uses (2×2.5) *NHXMH* cable for interior lighting, and to install exterior lighting (3×2.5) *NHXMH* and (4×4) *N2XH* cables are used.

The power, luminous flux, correlated colour temperature, colour rendering index and lifetime of luminaires with the incandescent, halogen and metal halide lamps used in the historical building of the El Aman Caravanserai are given in Table 2.

3. METHODOLOGY

3.1. Using LED luminaires

LED luminaires consume less energy than conventional luminaires do. Therefore, LED luminaires are widely used in both interior and exterior lighting. In historical buildings, lighting solutions fit the texture of the building can be provided with LED luminaires. For this reason, instead of fitting with metal halide, halogen and incandescent lamps, which are used in the interior and exterior lighting of the El Aman Caravanserai, it is proposed to use LED luminaires, which are suitable for the approximate value of luminous flux of these luminaires to improve the energy efficiency in lighting. The characteristics of the proposed LED luminaires are given in Table 3.

The characteristics of the luminaires used and proposed in the El Aman Caravanserai, such as the

Table 3. Characteristics of the Proposed LED Luminaires

Luminaire type	Power (W)	Luminous flux (lm)	Correlated colour temperature (K)	Colour rendering index (CRI)	Lifetime* (Hours)
LED (instead of metal halide)	90	10000	3000	70	10000–50000
LED (instead of halogen)	20	800	2000	80	10000–50000
LED (instead of incandescent)	15	1521	2700	80	10000–50000

Note to Table 3 by the scientific editor: here and below, the lifetime of luminaires based on LED is used for the characteristics of the LED itselves. However, it is necessary to take into account the lifetime also in relation to electronic components, not only the light source, but the driver too.

Table 4. Characteristics of the Luminaires Used and Proposed

Luminaire type	Power (W)	Luminous flux (lm)	Number of luminaire used (pc.)	Colour rendering index (CRI)	Total power (W)
Incandescent	100	1380	117	100	11700
LED (instead of incandescent)	15	1521	117	80	1755
Halogen	60	630	9	100	540
LED (instead of halogen)	20	800	9	80	180
Metal halide	150	12000	10	85	1500
LED (instead of metal halide)	90	10000	10	70	900

types of luminaires, their power, luminous flux, number of luminaires used, colour rendering index and their total power are given in Table 4.

In the El Aman Caravanserai, used as a cultural centre, it is assumed that the luminaires used for interior lighting work an average of 8 hours a day, and the luminaires used for exterior lighting work an average of 10 hours a day.

The existing electrical installation will use LED lamps, which are used instead of metal halide, halogen and incandescent lamps in interior and exterior lighting systems. Therefore, the extra installation fee, which is cable and workmanship, is not included in the calculations.

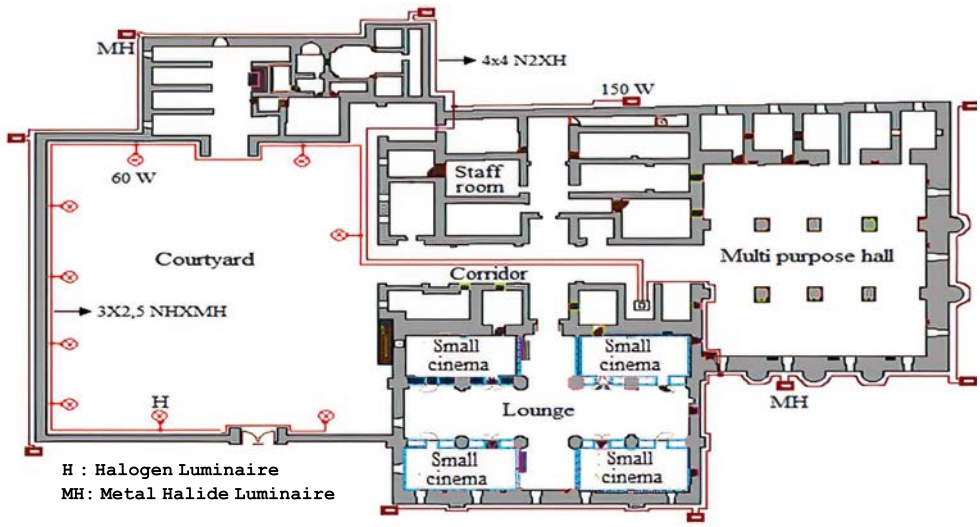

Fig. 5. Exterior installation project for outdoor lighting

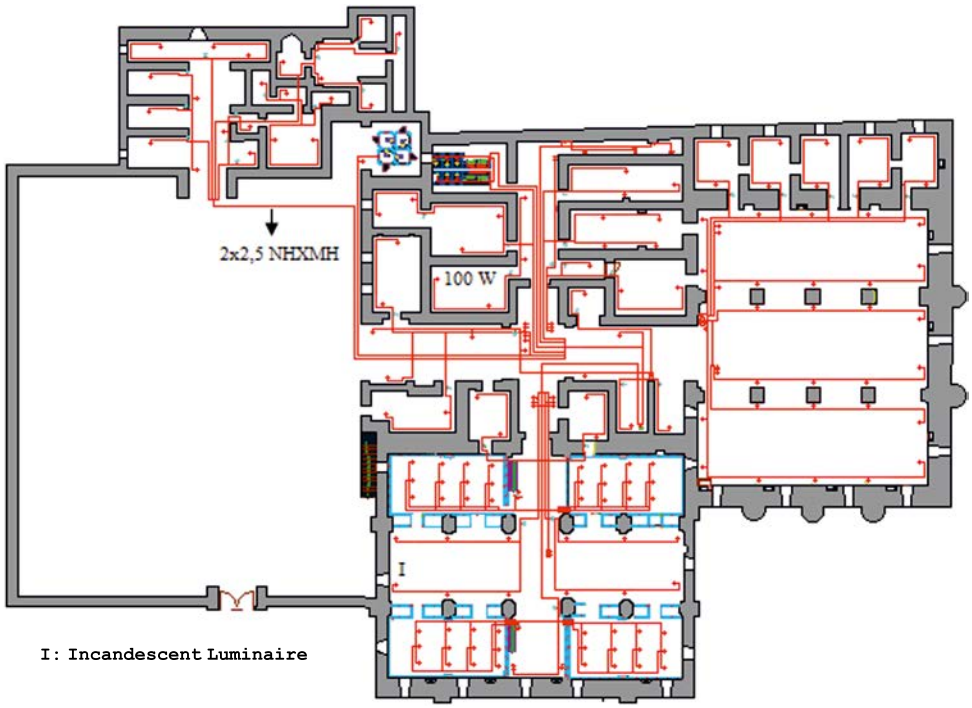

Fig. 6. Interior installation project for indoor lighting

3.2. Calculation of the Cost of the Luminaires that are Used

The costs have been calculated separately for luminaires with incandescent, halogen and metal halide lamps used in the historical building, which is the El Aman Caravanserai, and LED luminaires used instead of these ones.

The calculation of daily energy consumption for lighting installation with traditional lamps is presented below:

– With incandescent lamps

$117 \cdot 100\ W \cdot 8\ h = 93600\ W \cdot h = 93.6\ kW \cdot h;$

– With halogen lamps

$9 \cdot 60\ W \cdot 10\ h = 5400\ W \cdot h = 5.4\ kW \cdot h;$

– With metal halide lamps

$10 \cdot 150\ W \cdot 10\ h = 15000\ W \cdot h = 15.0\ kW \cdot h.$

Total daily energy consumption for lighting installation with incandescent, halogen and metal halide lamps is presented below:

$93.6\ kW \cdot h + 5.4\ kW \cdot h + 15.0\ kW \cdot h = 114\ kW \cdot h.$

Because the historic building is open and used every day of the year, the lighting installation was chosen to operate 365 days a year.

Yearly total energy consumption for lighting installation with incandescent, halogen and metal halide lamps is calculated below:

$114\ kW \cdot h / day \cdot 365\ day = 41610\ kW \cdot h.$

The cost of electricity (from September 2019) is 0.822018 Turkish Liras (TL) per 1 kW·h.

Annual energy consumption fee for lighting installation with incandescent, halogen and metal halide lamps is calculated below:

$41610\ kW \cdot h \cdot 0.822018\ TL / kW \cdot h =$

$= 34204.168\ TL.$

The calculation of daily energy consumption for lighting installation based on LED is presented below:

– Instead of incandescent lamps

$117 \cdot 15\ W \cdot 8\ h = 14040\ W \cdot h = 14.04\ kW \cdot h;$

– Instead of halogen lamps

$9 \cdot 20\ W \cdot 10\ h = 1800\ Wh = 1.80\ kW \cdot h;$

– Instead of metal halide lamps

$10 \cdot 90\ W \cdot 10\ h = 9000\ W \cdot h = 9.00\ kW \cdot h.$

Total daily energy consumption for LED luminaires is presented below:

$14.04\ kW \cdot h + 1.80\ kW \cdot h + 9.00\ kW \cdot h =$

$= 24.84\ kW \cdot h.$

Yearly total energy consumption for LED luminaires is calculated below:

$24.84\ kW \cdot h / day \cdot 365\ day = 9066.6\ kW \cdot h.$

Annual energy consumption fee for LED luminaires is calculated below:

$9066.6\ kW \cdot h \cdot 0.822018\ TL / kW \cdot h =$

$= 7452.908\ TL.$

Lifetime of incandescent lamp is 1000 h.

Annual operation time of the interior lighting system is calculated as

$8\ hour / day \cdot 365\ day = 2920\ h.$

Table 5. Average Prices for Luminaires

Luminaire type	Power (W)	Average cost per luminaire (TL)
Incandescent	100	6
Halogen	60	15
Metal halide	150	90
LED (instead of incandescent)	15	40
LED (instead of halogen)	20	106
LED (instead of metal halide)	90	650

The estimated time period, after which the incandescent lamp in the luminaire should be replaced (replacement time) based on the lifetime of it is calculated as $1000h/(2920\ h/year) = 0.342\ year$.

The lifetime of the LED luminaires varies from 10000 to 50000 hours. In the calculations, 30000 hours were selected, which is the average lifetime of the lamp.

So the LED luminaire (instead of luminaire with the incandescent lamp) replacement time is calculated as $30000h/(2920\ h/year) = 10.27\ year$.

Lifetime of halogen lamp is 3000 h.

Annual operation time of the exterior lighting system is calculated as

$10\ hour/day \cdot 365\ day = 3650\ h$.

Replacement time of the fitting with the halogen lamp is calculated as

$3000h/(3650\ h/year) = 0.822\ year$.

So the LED luminaire (instead of luminaire with the halogen lamp) replacement time is calculated as $30000h/(3650\ h/year) = 8.219\ year$.

Lifetime of metal halide lamp is 8000 h.

Replacement time of the luminaire with the metal halide lamp is calculated as

$8000h/(3650\ h/year) = 2.191\ year$.

So the LED luminaire replacement time (instead of luminaire with the metal halide lamp) is calculated as $30000h/(3650\ h/year) = 8.219\ year$.

Prices for the luminaires vary from brand to brand or from company to company. Therefore, the average prices for the luminaires according to market research data are shown in Table 5.

This way we can calculate the initial investment cost for lighting installation with traditional lamps:

– With incandescent lamps $6\ TL \cdot 117 = 702\ TL$;

– With halogen lamps $15\ TL \cdot 9 = 135\ TL$ 15;

– With metal halide lamps $90\ TL \cdot 10 = 900\ TL$.

Then total initial investment cost is

$702\ TL + 135\ TL + 900\ TL = 1737\ TL$.

Annual luminaire replacement cost for luminaires with traditional lamps is calculated below:

– With incandescent lamps

$6\ TL \cdot 117/0.342 = 702\ TL/0.342 = 2052.63\ TL$;

– With halogen lamps

$15\ TL \cdot 9/0.822 = 135\ TL/0.822 = 164.23\ TL$;

– With metal halide lamps

$90\ TL \cdot 10/2.191 = 900\ TL/2.191 = 410.77\ TL$.

Annual operating costs for fittings with incandescent, halogen and metal halide lamps are made up of annual charge for energy consumption and the annual cost of replacing the lamps. So, the annual operating cost for lighting system with traditional lamps is

$34204.168\ TL + 2627.63\ TL = 36831.798\ TL$.

Total cost of lighting installation with incandescent, halogen and metal halide lamps consists of initial investment costs and annual operating costs, and is equal to $1737\ TL + 36831.798\ TL = 38568.798\ TL$.

Similarly, we can calculate the initial investment cost for LED luminaires that is:

– 15 W LED luminaires (instead of incandescent) $40\ TL \cdot 117 = 4680\ TL$;

– 20 W LED luminaires (instead of halogen) $106\ TL \cdot 9 = 954\ TL$15;

– 90 W LED luminaires (instead of metal halide) $650\ TL \cdot 10 = 6500\ TL$.

Total initial investment costs of LED luminaires is $4680\ TL + 954\ TL + 6500\ TL = 12134\ TL$.

Annual fitting replacement cost for LED luminaires is calculated below:

– Instead of incandescent lamps

$40\ TL \cdot 117/10.27 = 4680\ TL/10.27 =$

$= 455.696\ TL$;

– Instead of halogen lamps

$106\ TL \cdot 9/8.219 = 954\ TL/8.219 = 116.07\ TL$;

– Instead of metal halide lamps

$650\ TL \cdot 10/8.219 = 6500TL/8.219 = 790.85\ TL$.

Then the total annual fitting peplacement cost for LED luminaires is equal to

$455.696\ TL + 116.07\ TL + 790.85\ TL =$

$= 1362.616\ TL$.

The annual operating cost for LED luminaires consists of the annual energy consumption fee and the annual fitting replacement cost, and calculated below as:

$$7452.908\ TL + 1362.616\ TL = 8815.524\ TL.$$

The total cost for LED luminaires consists of the initial investment cost and the annual operating cost, and calculated below as:

$$12134\ TL + 8815.524\ TL = 20949.524\ TL.$$

3.3. Calculation of the Amortization Period

According to the cost calculations, in case of using the LED luminaire, the cost is higher than when using fittings with incandescent, halogen and metal halide lamps. However, the amortization period has been calculated to determine the feasibility of using LED luminaires to improve the energy efficiency for the El Aman Caravanserai.

The amortization period when using LED luminaires instead of fittings with incandescent, halogen and metal halide lamps has been calculated, equation (1):

$$C_1 + A_p \cdot C_2 = C_3 + A_p \cdot C_4, \qquad (1)$$

where C_1 is the initial investment cost for fittings with traditional lamps (TL), C_2 is the annual operating cost for fittings with traditional lamps (TL), C_3 is the initial investment cost for LED luminaires (TL), C_4 is the annual operating cost for LED luminaires (TL), A_p is the amortization period (year).

The amortization period when using LED luminaires instead of luminaires with traditional lamps in case of the El Aman Caravanserai is calculated in accordance with (1):

$$1737\ TL + A_p \cdot 36831.798\ TL = 12134\ TL +$$
$$+ A_p \cdot 8815.524\ TL,$$
$$A_p \cdot (36831.798\ TL - 8815.524\ TL) =$$
$$= 12134\ TL - 1737\ TL,$$
$$A_p \cdot 28016.274\ TL = 10397\ TL,$$
$$A_p = 0.371\ year = 4.452\ months = 135.415\ days.$$

According to the calculation of amortization period, the cost of lighting in the historical building using LED luminaires have been amortized in about 135 days. This period is available period for improving energy efficiency in the lighting for historical building such as the El Aman Caravanserai.

4. CONCLUSION

The electrical energy used in lighting is 20 % of the total energy. Therefore, it is important to use LED luminaires. To ensure the energy efficiency of lighting, LED luminaires, which are consumed less energy than conventional luminaires should be preferable. As a result, it is predicted that the use of LED luminaires in general lighting will gradually increase.

In the El Aman Caravanserai, the annual energy consumption has been calculated 9066.6 kW·h in interior and exterior lighting using LED luminaires. On the other hand, the annual energy consumption has been calculated 41610 kW·h using luminaires with traditional lamps such as incandescent, halogen and metal halide lamps. Thus, it is expected that switching to LED luminaires will save approximately 78 % of the annual energy consumption compared to existing luminaires with traditional lamps.

The initial investment cost of LED luminaires (12134 TL) has been calculated approximately 86 % higher than the initial investment cost (1737 TL) of luminaires with incandescent, halogen and metal halide lamps. However, the annual operating cost of LED luminaires (8815.524 TL) has been calculated approximately 76 % less than the annual operating cost of luminaires with incandescent, halogen and metal halide lamps (36831.798 TL). According to the calculation, the cost of lighting in the historical building using LED luminaires will be amortized in approximately 135 days. After amortization period, lighting will be made with less energy consumption, and energy will be used efficiently.

Finally, the low energy consumption of LED lighting belongs to the widely discussed topic of how to save energy. Teherefore, the LED luminaire plays an important role in improving the energy efficiency of historical lighting. In other words, the author describe how it is possible to manage energy consumption for a lighting system, and shows how it is possible to obtain significant energy efficiency for historical buildings using lighting system based on LED luminaires.

ACKNOWLEDGEMENT

The author is grateful to the Rectorate of Bitlis Eren University for their support.

REFERENCES

1. Troi A., Bastian Z. "#Energy Efficiency Solutions for Historic Buildings, A Handbook, 2015.

2. www.thornlighting.co.uk (Access date:20.08.2019)

3. Górczewska M. Some aspects of architectural lighting of historical buildings. Conf. Light in Engineering, Architecture and the Environment, WIT Press, Southampton, Boston, ISSN: 1743–3509, 2011. pp. 107–116.

4. https://www.iac.es/system/files/documents/2019–09/opcc-otpc_guide.pdf.(Access date:15.06.2019)

5. Kocaman B., Rüstemli S. Comparison of LED and HPS luminaires in Terms of Energy Savings at Tunnel Lighting, Light & Engineering, 2019. V27, #3, pp. 67–74.

6. Claesson M., Broström T. Eight years of energy efficiency in historic buildings, Energy Efficiency and Comfort of Historic Buildings Brussels, Belgium 19th-21st October, 2016.

7. Troi A. Comfort and energy efficiency in historic buildings – the 3ENCULT experience, Energy Efficiency and Comfort of Historic Buildings Brussels, Belgium 19th-21st October, 2016.

8. Lucchi E. Energy Efficiency in Historic Buildings: a Tool for Analysing the Compatibility, Integration and Reversibility of Renewable Energy Technologies, World Renewable Energy Congress 2011, 8–13 May 2011, Linköping, Sweden.

9. Rezabek C., Mapp J., Smith, Cavallo J. Energy Efficient Lighting in Historic Buildings, 2008 American Council for an Energy-Efficient Economy (ACEEE) Summer Study on Energy Efficiency in Buildings, 2008.

10. Górczewska M., Mroczkowska S. Lighting of historical architectonic facilities and buildings using as an example the St. Joseph Church in Poznań, Computer Applications in Electrical Engineering, 2015. V13, pp. 394–403.

11. Balocco C., Volante G. A Method for Sustainable Lighting, Preventive Conservation, Energy Design and Technology Lighting a Historical Church Converted into a University Library, Sustainability 2019. #11, p. 3145.

12. Khan N., Abas N. Comparative study of energy saving light sources, Renewable & Sustainable Energy Reviews, 2011. V15, #1, pp. 296–309.

13. Braga M.F., Nogueira F.J., Campos M.F.C., Gouveia L.H.B., Braga H.A.C. A comparative study regarding linear fluorescent and LED lamps for indoor lighting, 2014 11th IEEE/IAS International Conference on Industry Applications (INDUSCON), 2014. pp. 1–7.

14. Jingyu Liu, Wen Zhang, Xiaodong Chu, Yutian Liu Fuzzy logic controller for energy savings in a smart LED lighting system considering lighting comfort and daylight, Energy Build, 2016. #127 (September), pp. 95–104.

15. Devesh Singh, Chandrajit Basu, Merve Meinhardt-Wollweber, Bernhard Roth, LEDs for energy efficient greenhouse lighting, Renewable & Sustainable Energy Reviews, 2015. V49, pp. 139–147.

16. Uddin S., Shareef H., Mohamed A. Power quality performance of energy-efficient low-wattage LED lamps, 2013. Measurement 46, pp. 3783–3795.

17. L. Ozolina, M. Rosˇa, A review of energy efficiency policy and measures for industries in Latvia, Management of Environmental Quality: An International Journal, 2012. V23, #5, pp. 517–526, doi:10.1108/14777831211255097.

18. Berg F., Donarelli A. Energy performance certificates and historic buildings: a method to encourage user participation and sustainability in the refurbishment process, Energy Efficiency and Comfort of Historic Buildings (EECHB-2016), 2016. 19th-21st October.

19. http://hasmutlu.com/blog/led-aydinlatma-ve-enerji-verimliligi/(Access date:15.08.2019)

20. Öztürk A.E., Aşkın M., Dal M., Korunur S., Kaymaz K. Konutlarda Yapay Aydınlatma Enerjisinin Etkin Yönetim, Munzur Üniversitesi, Bilim ve Gençlik Dergisi, 2017. V5, #2, pp. 1–17.

21. Kamaruzzaman S.N., Zulkifli N. A Review of the Lighting Performance in Buildings through Energy Efficiency, 2nd International Conference on Research in Science, Engineering and Technology (ICRSET'2014) March 21–22, Dubai, 2014.

22. http://www.yfu.com/kitapciklar/muzelerde_ve_burolarda_aydinlatma.pdf (Access date:28.09.2019)

23. Uluçay S. El Aman Hanı ve Köse Hüsrev Paşa Üzerine Bir Değerlendirme, Bitlis Eren Üniversitesi Sosyal Bilimler Enstitüsü Dergisi, 2012. V1, #1, pp. 70–83.

24. Özenç S., Menteşeoğlu D. İzmir'deki Kent Aydınlatmasına Yönelik Olumsuz Uygulamalar ve Çözüm Önerileri, TMMOB2. İzmir Kent Sempozyumu / 28–30 Kasım 2013. pp. 69–78.

Behcet Kocaman

received his B.Sc. degree in Electrical Engineering from Yıldız Techinal University in 1993. He received M.S. and Ph.D. degrees, all in Electrical Engineering, from Kocaeli University in 1997 and 2015, respectively. Currently, he is working as Assistant Professor at department of Electrical and Electronic Engineering at Bitlis Eren University. His research areas are energy efficiency, lighting, renewable energy sources, energy management, and transmission and distribution technologies

Light & Engineering
Vol. 28, No. 4, pp. 77–83, 2020
https://doi.org/10.33383/2020-09
Svetotekhnika #5, 2020

INTERIOR LIGHTING OF A HISTORICAL BUILDING BY USING LED LUMINAIRES: A CASE STUDY OF FATIH PAŞA MOSQUE

Serhat Berat Efe[1] and Derman Varhan[2]

[1]Department of Electrical Engineering, Bandırma Onyedi Eylül University, Turkey
[2]General Directorate of Foundations, Provincial Directorate of Diyarbakır, Turkey
E-mail: sefe@bandirma.edu.tr

ABSTRACT

In this study, a place of worship lighting in accordance with CIE standards was examined. Halogen lamps were used in the place of worship lighting, which was physically applied. Halogen lamp lighting and LED illuminated place of worship environment were compared in terms of luminance level and economic cost in a simulation environment. The illumination level should be 100 lx or above for places of worship according to CIE standards. Lighting using LED lamps, which provide 100 lx illuminance levels, has yielded 85 % more efficient results than illumination by halogen lamps.

Keywords: energy efficiency, LED, historical place, artificial lighting, illuminance, energy consumption

1. INTRODUCTION

Illuminance, which is physically defined as the luminous flux at the unit area, is also expressed as the perceptibility level of the environment or as a result of the light's usability. There are two types of lighting: day lighting and artificial lighting [1–2].

The lighting pattern of natural light differs hourly, seasonally, and would change according to weather conditions. Since it is not possible to provide illumination at any time with daylight, artificial lighting is preferred in the lighting of the places where the lighting needs are obvious [3–5]. Good and accurate lighting increases work efficiency and economic development, prevents accidents, prevents eye distortion, improves eye perception, and improves living comfort. The structure of the place to be illuminated and the reason for the illumination necessity determines the criteria of the lighting installation.

The characteristics of the area to be illuminated affect the criteria for determining the lighting element to be selected as the aesthetic quality of the architectural building. These characteristics should be considered in terms of comfort-related concepts such as glare, colour rendering index, and correlated colour temperature of the light sources used [6–8].

This study focuses on the lighting of a historical mosque located in Diyarbakır, Turkey. The topic was chosen because much too little study has been done on both lighting and modernization of illumination systems for historical buildings [9]. Within the scope of the study, principals about to lighting design of the historical buildings and the advantages of using LED lighting at such places are investigated in terms of energy savings. In the proposed study, modern and low energy consumption LED luminaires have been adapted instead of inefficient lighting elements in the historical building. In this way, while achieving illuminance levels in accordance with the standard, energy savings were achieved at the same time. During the design and assembly stages of the lighting elements, the originality of the building was fully protected.

A lighting project implemented in this study was analysed according to the International Lighting

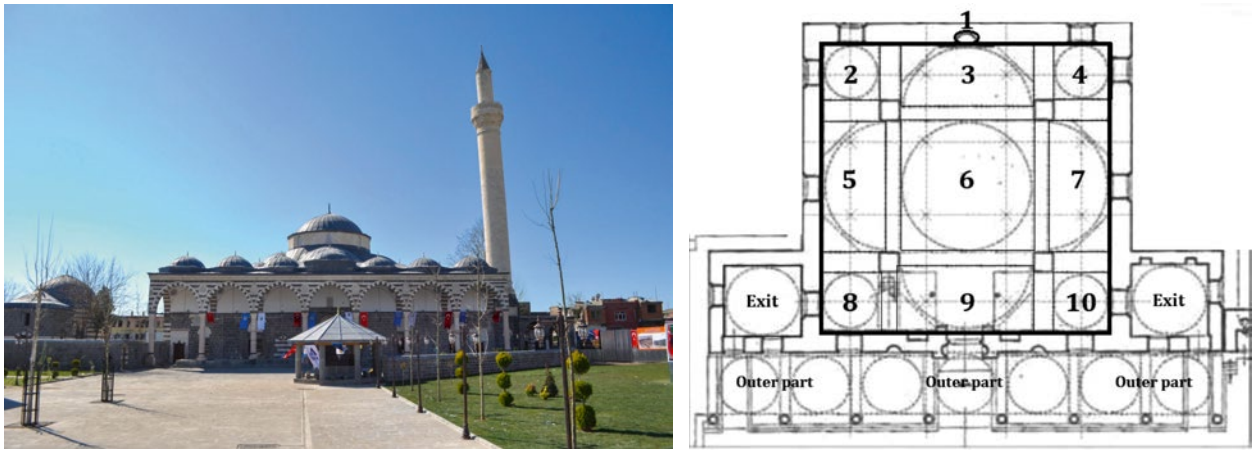

Fig. 1. Practiced place of worship and numbered lighting areas [28, 29]

Commission (CIE) standard [13]. For this purpose the lighting application in the project was compared by a non-commercial simulation program.

2. LED LIGHTING

Energy consumption for lighting increases day by day. Due to the unconscious use of energy resources, the lack of sufficient technical infrastructure to reach renewable energy sources, and the high-energy amounts, the importance of saving in lighting has increased remarkably [10–12].

In order to provide efficiency in protecting the health and comfort of users, it was established that fluorescent bulbs, which are used instead of incandescent lamps in new projects, have lost their effectiveness and LED lamps are preferred as much as possible. Light emitting diodes (LEDs), the latest technology used in artificial lighting, are regarded as the most important invention in the history of lighting after the electric lamp that Edison discovered centuries ago [14, 16].

Lighting elements with high efficiency and colour diversity have been obtained in lighting by developments in semiconductor technology. LEDs are also the product of this development. For example, instead of a 60 W incandescent filament lamp, 9W LED array can be used to save (80–85)% energy [17–22]. Because LEDs are used both as a single light source and as a fixture, the LEDs that enable the improvement of energy efficiency in lighting need to be evaluated differently than traditional light sources. For example, LED lamps can be used for all kinds of software and communication [23–26].

3. A PLACE OF WORSHIP LIGHTING WORK

Exhibition of the historical places in a proper and decent way has gained importance and in the last few years, many new and different methods have been used on it. Proper illumination is the best way to figure out these properties. The main goal of lighting is to provide excellent vision with low energy consumption. In addition, it is vital not to harm the historical buildings and their prominent features. In this paper, the illumination of a historical building has been discussed. An ancient mosque was selected as a status study. First, considering the indoor illumination level criteria identified by standards and using original architectural plans, the areas to be illuminated in this historical building were determined. Then, the designated areas were illuminated without damaging the historical place and giving importance to visualisation. Proposed systems were implemented experimentally to determine the most accurate results by the addition of environmental and architectural effects. One-year energy consumption comparison of two type lighting methods was proposed by using energy tariff data.

In general, the main objectives of the illumination design of a historical building should be:

- The main architectural elements, ornaments, valuable elements of the registered cultural heritage should be compatible with the original texture in a way that emphasizes the social and historical importance as well as the value of the moment and document along with the original pieces of that work;
- Make it possible to observe and perceive the area in a qualified way;

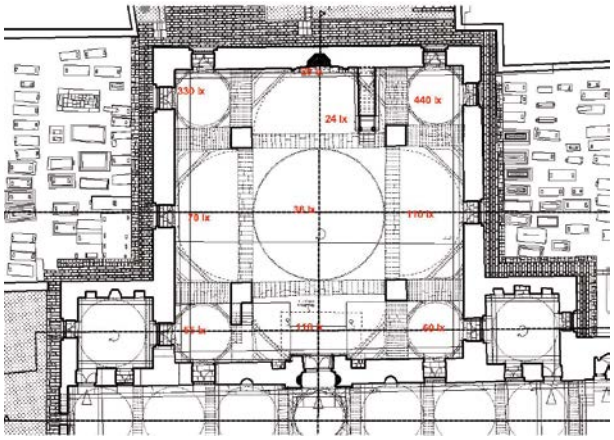

Fig. 2. Indoor daylight luminance levels measurement values

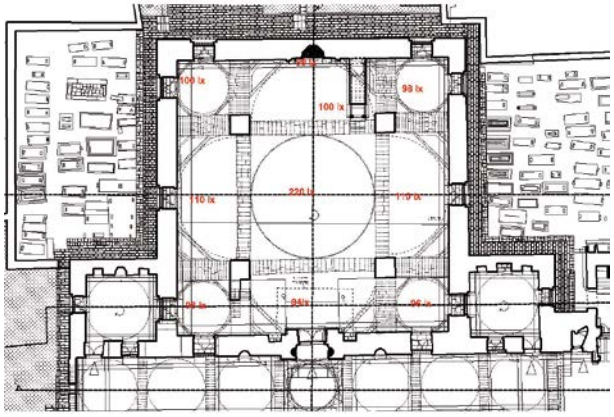

Fig. 4. Experimental measurement of indoor illuminance levels when using lighting elements at night

• To support the safety of works, especially in the old districts of cities, to increase user living, sightseeing and roaming comfort at night;

• To develop an approach that is appropriate to the principles of restoration besides aesthetics;

• Minimizing environmental impacts and maximizing energy savings while reaching desired illuminance levels [27].

Illumination of Fatih Paşa Mosque that built in Diyarbakır between 1516 and 1520 selected as a case study was performed according to these objectives. The place of worship and numbered lighting areas are shown in Fig. 1.

There are both indoor and outdoor illumination applications in this study. While the outdoor illumination is only for visualisation, this study focused on indoor illumination that has to meet standards. The minimum indoor illuminance level for worship is determined as 100 lx according to the CIE standard [13].

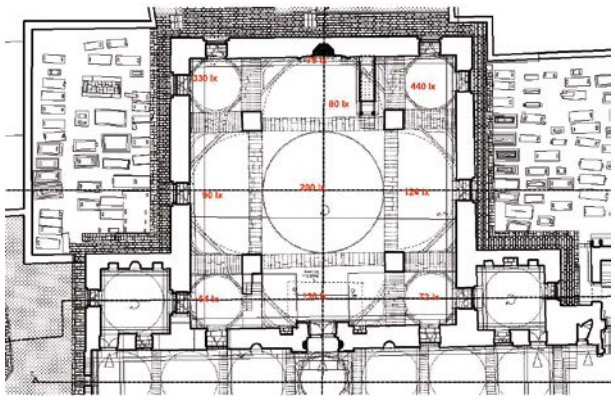

Fig. 3. Indoor experimental illuminance measurements with only the central luminaire open during daytime

In the Fatihpaşa Mosque, during the daylight hours, the illuminance levels were measured without lighting elements as shown in Fig. 2. It is seen that the illuminance levels are very high in some areas with daylight only and it is well below the desired in some areas.

Fig. 3 shows the measurements made using only the central lighting chandelier. It was observed that only the central chandelier was used during the day to provide the appropriate illumination levels for the place of worship. Fig. 4 shows measurements made using only lighting installations in the night. Indoor view of mosque after installation completed is given in Fig. 5. Table 1 shows the illuminance values according to the places of worship in manual measurements.

The lamps that operate actively during the day or at night are the lamps in Area-6. When Table 1 is examined, in the measurements made physically, 36 lx for 5 m height was measured in daylight in Area-6. During the day, when artificial lighting is made only in Area-6, 200 lx was measured. Again,

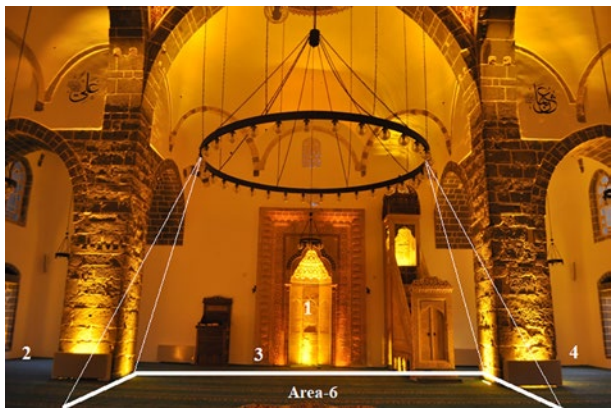

Fig. 5. Lighting scene with only embedded LED wall-washers

Table 1. The Illuminance Values According to the Places of Worship in Manual Measurements

Area	Daylight (no artificial lighting), lx	Daytime main lighting, lx	Night lighting (full capacity), lx
1	20	75	90
2	330	330	100
3	24	80	100
4	440	440	98
5	70	90	110
6	36	200	220
7	110	124	110
8	55	64	98
9	116	130	84
10	60	72	96

in the area-6 measurement at night, 220 lx was measured with the effect of other projectors. Accordingly, 36 lx value does not comply with CIE criteria in daylight free environment [1, 3, 30], because, at least, 100 lx illuminance is required for places of worship in the relevant CIE Standard [13]. If 32 halogen lamps are used in area-6, it is seen that unnecessary consumption is made if the lamp consumption is considered to be 60 W. If the lighting is realized with LED bulbs, a comparison has been made in the simulation environment for the energy consumption difference. In other words, 32 halogen lamps in area-6 were evaluated as LED lamps in the simulation environment and a comparison was made in terms of their illuminance levels. LED lamps used in the simulation have a power of 9W. These LED bulbs are in the daylight colour. 9W LED bulb and 60W halogen bulb are equivalent. The simulation used is prepared for the purpose of lighting.

It is a non-commercial simulation. The area to be illuminated is divided into equal parts. The calculated section is area-6 (12×12) m. The light source is at a height of 5 m. The maintenance factor is accepted as 0.92. Table 2 was calculated in the simulation environment according to the illuminance level values in the middle point of each region. The average illumination level according to Table 2 is $E_{average}$ = 118.29 lx. The illuminance level should be 100 lx or above for places of worship according to CIE Standard. Accordingly, it is understood that the use of a 9W LED lamp is more advantageous than a 60W halogen lamp. As a result of the data entered into the simulation, Table 2 shows the illuminnance levels of points in the place of worship.

4. ECONOMIC EVALUATION IN TERMS OF ENERGY CONSUMPTION

Daily energy consumption for each illumination device can be calculated as given in equation:

$$E = P_b n_a t_{op}, \quad (1)$$

where E (W·h) is the energy, P_b (W) is the power of one bulb, n_a is the number of chandelier arms, and t_{op} (h) is the operating time of luminaire, which has daily values of 2 hours, 5 hours, and 12 hours

Table 2. Illuminance at the Points in the Place of Worship, lx

E_{min}=18.56 lx E_{max}=399.94 lx $E_{average}$=118.29 lx

Meter/Meter	0.700	2.100	3.500	4.900	6.300	7.700	9.100	10.500	11.900	13.300
0.583	15.64	14.01	9.53	13.36	13.97	13.98	13.37	9.55	14,04	15.68
1.750	28.58	26.98	16.73	21.69	21.71	21.72	21.71	16.762	27.01	28.63
2.917	49.13	45.99	32.44	30.56	27.27	27.27	30.57	32.47	46.02	49.18
4.083	87.07	68.99	62.92	41.08	37.43	37.44	41.09	62.95	69.03	87.12
5.250	164.72	140.28	98.89	60.55	57.53	57.54	60.57	98.92	140.32	164.78
6.417	235.46	283.84	183.06	98.47	82.22	82.22	98.49	183.09	283.88	235.52
7.583	359.26	406.25	262.06	144.49	111.32	111.33	144.51	262.09	406.29	359.32
8.750	284.76	291.16	195.53	122.71	101.25	101.25	122.73	195.56	291.20	284.83
9.917	158.65	129.60	94.322	65.659	62.80	62.81	65.67	94.35	129.64	158.71
11.083	77.78	58.14	47.34	36.26	37.84	37.85	36.27	47.37	58.19	77.84
12.250	43.69	36.81	30.76	24.97	24.826	24.83	24.99	30.79	36.85	43.74
13.417	29.25	24.81	21.80	18.71	17.335	17.34	18.72	21.82	24.84	29.30

Table 3. Energy Consumption for Classic Luminaires

Equipment	Power per piece, W	Used pieces	Annual energy consumption, kW·h
Halogen Lamp	60	64	6912
Halogen Projector	50	48	8352
Halogen Projector	100	51	17244
TOTAL			32508

Table 4. Energy Consumption for LED Luminaires

Equipment	Power per piece, W	Used pieces	Annual energy consumption, kW·h
LED lamp	9	64	725.76
LED wall-washer	9	48	1503.36
LED wall-washer	18	51	3103.92
Total			5333.04

Table 5. Lighting Equipment Costs

Equipment	Power, W	Cost, TL/piece	Used pieces	Total cost for proposed study, TL
Halogen lamp	60	9	64	576
Halogen projector	50	25	48	1200
Halogen projector	100	40	51	2040
LED lamp	9	10	64	640
LED wall-washer	9	150	48	7200
LED wall-washer	18	250	51	12750

Table 6. Cost Comparison

Light source in fixture	Number of used elements	Annual energy consumption, kW·h	Annual energy cost, TL	Initial investment cost, TL	Total cost, TL
Halogen	163	32508	27228.7	3816	31044.7
LED	163	5333.04	4466.95	20590	25056.95
Saving		27174.96			5987.75

according to illuminator location as indoor and outdoor. Annual energy consumption of classical and LED illumination system components was calculated by using equation (1) and summarized in Table 3 and Table 4 respectively. In addition, equipment costs are given in Table 5.

According to the Electricity Market Regulatory Authority of Turkey data, as of 01.01.2020 per unit price of electricity was determined to be 0.8376 TL/kW·h and 27174.96 kW·h to be calculated for energy savings. So, annual energy saving is provided to be equal to 27174. 96 kW×h×0.8376 = 22761.7 TL. Difference with LED system will approximately be amortized total cost in about 9 months. It should be noted that lamp lifetimes are not taken into account. It is clear that payback period will further be reduced when considering lifetimes of both lamps. Annual cost comparison by adding initial investment costs is given in Table 6.

5. CONCLUSION

This study proposes the illumination of a historical building. An ancient mosque built in the early 16th century selected as a case study. The study includes the physical installation of lighting systems. Within the scope of the study, the installation of LED lighting systems was carried out while preserving the original state of the building.

In this study, the most important situation is the examination in terms of energy efficiency and saving. Cost calculations have been made for the cases where the lighting is done with classical and LED systems. As a result of the calculations, it has been observed that a great amount of energy can be saved when lighting installations with LED systems are using.

During the day lighting in area-6 with 32 lamps is needed. For the lighting in area-6 with 32 lamps during the day, 60W halogen lamp lighting application and 9W LED illuminated simulation were compared in terms of energy consumption. The instantaneous total energy consumed by halogen bulbs is 1920W and the instantaneous total energy consumed by 32 LED lamps is 288W. Accordingly, it is understandable that when an LED lighting that provides 100 lx and above are using ambient illumination, recommended by CIE Standard, is achieved with efficiency equal to 85 %. The average illuminance level for LED illumination in the simulation environment is equal to 118.29 lx.

ACKNOWLEDGEMENT

Author would like to thank General Directorate of Foundations of Provincial Directorate of Diyarbakır, Turkey, for their valuable contributions.

REFERENCES

1. Cengiz. M.S. Simulation and Design Study for Interior Zone Luminance in Tunnel Lighting// Light & Engineering, 2019, Vol. 27, #2, pp. 42–51.

2. Iacomussi, Rossi G., Soardo P. Energy Saving and Environmental Compatibility in Road Lighting// Light & Engineering, 2012, Vol. 20, #4, pp. 55–63.

3. Cengiz M.S. The Relationship between Maintenance Factor and Lighting Level in Tunnel Lighting//Light & Engineering, 2019, Vol. 27, #3, pp. 75–88.

4. Cole M., Driscoll T. The Lighting Revolution: If We Were Experts Before, We're Novices Now// IEEE Transactions on Industry Applications, 2014, Vol. 50, #2, pp. 1509–1520.

5. Coşkun. T., Gülhan Ö, Şahin C.D., Arsan Z.D., Akkurt G.G. The effect of spatial interventions on historic buildings' indoor climate (Case Study: Tire Necip Paşa Library. Izmir-Turkey)// Energy Procedia, 2017, Vol. 133. pp. 358–366.

6. Kamaruzzaman S. N., Zulkifli N. A Review of the Lighting Performance in Buildings through Energy Efficiency// Presented at the 2nd International Conference on Research in Science, Engineering and Technology (ICRSET'2014). March 21–22. 2014. Dubai (UAE).

7. Almodovar-Melendo J. M., Cabeza-Lainez J. M., Rodriguez-Cunill. I. Lighting features in historical buildings: Scientific analysis of the Church of Saint Louis of the Frenchmen in Sevilla// Sustainability, 2018, Vol. 10, #9, pp. 1–23.

8. Cesario E., Grifoni R.C., Leuzzi A., Paciotti D. Light design in historical buildings: Parameters and prototypes. Comparison of façade behaviour: Metal meshes vs. high-tenacity polymer composite meshes// Presented at International Conference on Environment and Electrical Engineering, 2016, pp. 1–5.

9. Zakaria S. A., Bahauddin A. Light Art for Historical Buildings: A Case Study of the Heritage Buildings in George Town. Penang Island// Procedia – Social and Behavioural Sciences, 2015, Vol. 184, pp. 345–350.

10. Salvadori G., Fantozzi F., Rocca M. & Leccese. F. The energy audit activity focused on the lighting systems in historical buildings// Energies, 2016, Vol. 9, #12, pp. 1–13.

11. Górczewska. M.. Some aspects of architectural lighting of historical buildings. WIT Transactions on the Built Environment. 2011. Vol. 121, pp. 107–116.

12. Balocco C., Volante G. A method for sustainable lighting, preventive conservation, energy design and technology-lighting a historical church converted into a university library//Sustainability, 2019, Vol. 11, #11. pp. 1–17.

13. CIE Standard "Lighting of Work Places – Part 1: Indoor" ISO 8995:2002(E)/ CIE S008/E-2001.

14. Xu X., Collin A., Djokic S.Z., Langella R., Testa A., Drapela J., Experimental evaluation and classification of LED lamps for typical residential applications// Presented at 2017 IEEE PES Innovative Smart Grid Technologies Conference Europe. ISGT-Europe 2017, pp. 1–6.

15. Kim J., Sa G., Kim Y., Baek J. LED-ID application for intelligent lighting// Presented at International Conference on Ubiquitous and Future Networks. ICUFN. 2015-August, pp. 225–227.

16. Matvoz D., Maksić M. Comparison of LED and CFL lamps and their impact on electric power network// Presented at Harmonics and Quality of Power (ICHQP). 2012 IEEE15th International Conference in Hong Kong, 2012, pp. 320–327.

17. Yurci Y., Cengiz Ç., Yapici İ., Cengiz M.S., Yildirim S., Eren M., Palta O., Atiç S. Analysis of Energy Productivity in LED Illumination by Active or Passive Methods// International Conference on Multidiscipli-

nary Engineering, Science, Education, and Technology, 2017, Baku.

18. Onaygil S., Güler Ö., Erkin E. Cost Analyses of LED Luminaires in Road Lighting// Light & Engineering, 2019, Vol. 20, #2, pp. 39–45.

19. Cengiz Ç., Kaynaklı M., Gencer G., Eren M., Yapici İ., Yildirim S., Cengiz M.S. Selection Criteria and Economic Analysis of LEDs// Book of Abstracts. Imeset Int. Conf. Mult. Sci. Eng. Tech., October 27–29, 2017, Bitlis, Turkey.

20. Yurci Y., Yildirim S., Palta O., Cengiz Ç., Atiç S., Yapici İ., Cengiz M.S., Eren. M. Numerical Analysis of LED Illumination Productivity Parameter// International Conference on Multidisciplinary, Engineering, Science, Education, and Technology, 2017, (IMESET'17 Baku).

21. Yıldırım S., Yapıcı İ., Atiç S., Eren M., Palta O., Cengiz Ç., Cengiz M.S., Yurci Y. Numerical Analysis of Productivity and Redemption Periods in LED Illimunation// Imeset Book of Abstracts. Int. Conf. Mult. Sci. Eng. Tech., 12–14 July, 2017, Baku.

22. Cengiz M.S., Cengiz Ç. Numerical Analysis of Tunnel LED Lighting Maintenance Factor// IIUM Engineering Journal, 2018, Vol. 19, #2, pp. 154–163.

23. Çıbuk M., Arı D., Ağgün F. Relay Mechanism with Three way Handshake for Wireless Sensor Networks// Presented at the 8th International Advanced Technologies Symposium, Elazığ, 2017.

24. Çıbuk M., Cengiz M.S. Determination of Energy Consumption According to Wireless Network Topologies in Grid-Free Lighting Systems// Light & Engineering, 2020, Vol. 28, #2, pp. 67–76.

25. Cengiz M.S., Cengiz Ç. IOT and Lighting Automation// International Conference on. Imeset Book of Abstracts. Int. Conf. Mult. Sci. Eng. Tech., 12–14 July, 2017, Baku.

26. Arı D., Çıbuk M., Ağgün F. Effect of Relay Priority Mechanism on Multi Hop Wireless Sensor Networks// Bitlis Eren University Journal of Science and Technology, 2017, Vol. 7, #2. pp. 145–153.

27. Dos Santos Oliveira G., De Oliveira E.P., Da Silva A.P., De Moura Carvalho C.C.M. Power quality of LED lamps// Presented at International Conference on Harmonics and Quality of Power, ICHQP, 2016-December, pp. 575–580.

28. Varhan D. LED Lighting in Historical Spaces and Applications// Master Thesis. Bitlis Eren University. Turkey. October 2019.

29. Tuncer O.C. Diyarbakır Mosques. Diyarbakır Metropolitan Municipality// Culture and Art Publications, Diyarbakır, 1996.

30. Onaygil S. Turkish Electrical Distribution Company Illumination Training Seminar, 23–24 January, 2007, Ankara, Turkey.

Serhat Berat Efe
received his Ph. D. degree from Fırat University, Turkey, in 2014. His main research areas are power system analysis, power quality and renewable energy sources. He is currently working at Bandırma Onyedi Eylül University as Assistant Professor with the Electrical Engineering department

Derman Varhan
received his M. Sc. degree in the field of Electrical and Electronics Engineering from Bitlis Eren University, Turkey, in 2019. He is currently working at General Directorate of Foundations, provincial directorate of Diyarbakır, Turkey, as electrical and electronics engineer

Light & Engineering
Vol. 28, No. 4, pp. 84–90, 2020

https://doi.org/10.33383/2019-083
Svetotekhnika #2, 2020, pp. 63–66

STUDY OF OPERATING MODES OF A CONTROLLABLE LIGHTING SYSTEM CONSISTING OF A TRIAC DIMMER AND A LED LIGHT SOURCE WITH A CONTROLLABLE DRIVER

Nadezhda P. Kondratieva[1], Dmitry A. Filatov[2], and Pavel V. Terentiev[2]

[1] Izhevsk State Agricultural Academy
[2] Nizhny Novgorod State Agricultural Academy
E-mail: filatov_da@inbox.ru

ABSTRACT

The article covers the study of the effect of a dimmer on operation of a light source and electromagnetic compatibility of a controllable lighting system. It is found that with reduction of active power ***P*** of a light source its luminous flux and bulb heating temperature decrease, the power factor of the lighting system decreases too with increasing of the total harmonic distortion current factor of the lighting system. The changes are non-linear. Mathematical expressions related to changes of luminous flux, heating temperature, power factor and total harmonic distortion caused by change of active power of a light source are obtained. A conclusion is made that together with an opportunity to save energy and to increase the operating life of the controllable lighting system application of a dimmer leads to reduction of electric power quality and electromagnetic compatibility of this system. The study also demonstrated that changes in supply voltage also affect operation of the controllable lighting system. Reduced supply voltage causes the highest effect on characteristics of the lighting system. Change in the supply voltage strongly affects the luminous flux and the heating temperature of the light source and the power factor of the lighting system in operating modes at 0.25 of $\boldsymbol{P_{nom}}$ and 0.5 of $\boldsymbol{P_{nom}}$ and the total harmonic distortion in operating modes at 0.75 of $\boldsymbol{P_{nom}}$ and $\boldsymbol{P_{nom}}$.

Keywords: TRIAC dimmer, LED light source, controllable driver

1. INTRODUCTION

In Russia, 10 % of all annual electric power generation is used for lighting purposes [1]. The electricity tariffs growth makes the issue of energy saving and transfer to more energy-efficient technologies in lighting system still relevant. Nowadays light sources based on light emitting diodes (LED) are being introduced in different industries more actively. One of the advantages of LEDs is capability to control them. The control is based on such parameters as operating time and illuminance level. The operating time is controlled by means of a timing relay and the illuminance level is controlled by a dimmer. Analysis of works on controllable lighting systems [2–7] has shown that they aim at development of configurations or particular elements of such systems as well as their cost-efficiency. There are virtually no studies of the influence of dimmers on operation of light sources and electromagnetic compatibility (EMC) of a controllable lighting system. EMC of a technical device is its capability to function with a set quality level in the set electromagnetic environment and not to generate unacceptable electromagnetic interference (EMI) into operation of other technical means [8]. Level of electromagnetic compatibility of a power supply system: standardised level of conductive EMI used as reference for coordination between the acceptable level of interference caused by technical means of electric power network users and the level of interference received by technical means con-

Table 1. The Results of Studying the Characteristics in Absolute Values

***P*, W**	***K_m*, per unit**	***THDi*, %**	***E*, lx**	***Kn*,%**	***T*, °C**
Supply voltage 220V					
3	0.84	92.7	50.2	25.6	41.9
6	0.94	91.3	65.4	26.7	47.1
9	0.99	82.3	171.3	28.8	70
12	1	34.8	266	21.4	81.9
Supply voltage 198V					
3	0.66	91.9	20.9	22	40.2
6	0.88	90.9	47.9	25.2	46.2
9	0.99	78.3	150.7	27.5	69.3
12	1	29.2	266	20.9	81.9
Supply voltage 242V					
3	0.9	93	63.5	26.7	43.6
6	0.97	92.1	80	27.2	48.1
9	0.99	86.7	187	29.7	70.7
12	0.9	40	266	21.1	82

nected to an electric power network without prevention of their normal functioning. Conductive EMI is electromagnetic interference propagating via electric power network conductors [9]. Conductive EMI may reduce quality of functioning of devices, electric installations or systems, or damage them [10, 11]. That is why the problem of the determination of dimmer effect on operation of light sources and electromagnetic compatibility of a controllable lighting system is relevant.

2. MATERIALS AND METHODS

The controllable lighting system consisting of a LED light source and a dimmer was studied in the Lighting Engineering laboratory of the Nizhny Novgorod State Agricultural Academy. The study was conducted with the electric system (Fig. 1) consisting of: RNO-250–2-M regulating linear autotransformer –1, *Circutor* AR-6 electric power quality analyser – 2, IEK BCP-10–1–0 dimmer – 3, voltmeter – 4, TKA-PKM 08 flicker and illuminance meter, JazzWay PLED-DIM A60 LED light source with dimming functionality. Dimmer power regulation is up to 400 W. Dimming range of the LED light source is (25–100)%. The regulation of the active power was four-step: 0.25 P_{nom}; 0.5 P_{nom}; 0.75 P_{nom} and P_{nom}. Each step was measured 3 times.

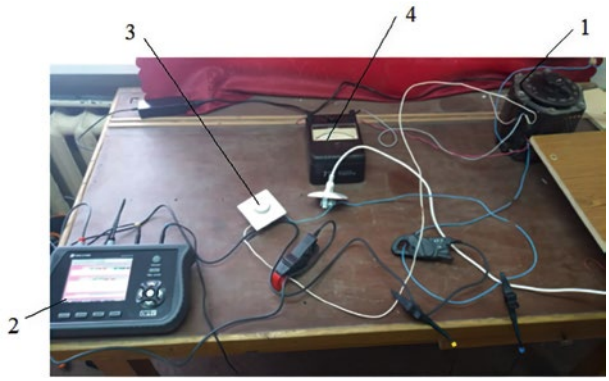

Fig. 1. The electric system for studying the controllable lighting system consisting of a LED light source and a dimmer

3. RESULTS AND DISCUSSION

The studied characteristics of the controllable lighting system included luminous flux of the light source, heating temperature of the light source, power factor and total harmonic distortion. The results of studying these characteristics at nominal points are shown in Table 1 in absolute values.

The results of the study of the light source luminous flux Φ_v dependence on active power consumption P are shown in Fig. 2.

It is found that luminous flux of the light source decreases with decrease in active power. With decrease in active power of 25 %, luminous flux decreases by 36 %. With decrease in active power of

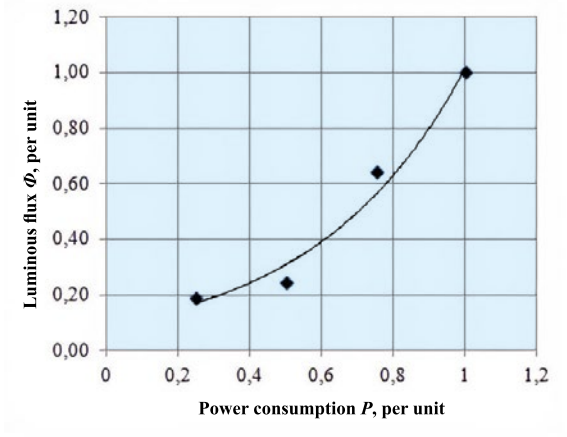

Fig. 2. The luminous flux dependence on active power consumption change

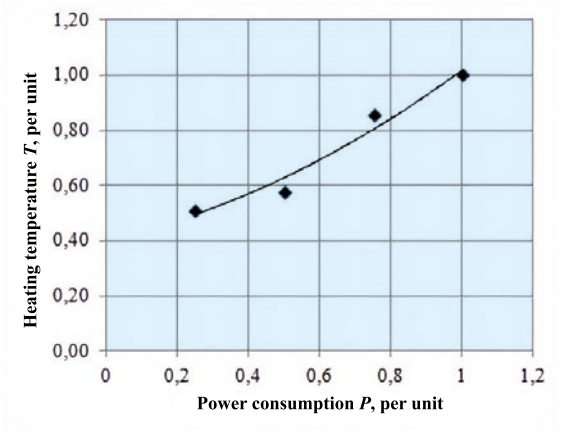

Fig. 3. Heating temperature dependence on active power consumption change

50 %, luminous flux decreases by 75 %. With decrease in active power of 75 %, luminous flux decreases by 81 %. The dependence of change of luminous flux and change of active power is non-linear and may be described by means of a mathematical expression derived using MS Excel:

$$\Phi_{\upsilon} = \Phi_{\upsilon nom} \cdot (\alpha \cdot \exp^{\beta \cdot K_P}), \quad (1)$$

where $\Phi_{\upsilon nom}$ is the nominal luminous flux, lm; α, β are constant factors depending on the manufacturer of a given light source (for the studies light source, α=0.095; β=2.3689); $K_p = \frac{P_\Phi}{P_{nom}}$ is the change of the level of active power of the light source, per unit; P_Φ is the actual active power consumption, W; P_{nom} is the nominal active power consumption, W.

The results of studying the dependence of the light source heating temperature T change and active power consumption P change are shown in Fig. 3.

It is found that heating temperature of the light source decreases with decrease in active power. With decrease in active power of 25 %, heating temperature decreases by 15 %. With decrease in active power of 50 %, heating temperature decreases by 42 %. With decrease in active power of 75 %, heating temperature decreases by 49 %. The dependence of heating temperature change and change of active power is non-linear and may be described by means of a mathematical expression derived using MS Excel:

$$T = T_{nom} \cdot (a \cdot K_p^{\,2} + b \cdot K_p + c), \quad (2)$$

where T_{nom} is the heating temperature at nominal power consumption, °C; a, b, c are the constant

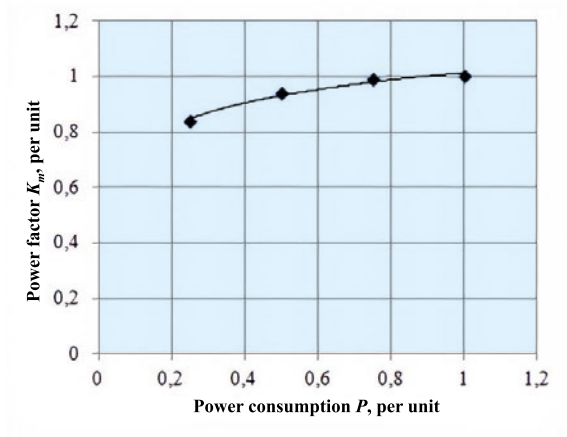

Fig. 4. Dependence of power factor change on active power consumption change

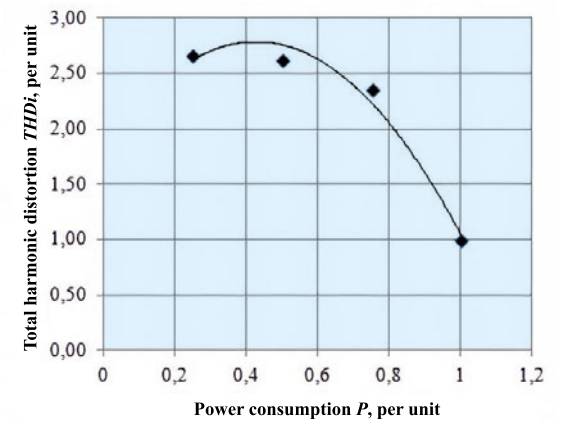

Fig. 5. Dependence of total harmonic distortion change on active power consumption change

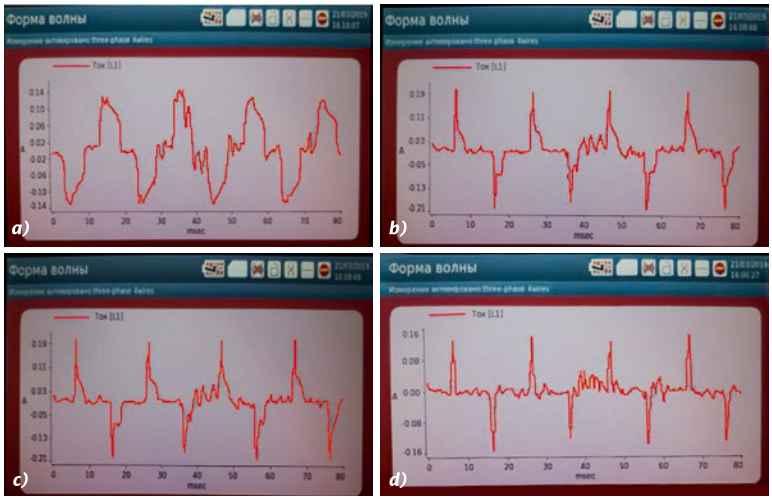

Fig. 6. The current's waveforms of the lighting system at: a) P_{nom}, b) 0.75 P_{nom}, c) 0.5 P_{nom}, d) 0.25 P_{nom}

factors depending on the manufacturer of a given light source (for the studied LED light source, a = 0.3272; b = 0.2889; c = 0.4014).

The results of studying the dependence of power factor K_m change and active power consumption P change are shown in Fig. 4.

It is found that power factor of the light source decreases with decrease in active power. With decrease in active power of 25 %, power factor decreases by 1 %. With decrease in active power of 50 %, power factor decreases by 6 %. With decrease in active power of 75 %, power factor decreases by 16 %. The dependence of power factor change and change of active power is non-linear and may be described by means of a mathematical expression derived using MS Excel:

$$K_M = K_{nom} \cdot (a \cdot \ln(K_p) + b), \qquad (3)$$

where K_{nom} is the nominal power factor, per unit; a, b are the constant factors depending on the manufacturer of a given light source (for the studied LED light source, a = 0.1201; b = 1.0135).

The results of studying the dependence of total harmonic distortion *THDi* change and active power consumption P change are shown in Fig. 5.

It is found that total harmonic distortion increases with active power decrease. With decrease in active power of 25 %, total harmonic distortion increases by 2.36 times. With decrease in active power of 50 %, total harmonic distortion increases by 2.62 times. With decrease in active power of 75 %, total harmonic distortion increases by 2.66 times. The effect of total harmonic distortion change on active power is non-linear and may be described by means of a mathematical expression derived using MS Excel:

$$THDi = THDi_{nom} \cdot (a \cdot K_P{}^2 + b \cdot K_P + c), \qquad (4)$$

where $THDi_{nom}$ is the nominal total harmonic distortion, per unit; a, b, c are the constant factors depending on the manufacturer of a given light source (for the studied LED light source, a = –5.2989; b = 4.5236; c = 1.8197).

Increase in total harmonic distortion negatively affects electric power quality. The oscillograph records (waveforms) of the current (Fig. 6) confirm it.

The results of studying the dependence of flicker index K_p change and active power consumption P change are shown in Fig. 7.

It is found that, generally, with decrease in active power, flicker index of luminous flux increases as compared to the nominal mode. With active power decrease by 25 %, flicker index of luminous

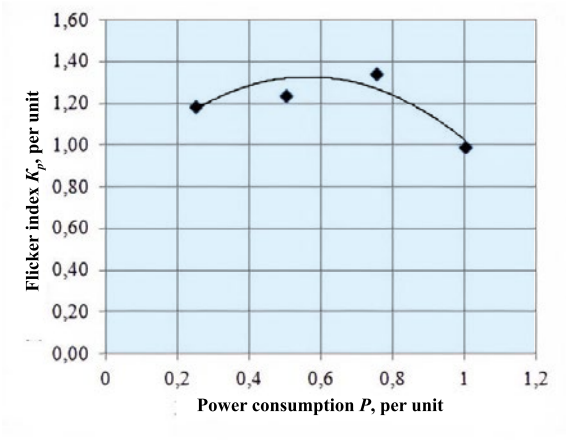

Fig. 7. Dependence of luminous flux flicker index change on active power consumption change

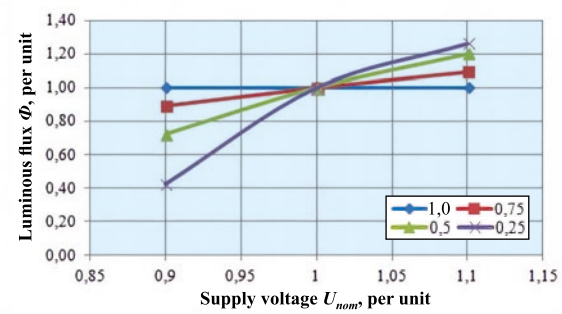

Fig. 8. The effect of supply voltage change on luminous flux of the light source with change of active power

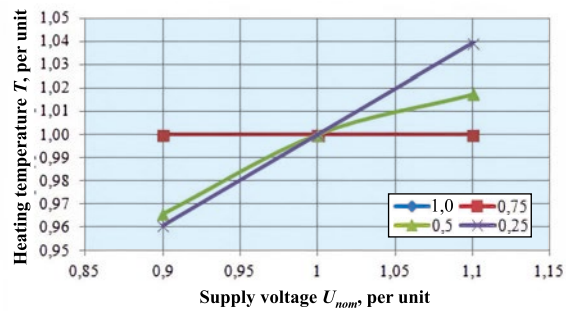

Fig. 9. The effect of supply voltage change on heating temperature of the light source with change of active power

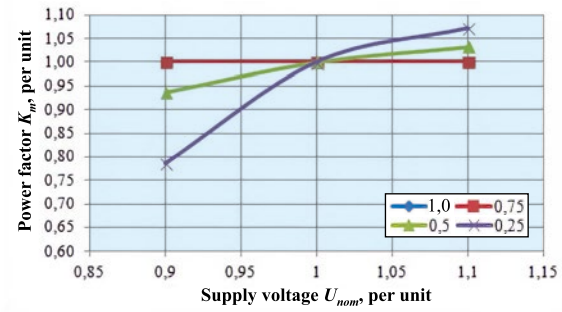

Fig. 10. The effect of supply voltage change on power factor of the light source with change of active power

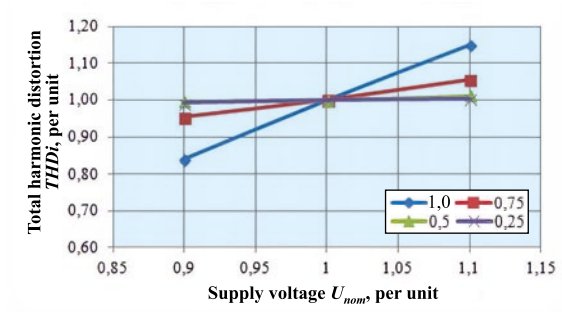

Fig. 11 The effect of supply voltage change on total harmonic distortion of the light source with change of active power

flux increases by 35 %. With active power decrease by 50 %, flicker index of luminous flux increases by 25 %. With decrease in active power of 75 %, flicker index of luminous flux increases by 20 %. The dependence of luminous flux flicker index change and change of active power is non-linear and may be described by means of a mathematical expression derived using MS Excel:

$$K_p = K_{Pnom} \cdot (a \cdot K_p^{\,2} + b \cdot K_p + c), \qquad (5)$$

where K_{Pnom} is the nominal luminous flux flicker index,%; a, b, c are the constant factors depending on the manufacturer of a given light source (for the studied LED light source, a = –1.5888; b = 1.7897; c = 0.8236).

Slow change of supply voltage is one of the main characteristics of electric power quality characterising EMI. According to [9], voltage fluctuations at balance sheet attribution border of $\pm U_{nom}$ are acceptable.

The study of the effects of supply voltage changes on a light source without a dimmer has shown that, irrespective of voltage level, luminous flux, heating temperature, and power factor remain constant.

The effect of supply voltage change on operation of a controllable lighting system (with a dimmer) is studied. The results of the study are presented below.

Fig. 8 shows the effect of supply voltage change on luminous flux of the light source with change of active power.

It is found that change of supply voltage affects luminous flux of the light source with change of active power. The most significant effect is caused by reduction of supply voltage. At 0.9 U_{nom} and with decrease in active power of 25 %, luminous flux decreases by 11 %, with decrease in active power of 50 %, luminous flux decreases by 28 %, with decrease in active power of 75 %, luminous flux decreases by 58 % as compared to the nominal mode. Increase in supply voltage causes less effect. At 1.1 U_{nom} and with decrease in active power of 25 %, luminous flux increases by 9 %, with decrease in active power of 50 %, luminous flux increases by 20 %, with decrease in active power of 75 %, luminous flux increases by 26 % as compared to the nominal mode.

Fig. 9 shows the effect of supply voltage change on heating temperature of the light source with change of active power.

It is found that change of supply voltage does not affect heating temperature of the light source with change of active power from P_{nom} down to $0.75P_{nom}$

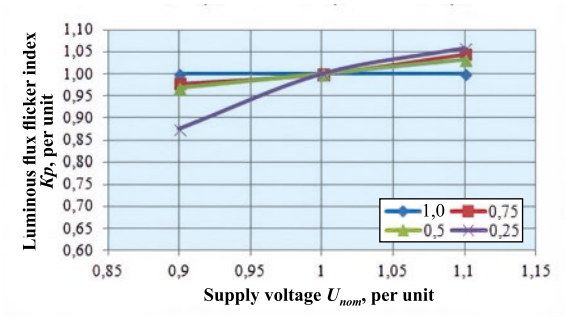

Fig. 12 The effect of supply voltage change on luminous flux flicker index of the light source with change of active power

and insignificantly affects heating temperature of the light source with change of active power from $0.5P_{nom}$ down to $0.25P_{nom}$. At $0.9U_{nom}$ and with decrease in active power of 50 %, heating temperature decreases by 3 %, with decrease in active power of 75 %, heating temperature decreases by 4 % as compared to the nominal mode. At $1.1U_{nom}$ and with decrease in active power of 50 %, heating temperature increases by 2 %, with decrease in active power of 75 %, heating temperature increases by 4 % as compared to the nominal mode.

Fig. 10 shows the effect of supply voltage change on power factor of the light source with change of active power.

It is found that change of supply voltage does not affect power factor of the lighting system with change of active power from P_{nom} down to $0.75P_{nom}$ and affects power factor of the lighting system with change of active power from $0.5P_{nom}$ down to $0.25P_{nom}$. At $0.9U_{nom}$ and with decrease in active power of 50 %, power factor decreases by 6 %, with decrease in active power of 75 %, power factor decreases by 21 % as compared to the nominal mode. At $1.1U_{nom}$ and with decrease in active power of 50 %, power factor increases by 3 %, with decrease in active power of 75 %, power factor increases by 7 % as compared to the nominal mode.

Fig. 11 shows the effect of supply voltage change on total harmonic distortion of the light source with change of active power.

It is found that changing supply voltage does not affect total harmonic distortion of the lighting system at active power of $0.25P_{nom}$ and $0.5P_{nom}$ and affects total harmonic distortion of the lighting system at active power of P_{nom} and $0.75P_{nom}$. At $0.9U_{nom}$ and with decrease in active power of 25 %, total harmonic distortion decreases by 5 %, at 100 % of active power, total harmonic distortion decreases by 16 % as compared to the nominal mode. At $1.1U_{nom}$ and with decrease in active power of 25 %, total harmonic distortion increases by 6 %, at 100 % of active power, total harmonic distortion decreases by 16 % as compared to the nominal mode.

Fig. 12 shows the effect of supply voltage change on luminous flux flicker index of the light source with change of active power.

It is found that changing supply voltage affects luminous flux flicker index of the light source with change of active power. The most significant effect is caused by reduction of supply voltage. At $0.9U_{nom}$ and with decrease in active power of 25 %, luminous flux flicker index decreases by 2 %, with decrease in active power of 50 %, luminous flux flicker index decreases by 3 %, with decrease in active power of 75 %, luminous flux flicker index decreases by 12 % as compared to the nominal mode. Increase in supply voltage causes less effect. At $1.1U_{nom}$ and with decrease in active power of 25 %, luminous flux flicker index increases by 4 %, with decrease in active power of 50 %, luminous flux flicker index increases by 3 %, with decrease in active power of 75 %, luminous flux flicker index increases by 6 % as compared to the nominal mode.

4. CONCLUSION

The conducted study has shown that TRIAC affects operation of light sources and the power supply system.

It is found that, with reduction of active power of a light source, its luminous flux decreases, its heating temperature decreases, power factor of the lighting system decreases and total harmonic distortion of the lighting system and luminous flux flicker index of the light source increase. The changes are non-linear. Mathematical expressions related to changes of luminous flux, heating temperature, power factor, total harmonic distortion and flicker index caused by change of active power of a light source are obtained. It is possible to make a conclusion that together with an opportunity to save energy and to increase the operating life of a controllable lighting system application of a dimmer leads to reduction of electric power quality and luminous flux flicker index.

The study also demonstrated that changes in supply voltage also affect operation of the controllable lighting system. Reduced supply voltage causes the highest effect on characteristics of the lighting sys-

tem. Changing supply voltage strongly affects luminous flux and heating temperature of the light source, power factor of the lighting system and luminous flux flicker index in operating modes at $0.25P_{nom}$ and $0.5P_{nom}$ and total harmonic distortion in operating modes at $0.75P_{nom}$ and P_{nom}.

REFERENCES

1. Bagin G. Ya., SolNtsev E.B., Malafeev O. Yu. Evaluation of Characteristics of Russian Lighting Systems [Otsenka kharakteristik sistem osvescheniya v Rossii] // Bulletin of the Samara State Technical University. Technical Sciences, 2016, Vol. 3 (51), pp. 78–86.

2. Nikolaev P.L. Architecture of a Smart House Control System Integrated in a Cloud Environment [Arkhitektura integrirovannoy v oblachnuyu sredu sistemy upravleniya umnym domom] // Programmnyie produkty i sistemy, 2015, Vol. 2 (110), pp. 65–69.

3. Galliulin R.R., Karimov I.I. Efficiency of LED Luminaires Application in Greenhouse Facilities [Effektivnost ispolzovaniya svetodiodnykh svetilnikov v teplichnykh khozyaystvakh] // Elektrotekhnicheskiye i informatsionnyye kompleksy i sistemy, 2016, Vol. 1, pp. 34–39.

4. Stepanchuk G.V., Yudaev I.V., Zharkov A.V. Energy-efficient Greenhouse Irradiating System [Energoeffektivnaya sistema oblucheniya v teplitse] // Tekhnologii, sredstva mekhanizatsii i energeticheskoye oborudovaniye, 2016, Vol. 1 (33), pp. 5–12.

5. Minaev I.G., Molchanov A.G., Samoilenko V.V. Energy-saving Greenhouse Optical Radiation Control System [Energosberegayuschaya sistema upravleniya istochnikami opticheskogo oblucheniya v teplitsakh] // Innovative Developments of Young Scientists of Southern Russia: abstracts of the scientific and practice conference, 2012, pp. 37–40.

6. Assonova M.L., Olkhovoy A.A., Iliin S.V. Energy-saving Technologies for Industrial Greenhouse Lighting Systems [Energosberegayuschiye tekhnologii dlya sistem osvescheniya promyshlennykh teplits] // Novyye informatsionnyye tekhnologii v avtomatizirovannykh sistemakh, 2014, Vol. 17, pp. 456–459.

7. Plotnikov V.V., Kuramshina L.F., Vakhitov A.R. Some Aspects of Design of Light Control Systems [Nekotoryye aspekty proektirovaniya sistem upravleniya svetom] // Bulletin of Kazan Techological University, 2013, Issue 4, Vol. 16, pp. 235–239.

8. GOST R50397–2011. Electromagnetic compatibility of technical equipment. Terms and definitions. Moscow: STANDARTINFORM, 2014, 57 p.

9. GOST 32144–2013. Electromagnetic compatibility of technical equipment. Power quality limits in the public power supply systems. Moscow: STANDARTINFORM, 2014, 16 p.

10. Kondratieva, N.P., Terentiev, P.V., Filatov, D.A. Comparative Experimental Analysis of Electromagnetic Compatibility of Discharge and LED Artificial Light Sources for Plant-Growing [Sravnitelnyy experimentalnyy analiz po elektromagnitnoy sovmestimosti razryadnykh i svetodiodnykh iskusstvennykh istochnikov sveta dlya rasteniyevodstva] // Bulletin of NGIEI, 2018, Vol. 12 (91), pp. 39–49.

11. Kondratieva N.P., Filatov, D.A., Terentiev, P.V. Selection of 0.4kV Cable Lines for Greenhouse Facilities [Vybor kabelnykh liniy 0.4 kV dlya teplichnykh kombinatov] // Elektrotekhnologii i elektrooborudovaniye v APK, 2019, Vol. 2 (35), pp. 17–25.

Nadezhda P. Kondratieva,
Prof., Dr. of Tech. Sc. In 1978, she graduated from Chelyabinsk Institute of Mechanization and Electrification of Agriculture. At present, she is a Head of the Chair of Automated Electric Drive Izhevsk State Agricultural Academy (IzhGSHA). She has its own science school in the field of agricultural lighting and developing of energy saving lighting technologies for agricultural enterprises is her field of interests. Also, she has got the title of "Honorary Worker of Higher Vocational Education of Russian Federation"

Dmitry A. Filatov,
Ph.D. of Tech. Sc., Associate Prof. In 2009, he graduated from R.E. Alekseev Nizhny Novgorod State Technical University. Currently, he is docent of the Chair of mechanization of livestock and rural agricultural electrification economy at Nizhny Novgorod State Agricultural Academy. His scientific interests are light sources, electromagnetic compatibility, and quality of electricity

Pavel V. Terentiev,
Ph.D., Associate Prof. In 2009, he graduated from R.E. Alekseev Nizhny Novgorod State Technical University.
At present time, he is docent of the Chair of mechanization of livestock and rural agricultural electrification economy at Nizhny Novgorod State Agricultural Academy. His scientific interests are light sources, electromagnetic compatibility, and quality of electricity

Light & Engineering
Vol. 28, No. 4, pp. 91–102, 2020

https://doi.org/10.33383/2020-027
Svetotekhnika #4, 2020

REDUCING ENERGY CONSUMPTION IN SINGLE-HOP AND MULTI-HOP TOPOLOGIES OF ROAD LIGHTING COMMUNICATION NETWORK

Musa Cıbuk

Department of Computer Engineering, Bitlis Eren University, Turkey
E-mail: mcibuk@beu.edu.tr

ABSTRACT

This study aims to make the wireless sensor network based on a linear topology required in road lighting energy-efficient using the proposed new methods. Because the physical installation of road lighting systems will result in costliness and time-labour loss, the mentioned scenarios were created and analysed in a simulation design. Two new methods were proposed to organize the lighting system more quickly and to increase the speed performance of sensors that join the network and carrying the luminaire data. This is the proxy-based network connection method and a new time-division method for the nodes' common channel access. Energy consumption scenarios for lighting systems with 50, 100, 150, and 200 luminaires were analysed comparatively during data exchange using wireless sensor networks. Accordingly, the classical method and the proposed novel method were evaluated for the single- and multi-hop scenarios. In the communication between luminaires, the proposed new method for a single-hop scenario was at least 80 % more efficient than the classical method in terms of total energy consumption. In linear topology lighting systems for the same scenario, if the classical method is compared with the proposed new method for 3-hop structures, 58 % efficiency of total energy consumption is achieved.

Keywords: intelligent lighting, wireless sensor network, energy efficiency, linear lighting

1. INTRODUCTION

In the linear wireless sensor network (WSN), nodes are ordered one after the other. The data is transmitted from the source node to the coordinator via other nodes. As the number of nodes increases, the end-to-end delay of packets and the data traffic of nodes near the coordinator increases. In addition, if the number of nodes in linear topology increases, the probability of collision and jamming increases. Protocols developed for ideal linear topologies need characteristics such as being delay-sensitive, having no connection problems, and error-free transmission of data to the centre.

With energy consumption, the rate of lighting in total energy consumption increases day by day. Intelligent lighting systems are needed to provide a sustainable and uninterrupted lighting service [1–5]. Wireless networks are frequently used for intelligent lighting in automation of remote monitoring and remote control systems [6–9].

Nodes are heavily used in many WSN applications. The increasing number of nodes is preventing WSN from organizing quickly. Connection patterns and sequences of nodes (topology) have a direct effect on the performance and life span of the network [10, 11]. Topology selection is important for self-organization of the network, reducing collisions on communication lines, reducing jams and interferences, saving energy and extending network lifetime [12, 13]. However, there is no choice of topology in linear road lighting. For linear road lighting, it is mandatory to use WSNs with linear topology

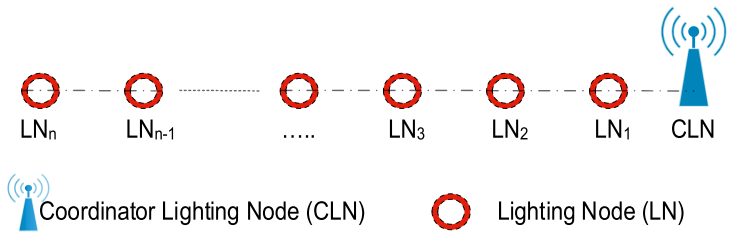

Fig. 1. Linear wireless sensor networks

[14–16]. Therefore, in road lighting with linear topology, we need to prevent data conflicts and jams of WSN during communication and reduce interference. We should be especially careful to use energy savings when performing these operations [8, 17].

In this study, an efficient novel method was proposed to minimize the energy expended by linear topology based WSN in road lighting. Each lighting node (LN) in this work represents a luminaire. The transformer pole is also called the coordinator lighting node (CLN).

The remote monitoring and control system that is subject of this study records various parameters. They are the luminance level of the LNs belonging to the luminaire, the decrease in luminous flux compared to the first day's luminance level, fog in the air, humidity, air temperature regardless the luminaire is turned on or not, and the angular position of the luminaire compared to the location, etc. In this way, the information coming from the luminaires will be collected and the information about the maintenance factor of the road lighting system will be reached by automation [8, 16, 18–20].

2. APPLYING WIRELESS SENSOR NETWORKS TO LIGHTING

The two basic elements that constitute the network in linear WSNs for illumination purposes are CLN and LN. CLN organizes the network and manages the LNs, enabling data communication. If the number of luminaires is small and there is no linear topology, then the communication of LNs is usually achieved by single-hop communication. If the luminaire topology is linear, then multi-hop communication is required. LNs that do not have direct access to CLN reach it using other LNs due to the long-distance [8, 16, 18–20]. Fig. 1 shows an example of a linear WSN.

Lighting with a linear topology is performed along the line of the road, as shown in Fig. 1. This sequence is the most widely used topology in road and tunnel lighting. [4, 6, 21, 22].

In linear topology, the LNs transmit the information of the previous LN to the CLN. LNs can be transferred with single or multi hops. As the distance between the luminaires increases, the amount of energy consumed by the nodes per packet increases. In addition, the number of hops directly affects the end-to-end delay of packets. As the number of luminaires increases, the end-to-end delay of information packets increases. Data exchange traffic on LNs close to the CLN increases in direct proportion to the size of the network. As in this study, the collision and the jam is increased with increasing number of luminaires in lighting systems with linear topology. Therefore, since the road lighting created for the lighting system must have a linear topology, the developed protocols must be delay-sensitive, have no connection problems, and have characteristics such as transmitting the data to the centre without errors [8, 23–25]. In WSNs based on linear topology, the delivery of information packets between the luminaires themselves (LN) and to the CLN is represented in Fig. 2 as 1-hop, 2-hop, and 3-hop.

When choosing the optimum conditions targeted during data exchange in WSNs, you can rely on the following parameters:

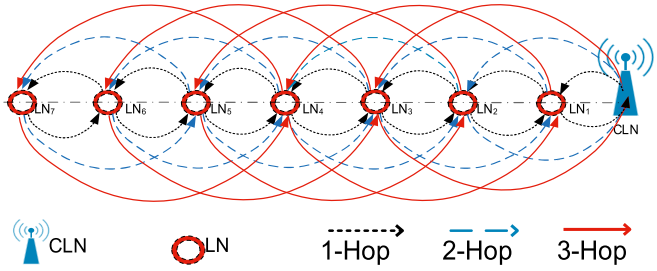

Fig. 2. 1-hop, 2-hop, and 3-hop linear WSN structure

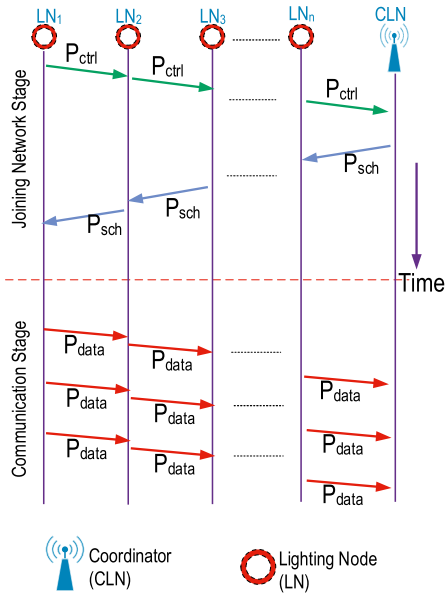

Fig. 3. The classic approach to the network joining in WSN

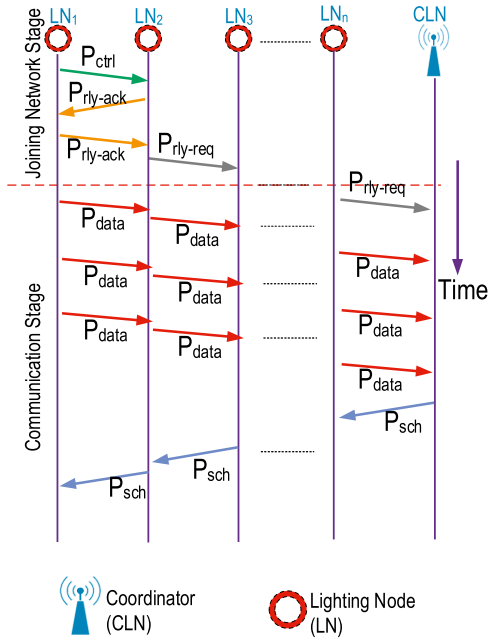

Fig. 4. Proxy-based network joining method

– low energy consumption;
– non-conflicting information packets;
– joining all nodes to the network;
– not being late in joining the network;
– not breaking out, and if the whole system is disabled for any reason;
– data exchange must be provided in a short time when the system is restarted [8, 25, 26].

In a single-hop connection model, lighting nodes (LN) communicate directly with the CLN. In the multi-hop connection model, CLN communicates with LNs that are out of coverage zone through LNs that are in the coverage zone. Therefore, in multi-hop WSNs, LNs have different energy consumption. That is why the amount of data exchange is different for each LN. Since LNs close to CLN serve as routers for more remote LNs, the amount of data exchange is significantly higher than the rest. This causes LNs close to CLN to consume more energy. Therefore, when the energy of LNs close to CLN is rapidly depleted, the communication with WSN is interrupted. In remote LNs connected to this LN, even if their energy is not exhausted, they are disconnected from the network. Therefore, the data exchange is interrupted. In such cases, the topologies using the energy efficiently should be preferred to make WSN implementation optimal. However, the use of linear topology is mandatory in road lighting. Therefore, it is necessary to develop solutions to the problems of WSN in linear road lighting systems [8].

2.1. Proxy-Based Network Joining

In multi-hop WSNs, packets of the sensor nodes are transmitted over other nodes and delivered to the coordinator node. Nodes between the target and the source perform their sensing tasks and forward data from other nodes to the next node. Fig. 3 shows the classic approach to network joining.

WSNs adopt a central approach to channel and time slot allocation in classic network scenarios. As shown in Fig. 3, it gets dark in the evening, thus the luminaire sends a request to join the network (P_{ctrl}) when the power is turned on for the first time. The neighbouring luminaire that receives this request transmits the incoming demand to the next luminaire within its own time slot. The network connection request is then transferred until it reaches the coordinating node (CLN). The coordinator receiving the connection request allocates channels and a time slot for the request. Then it creates a global schedule packet and forwards it along the road that the request came from. The schedule package created by the coordinator is delivered to the end luminaire that makes the request through the luminaires. If the end luminaire finds its own data in the schedule packet, it joins the network by setting its own channel and time slot. After this, the network joining phase is complete. The corresponding luminaire begins transmitting data. With such classic approaches, both time and energy consumption is high. For this reason, organizing the network and

Table 1. Energy Consumption Values of the Nordic Platform

Bandwidth (KHz)	Data rate (bps)	Power consumption type	Power (W)
100	5.95E+05	P_{Tx}	0.0330
		P_{Rx}	0.0366
200	1.19E+06	P_{Tx}	0.0900
		P_{Rx}	0.0384
No signal		P_{Sp}	0.0003
		P_{LPL}	3,75E-05

reconnecting nodes that are disconnected from the network are costly and slow in terms of energy consumption [8, 27].

This study adopted a proxy-based network joining approach in order to improve the energy consumption and performance of the classic approach. Fig. 4 displays a proxy-based approach to connecting to the network.

In the proposed proxy-based network joining method, a local approach is adopted instead of a central system for the channel and time slot assigning. In linear topology, nodes use a common communication channel in a sequence [28]. Nodes in the network use this channel as a time-shared system. When the node attempts to join the network, it sends a request to join the network (P_{ctrl}) to the neighbour node, as shown in Fig. 4. When the neighbour node connected to the network receives a request to join the network, it shares own channel and time slot information with that node, allowing it to join the network if appropriate. Only the information of the node that attempts to join the network is sent to the CLN. Thus, the node that attempts to join the network can do it without having to receive a scheduled packet (P_{sch}). With this method, the time to join the node to the network becomes much shorter. This ensures that the delay in joining the network, which is sourced from end-to-end packet transmission, is reduced. In addition, the request packet (P_{ctrl}) is not repeated over other nodes, resulting in a great energy savings.

In this study, the total energy consumptions of *n* pcs of LN and one CLN during sleep mode, LPL (low power listening mode) and package exchange were calculated as follows [8]. The power consumption of other parameters that may cause to power consumption was ignored. The amount of energy required for a node to receive a packet is calculated according to Eq. 1:

$$P_R = \frac{L_{pkt}}{R_{ch}} P_{Rx}, \quad (1)$$

where P_R is the power consumed for each packet reception, P_{Rx} is the power consumed by the receiver, L_{pkt} is the bit length of the packet, and R_{ch} is the data transmission capacity (bps) value of the transmission channel.

The energy calculation that any LN attempting to send data uses in radio transmission to transmit a packet is shown in Eq. 2:

$$P_T = \frac{L_{pkt}}{R_{ch}} P_{Tx}, \quad (2)$$

where P_T is the power spent to send each package, P_{Tx} is the power of the transmitter circuit power, L_{pkt} is the bit length of the packet, and R_{ch} is the data transmission capacity (bps) of the transmission channel.

The total amount of energy E_T expended by a network with ($N_C = n + 1$) nodes consisting of *n* pcs of LN nodes ($n > 2$) and at least one CLN is calculated as shown in Eq. 3:

$$E_T = \sum_{n=1}^{N_C} \left\{ \left(P_R \cdot N_{Rpkt} \right) + \left(P_T \cdot N_{Tpkt} \right) + P_{SM} + P_{LPL} \right\}, \quad (3)$$

where N_{Rpkt} is the number of packets received by the nodes, N_{Tpkt} is the number of packets transmitted by the node, P_{SM} is the energy the node spends in sleep mode, and P_{LPL} is the amount of energy the node spends in LPL mode.

As can be seen in Fig. 3, the process of joining a node to the network in the classic approach does not end until the timing packet (P_{sch}) sent by CLN reaches the node requesting to join the network. If there are at least 2 or more LNs on the network, then the other nodes between the requesting LN and the CLN perform the transfer task. LNs in transmitting state, they expend the same amount of energy as ($P_R + P_T$) to receive the packet and then transfer it to the next node. Therefore, in the classic approach, the total amount of energy expended for a node to join the network is as in Eq. 4:

$$P_{classic} = N_C \cdot \left(P_R + P_T \right) = \left(n+1 \right) \cdot \left(P_R + P_T \right), \quad (4)$$

where $P_{classic}$ represents the total energy spent by a node to join in the network based on the classic approach.

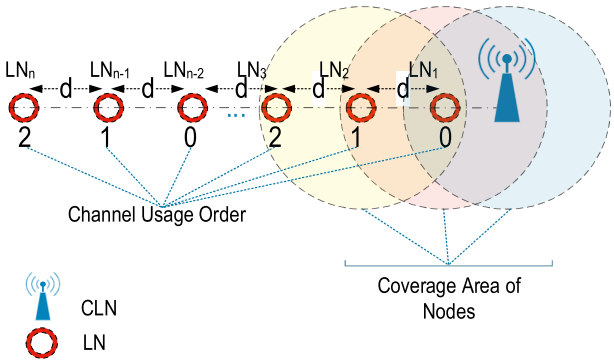

Fig. 5. Schematic representation of the time-division method

Similarly, in the proposed proxy-based network joining approach, as can be seen in Fig. 4, the process of joining a node to the network occurs only by exchanging a packet between the neighbouring node that has joined the network before. At the first moment, there is no need to wait for the schedule packet (P_{sch}) sent by CLN. Except of the neighbour LN, other LNs on the network and the CLN do not spend any energy for this process. Therefore, in the proposed proxy-based network joining approach, the total energy spent by a node to join the network is the same as in Eq. 5:

$$P_{proposed} = 3 \cdot (P_R + P_T). \quad (5)$$

In case the control (P_{ctrl}) and transfer (P_{rly}) packet sizes are constant (see Table 2), it is clear that the amount of energy spent by a node to join the network is independent of N_C and is constant in the proxy-based network participation approach in Eq. 5. Therefore, the amount of energy (P_j) spent for joining the network by all nodes in a structure with n node is $P_{jclassic} = n \cdot (n+1) \cdot (P_R + P_T)$ in the classic approach, while $P_{jproposed} = 3 \cdot n \cdot (P_R + P_T)$ in the recommended proxy-based network joining approach.

Table 2. Types and Sizes of Packaging

Packet type	Length (byte)
Scheduled Packet (*Psch*)	Variable
Control Packet (*Pctrl*)	32
Relay Packet (*Prly*)	52

As a result, as the number of nodes on the network increases, the power spent in the classic approach increases exponentially depending on the number of nodes spent, while the recommended approach will increase linearly. Depending on the fact that the network should have at least two LNs and one CLN, it will always be $P_{jproposed} < P_{jclassic}$ $\{n > 2\}$.

2.2. A New Time Division Method

In classic approaches, collision-based data losses occur because LNs use common channels simultaneously. Therefore, a new time-division method has been proposed to prevent channel access simultaneously with other LNs in the coverage of LNs in linear topology [29].

The proposed time-division method is also implemented in the communication channel that nodes use to transmit data to the CLN. In this method, a node at the n^{th} level transmits data belonging to itself and its neighbours. If the transmission direction is towards the CLN, it transmits to the node (n - *1*), and if the transmission direction is downwards from the CLN, it transmits to the node (n + *1*). In the coverage area of each luminaire, there are two luminaires, the previous one and the next one. A schematic representation of the proposed time-division method is given in Fig. 5.

As shown in Fig. 5, the time-division method is based on how the sensor node uses the channel in a specific sequence order that repeats itself with its neighbour nodes. In this approach, there are two

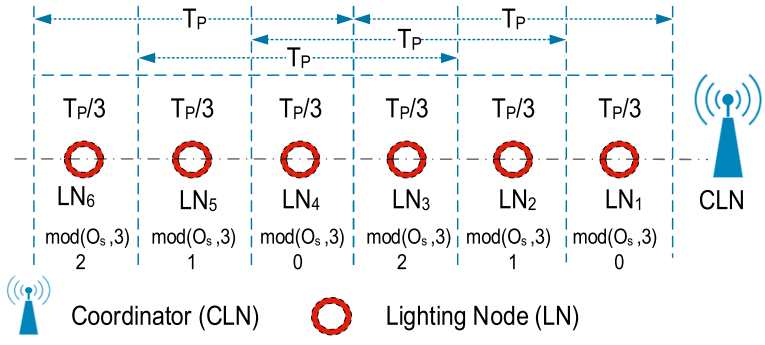

Fig. 6. Time zones for nodes

Table 3. Simulation Parameters for Scenarios Created for Simulation

Scenario/ Node count	Signal coverage of nodes (m)	Distance between nodes (m)	Number of coordinator nodes	Total distance of network (km)
S50/50	120	25	1	1.25
S100/100	120	25	1	2.5
S150/150	120	25	1	3.75
S200/200	120	25	1	5

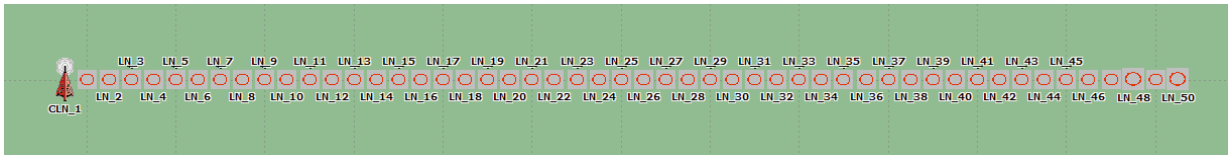

Fig. 7. Linear lighting topology in simulation environment

channels: control channel and data channel. The control channel is used by the luminaire to send the corresponding packets (*ctrl*, *sch*, *relay*) to join the network. In this channel, as the CLN is approached, the data exchange increases due to the property of the linear topology. In the data channel, the LNs transmit data packets to the CLN. Each node transfers both its own data and the data of the lower-level nodes. This channel uses the proposed time division-method. Collision and jam are prevented by using a multi-channel structure in this way. Fig. 6 shows time zones for nodes.

Each node uses the common channel with neighbour nodes in sequence, as shown in Fig. 6. Eq. 7 is used to time division [29]:

$$S_d = \left(\frac{T_p}{3} \right) mod(O_s, 3), \qquad (7)$$

where T_p is the packet transmission period, S_d is the node time zone, and O_s is the channel allocation order (0, 1, 2,…, n).

As the LNs join the network, channel usage sequences are determined. The first user is assigned "0". Then 1, 2, 3, … n sequences are assigned to the luminaires in order. LNs learn channel usage sequences with timing packets when they first join the network. When calculating time slots, as seen in Eq. 7, to give nodes an equal time slot, the fixed packet transmission period is division by 3, and the channel usage order is multiplied by mode (3). As the number of luminaires increases according to the mode of use of the channel (3), it periodically produces results 0, 1 and 2. In this way, each luminaire (LN) on WSN does not use the existing channel simultaneously with the adjacent luminaire through all the way. This prevents collisions and jams. Data is not lost.

3. SIMULATION AND PERFORMANCE ANALYSIS

There is no need to pre-determine the locations of the sensor nodes when creating the WSN. In lighting systems, however, the positions of the luminaires are precise and clear. Various WSN protocols have been used in applications for lighting purposes to create a remotely controlled intelligent system [6, 21, 22, 30–33]. The most preferred network systems in these studies are *Zigbee* and *GPRS*.

Although using the *Zigbee* protocol increases energy efficiency, *Zigbee* has a low data transmission capacity, so it is insufficient when high data transmission is needed. The most commonly used method after *Zigbee* in remote control applications of lighting is *GSM*-based *GPRS*. In many studies in the literature, remote control operation in intelligent lighting systems has been done with *GPRS-GSM* [34–36].

Due to *Zigbee's* inadequate bandwidth, as well as the high energy consumption of its *GPRS-GSM*-based WSN protocols, this study preferred *nRF905* [37] single chip 433 MHz / 868 MHz / 915 MHz transceiver, which is more up-to-date new technologies, easy to use, and has very low energy consumption during data exchange. Thus, *nRF905* was used for WSN data exchange in the lighting system.

This research was done for systems with 50, 100, 150, and 200 road lighting poles with linear topology. A simulation design was preferred for the analysis of the modelling method. The physical implementation of a real application in WSNs results in

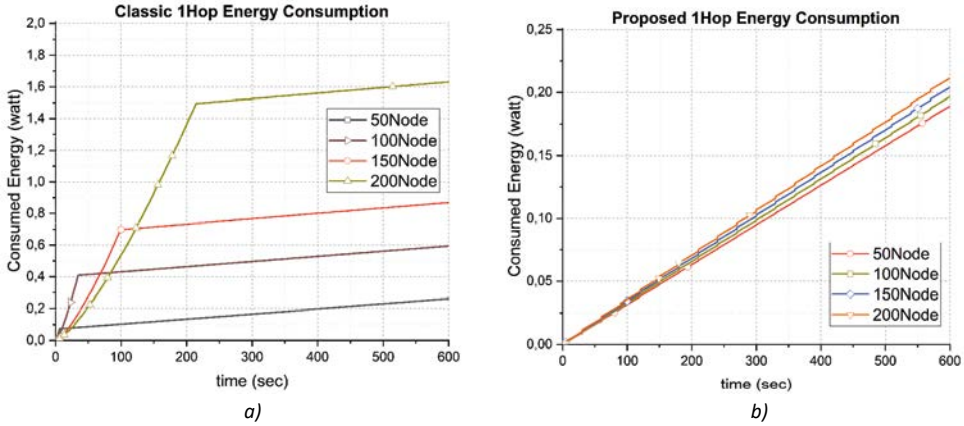

Fig. 8. Comparison of the total energy consumption for single-hop of classical (a) and proposed (b) approaches CLN-based

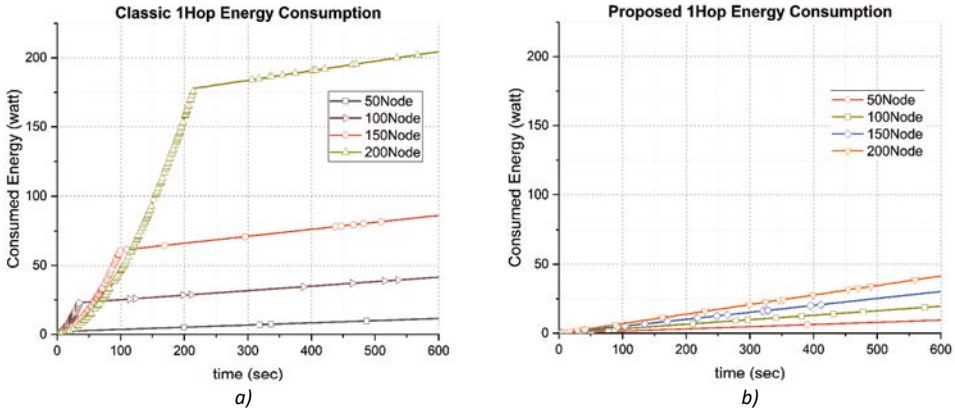

Fig. 9. The comparison of total LN-based energy consumption for single-hop of classic (a) and recommended (b) approaches

loss of time, labour and cost. In this case, first, it is necessary to conduct a simulation that produces real-life results.

The developed WSN application was modelled in the *Riverbed Modeler* simulation design. *Riverbed Modeler* is a network simulation software where simulation of all network projects can be done [38]. It allows doing many things, such as monitoring the behaviour of the network, performance analysis, testing its superiority. When designing model behaviour, it uses software-specific *ProtoC* language based on *C* programming.

Riverbed Modeler enables discrete event-based simulations to analyse the developed network model [10, 23, 38–40].

In this study, two types of nodes were designed in the simulation platform. These nodes are CLN for the central administrative point and LN for luminaires. The topological distribution of the lighting system is designed with linear topology representing road and tunnel lighting. Linear lighting topology in simulation environment is presented in Fig. 7.

The energy consumption of Nordic radios used in node models designed in the simulation environment is presented in Table 1 [8, 37].

One of the parameters that affect energy consumption is the size of data exchange packages used in WSNs. Thus, the WSNs developed as part of this study use 3 different package types for network connectivity and network continuity. Types and sizes of packaging can be seen in Table 2. The sizes of data packets vary depending on the data to be sent.

The scheduled packet was used by CLN to transmit the channel information assigned to the LNs. Control packets are used by LNs to join directly in the network and maintain continuity in the network. LNs also use relay packets to join the network through other nodes.

In this study, four different scenarios have been developed, and the simulation parameters are shown in Table 3.

The WSN node (LN) numbers are set to 50, 100, 150, and 200 luminaires, respectively, for simulation scenarios. Thus, the effect of increasing the number of nodes on linear topology is seen.

The coverage of the luminous sensors was set to 120 m for the formation of a single-hop structure. In this way, a luminaire in the linear network can only communicate with two adjacent luminaires.

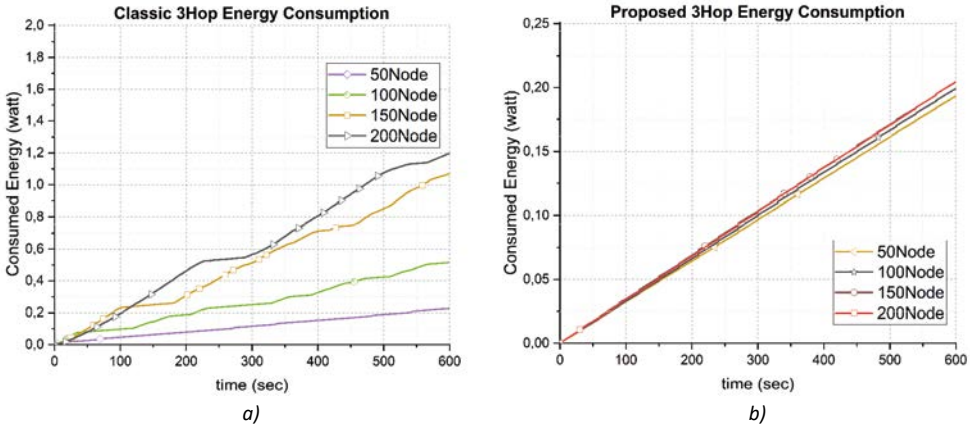

Fig. 10. Comparison of total energy consumption of the classical (a) and the proposed (b) approaches CLN-based for 3 hops

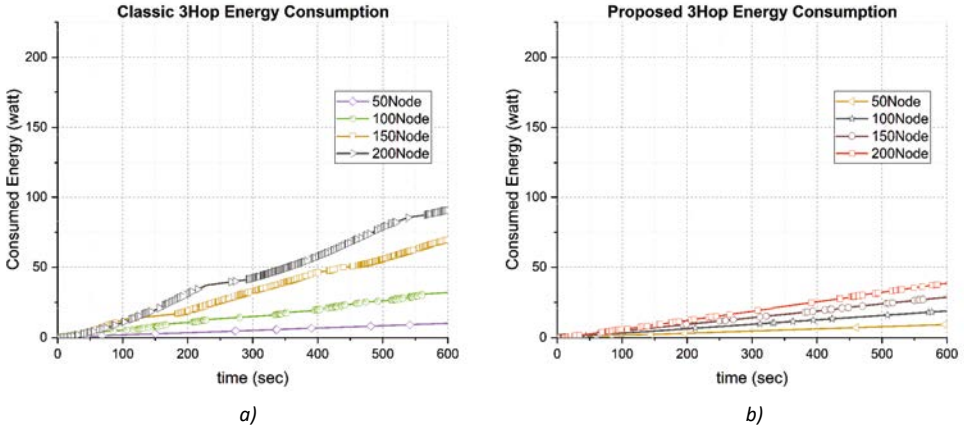

Fig. 11. Comparing of the total energy consumption of classic (a) and recommended (b) approaches LN-based for 3-hop

4. RESULTS AND DISCUSSIONS

In all scenarios that were simulated in this study, a single CLN was used. Because of simulations, the energy consumption of LNs was examined for single- and multi-hop scenarios. A comparison of networks created using classical approaches and the proposed approaches in this study is made.

First, Fig. 8 shows comparison of the total energy consumption of classical (a) and proposed (b) for single-hop approaches CLN-based.

As shown in Fig. 8, in the classical approach, a sudden energy demand occurs at the moment of joining the network. The energy consumed by the CLN of the 200 luminaires system, which consumes the most energy at the first moment, is 1.5 W when all LNs join the network. In the proposed approach, the energy consumption of CLN is 0.0116 W for the same situation. The advantage of all LNs joining the network is 99.23 %. This can be explained as follows: in the classic approach, LNs create severe packet traffic to join the network at the first moment. The CLN processes every connection request that reaches it and responds back, thus expending a lot of energy. Since the proposed approach adopts a proxy-based network connection, the relevant neighbour LN, not CLN, makes the network connection process. This allows the CLN to be less busy with fewer packets. This reduces the energy expended by the CLN during the network connection phase. For other scenarios, this situation is the same as can be seen in Fig. 8. With a similar approach, LN-based total energy consumption for single-hop is shown in Fig. 9.

As shown in Fig. 9, LNs create heavy packet traffic in the classic approach to join the network at the first moment. In the experiment of 200 LNs, which is the most difficult scenario, the energy consumed by the nodes is 175 W, while the energy consumption in the proposed approach is 0.235 W. The advantage provided is 99.86 %.

Fig. 10 (a) shows the amount of energy spent by the CLN in simulation scenarios with 50, 100, 150, and 200 lighting poles with 3 hops in the classical approach. In the scenario of 200 LN, which is the most difficult scenario in the classical approach, the process of connecting all the LNs to the network takes 225 seconds. At this point, the CLN consumed 0.552 W. In the proposed approach shown in Fig. 10 (b), the power consumption of the CLN is

Table 4. Total LNs Energy Consumption by Hop Numbers for the Simulations of 200 LNs

	1-hop	2-hop	3-hop
Classic (W)	205.92	89.71	91.81
Proposed (W)	41.63	37.59	38.57
Advantage (%)	~80	~58	~58

Table 5. Total CLN Energy Consumption Based on Hop Numbers for Simulation of 200 LNs

	1-hop	2-hop	3-hop
Classic (W)	1.63	1.08	1.20
Proposed (W)	0.211	0.200	0.205
Advantage (%)	~87	~81	~83

Table 6. Total (CLN + 200 LNs) Energy Consumption of the System Based on Hop Numbers for Simulation of 200 LNs

	1-hop	2-hop	3-hop
Classic (W)	207.55	90.79	93.010
Proposed (W)	41.841	37.79	38.775
Advantage (%)	~80	~58	~58

only 0.0086 W in the most difficult scenario of 200 LNs, when all the LNs join to the network. Accordingly, the proposed approach provides an advantage of 98.35 % in the network connection phase of LNs compared to the classical approach.

Similarly, Fig. 11 shows comparison of the total energy consumption of the classic (a) and proposed (b) the LN-based approaches for 3-hop.

According to Fig. 11, in the analysis of 200 LN that is the most difficult scenario of the classic method with 3-hop, the energy consumption required for all LNs to join the network in full performance is 39 W. In the proposed approach of this study, the energy consumed is 0.387 W for the same scenario. Here, the proposed approach provides a 99 % advantage.

According to the node numbers (LN) of the network, the comparison of the total energy consumption of LNs in the simulation scenarios 50, 100, 150, and 200 LNs for different hop numbers of the classical and proposed approaches is shown in Fig. 12.

In Fig. 12, the total amounts of energy expended by all LNs (except CLN) in connection between LNs in 1-hop, 2-hop, and 3-hop scenarios were compared in terms of the classical and proposed method. In this study, it was observed that the classic method consumes much more energy. Accordingly, the total energy consumption and savings obtained according to the hop numbers for the 200 LNs simulation that is the most difficult scenario are seen in Table 4.

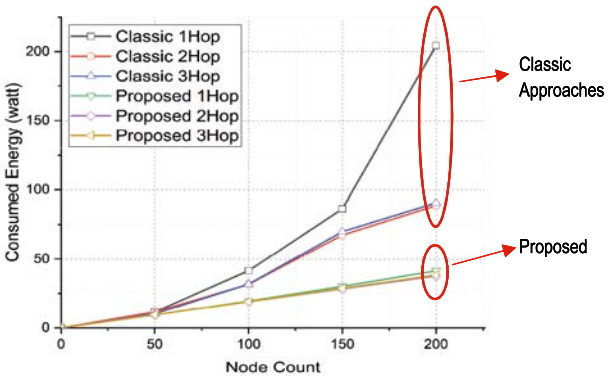

Fig. 12. Comparison of the total energy consumption of LNs

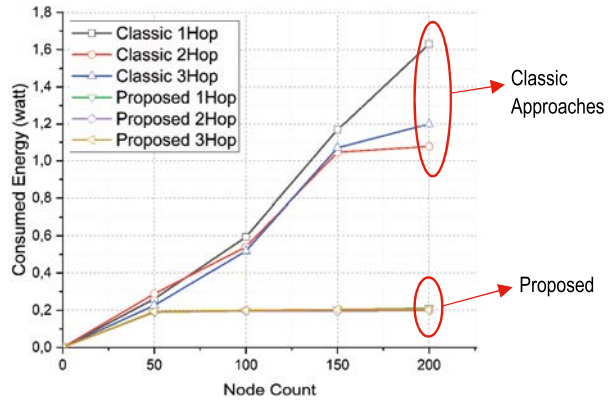

Fig. 13. CLN energy consumption comparison

The comparison of CLN energy consumption in 50, 100, 150, and 200 LNs simulation scenarios for different hop numbers of classic and recommended approaches is shown in Fig. 13.

As shown in Fig. 13, the energy that CLN expends in the 1-hop, 2-hops and 3-hops is compared in terms of the classical and proposed method. In all scenarios of 50, 100, 150, and 200 LNs, it is seen that the proposed method is much more efficient in terms of total energy consumption. For example, in a linear topology scenario with 200 poles, the comparison of energy consumption and the resulting savings amounts are shown in Table 5.

Table 6 shows the total (CLN + 200 LNs) energy consumption of the system based on hop numbers for simulation of 200 LNs.

Table 6 shows the total energy consumption of the system with 200 luminaires, which is the most difficult scenario. When comparing the classic and

proposed approaches, you can see savings of ~80 %, especially in a single hop situation.

5. CONCLUSION

In the classic approach, the energy consumption during the first join of the LNs to the network is higher, and this is due to the frequent use of schedule, control and relay packets at the first time the system is energized. In the proposed approach, the proxy-based network joining method eliminates this situation. The proposed approach gives an advantage of 98.23 % in a single-hop structure. Thus, the minimum energy consumption is achieved during the connection phase to the network, where the energy is consumed the most.

The excess of total energy consumption is particularly prominent in linear scenarios. The main reason for the increase in total energy consumption is related to the increase in the number of luminaires. As the number of LNs increases, the maximum number of hops in the system will also increase. Each hop means extra packet transfer and repetition. This will result in more energy consumption.

The approach to implementing WSN based on linear topology proposed in this study works better than the classic approach. As the number of LNs increased, the packet traffic of the LNs close to the CLN increased, but no collision was seen. End-to-end delay, one of the most important performance parameters in linear topologies, is acceptable, although the number of LNs increases. All scenarios in this study used a single CLN and were intended to maximize WSN's performance under these circumstances. On the other hand, as the number of CLN increased, it was observed that LNs connected to the network faster and that the end-to-end delay was much less. In this study, all LNs in WSN used the recommended time-division method for data transmission and control communication.

In simulations, it can be observed that as the number of LNs increases in the classical approach, the length of time that nodes will be involved in the network increases. Also, in the same scenarios with the numbers of nodes 50, 100, 150, and 200, the time for joining nodes to the network increases parabolically (5 sec., 18 sec., 99 sec., 210 sec., respectively). In WSN applications, where the number of nodes is much bigger, these periods are much longer. However, due to the proxy-based network joining method proposed in this study, it could be observed that these times are very much decreased to very low acceptable values (0.3 sec., 0.89 sec., 1.53 sec., and 2.4 sec.). In addition, the proposed approaches enabled quicker organization of the network. In case of a possible breakaway, the network the network itself will quickly reorganize.

As a result, the development of energy- and time-sensitive methods in linear WSN applications used in lighting systems is imperative in terms of network performance and efficiency of the application. Thanks to the proposed solutions, energy consumption was reduced by 80 % and 58 % depending on different scenarios.

REFERENCES

1. Dong P. Application of intelligent lighting control system in different sports events in sports venues. Light & Engineering, 2018. V26, #4, pp. 165–171.

2. Cheng R. Classroom Lighting Energy-Saving Control System Based on Machine Vision Technology. Light & Engineering, 2018. V26, #4, pp. 143–149.

3. Sun E. Solar Photovoltaic Power Generation Wireless Monitoring System Based on IOT Technology. Light & Engineering, 2018. V26, #4, pp. 130–136.

4. Sanaz Bozorg Chenani, Rami-Samuli Rasanen, Eino Tetri, Advancement in Road Lighting. Light & Engineering, 2018. V26, #2, pp. 99–109.

5. Iacomussi P., Rossi G., Soardo P. Energy saving and environmental compatibility in road lighting. Light & Engineering, 2012. V20, #4, pp. 55–63.

6. Hao L., Gao J. Intelligent Lighting System of Urban Road Based on Internet of Things. Light & Engineering, 2018 V26, #4, pp. 150–156.

7. Cao S. Intelligent Lighting Control System in Large-Scale Sports Competition Venues. Light & Engineering, 2018. V26, #4, pp. 172–182.

8. Çıbuk M., Cengiz M.S. Determination of Energy Consumption According To Wireless Network Topologies In Grid-Free Lighting Systems. Light & Engineering, 2020. V28, #2, pp. 67–76.

9. Zou Q. Lighting and Control Design of Large-Scale Stadium Skating Competition. Light & Engineering, 2018. V26, #4, pp. 183–190.

10. Arı D., Çıbuk M., Ağgün F. Effect of Relay-Priority Mechanism on Multi-hop Wireless Sensor Networks. Bitlis Eren University Journal of Science and Technology, 2017. V7, #2, pp. 145–153.

11. Çıbuk M. A New Fast Network Joining Algorithm for Single-Hop Wireless Sensor Networks. Bitlis

Eren Üniversitesi Fen Bilimleri Dergisi, 2018. V7, #1, pp. 72–83.

12. Shrestha A., Xing L. A performance comparison of different topologies for wireless sensor networks, in 2007 IEEE Conference on Technologies for Homeland Security: Enhancing Critical Infrastructure Dependability, 2007. pp. 280–285.

13. Mamun Q. A Qualitative Comparison of Different Logical Topologies for Wireless Sensor Networks. Sensors, 2012. V12, #11, pp. 14887–14913.

14. Efe S. B. UPFC Based Real-Time Optimization of Power Systems for Dynamic Voltage Regulation. Computer Modeling in Engineering & Sciences, 2018. V116, #3, pp. 391–406.

15. Efe S. B., Cebeci M. Power Flow Analysis by Artificial Neural Network. International Journal of Energy and Power Engineering, 2013. V2, #6, pp. 204–208.

16. Cengiz M.S. Simulation And Design Study For Interior Zone Luminance In Tunnel Lighting. Light & Engineering, 2019. V27, #2, pp. 42–51.

17. Yetgin H., Cheung K.T.K. El-Hajjar, M., Hanzo, L., A Survey of Network Lifetime Maximization Techniques in Wireless Sensor Networks. IEEE Communications Surveys & Tutorials, 2017. V19, #2, pp. 828–854.

18. Cengiz M. S., Cengiz Ç. Numerical Analysis of Maintanance Factor for Tunnel and Road In Solid State Lighting, in International GAP Renewable Energy and Energy Efficiency Congress, 2018. pp. 347–348.

19. Cengiz M. S., Cengiz Ç. Numerical Analysis of Tunnel LED Lighting Maintenance Factor. IIUM Engineering Journal, 2018. V19, #2, pp. 154–163.

20. Cengiz M.S. The Relationship between Maintenance Factor and Lighting Level in Tunnel Lighting. Light & Engineering, 2019. V27, #3, pp. 75–88.

21. Peixoto J. P. J., Costa D.G. Wireless visual sensor networks for smart city applications: A relevance-based approach for multiple sinks mobility. Future Generation Computer Systems, 2017. V76, pp. 51–62.

22. Karun R., Johny M. Street Light Commander System Using Zigbee Network of Devices. International Journal of Engineering and Innovative Technology (IJEIT), 2014. V4, #4, pp. 165–169.

23. Çıbuk M., Arı D., Ağgün F., Relay Mechanism with Three-way Handshake for Wireless Sensor Networks, in International Advanced Technologies Symposium (IATS17), 2017. pp. 3459–3466.

24. Bathla M., Sharma N. Topology Control in Wireless Sensor Networks. International Journal of Advances in Computer Networks and its Security, 2009. pp. 161–164.

25. Varshney S., Kumar C., Swaroop A. Linear Sensor Networks: Applications, Issues and Major Research Trends, in International Conference on Computing, Communication and Automation (ICCCA2015), 2015. pp. 446–451.

26. Chen Q., Wang K., Ying K., Miao C., Dai G. An Energy Efficient MAC Protocol for Linear WSNs. Chinese Journal of Electronics, 2015. V24, #4, pp. 725–728.

27. Çıbuk M., Arı D., Çınar H. A New Multi-Channel Algorithm Of Join The Network For Single Hop Multi-Node Sensor Networks, in International Engineering, Science and Education Conference – INESEC2016, 2016. #December, pp. 1–3.

28. Arı D., Çıbuk M., Ağgün F. A New Proxy-Based Network Joining Method for Linear Wireless Sensor Networks, in International Engineering and Natural Sciences Conference (IENSC2018), 2018. pp. 715–723.

29. Arı D., Çıbuk M., Ağgün F. Doğrusal Kablosuz Algılayıcı Ağlar için Yeni Bir Zaman Dilimleme Metodu, in 1st International Engineering and Technology Symposium, 2018. pp. 1166–1170.

30. Srinath V., Srinivas S. Street Light Automation Controller using Zigbee Network and Sensor with Accident Alert System. International Journal of Current Engineering and Technology, 2015. V5, #4, pp. 2819–2823.

31. Bhargavi R., Busupalli P. Development of Automatic Street Light Illumination and Vehicle Speed Controlling System on Arm7 for Roadways. International Journal of Research in Advanced Engineering Technologies, 2016. V5, #3, pp. 16–22.

32. Gomez C., Paradells J. Wireless Home Automation Networks- A Survey of Architectures and Technologies.pdf. CONSUMER COMMUNICATIONS AND NETWORKING, 2010. #June, pp. 92–101.

33. Radmand P., Talevski A., Petersen S., Carlsen S. Comparison of industrial WSN standards. 4th IEEE International Conference on Digital Ecosystems and Technologies – Conference Proceedings of IEEE-DEST 2010, DEST 2010, 2010. pp. 632–637.

34. Caponetto R., Dongola G., Fortuna L., Riscica N., Zufacchi D. Power consumption reduction in a remote controlled street lighting system, in SPEEDAM 2008 – International Symposium on Power Electronics, Electrical Drives, Automation and Motion, 2008. pp. 428–433.

35. Dingfang L., Suiping Q., Tundong L., Shou-Zhi Y., Funchun S. The design and realization of communication technology for street lamps control system. Proceedings of 2009 4th International Conference on Computer Science and Education, ICCSE2009, 2009. pp. 259–262.

36. Nasirudin M. A., Za'bah U. N., Sidek O. Fresh water real-time monitoring system based on Wireless Sen-

sor Network and GSM. Open Systems (ICOS), 2011 IEEE Conference on, 2011. pp. 354–357.

37. Nordic Semiconductor, nRF905 Single chip 433/868/915MHz Transceiver, 2008.

38. Riverbed, OPNET Technologies – Network Simulator, 2018. https://www.riverbed.com/gb/products/steelcentral/opnet.html (accessed May 02, 2018).

39. Vançin S., Erdem E. Design and simulation of advance MODLEACH for wireless sensor network, in International Journal of Computer Networks and Applications (IJCNA), 2015. V2, #3, pp. 135–143.

40. Cengiz M. S., Cengiz Ç. IOT and Lighting Automation, International Conference on Multidisciplinary, Engineering, Science, Education and Technology (IMESET'17 Baku) Book of Abstracts, 12–14 July 2017, Baku, pp. 8.

Musa Cıbuk,
received his M. Sc. and Ph.D. degrees from Fırat University, Turkey in 2002 and 2009, respectively. His research interests include WSNs, MAC, Computer Networks, Digital Communication and Image Processing. From 2000 to 2010, he worked at the University of Fırat. Currently, he works at Bitlis Eren University, serving as the Head of Department at Computer Engineering

Light & Engineering
Vol. 28, No. 4, pp. 103–110, 2020

https://doi.org/10.33383/2019-012
Svetotekhnika #3, 2020, pp. 71–77

A COST-EFFECTIVE ILLUMINANCE SENSOR FOR DAYLIGHT-HARVESTING LIGHTING CONTROL SYSTEMS

Moutusi Bag, Saswati Mazumdar, and Kalyan Kumar Ray

Jadavpur University, Kolkata, India
E-mails: bag12moutusi@gmail.com,
saswati.mazumdar@gmail.com,
kalyancs.ray@gmail.com

ABSTRACT

A cost-effective two-wire industrial standard illuminance sensor (4–20) mA has been proposed. It can be used for daylight harvesting control of indoor illuminance and other applications. The basic sensor used is a cadmium sulphide (*CdS*) light dependent resistor, whose relative spectral characteristic almost corresponds to the human eye. The method of sensor calibration has been presented and static and dynamic performance characteristics of the sensor have been experimentally determined.

Keywords: daylight-harvesting, relative spectral response, light dependent resistor (LDR), silicon *PIN* photodiode, current controlled current sink, infrared-cut filters, static performance, dynamic performance, points-of-control

1. INTRODUCTION

1.1. General Background

Two-wire sensors have been very popular in measurement of commonly encountered process variables like temperature, pressure, traffic flow, level of illuminance, etc. [1–4]. The most important reasons for their popularity are the absence of any auxiliary power supply, low cost of wiring and simplicity of installation. The necessity of using a two-wire sensor for illuminance measurement was felt during the development of a daylight-harvesting lighting scheme, in which natural daylight supplements artificial dimmable light emitting diode (LED) luminaires to provide a highly energy-efficient lighting system [5–9], [20–21]. As commercially available sensors for the purpose were either not easily available or were costly, it was necessary to develop one with a high performance/cost ratio. A large number of sensors (typically 1 to 4 per thousand m^2) may be required to maintain a uniformity of illuminance. This makes the cost of the sensor and the wiring cost very important factors in the design.

1.2. LDR as an Illuminance Sensor

Our initial attempt to develop a cost-effective indirect illuminance measurement system for daylight harvesting applications was biased towards using a silicon *PIN* photodiode (SIPD) as the basic sensing element. The obvious fact of high linearity of the short-circuit photocurrent as a function of the incident illuminance LED to this bias [13]. However, several disadvantages of this sensor were apparent during the development process. Firstly, the amplifier needed to amplify the photocurrent to the level of usable current or voltage required a bipolar power supply, which required two supply wires (apart from the ground). Another approach was to use an on-board positive-to-negative voltage converter, causing increase of complexity, cost and supply current requirements. A supply current more than 4 mA implied that an industry-standard 2-wire (4–20) mA signal output could not be produced. This

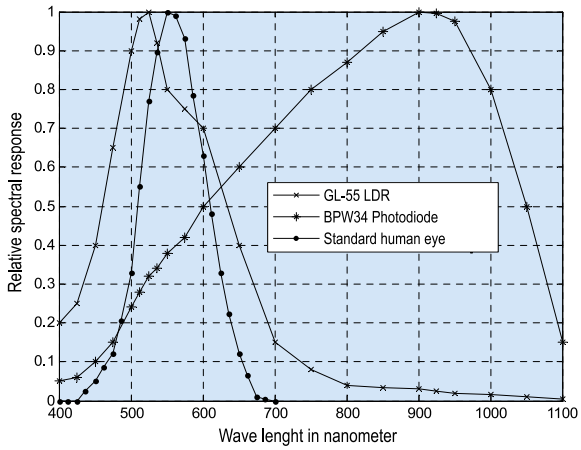

Fig. 1. Relative spectral response characteristics of a typical *Si PIN BPW 34* photodiode, a LDR and standard human eye

meant that one has to remain satisfied output of (0–10) V or (0–5) V with all associated demerits of a voltage-type sensor [3]. It would take four or at least three wires to connect such a sensor to a remote instrument or controller.

The second factor, which made an SIPD not very amenable to our application, was a great mismatch between its spectral response and the response of the human eye. The relative spectral response characteristic of a typical SIPD is shown in Fig. 1. An average human eye responds to wavelengths from 360 nm to 720 nm and has a peak of response of about 555 nm. The 10 % of the peak response occurs at about 425 nm and 675 nm. As shown in Fig. 1, 10 % of the peak response of an SIPD extends wide into the infrared region, up to about 1080 nm, thereby making it quite sensitive for wavelengths above the visible spectrum. Unless it is used along with a proper infrared-stop optical filter, an SIPD produces a higher output for a source containing infrared light (e.g. daylight or incandescent source) than one, which does not contain it (e.g. white LED or fluorescent lamp), while same produces the same illuminance in the visible range. Since the required infrared-cut filters were expensive and not very available, the research in this direction was abandoned. A photodiode with an integral optical filter was announced, which has a spectral response almost corresponding to the human eye, as *TEMT6200FX01* [14]. Issues of availability and cost kept us from using it in this study.

The peak spectral response of human eye for photopic vision occurs at 555 nm. The relative spectral responses (RSR) of a *CdS* LDR and a Si PIN photodiode are shown in Fig. 1. The RSR of common *CdS* LDRs [15–16] has a spectral peak at 525 nm. In addition, at 800 nm, which is above the visible range, the RSR falls only to 0.04. In contrast, a *PIN* diode sensor has an RSR of 0.87, which is completely unacceptable.

The basic equation representing the variation of the terminal resistance *R (E)* depending on the incident illuminance *E* is given in [16]

$$R\left(E\right)\cdot E^{\gamma} = K, \tag{1}$$

where γ is a constant known as illuminance index of the LDR and *K* is a constant.

Considering two illuminances E_1 and E_2 the following can be obtained

$$R\left(E_1\right) \,/\, R\left(E_2\right) = \left(E_2 \,/\, E_1\right)^{\gamma}. \tag{2}$$

Manufacturers determine the value of γ based on two measurements at E_1 = 10 lx and E_2 = 100 lx. Thus, we get

$$R\left(10\right) \,/\, R\left(100\right) = 10^{\gamma} \quad \text{or} \quad \gamma = lg\frac{R\left(10\right)}{R\left(100\right)}. \tag{3}$$

Section 3 describes an experimental method for evaluation of an approximate value of γ.

2. PRINCIPLE OF OPERATION OF THE SENSOR

2.1. Block Diagram Description

The principle of operation can be understood by considering the cascade combination of three blocks, as shown in Fig. 2. The first block converts the incident illuminance *E* into a low-level voltage u_1 with a typical full-scale value of 90 mV. This voltage is amplified to a higher-level u_2 using an amplifier *A*1. A typical full-scale value of u_2 is about 1 V. To improve the linearity of the transmitter at low values of *E*, a fixed offset is also added to the output.

The second block generates two currents i_{21} and i_{22} using two 2-terminal components marked as *VIC*1 and *VIC*2. *VIC*1 is actually a variable linear resistor. *VIC*2, on the other hand, is a non-linear resistor, as discussed in section 2.2. The *VIC*s are se-

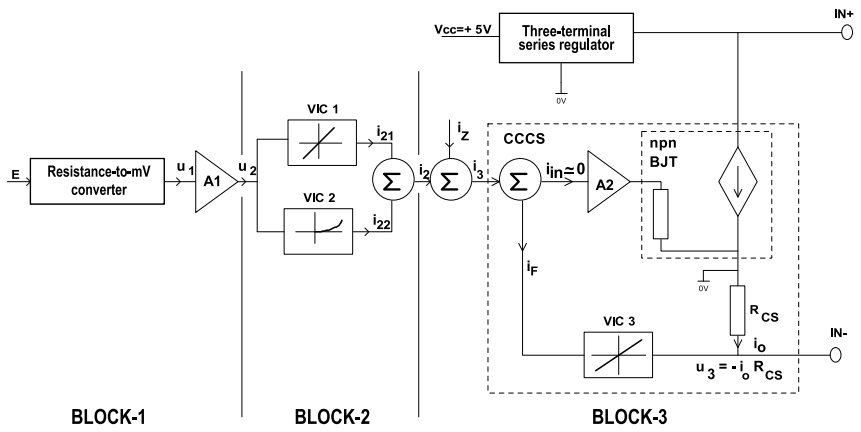

Fig. 2. Simplified block diagram of the sensor

lected in such a way that the sum i_2 of the two-component currents i_{21} and i_{22} is a linear function of the illuminance E.

The third block takes the sum of i_2 and adjustable current i_z to produce the current i_3. The current i_3 is then fed to the current controlled current sink (CCCS), so that the current i_o drawn between the transmitter terminals *IN+* and *IN-* is an amplified replica of i_3. This block utilizes an op-amp and a medium-power *NPN* bipolar junction transistor (BJT). A detailed explanation is given at the end of this section.

An expression for the output current i_o may be considered now. Clearly, i_o is given by

$$i_o = G_i \cdot (i_2 + i_z), \tag{4}$$

where G_i is the gain of the CCCS.

Since i_2 is proportional to E, Eq. 4 is modified to

$$i_o = K_1 \cdot E + K_2, \tag{5}$$

where K_1 is a constant and $K_2 = G_i \cdot i_z$ is also a constant. For an ideal transmitter K_2 caters for the "live-zero" component of the output current, which is commonly 4 mA.

2.2. Circuit Realization of the Functional Blocks

The circuit diagram of the first block is shown in Fig. 3. The photocurrent of the LDR, which is a function of incident illuminance E, flows through the variable resistor $R1$ and produces the input voltage u_1 of the amplifier [17]. The resistor $R1$ should have a value small in comparison with the resistance of the LDR at the full-scale value of E. For the supply voltage Vcc = 5 V the value of u_1 is kept within 90 mV at full scale. This ensures that the terminal voltage across the LDR is nearly constant.

The amplifier uses one-half of a common *LM358* operational amplifier in a non-inverting configuration in [17] and [18]. If there is no resistor $R4$, the gain of the amplifier $G_v = u_2 / u_1$ is set by

$$G_v = 1 + R2 / R3, \tag{6}$$

where $R2$, $R3$, and $R4$ are appropriate resistors on the circuit in Fig. 3.

However if $R4$ is present in the schema the expression for u_2 is modified as follows:

$$u_2 = (1 + R2 / R3) \cdot u_1 - (R2 / R4) \cdot V_{cc}.$$

The above expression reduces to the following

$$u_2 = G_v \cdot u_1 + u_{20}, \tag{7}$$

where

$$u_{20} = -(R2 / R4) \cdot V_{cc}. \tag{8}$$

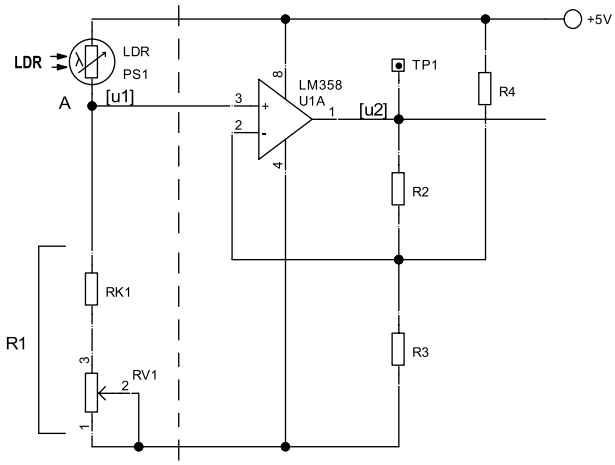

Fig. 3. Illuminance to voltage converter and linear amplifier

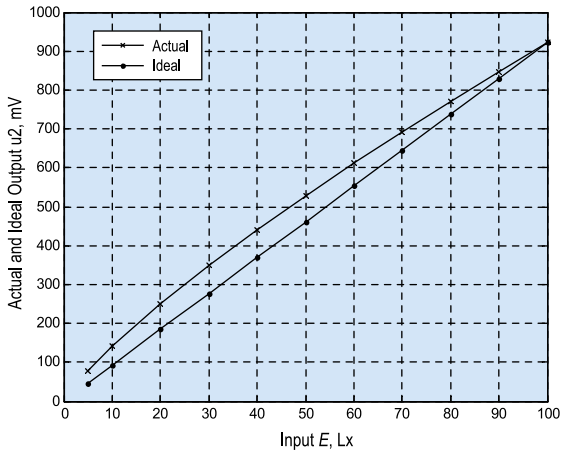

Fig. 4. Amplifier 1 output as a function of incident illuminance *E*

In our study, we have used values of *R*2 and *R*3 as 10 K and 1 K, respectively, so as to get a G_v of 11. A fixed *R*4 value of 1 MΩ produced a fixed output offset of 5 mV, which was good enough for all transmitters. The value of *RV*1 the variable part of *R*1 was adjusted so that at 40 % of E_{FS}, the full scale value of *E*, the value of the output u_2 becomes 440 mV.

For a typical LDR with a γ = 0.81 and *R* (100) = 7.1 KΩ, the variation of u_2 as a function of *E* is shown in Fig. 4. It may be observed here that the function is nonlinear. The maximum deviation of about 72 mV occurs at 40 % of span. The slope of *E* (u_2) graph is a monotone decreasing function of *E*. The latter observation is true irrespective of the values of γ and *R* (100).

The circuit realization of the second block is shown in Fig. 5. The ground terminal shown on the right side of this figure attains a potential very close to ground due to reasons explained in the next section. Thus, the current in the upper branch i_{21} is set as follows:

$$i_{21} = u_2 / R5 \quad , \tag{9}$$

where *R*5 is a variable resistance consisting of a series combination of series resistance of *RK*5 and *RV*5. Thus, the value of i_{21} corresponding to any u_2 can be adjusted using *RV*5. Graph i_{21} as a function of *E*, by virtue of Eq. 9, has the same form as Fig. 4. Since $\frac{du2}{dE}$ is a monotonically decreasing function of *E* and $i_{21} = u_2/R5$, the same nature is found in the function i_{21} (*E*). The voltage to current converter *VIC*2 produces a complementary non-linearity,

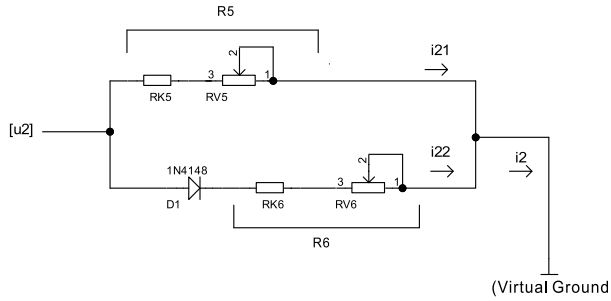

Fig. 5. Amplifier output to linear and non-linear current converter

whose slope is monotone increasing in nature. The character of the latter complementary function i_2 should be such that the sum of the component currents i_{21} and i_{22} becomes a linear function of *E* over the operating range.

Assuming that *D*1 to be an ideal diode with a fixed threshold voltage V_F and a negligible dynamic resistance, i_{22} is given as follows:

$$i_{22} = 0, \; if \; u_2 < V_F,$$

$$i_{22} = (u_2 - V_F)/R6, \; if \; u_2 \geq V_F, \tag{10}$$

where *R*6 consists of a fixed part of *RK*6 and a variable part of *RV*6 sequentially.

It is easy to graph the characteristics of u_2 (i_{22}) given by Eq. 10. It will have a zero slope until the voltage reaches the value of V_F and a slope of 1/*R*6 for higher voltages. Such an abrupt change in slope is not observed when using a physical low-signal diode e.g. *1N4148* is used. The u_2 (i_{22}) graphs for three different *R*6 values, namely 8.2 KΩ, 10 KΩ, 12 KΩ, in series with the *1N4148* are shown in Fig. 6. It is observed that for a fixed u_2, the current i_{22} reduces with increasing *R*6, and for a fixed *R*6 the slope of the graph monotonically increases with increasing u_2.

The circuit realization of the third block is now considered. The output stage of the sensor that works as a current-controlled current sink [19] is shown in Fig. 7. Of the two output terminals marked *I*+ and *I*-, the former is connected to the positive side of the loop supply of (8–24) V range, and the latter is connected to the ground side of the same supply via a current sensing resistor R_{cs} (not shown in the figure). The drop across R_{cs} is used to measure the current output of the sensor. The path of the output current I_o is shown by thick lines in the same figure. Due to the flow of I_o, a voltage u_3 is generated across *R*14

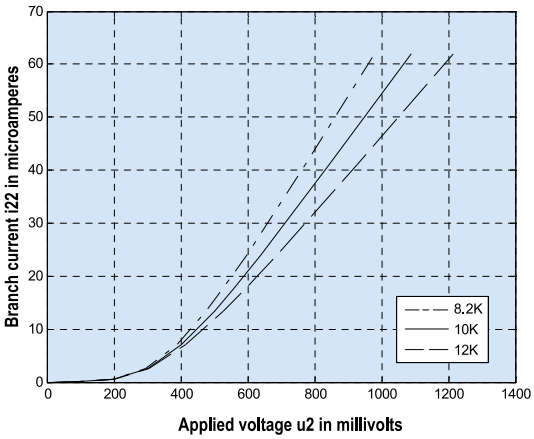

Fig. 6. i_{22} as function of u_2 for various values of $R6$

$$u_3 = -i_o \cdot R14. \tag{11}$$

This consequently produces a current i_F in the indicated direction given by

$$i_F = u_3 / R13. \tag{12}$$

Combination of Eq. 11 and Eq. 12 gives

$$I_O = i_F \cdot G_I, \tag{13}$$

where G_I is the current gain factor given by

$$G_I = R13 / R14. \tag{14}$$

The required expression of the output current as a function of the currents i_2 and i_Z can be obtained by considering the *Kirchhoff's* current equation at node *B*, which is

$$I_2 + i_Z = i_F,$$

since the input current I_{in} at the non-inverting input of the opamp *U*1 can be neglected in comparison with other terms. Substitution of i_F from Eq. 13 and the fact that

$$i_Z = V_{cc} / R7, \tag{15}$$

therefore, yields that

$$i_O = G_I \cdot \left(i_2 + V_{cc} / R7\right). \tag{16}$$

Eq. 16 indicates that at zero illuminance (E = 0), since both i_{21} and i_{22} have zero values, i_2 has a zero value and the output current assumes a value of V_{cc} / *R*7, which can be adjusted to its nominal value of 4 mA by adjustment the variable part of *R*7, namely

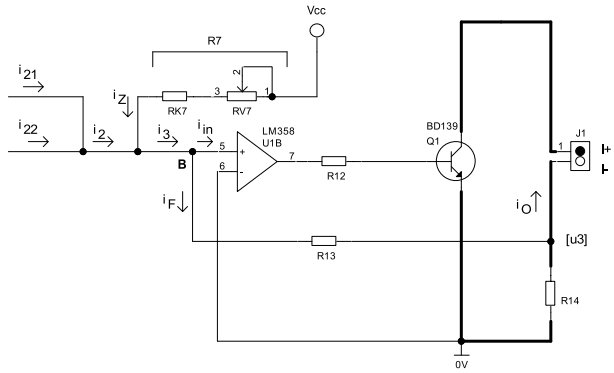

Fig. 7. Current summer and output current converter

*RV*7. As will be seen later, this will form a step in the calibration procedure of the sensor.

3. APPROXIMATE DETERMINATION OF γ AND SELECTION OF A SUITABLE LDR

Under the condition, that the voltage u_1 is very small compared to *Vcc*. The values of u_1 at 10 lx and 100 lx are given by

$$u_1(10) \approx \frac{Vcc}{R(10)} R_1, \tag{17}$$

$$u_1(100) \approx \frac{Vcc}{R(100)} R_1. \tag{18}$$

Division of Eq. 18 by Eq. 17 yields

$$\frac{u_1(100)}{u_1(10)} \approx \frac{R\ (10)}{R\ (100)}\ . \tag{19}$$

In the absence of the output offset voltage u_{20}, which can be ensured by omitting *R*4 in Fig. 3, the left side of Eq. 19 can be replaced by u_2 (100) / u_2 (10), since u_1 and u_2 are related by a constant gain factor *Gv*. Thus,

$$\frac{u_2(100)}{u_2(10)} \approx \frac{R\ (10)}{R\ (100)}\ . \tag{20}$$

A combination of Eq. 20 with Eq. 3 therefore produces

$$\gamma \approx lg\ \frac{u_2(100)}{u_2(10)}. \tag{21}$$

Eq. 21 gives us a convenient way of determining the approximate γ. Our experience shows that if the approximate γ lies in the range (0.7–0.85), the resulting sensor can give a linearity of better than 1 %. Thus, an LDR with the measured γ outside the range was rejected.

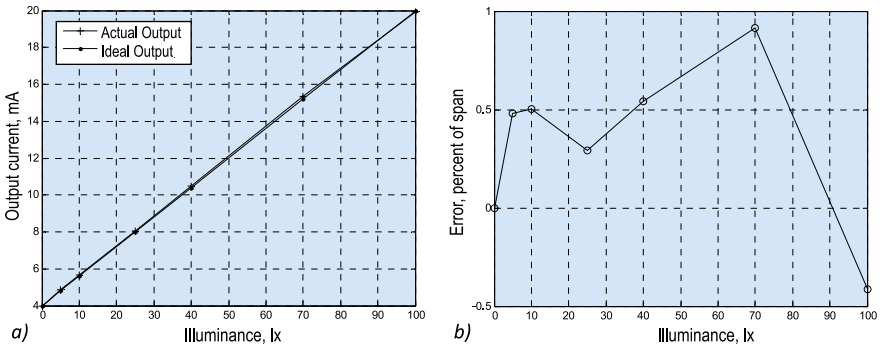

Fig. 8. Actual and ideal output characteristics (a) and graph of the sensor error (b)

4. CALIBRATION OF THE SENSOR

To calibrate the sensor, the sensor head was placed in close proximity of a calibrated illuminance meter placed in a light tight box. A white LED light source was placed above the sensor, and the current values of the LED were selected so that when two switches with appropriate marking were turned on, it was possible to obtain illuminances of 40 lx and 100 lx. Turning off both switches creates a zero illuminance condition on the sensor. The *IN*+ and *IN*- terminals of the sensor are connected to a 12 V DC power supply via a milliammeter. The following steps are then executed to calibrate the sensor.

1. Create 0 lx condition. Adjust *RV*7 (Fig. 7) so that i_O = 4 mA.

2. Keep *RV*6 at its maximum value.

3. Set *E* = 100 lx and adjust *RV*5 (Fig. 5) so that i_O becomes 90 % of its full scale value, i.e. 18 mA.

4. Set *E* = 40 lx and adjust *RV*6 (Fig. 5) so that i_O becomes (4+0.4·16), i.e. 10.4 mA.

5. Set *E* = 100 lx and adjust *RV*5 (Fig. 5) so that i_O becomes 20 mA.

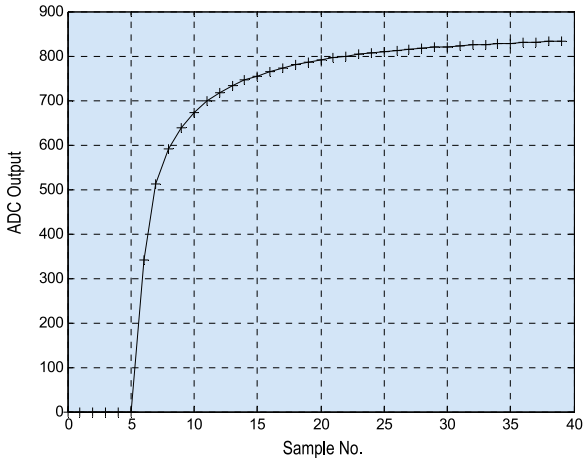

Fig. 9. Step response of the sensor

Repeat steps (4) and (5) until the sensor is calibrated at both 40 lx and 100 lx.

The performance of the sensor over the entire range of (0–100) lx is described in the next section.

5. EXPERIMENTAL RESULTS

The results given in this section have been obtained for a sensor using an LDR with an approximate γ of 0.78, as determined by the method in section 3.

5.1. Static Performance

The ideal and actual output currents of the sensor are shown in Fig. 8.(a), where the measured values correspond to *E* = 0 lx, 5 lx, 10 lx, 25 lx, 40 lx, 70 lx, and 100 lx. The error is so small that it is impossible to accurately measure with the help of the graph. The graph of the function *Error (E)* is therefore presented in Fig. 8.(b). It is observed that the maximum error magnitude is less than 1 % of the span of 16 mA.

5.2. Dynamic Performance

An experiment was performed to evaluate the time constant of the first-order model of the sensor. The terminal current is made to pass through a 100 Ω resistor. The resulting voltage drop is converted to a number using a 10 bit A-to-D converter. A step increment in *E* from 0 lx to 100 lx is applied, and the resulting output of the ADC is stored for 800 ms at 20 ms intervals. A graph of the stored values is shown in Fig. 9 where the step in *E* has been applied at 100 ms. Observing that the steady state ADC output is about 840, the time constant of the sensor is approximately 40 ms, which is equal to the time taken to reach 0.632 times the steady-state value.

Fig. 10. Photo of the typical wall mounted sensor

6. CONCLUSION

6.1. Hardware Variants of the Sensor

Two different hardware variants of the sensor were built using the LDR sensor and its associated circuit. The first one is wall-mounted, and the second one is for ceiling mounting. A photo of the wall-mounted version is shown in Fig. 10. The sensor head is placed at the back of the cylinder with a diameter of 25 mm and length of 30 mm. The cylinder makes an angle of 45° with a matte-white horizontal platform. The incident light on the platform which, is the result of different light sources in a room, generates the light incident on the sensor. In a typical lighting control system, the output variable from several sensors can be combined to calculate the illuminances at several points of interests in the room.

Another version of the sensor, meant for ceiling mounting, has a simpler construction. The LDR is placed behind a cylinder with a diameter of 20 mm and a length of 20 mm long, the open end of which faces the floor. The results in a conical zone with a total viewing angle of about 53 °. The output of such a sensor is a function of the illuminance on the work surface is included in the viewing area.

6.2. Applications

The sensor described in this study can be used in applications where the primary requirements are low cost, two-wire connection, and indirect placement (on wall or ceiling) [11]. In addition, since the self-low cost components have been used, the system specification costs are very low compared to commercially available sensors. The latter requirement is based on the fact that in most cases the required sensor can not be installed directly on the work surface.

In our study, this type of sensor is used in an integrated feedback lighting system where daylight is used to supplement artificial dimmable luminaires based on LED. This concept of daylight harvesting control gives significant savings in electrical energy and uniformity of illuminance at preselected points-of-control (POC) on the work surface [10, 12]. In the present scheme, there are six ceiling-mounted LED luminaires and four wall-mounted sensors in a (6.2 m × 4.1 m) room with windows on one side. There are 6 POCs where the illuminances due to the combined contributions of artificial lighting and daylighting are to be maintained at set-point values. The illuminance data available from the four sensors are converted into the six illuminances at the POCs by using a suitable matrix transformation.

REFERENCES:

1. Bela G. Liptak. Instrument Engineers Handbook. Boca Raton, London, New York, Washington: D.C., CRC Press, 4th Edition, 2003.

2. John G. Webstar. The Measurement, Instrumentation And Sensors Hand book. N.W., Boca Raton: CRC Press, and IEEE Press, 1999.

3. Carlos A. dos Reis Filho, An integrated 4–20 mA two-wire transmitter with intrinsic temperatures sensing capability, IEEE Trans. Solid-State Circuits, Aug., 1989. V24, #4, pp. 1136–1142.

4. Murata Power Solutions, DMS Application Note 20: 4–20 mA Current Loop Primes. [Online]. Available: www.murata-ps.com/support.

5. Li S., Pandharipande A. Daylight sensing LED lighting system, IEEE sensors journal, May 1, 2016. V16, #9, pp. 3216–3223.

6. Pandharipande A., Li S. Light-harvesting wireless sensors for indoor lighting control, IEEE sensor journal, December, 2013. V13, #12, pp. 4599–4606.

7. Pandharipande A., Caicedo D., Smart indoor lighting systems with luminaire-based sensing: A review of lighting control approaches, Energy Buildings (Oct. 2015). V104, pp. 369–377.

8. D. Caicedo, A. Pandharipande, F. M.J. Willems, Light sensor calibration and dimming sequence design in distributed lighting control systems, Proc. IEEE11th Int. Conf. Netw. Sens. Control (ICNSC), Apr. 2014. pp. 344–349.

9. D. Caicedo, A. Pandharipande, F. M.J. Willems, Illumination gain estimation and tracking in a distributed lighting control system, Proc. IEEE Multi-Conf. Syst. Control (MSC), Oct. 2014. pp 1650–1655.

10. A. Pandharipande, S. Li, Illumination and light sensing for daylight adaptation with an LED array: Proof-of-principle, Proc. 39th Annu. Conf. IEEE Ind. Electron. Soc. (IECON), Nov., 2013. pp. 6081–6086.

11. P. Dietz, W. Yerazunis, D. Leigh, Very low-cost sensing and communication using bidirectional LEDs, Proc. 5th Int. Conf. Ubiquitous Comput, Oct., 2003. pp. 175–191.

12. M. G. Villalva, J.R. Gazoli, E.R. Filho, Modeling and circuit-based simulation of photovoltaic arrays, Proc. Power Electron. Conf. (COBEP), 2009. pp. 1244–1254.

13. BPW34 datasheet, Vishay Semiconductors. [Online]. vailable: www.vishay.com/doc?91000.PDF

14. TEMT6200FX01 datasheet, Vishay Semiconductors.[Online]. Available: www.vishay.com/doc?91000.

15. Plastic coated CdS photocells. [Online]. Available: www.selcoproducts.com

16. PGM CDS Photo resisters, version 2010. [Online]. Available: www.token.com/tw

17. A. S. Sedra and K.C. Smith, Microelectronic Circuit, New York: Oxford University press, 1998.

18. Sergio Franco, Design with operational amplifiers and analog integrated circuits. NY, USA: McGraw-Hill Education, 2015.

19. Toumazou, C., Lidgey, F. J. and Haigh, D. G., (EDS), Analogue IC design: the current-mode approach. London: IEE, Peter Peregrinus Ltd, April 1990.

20. GaspareBoscarino, MehrdadMoallem, Daylighting control and simulation for LED-based energy-efficient lighting systems, IEEE transsactions on industrial informatics, February 2016. V12, #1, pp. 301–308.

21. Karl W. Boer, Cadmium sulfide enhances solar cell efficiency, Energy conversion and management, Elsevier, 2011. #52, pp. 426–430.

Moutusi Bag

received her M. Sc. degree in Instrumentation and Control Engineering from University of Calcutta, India in 2010. She is currently pursuing Ph.D. in Engineering at Jadavpur University, India. Her research interests are in the area of daylight harvesting for indoor lighting control and solar based lighting system

Kalyan Kumar Ray

received the B. Sc. degree from Jadavpur University, Kolkata, India, in 1968, where he was adjudged the best student in the Faculty of Engineering and Technology, the M. Sc. degree from the Indian Institute of Technology, Kanpur, India, in 1970, and the Ph.D. degree from Jadavpur University in 1979, all in electrical engineering. He was a Senior Research Assistant in the Indian Institute of Technology, Kanpur, from 1968 to 1973. In 1973, he joined Jadavpur University, Kolkata, India, as a Lecturer. He served in the Departments of Electrical Engineering and Instrumentation and Electronics Engineering for 39 years and retired as a Professor. He was Principal Investigator in several Government-funded projects. He is currently a Consultant to industries manufacturing electronic systems. His primary research interests include control of power electronic converters, embedded control and instrumentation, solar photovoltaic conversion, and vehicular electronics

Saswati Mazumdar

received the B. Sc., M. Sc., and Ph.D. degrees in electrical engineering (EE) from Jadavpur University (JU), Kolkata, India, in 1982, 1984, and 1996, respectively. She worked first as CSIR Senior Research Fellow, then System Development Engineer in a DOE-funded Project in the Department of EE, JU. From 1987, she joined in teaching in the department of EE, JU. She acted as Director of School of Illumination Science, Engineering and Design, JU from 2006 to 2014. She is currently working as a Professor in the Department of EE, JU, Kolkata, India. She has now 33 years of experience in lighting research and teaching. She developed a modernized Illumination Engineering Laboratory in Department of EE, JU. She has founded one full-time Master's Course on illumination engineering and another part-time Master's course on illumination technology and design in JU. She has executed a large number of R&D and Consultancy Projects on illumination and allied fields. Her primary research areas are controllers of lighting systems, renewable energy-based lighting systems, smart lighting systems, LEDs and LASER communication, interior and exterior lighting design, and colour control of modern lighting systems

Light & Engineering
Vol. 28, No. 4, pp. 111–122, 2020
https://doi.org/10.33383/2019-100
Svetotekhnika # 4, 2020

GENDER DIFFERENCE IN COLOUR PREFERENCE OF LIGHTING: A PILOT STUDY

Zheng Huang[1], Qiang Liu[1, 2*], Ying Liu[1], Michael Pointer[3], Peter Bodrogi[4], Tran Quoc Khanh[4] and Anqing Liu[5]

[1]*School of Printing and Packaging, Wuhan University, Wuhan, China*
[2]*Hubei Engineering Research Centre for Digitization and Virtual Reproduction of Colour Information in Cultural Relics, Wuhan, China*
[3]*School of Design, University of Leeds, Leeds, United Kingdom*
[4]*Laboratory of Lighting Technology, Technische Universität Darmstadt, Darmstadt, Germany*
[5]*Shenzhen Chromatech Lighting Co., Ltd., Shenzhen, China*
[*]*E-mail: liuqiang@whu.edu.cn*

ABSTRACT

Gender difference has been widely reported in many research fields. However, in the topic of colour preference of lighting, such an issue has not aroused much attention. In this study, therefore, three groups of visual experiments with different illuminance (*E*) levels (50 lx, 200 lx, 600 lx) were conducted which investigated the preferred correlated colour temperature (CCT: 3500 K, 5000 K, 6500 K) for six single-coloured decorative artificial bird-shaped objects (red, green, yellow, blue, white and black). Twenty subjects, ten males and ten females, were invited to respond with their visual colour preference of the experimental objects. The aim of this work was to investigate if gender difference exists when the observers judge objects with different colours under different *E*-CCT conditions. The results indicate that there is significant difference between males and females for the 200 lx and 600 lx conditions, especially for the cases with higher CCTs (5000 K and 6500 K). In addition, it was found that under certain *E*-CCT conditions the preference ratings of males and females for certain colours were obviously different. Similarly, for some scenarios the subjective ratings from observers of the same gender also varied with object colour.

Keywords: gender difference, colour preference, correlated colour temperature, illuminance

1. INTRODUCTION

Colour preference of lighting is currently an intensively examined topic in the field of lighting quality evaluation [1–7]. The aim of those studies was to investigate under which kind of light sources subjects prefer the rendered colours of the illuminated object [1, 8–10] to explore the influencing factors of visual colour preference perception [1, 8, 11–16] and to set up an objective metric which correlates with the subjective responses of the observers obtained from psychophysical experiments [17–21]. According to current literature, the colour preference of lighting is influenced by several factors including lighting application [13–14], regional or cultural difference [6, 16, 22–23], illuminance [24], familiarity with the experimental object [11], colour features of illuminated objects [25] as well as the whiteness of the light sources [1, 8, 26–27].

In our latest work on investigating the optimal lighting for jeans, significant gender difference was found in colour preference and colour discrimination [2]. According to that study, gender difference in colour preference varies with lighting application. Female participants exhibited better colour

Fig. 1. Experimental scene in the light booth with the red bird (an artificial decorative bird-shaped object)

discrimination ability than males. In fact, similar findings have been extensively reported by related research from multiple subjects, including genetics [28], neuroscience [29], ophthalmology [30], biology [31] as well as colour science [32]. For instance, genetically speaking, the spectral sensitivities of many of the photoreceptors in the retina are determined by genes on the X chromosome [33] and it is regarded as one possible explanation for the basis of gender differences in colour perception [34]. Moreover, as reported by Hurlbert *et al*., such differences may also be attributed to the gender specific functional specialisations in the evolutionary division of labour [31].

However, although many studies in related subjects have proved such a difference between men and women, currently for the topic of colour preference of lighting, that issue has not been paid enough attention. In fact, the unbalanced recruitment of male and female observers [13,14, 16, 24, 35–46] in current literature is common and we suspected that such neglect might to some extent lead to a potential bias in the overall conclusions.

In this study, therefore, three groups of psychophysical experiments were implemented with the aim of validating the gender difference in colour preference of lighting. We speculate that such differences might be related to specific lighting conditions as well as to the colour attributes of the experimental objects, so light sources of different illuminance (E) and correlated colour temperature (CCT) levels were adopted, together with the decorative artificial bird-shaped objects of different saturated colours. In addition to this, since the experiments were grouped by E levels (i.e. for each experiment, the observers rated their colour preference for different CCTs with a constant E value), the results of this work should also provide a deeper understanding of the preferred CCT under different illuminance levels.

2. EXPERIMENTAL METHOD

2.1. Experimental Setup

The visual experiments in this work were conducted in a light booth, as shown in Fig. 1. The size of the booth was 50 cm×50 cm×60 cm (W×D×H) and its walls and floor were uniformly painted with medium-grey matt paint (Munsell N7). A chair was placed approximately 40 cm in front of the booth, which resulted in a viewing angle of approximately 30°. In addition, the height of the chair was adjustable such that each observer was unable to see the lighting module in the roof of the booth during the test.

Nine light spectra were generated by an LED cube spectral tuneable smart lighting system provided by Changzhou Thouslite Ltd. This device can simulate a wide range of spectral power distributions in a temporally stable manner by blending the 11 LED channels fitted inside the lighting

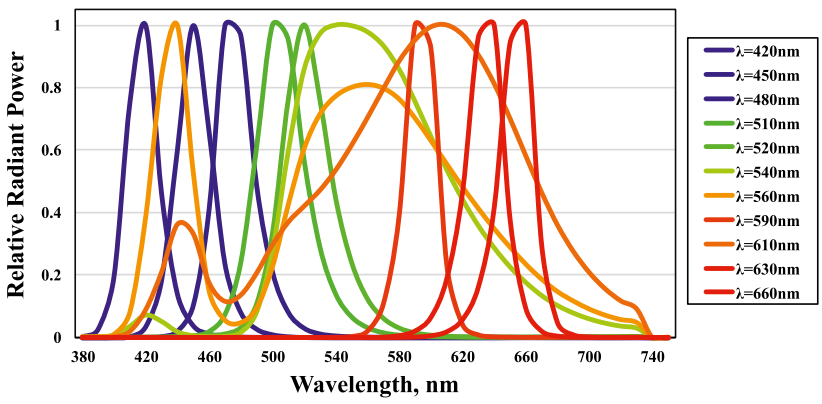

Fig. 2. Relative spectral power distribution of the 11 LED channels fitted in the LED cube system

Table 1. Colorimetric Data of the Experimental Light Sources

ID*	1	2	3	4	5	6	7	8	9
E-level (lx)	50	200	600	50	200	600	50	200	600
CCT-level (K)	3500	3500	3500	5000	5000	5000	6500	6500	6500
Measured *E* (lx)	52	203	603	48	210	600	52	204	602
Measured CCT (K)	3412	3523	3529	4956	5005	5102	6624	6520	6604
Duv	0.0032	0.0036	0.0012	0.0031	0.0011	0.0014	0.0036	0.0011	0.0012
CRI (R_a)	91	92	92	90	90	90	95	93	93
GAI	59	62	65	88	90	90	101	101	102
Q_a (9.0.3)	91	90	91	90	92	92	94	94	93
Q_f (9.0.3)	91	90	91	89	92	92	93	93	92
Q_g (9.0.3)	92	93	94	99	99	99	102	101	101
Q_p (7.4)	90	90	91	91	94	94	96	96	95
CRI2012	92	92	93	91	91	94	97	97	97
MCRI	89	89	89	91	91	91	90	90	90
R_f	87	87	88	86	86	87	94	94	93
R_g	93	93	94	98	97	97	101	101	101
GVI	80	81	81	91	89	89	92	90	90

**Note to Table1:* Duv is the distance from the test chromaticity coordinates at the Planck's locus; CRI is the general Colour Rendering Index [18]; GAI is the Gamut Area Index [19]; CQS (Q_a, Q_f, Q_p, Q_g) is the Colour Quality Scale [20]; CRI2012: An updated version of CRI [47], MCRI is the Memory Colour Rendering Index [48]; R_f and R_g is the IESNA TM-30 metrics [49]; GVI is the Gamut Volume Index[17].

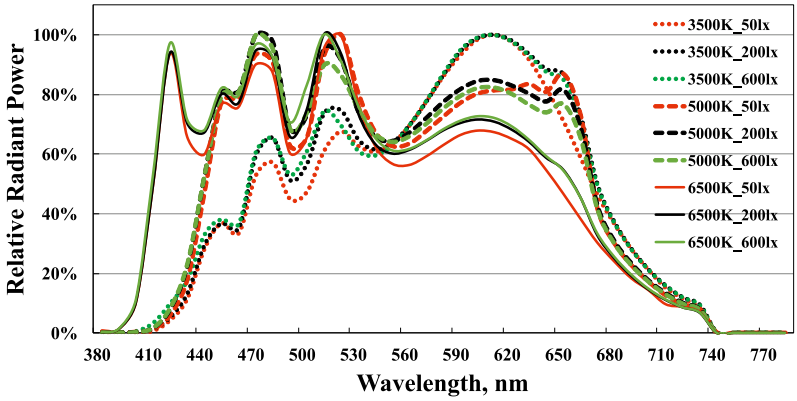

Fig. 3. Relative spectral power distributions of the experimental light sources

unit, as shown in Fig. 2. The chosen experimental light sources had 3 CCT values (3500 K, 5000 K and 6500 K) at 3 *E*-levels (50 lx, 200 lx and 600 lx). An *X-Rite i1 Pro 2* spectrophotometer was used to measure these spectra. The spectral power distributions (SPDs) of the light sources are shown in Fig. 3. The colour parameters of the experimental light sources were calculated, together with several typical colour quality measures, see Table 1.

From Table 1, it is clear that the values of the colour quality metrics of the light sources with a similar CCT are consistent. Therefore, among different *E*-level conditions, the difference of the experimental results could be attributed to *E* levels. Meanwhile, note that the Duv values of the constant-CCT light sources are not completely consistent due to the limitation of the smart lighting device. That is, when we tuning the lights to make the colour quality metrics consistent, those Duv values were the best value our device could achieve. We believe such smaller errors in Duv (~0.002) are negligible when compared to the large variations in CCT (~1500 K). In addition, the CRI values are no less than 90, which indicates that the gamut shapes [14] of those lights are normal and consistent as well.

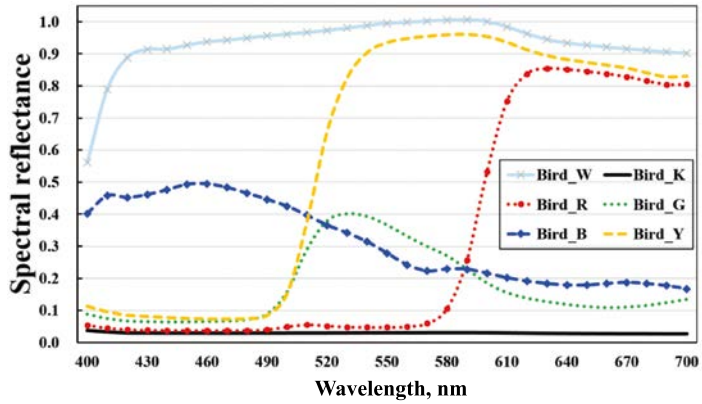

Fig. 4. Spectral reflectance of the experimental objects (artificial bird shapes of different colour). W: white; R: red; B: blue; K: black; G: green; Y: yellow

2.2. Experimental Design

Six decorative artificial bird-shaped objects (see Fig. 1) of similar shape and size (approximately 10 cm×37 cm×28 cm) were adopted as the experimental objects. The birds had the following colours: red, green, blue, yellow, black and white with moderate saturation. Their spectral reflectances were measured using a calibrated spectroradiometer (*X-Rite SpectroEye*). Figs. 4 and 5 show the spectral reflectance of the matt surface objects and their chromaticity coordinates in CAM16-UCS uniform colour space [50] respectively. It is worth mentioning that we did not adopt natural or familiar objects (e.g. fruit and vegetables) in this study since no such objects are of consistent shape and size while of different colours. Moreover, the other reason well-known objects were not used lies in the concern that the ratings of the observers might be influenced by their colour memory [51]. For instance, when rating the colour of an apple, it is possible that a red apple will be preferred while a blue one will not be appreciated.

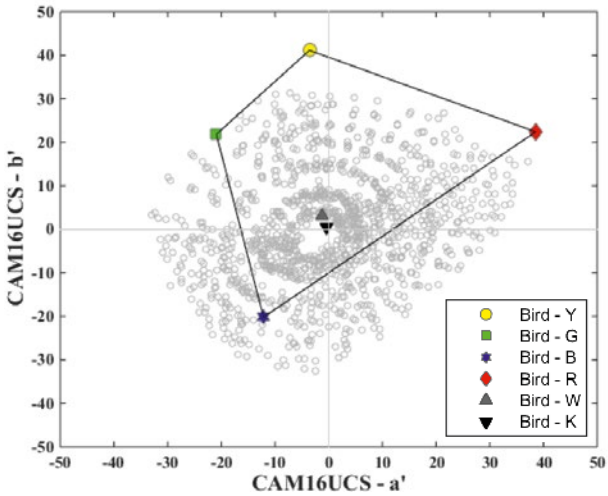

Fig. 5. CAM16-UCS chromaticity coordinates of the experimental objects (artificial bird shapes) at 50 lx and 3500 K. The scattered grey points indicate the location of the Munsell matt colour samples

Twenty observers, ten females and ten males, took part in the visual experiments. These participants were students of Wuhan University. Their age ranged between 17 and 22 years, with a mean of 19.1 years. All the observers passed the Ishihara Colour Vision Test. None knew the research intent before the test.

A 7-point rating scale was used to quantify the colour preference of the observers. Participants were asked to respond with –3, –2, –1, 0, 1, 2, 3, respectively, denoting *strongly dislike, moderately dislike, slightly dislike, neutral, slightly like, moderately like and strongly like*. Within an equi-illuminance level, each observer rated a randomly selected *E*-CCT combination twice; the participants were unaware which equi-illuminance level they were viewing. Such a setting aimed to quantify the intra – observer variability of each participant.

2.3. Experimental Procedure

Upon arrival, the participant was asked to sign a consent form and carry out the Ishihara Test. The experimenter then asked the qualified observer to put on a grey coat so that there would be no coloured light rays reflected from their coloured clothes onto the test object.

After leading the observer to the booth, the experimenter asked him/her to adjust the height of the chair to make sure that the lighting module in the booth could not be seen. Subsequently, the ambient lights were switched off so that the experimental lighting was the only illumination in the otherwise dark room. The experimenter then read the instructions to the observer and asked him/her to respond orally during the test. This protocol was designed in

Table 2. Standard Deviations of the Colour Preference Ratings for Different *E*-CCT Combinations with Different Experimental Objects

Object	50 lx			200 lx			600 lx		
	3500 K	5000 K	6500 K	3500 K	5000 K	6500 K	3500 K	5000 K	6500 K
Bird_K	1.63	1.58	1.51	1.24	0.94	1.06	1.74	0.92	1.19
Bird_W	1.33	1.18	1.12	1.72	0.98	0.97	1.44	1.05	1.41
Bird_R	1.52	1.16	1.20	1.69	1.09	1.44	1.53	1.36	1.79
Bird_Y	1.39	1.11	1.16	1.50	1.09	1.28	1.69	1.23	1.53
Bird_B	1.22	1.37	1.30	1.06	0.80	1.02	1.26	0.99	1.37
Bird_G	1.13	1.19	1.34	1.39	1.03	0.99	1.49	1.10	1.44

order to avoid the influence of reflected light on the observer's visual adaptation condition which might be caused if the observer were to write the answers onto a piece of white paper.

Since it takes a longer time to adapt from a high to a low illuminance level, in this experiment the light sources with low *E* values (50 lx) were evaluated first and then the middle (200 lx) and the high (600 lx) levels. Within a subgroup of constant *E* values, the presentation order of CCTs and experimental objects was randomized and counterbalanced between observers. At the very beginning, each participant was allowed 1 minute to adapt to the initial light which was randomly selected from the candidate lights with an *E* value of 50 lx. Afterwards, with a randomly selected colour bird, a training section was provided to help the observer get used to the evaluation process.

After the training session, the formal experiment began with the subgroup of 50 lx light sources. Using a randomly selected CCT, the participant was first asked to rate his/her visual colour preference of the empty booth and then the colour preference of the 6 colour birds (one at a time, with a random order). When the experimenter changed the light source, the observer was asked to keep his/her eyes closed for about 30 seconds to eliminate the short-term memory effect caused by the former lighting condition. Such a wash-up time was determined according to our previous work on evaluating colour preference of different CCTs [9, 11]. Subsequently, the observer was asked to open their eyes and observe the illuminated environment in the empty booth for 1 minute. After this chromatic adaptation step, the experimenter asked the participant to rate their colour preference of the illuminated booth and then the colour preference of the coloured birds. For each judgment, the observer was provided with as much time as they needed.

When the observer announced that they had finished their rating (for the last bird) and confirmed the results, the experimental lighting condition was changed. Meanwhile, when all the trials for a constant illuminance had been completed, the experimenter gave the participant 1 minute for wash-up (with eyes closed) and 2 minutes to fully adapt to the new illuminance level in the empty booth. Afterwards, the visual judgment workflow described above was repeated for every *E*-CCT combination. It took about 100 minutes for an observer to finish the whole experimental session.

3. RESULTS AND DISCUSSION

3.1. Inter – Observer and Intra – Observer Variability

The inter – observer variability of the participants responses was quantified by the standard deviations of their ratings, as summarized in Table 2. It can be seen that these measures are consistent with regard to each experimental object. These results also agree well with those of our previous work, in which similar experimental settings, protocols and the same 7-point rating approach were used [2, 9, 11–12, 52].

For quantifying the intra – observers variability, the absolute-difference method adopted in our previous work [1–2, 9, 11] was followed. As described above, during the test the observers were asked to rate a randomly selected *E*-CCT combination twice (for all the objects) without being informed of this point. If the absolute difference of the two responses was larger than 2 (e.g. –3 for the first time while 0 for the second time), that pair of ratings was classified as abnormal data. Subsequently, the intra – observer variability was represented by the ratio of the number of abnormal data

points to the total number of data points. The average value for this experiment was 9 %, which is within the range of average values from previous studies (3–17)%.

It was found that the intra – observer variability for the objects with lower lightness values (i.e. black, blue and green, as shown in Fig. 4) was higher, with values between (15–20)%, while for high-lightness colours (i.e. white, red and yellow) the intra – observer variability values were much lower (0–5)%. This finding prompted us to revisit our latest work on colour preference for jeans, in which the preferred CCT for 7 pairs of jeans with a colour gradient pattern was discussed [1]. Interestingly, it was found in that study that the jeans with lower lightness values also exhibited higher intra – observer variability. This suggests that perhaps the lightness of the experimental object impacts the intra – observer variability. In addition to this, another finding was that the intra – observer variability was also associated with the degree of familiarity. For the objects, which the observers were familiar with, such values were lower (jeans [1–2]: 4.8 % and 6.2 %, fruit and vegetables [1]: 3.3 %, oil painting with a seaside scenery [11]: 5.6 %, black and white object [1]: 6.7 %) while for unfamiliar objects those values were higher (artificial flowers [11]: 16.6 %, reproduction of ancient mural painting [11]: 15 %). For inter-observer variability, the impact of the lightness and similarity of the experimental object was not observed.

3.2. Overall Analysis

The overall result of this study is summarized in Fig. 6. From this figure we can conclude that for some conditions there is indeed a trend for the ratings of men and women to be different. For instance, for the 200 lx and 600 lx scenarios, it is clear that the ratings of female observers are higher than those of male observers while for the 50 lx condition, the results are not so obvious. Meanwhile, when examining the ratings for 5000 K and 6500 K we find that female observers prefer 6500 K no matter under which *E*-level condition, but such a trend is not so significant for male observers. Therefore, it seems that females have stronger demand for higher illuminance and whiter illumination, at least for the condition of this work. In addition, as shown in Table 1, since the light sources of a similar CCT are of consistent colour rendition properties, the data in Fig. 6 also illustrate the impact of illuminance for preferred CCT.

A multivariate analysis of variance (MANOVA) approach was adopted to investigate the influence of CCT, gender and object colour on the colour preference ratings for each group of a constant *E* level. The results show that for the 50 lx condition, only the influence of CCT is significant ($F=29.087$, $p<0.001$) while for the cases of 200 lx and 600 lx, both CCT (200 lx: $F=54.697$, $p<0.001$; 600 lx: $F=31.653$, $p<0.001$) and gender (200 lx, $F=5.276$, $p<0.05$; 600 lx, $F=11.669$, $p<0.05$) impact the preference ratings significantly. In addition to this, the *post hoc* comparison test reveals that for the 50 lx condition significant difference ($p<0.05$) is found between any two of the three CCTs while for 200 lx and 600 lx, only 3500 K is significantly different ($p<0.05$) from 5000 K and 6500 K. Those results agree well with Fig. 6 and strengthen our former statements. Besides, for this analysis the influence of object colour is not significant, regardless of *E* level.

Meanwhile, it must be pointed out that some expressions in this paper like “the preferred CCT” or “CCT influences colour preference” are not theoretically rigorous, since according to colorimetry a CCT corresponds to numerous SPDs and the colour renditions properties of light sources (the metrics shown in Table 1) also impacts colour preference perception. From this point of view, it is not wise to conclude that the finding of this study will be valid for any situations.

However, please note that from the perspective of practical application, it is indeed meaningful to discuss such a topic. The reason is clear: CCT is one of the most fundamental properties of a light source and it is quite common that naive users always have to make choices among light sources of different CCTs with different colour rendition properties. In fact, according to recent studies about “the preferred CCT” [1, 9, 11, 53–55], although the colour quality metrics of the experimental lights in those studies were different, consistent results were found that observers generally prefer CCTs around 4500 K to 5500 K while they dislike the colour rendition of light sources with low CCTs (2500–3500) K, or high CCTs (higher than 6000 K). Such consistency indeed validates the research manner of this work and, as far as we are concerned, it should be ascribed to the correlation between CCT and colour rendition properties. That is, although CCT

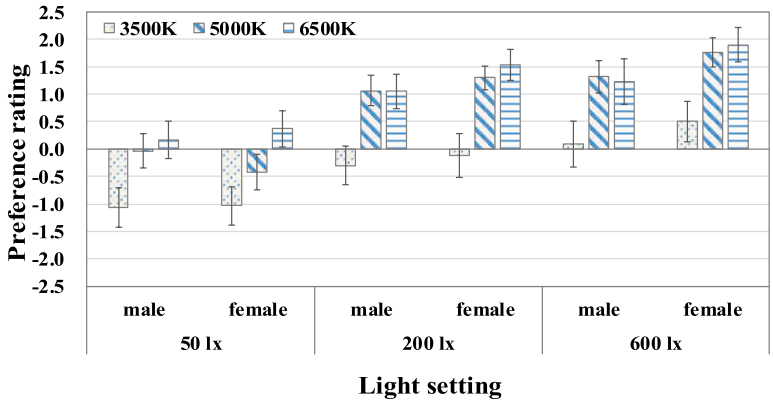

Fig. 6. Average colour preference ratings of the six experimental objects (artificial bird shapes of different colour) with regard to different gender and *E*-CCT combinations. The error bars are 95 % confidence intervals

does not influence colour perception directly, it is highly correlated with many colour rendition metrics [56] so that it has certain, or even significant "impact" on colour perception.

3.3. Gender Difference for a Certain *E*-CCT condition

In Fig. 6, it is quite clear that the gender difference in ratings varies with *E*-CCT settings. Thus, the same MANOVA approach was applied for the data of each *E*-CCT scenario. The result shows that for 200 lx at the 6500 K, 600 lx at the 5000 K and 600 lx at the 6500 K significant gender difference ($p<0.05$) could be observed while for other *E*-CCT scenarios there is no such significant difference. In addition, only in the scenario of 200 lx at the 6500 K we can observe significant influence ($p<0.05$) of object colour on preference rating and the *post hoc* comparison test demonstrates that in this condition the ratings of the blue bird are significantly different ($p<0.05$) from those of the black, red and green birds while the ratings of the white and the red birds are also significantly different ($p<0.05$). What is more, although for the 50 lx at the 6500 K scenario the influence of object is not remarkable according to MANOVA, by *post hoc* significant difference ($p<0.05$) is found between the ratings of the black and blue birds, as well as between the red and blue birds. Despite of the findings noted above, there are no other significant factors that influence the colour preference ratings for each *E*-CCT scenario.

Fig. 7 illustrates the above findings intuitively, where gender difference in preference ratings of different *E*-CCT combinations and different object colours is shown. First of all, it is clear that for every group of scenarios with a constant *E* value, the preference ratings for multiple objects seen under different CCTs show a similar trend (3500 K is not preferred while 5000 K and 6500 K are relatively appreciated). Such a result strengthens our former conclusion that light dominates colour preference when CCT differs [11].

As can be seen from Fig. 7, for the 200 lx at the 6500 K, 600 lx at the 5000 K, and 600 lx at the 6500 K conditions the average ratings of male observers of different coloured birds are relatively scattered while for female observers the average ratings are relatively concentrated. This explains why significant gender difference is found according to MANOVA as described previously. Similarly, although it has not been validated by MANOVA ($p>0.05$), from Fig. 7 it can also be observed that for the scenarios of the low CCT (3500 K), the average ratings of female observers are relatively scattered while for male observers the average ratings are relatively concentrated. Inspired by the work of Hurlbert [31] and Palmer [57], we suspect that such a finding might be ascribed to the biological long-term adaptations of the human visual system during evolution. That is, according to the hunter-gatherer theory, the vision system of males is more adapted to outdoor behaviour under daylight conditions with high CCTs, while females are more adapted to the indoor behaviour with lighting of lower CCTs (e.g. firelight). Thus, under the higher CCT conditions males are more biologically adapted in vision so that they could response diversely upon different colours while females are more adapted to lower CCT conditions and, thus, more sensitive in judging colours in those situations.

3.4. The Influence of Object Colour

As noted above, for the 50 lx at the 6500 K condition the ratings of the blue bird are significantly different from those of the black and the red birds. For the 200 lx at the 6500 K condition, similar re-

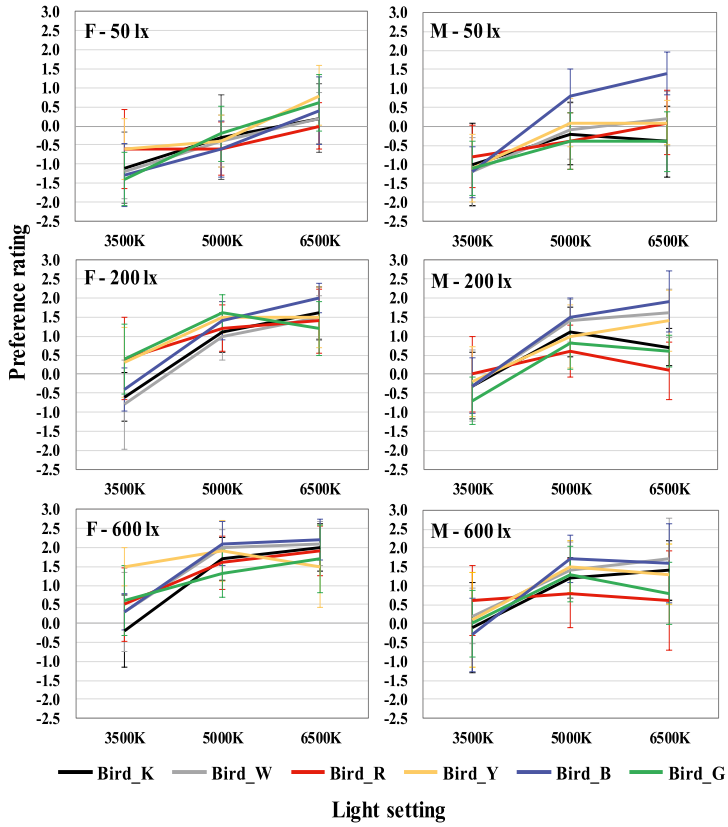

Fig. 7. Gender difference in colour preference ratings of different *E*-CCT combinations and different object colours (F: females, M: males, Error bars: 95 % confidence intervals)

sults are also obtained between the blue bird and the black, red and green birds, as well as between the white and red birds. From Fig. 7 we can conclude that those results are largely due to the ratings from male observers. Such a finding reminds us to consider the impact of object colour when investigating the gender difference in this study.

When investigating the gender difference for ratings of a certain coloured bird under a certain *E*-CCT condition Student t-test approach was adopted. It was found that for the 50 lx at the 5000 K condition, the ratings between males and females on the blue bird differed significantly ($p<0.05$) and it can be seen in Fig. 7 that the ratings of males is obviously higher. Similar result could be found for the 50 lx at the 6500 K condition (for the blue bird), although it has not been statistically validated by the t-test ($p=0.094$). Meanwhile, it was found that under the 200 lx at the 6500 K condition, there is still significant gender difference ($p<0.05$) when judging the red bird but for this case the ratings of female observers are higher. In fact, as for 600 lx at the 6500 K, such a difference could also be observed in Fig. 7, but was not significant at the 10 % level ($p=0.115$). Despite the above noted findings we suspect that there might be a gender difference for other cases as well (e.g. 200 lx at the 6500 K – black, $p=0.063$; 600 lx at the 3500 K – yellow, $p=0.070$; 200 lx at the 3500 K – green, $p=0.086$, 200 lx at the 5000 K – green, $p=0.090$), which could be observed in Fig. 7 but denied by the t-test ($0.05<p<0.1$). Those assumptions need further validation in future work with a larger number of observers.

In addition, the rating difference for multiple colours from a single gender is also discussed. According to Fig. 7 and the t-test a very interesting result was found. That is under the 600 lx at the 3500 K condition the females' ratings on the yellow birds are significantly higher ($p<0.01$) than those of the blue and black birds while, symmetrically, under the 50 lx at the 6500 K condition, the ratings of males on the blue bird are significantly higher ($p<0.05$) than those of all the other birds. Moreover, male observers also significantly prefer the blue bird under the 50 lx at the 5000 K condition (compared to the red and green birds, $p<0.05$) and for the 200 lx at the 6500 K condition, their ratings on the blue and white birds are significant higher (compared to the black, red and green birds, $p<0.05$) as well. Obviously, such results demonstrate the impact of the object colour upon the gender difference in a preferred *E*-CCT combination. When discussing relevant topics, such a factor should also be considered.

4. CONCLUSION

In this study, three groups of visual experiments with different illuminance levels were conducted, which tested the preferred correlated colour temperature for six single-coloured decorative artificial bird-shaped objects. The main finding of this work lies in the validation of gender difference for defined *E*-CCT conditions. Based on the above findings, we recommend that in future studies the number of female and male observers invited for a visual test should be equal or at least similar, since an unbalanced recruitment of male and female observers may lead to a potential bias in the overall conclusions, especially for some extreme conditions.

Meanwhile, with the aim of drawing safe conclusions, it must be acknowledged that this pilot study only represents a small set of variations in a big, multi-dimensional world. In future work, many influencing factors should be taken into account in order to further investigate this topic. These include the colour rendition properties of light sources, cultural or regional difference, the illuminance range, and other possible variations among the objects.

ACKNOWLEGEMENT

This work is supported by the National Natural Science Foundation of China (Project No. 61505-149) and the Young Talent Project of Wuhan City of China (Project No. 2016070204010111).

REFERENCES

1. Huang Z., Liu Q., Pointer M.R., Luo M.R., Wu B., Liu A. White lighting and colour preference, part A: correlation analysis and metrics validation based on four groups of psychophysical studies// Lighting Research & Technology, 2020, Vol. 52, № 1, pp. 5–22.

2. Huang Z., Liu Q., Y. Liu, M.R. Pointer, M.R. Luo, Q. Wang, Wu B. Best lighting for jeans, Part 1: Optimizing colour preference and colour discrimination with multiple correlated colour temperatures// Lighting Research & Technology, 2019, Vol. 51, № 8, pp. 1208–1223.

3. Khanh, T.; Bodrogi, P.; Guo, X.; Anh, P.Q. Towards a user preference model for interior lighting Part 1: Concept of the user preference model and experimental method. 2019,, Vol. 5, #7, pp. 1014–1029.

4. Khanh T., Bodrogi P., Vinh Q., Stojanovic D. Colour preference, naturalness, vividness and colour quality metrics, Part 1: Experiments in a room// Lighting Research & Technology, 2017**,** Vol. 49, № 6, pp. 697–713.

5. Dangol R., Islam M.S., Hyvärinen M., Bhusal P., Puolakka M., Halonen L. User acceptance studies for LED office lighting: Preference, naturalness and colourfulness// Lighting Research & Technology, 2015**,** Vol. 47, № 1, pp. 36–53.

6. Dugar A. M., Agarwal D. A pilot study assessing short-term chromatic adaptation preferences for correlated colour temperature in India// Light & Engineering, 2019**,** Vol. 27, № 1, pp. 38–45.

7. Ohno Y, Fein M., Miller C. Vision experiment on chroma saturation for colour quality preference// Light and Engineering, 2015**,** Vol. 23, № 4, pp. 6–14.

8. Huang, Z.; Liu, Q.; Luo, M. R.; Pointer, M. R.; Wu, B.; Liu, A., The whiteness of lighting and colour preference, Part 2: A meta-analysis of psychophysical data//Lighting Research & Technology, 2019, Vol. 52, #1, pp. 23–35.

9. Liu Q., Huang Z., Pointer M.R., Luo M.R., Xiao K., Westland S. Evaluating colour preference of lighting with an empty light booth// Lighting Research & Technology, 2018**,** Vol. 50, № 8, pp. 1249–1256.

10. Jost-Boissard S., Fontoynont M., Blanc-Gonnet J. Perceived lighting quality of LED sources for the presentation of fruit and vegetables// Journal of Modern Optics, 2009**,** Vol. 56, № 13, pp. 1420–1432.

11. Huang Z., Liu Q., Westland S., Pointer M.R., Luo M.R., Xiao K. Light dominates colour preference when correlated colour temperature differs// Lighting Research & Technology, 2018, Vol. 50, № 7, pp. 995–1012.

12. Tang Y., Lu D., Xun Y., Liu Q., Zhang Y., Cao G. In Proceedings of "*The influence of individual colour preference on LED lighting preference"* 49th Conference of the International Circle of Education Institutes for Graphic Arts Technology and Management (IC) and 8th China Academic Conference on Printing and Packaging, 2017, May 14–16,, Beijing, China, Springer Verlag: Beijing, China, 2018; pp 77–87.

13. Lin Y., Wei M., Smet K., Tsukitani A., Bodrogi P., Khanh T.Q. Colour preference varies with lighting application// Lighting Research and Technology, 2017**,** Vol. 49, № 3, pp. 316–328.

14. Wei M., Houser K., David A., Krames M. Colour gamut size and shape influence colour preference// Lighting Research & Technology, 2017**,** Vol. 49, № 8, pp. 992–1014.

15. Wei M., Houser K.W. What is the Cause of Apparent Preference for Sources with Chromaticity below the Blackbody Locus?// LEUKOS, 2016**,** Vol. 12 (1–2), pp. 95–99.

16. Liu A., Tuzikas A., Zukauskas A., Vaicekauskas R., Vitta P.I., Shur M. Cultural preferences to colour quality of illumination of different artwork objects revealed by a colour rendition engine// Photonics Journal, *IEEE2*013**,** *5* (4), 6801010–6801010.

17. Liu Q., Huang Z., Xiao K., Pointer M.R., Westland S., Luo M.R. Gamut Volume Index: a colour preference metric based on meta-analysis and optimized

colour samples//Optics Express, 2017**,** Vol. 25, № 14, pp. 16378–16391.

18. Nickerson D., Jerome C.W. Color rendering of light sources: CIE method of specification and its application// Illum. Eng., 1965**,** Vol. 60, *# 4*, pp. 262–271.

19. Freyssinier J. P., Rea M. In Proceeding "A two-metric proposal to specify the colour-rendering properties of light sources for retail lighting"// SPIE Optical Engineering + Applications, 2010, 7784, 6.

20. Davis W., Ohno Y. Color quality scale// Optical Engineering, 2010**,** Vol. 49, #3, 033602–033616.

21. Houser K. W., Wei M., David A., Krames M.R., Shen X.S. Review of measures for light-source color rendition and considerations for a two-measure system for characterizing color rendition// Optics Express, 2013**,** Vol. 21, # 8, pp. 10393–10411.

22. Wei R., Wan X., Liu Q., Cao G., Wang H. Regional Culture Preferences to LED Light Colour Rendering// Lecture Notes in Electrical Engineering, 2017**,** Vol. 417, pp. 33–40.

23. Bodrogi P., Khanh T.Q. Stojanovic D., Lin Y. Intercultural Colour Temperature Preference of Chinese and European Subjects Living in Germany// Light & Engineering, 2016**,** Vol. 24, #1, pp. 8–11.

24. Wei M., Bao W., Huang H.P. Consideration of Light Level in Specifying Light Source Color Rendition// Leukos the Journal of the Illuminating Engineering Society of North America, 2018, Vol. 16, # 1, pp. 55–65.

25. Lasauskaite Schüpbach R., Reisinger M., Schrader B. Influence of lighting conditions on the appearance of typical interior materials// Color Research & Application, 2015**,** 40 (1), 50–61.

26. Rea M., Freyssinier J., White lighting// Color Research & Application, 2013**,** 38 (2), 82–92.

27. Rea M., Freyssinier J. White lighting for residential applications// Lighting Research & Technology, 2013**,** Vol. 45, #3, pp. 331–344.

28. Vanston J. E., Strother L. Sex Differences in the Human Visual System// J. Neurosci. Res., 2017**,** Vol. 95 (1–2), pp. 617–625.

29. Palmer S. E., Schloss K.B., Sammartino J. Visual aesthetics and human preference// Annual review of psychology 2013, #64, pp. 77–107.

30. Panorgias A., Parry N.R. A., McKeefry D. J., Kulikowski J.J., Murray I.J. Gender Differences in Peripheral Colour Vision; A Colour-Matching Study// Investigative Ophthalmology & Visual Science, 2010, Vol. 51, #13, p. 2.

31. Hurlbert A. C., Ling Y. Biological components of sex differences in color preference// Current Biology, 2007**,** Vol. 17, #16, R623-R625.

32. Bimler D. L., Kirkland J., Jameson K.A. Quantifying Variations in Personal Color Spaces: Are There Sex Differences in Color Vision?// Color Research and Application, 2004, Vol. 29, #2, pp. 128–134.

33. Foote K. G., Neitz, M., Neitz, J. Comparison of the Richmond HRR4th edition and Farnsworth-Munsell 100 Hue Test for quantitative assessment of tritan color deficiencies// J. Opt. Soc. Am. A Opt. Image. Sci. Vis., 2014, Vol. 31, #4, pp. 186–188.

34. Seshadri J., Lakshminarayanan V., Christensen J. Farnsworth and Kinnear method of plotting the Farnsworth Munsell 100-Hue test scores: A comparison//Journal of Modern Optics, 2006, Vol. 53, # 11, pp. 1643–1646.

35. Khanh T. Q., Bodrogi P., Vinh, Q. T., Stojanovic D. Colour preference, naturalness, vividness and colour quality metrics, Part 1: Experiments in a room// Lighting Research & Technology, 2016, Vol. 49, # 6, pp. 697–713.

36. Khanh T. Q., Bodrogi P., Vinh Q.T., Stojanovic D. Colour preference, naturalness, vividness and colour quality metrics, Part 2: Experiments in a viewing booth and analysis of the combined dataset// Lighting Research & Technology, 2016, Vol. 49, # 6, pp. 714–726.

37. Khanh T. Q., Bodrogi P. Colour preference, naturalness, vividness and colour quality metrics, Part 3: Experiments with makeup products and analysis of the complete warm white dataset//Lighting Research & Technology, 2018, Vol. 50, # 2, pp. 218–236.

38. KhanhT. Q., Bodrogi P., Vinh Q.T., Guo X., Anh T.T. Colour preference, naturalness, vividness and colour quality metrics, Part 4: Experiments with still life arrangements at different correlated colour temperatures// Lighting Research & Technology, 2018, Vol. 50, # 6, pp. 862–879.

39. Nascimento S. M. C., Linhares J.M. M., Montagner C., João C.A. R., Amano K., Alfaro C., Bailão A. The colors of paintings and viewers' preferences// Vision Research, 2017, #130, pp. 76–84.

40. Wei M., Houser K.W., Allen G.R., Beers W.W. Color Preference under LEDs with Diminished Yellow Emission// LEUKOS, 2014, Vol. 10, # 3, pp. 119–131.

41. Rea M. S., Freyssinier-Nova J.P. Color rendering: A tale of two metrics// Color Research & Application, 2008, Vol. 33, #3, pp. 192–202.

42. O'Connor D. A., Davis R.G. Lighting for the elderly: The effects of light source spectrum and illuminance on color discrimination and preference//Leukos, 2005, Vol. 2, # 2, pp. 123–132.

43. Jost-Boissard S., Avouac P., Fontoynont M. Preferred Color Rendition of Skin under LED Sources//Leukos, 2016, Vol. 12 (1–2), pp. 79–93.

44. Wei M., Houser K.W. Systematic Changes in Gamut Size Affect Color Preference. LEUKOS, 2017, Vol. 13, #1, pp. 23–32.

45. Lin Y., He J., Tsukitani A., Noguchi H. Colour quality evaluation of natural objects based on the Feel-

ing of Contrast Index//Lighting Research & Technology, 2016, Vol. 48, # 3, pp. 323–339.

46. Zukauskas A., Vaicekauskas R., Vitta P., Tuzikas A., Petrulis A., Shur M. Color rendition engine// Optics Express, 2012, Vol. 20, # 5, pp. 5356–5367.

47. Smet K. A. G., Schanda J., Whitehead L., Luo R.M. CRI2012: A proposal for updating the CIE colour rendering index//Lighting Research & Technology, 2013, Vol. 45, #6, pp. 689–709.

48. Smet K. A. G., Ryckaert W.R., Pointer M.R., Deconinck G., Hanselaer P. Memory colours and colour quality evaluation of conventional and solid-state lamps//Optics express, 2010, Vol. 18, # 25, pp. 26229–26244.

49. David A., Fini P.T., Houser K.W., Ohno Y., Royer M.P., Smet K.A., Wei M., Whitehead L. Development of the IES method for evaluating the color rendition of light sources// Optics Express, 2015, Vol. 23, #12, pp. 15888–15906.

50. Li C., Li Z., Wang Z., Xu Y., Luo M.R., Cui G., Melgosa M., Brill M.H., Pointer M. Comprehensive color solutions: CAM16, CAT16, and CAM16-UCS//Color Research and Application, 2017, Vol. 42, #6, pp. 703–718.

51. Hansen T., Olkkonen M., Walter S., Gegenfurtner K.R. Memory modulates color appearance// Nature neuroscience, 2006, Vol. 9, #11, pp. 1367–1368.

52. Liu Q., Tang M.-H. Influence of light source and paper colour on the exhibiting preference of traditional calligraphy// Guang Pu Xue Yu Guang Pu Fen Xi/ Spectroscopy and Spectral Analysis, 2016, Vol. 36, #11, pp. 3664–3670.

53. Wang Q., Xu H., Zhang F., Wang Z. Influence of color temperature on comfort and preference for LED indoor lighting// Optik-International Journal for Light and Electron Optics, 2017, #129, pp. 21–29.

54. He J., Lin Y., Yano T., Noguchi H., Yamaguchi S., Matsubayashi Y. Preference for appearance of Chinese complexion under different lighting//Lighting Research & Technology, 2015, Vol. 49, #2, pp. 228–242.

55. Dikel E. E., Burns G.J., Veitch J.A., Mancini S., Newsham G.R. Preferred chromaticity of colour-tunable LED lighting// Leukos, 2014, Vol. 10, #2, pp. 101–115.

56. Wang W., Gao S., Lin H., Liu Y., Liu Q. (2019) Objective Colour Quality Assessment for Lighting. In: Zhao P., Ouyang Y., Xu M., Yang L., Ren Y. (eds) Advances in Graphic Communication, Printing and Packaging. Lecture Notes in Electrical Engineering, vol 543. Springer, Singapore.

57. Palmer S. E., Schloss K.B. An ecological valence theory of human color preference// Proceedings of the National Academy of Sciences 2010, Vol. 107, # 19, pp. 8877–8882.

Zheng Huang,
M.Eng. He graduated from Wuhan University, China. At present, he is the master student of Graphic Communication Engineering at School of Printing and Packaging, Wuhan University. He used to be the Research Assistant in the Department of Building Services Engineering, Hong Kong Polytechnic University. He has authored more than 20 journal articles and conference papers. His scientific interests are lighting engineering, colorimetry, and colour science

Qiang Liu
received the Ph.D. degree in computer science from Wuhan university in 2013 (Wuhan, Hubei, China). He is an Associate Professor with the School of Printing and Packaging of Wuhan University and serves as a technical committee member of CIE Division 1. His research interests include colour, lighting and vision. He has over 60 publications and 20 patents in the areas of colour imaging and LED lighting

Ying Liu,
B.S. She has studied at School of Printing and Packaging, Wuhan University, since 2016. Her scientific interests are colour quality of light sources, focusing on colour preference and colour discrimination. She has published 6 paper in journals and conferences

Michael R. Pointer
received his Ph.D. from Imperial College, London in 1972. He then worked in the Research Division of Kodak Limited for 28 years and is now a Visiting Professor at the University of Leeds and Technical Advisor to the Colour Engineering Laboratory at Zhejiang University, Hangzhou, China. He is the co-author, with Robert W G Hunt, of Measuring Colour, now in its 4th Edition

Anqing Liu,
Dr. He is a researcher at Chromatech Lighting Limited, Shenzhen, China. He finished his Ph.D. in Rensselaer Polytechnic Institute, Troy, United States. He worked as a research assistant in Smart Lighting Engineering Research Center in United States. After his Ph.D. study, he was a research scientist in Philips Lighting Research North America, Cambridge, United States. He serves as a technical committee member of CIE Division 1. His interest concern colour and imaging, human centric lighting and applied optics

Peter Bodrogi,
Dr. He is Optoelectronic Engineer at ERCO GmbH, Lüdenscheid, Germany. He studied physics at the Lorand Eotvos University in Budapest, Hungary. He obtained his Ph.D. degree in Information Technology from the University of Pannonia (Veszprém, Hungary). He obtained his Lecture Qualification Thesis (habilitation) in Lighting Engineering from the Technische Universität Darmstadt (Darmstadt, Germany). His interests concern lighting engineering, colorimetry, colour science, modern software technologies and LED lighting systems

Tran Quoc Khanh, Dr., Prof. He is studied from 1980 to 1985 Machine Engineering and Technical Optics before he finished his Ph.D. thesis on the Spectroscopy of UV-VIS Radiation Sources in 1989. Between 1990–1997 and 1997–1999, he was laboratory leader and project manager for photometry, radiometry and colorimetry at PRC Krochmann and Gigahertz Optik. Between 2000 and 2006, he was technical manager for optical imaging systems at ARRI, developed a digital CMOS camera, a film scanner and a laser recorder and optimized colour image processing for cinematography and TV signal processing. In 2005, he completed his Lecture Qualified Thesis (habilitation) on colour appearance and visual performance and started his current work as a Professor for Lighting Technology and Solid-State Lighting at the Technische Universität Darmstadt. He is conducting research and development projects on LED lighting technology. He is also the Chairman of the International Symposium for Automotive Lighting (ISAL). He is author of several books and scientific articles and inventor of patents on lighting technology and related subjects. He is currently Dean of the Department of Electrical Engineering and Information Technology at the Technische Universität Darmstadt

IN MEMORY OF EUGENE ROZOVSKY (09.09.1947–26.06.2020)

On June 26, 2020, at the seventy-third year of life, Eugene Isaakovich Rozovsky, a leading researcher of VNISI, senior scientific editor of the Svetotekhnika/ Light & Engineering Journals, a man of brilliant mind and a selfless worker, suddenly died. He has passed away unexpectedly and early, striving to live, work, argue, to defend his point of view to the end. The entire lighting engineering community has lost a remarkable person of amazing inner intelligence and culture, a highly trained specialist and expert, a beloved friend and comrade, who died from severe covid-19. This is an irreparable loss for all of us…

Eugene Rozovsky was born in 1947 in Moscow. In 1965 he entered the Moscow Power Engineering Institute, from which he graduated with honors in 1971 with a degree in Lighting Engineering and Light Sources, and immediately after graduation he took up the post of an engineer at the All-Union Scientific Research Institute of Lighting Engineering (VNISI) named after S.I. Vavilov. In 1975 E.I. Rozovsky graduated from the evening department of the Institute of Electronic Engineering with a degree in Applied Mathematics. In 1983 he defended his thesis for the degree of candidate of technical sciences on the topic "Research of Applied Processes in Arc Light Sources and the Development of a Method for Calculating the Design Parameters of the Cathodes of Ultrahigh-range Xenon Lamps". Eugene Rozovsky's scientific career is inextricably linked with VNISI, in which he worked all his life, going from an engineer and a junior researcher to a leading researcher at the institute. For more than 30 years E.I. Rozovsky worked in the laboratory of irradiation devices for photo-technological processes at VNISI. As a talented scientist and highly qualified specialist, Eugene Rozovsky played a key role in many important works for the institute. Among the latter are the development of a series of standards for LED lighting, including for agriculture and museum lighting, the development of lighting applications to the TR CU "Requirements and characteristics of energy efficiency, rules for determining these characteristics and forms of confirmation of compliance with the requirements for energy efficiency of light sources", research work in the fields of plant photo-culture and museum lighting. It is also important to note the serious contribution of E.I. Rozovsky in the work of the Russian National Committee of the CIE and expert activities in the projects of the IEC. On the account of E.I. Rozovsky more than 60 publications in Russian and foreign scientific journals.

The VNISI team and the Editorial Board of the Svetotekhnika/Light & Engineering Journals have lost a truly irreplaceable employee, researcher, and comrade. Modesty, benevolence and intelligence of E.I. Rozovsky, his outlook and erudition, spreading much wider than professional knowledge, reverent and respectful attitude to relatives and colleagues will forever remain in our memory and in our hearts…

CONTENTS

VOLUME 28 **NUMBER 5** **2020**

LIGHT & ENGINEERING
(SVETOTEKHNIKA)

PARTNERS OF LIGHT & ENGINEERING JOURNAL

Editorial Board with big gratitude would like to inform international lighting community about the Journal Partners Institute establishment. The list with our partners and their Logo see below. The description of partner's collaboration you can found at journal site *www.sveto-tekhnika.ru*

BL Group
International Lighting Engineering Corporation
BOOS LIGHTING GROUP

ВНИСИ

RE FLUX
HID Lighting systems

interlight RUSSIA | intelligent building RUSSIA

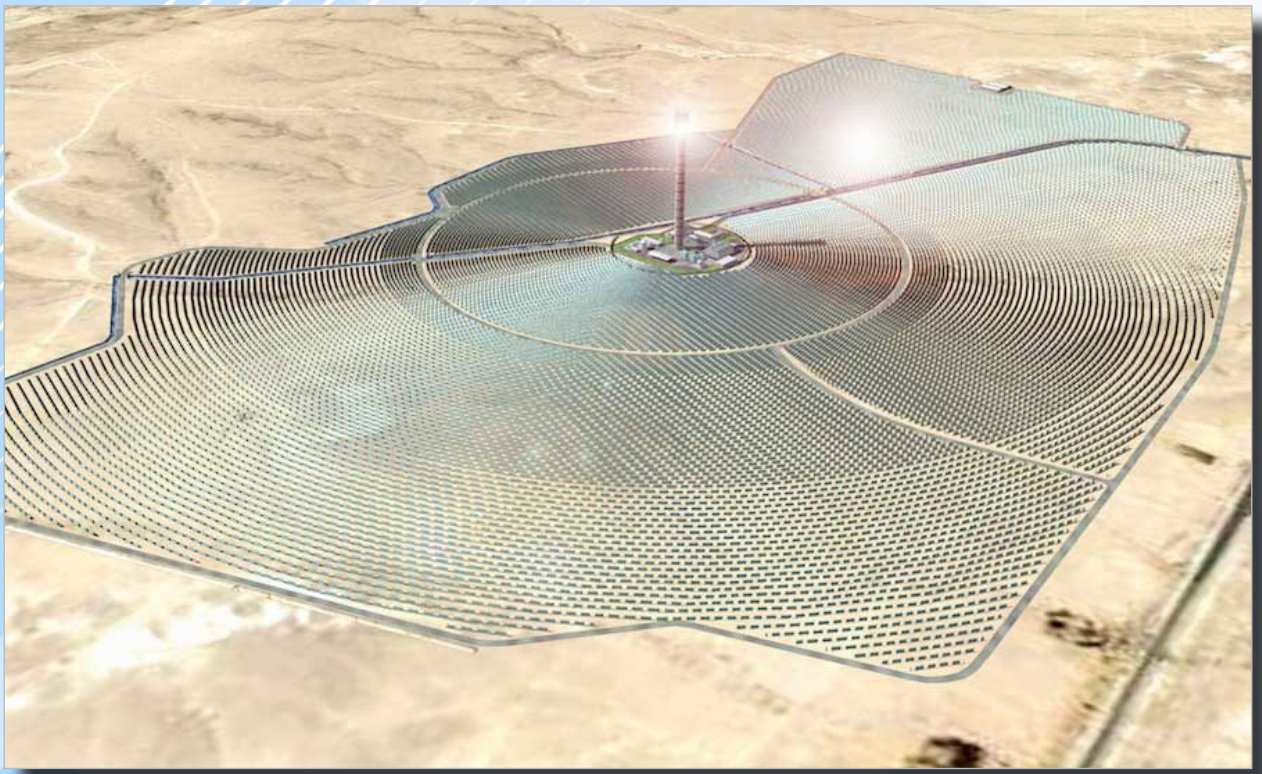

DESERT MIRRORS

In the Negev desert (Israel), a tower-type solar power station reached its design capacity. The principle of its operation is to obtain water vapour using solar radiation. In the centre of the solar power station (SPS) stands a tower, on top of which there is a reservoir of water.

This solar thermal power plant ASHLIM is located near a kibbutz of the same name in the Negev desert. The station is powered by BRIGHTSOURCE technology developed in Israel. SPS is considered one of the most advanced and largest facilities of this type in the world.

In an area of 400 football fields (approximately a million square meters), 55,000 mirrors are placed that reflect sunlight in the direction of the tallest solar tower in the world with a height of 240 meters. Mirrors are controlled by computers, tracking the movement of the sun. The tower has an installed capacity of 121 MW and a capacity of 320 GW of electricity per year, which allows providing 120,000 private houses with electricity.

For this station, scientists from Ben-Gurion University proposed an ingenious and simple way to clean the solar panels from dust, which significantly reduces the efficiency of the panels, especially in the desert. A special water-repellent coating was created, thanks to which the water flowing through the panels captures the bulk of the dust with it. The discovery was made possible by observing lotus leaves that are not exposed to dust due to the special surface covered with natural hydrophobic tissue.

A desert power station will allow Israel to move closer to the government's goal: to provide 10 % of the energy consumed from renewable energy sources.

Yefim A. Lesman
Power engineer,
Light & Engineering Journal
Correspondent,
St. Petersburg